NASA CR-
144629

[redacted]

Axiomatix

Marina del Rey • California

STUDY TO INVESTIGATE AND EVALUATE MEANS OF OPTIMIZING THE RADAR FUNCTION

Final Report

Contract No. NAS 9-14614

Prepared for

NASA Lyndon B. Johnson Space Center
Houston, Texas 77058

Prepared by

Axiomatix
13900 Panay Way, Suite 110M
Marina del Rey, California 90291

Axiomatix Report No. R7511-3
November 24, 1975

TABLE OF CONTENTS

LIST OF FIGURES

LIST OF TABLES

1.0 INTRODUCTION

This is the final report for the "Study to Investigate and Evaluate Means for Optimizing the Radar Function" for the Space Shuttle. The radar function is required by the Shuttle for rendezvous with either the passive or the cooperative (i.e., transponder equipped) targets. At the terminal phase of the rendezvous the purpose of the radar function is to provide the data necessary for stationkeeping.

At the onset of this study the objectives were to consider the radar function optimization without regard to any other function, such as the Ku-band communication system also carried on board the Shuttle. However, as the study progressed, a previously established concept of time-sharing the Ku-band equipment between the radar and the communication functions regained a major predominance in NASA's design philosophy. Consequently, the optimization of the radar function, per se, was modified accordingly to conform with the ultimate goal of an integrated radar/communication system design. For example, the considerations of the radar operating frequency were narrowed down to the region of the Ku-band communication function.

Also, the two-axis monopulse angle tracking, which is one of the major functions performed by the radar subunit, was considered in terms of its compatibility with the communication signal tracking requirements. Transmitter and receiver filtering, not necessarily a critical design area for the radar operation alone, were reconsidered in view of the ultimate requirements for time-sharing the components of an integrated system between the radar and communication functions.

Furthermore, the considerations of the angular search methods for the radar mode indicate that these methods can be easily adapted to the requirements of the communication mode, thus increasing the areas of compatibility between the two modes. Thus, it appears that a properly designed integrated radar/communication system can provide overall savings in components requirements by time-sharing the two functions.

At the two extremes of the modulation format for the radar are the noncoherent pulse system and the coherent pulse doppler system. The former is characterized by a high peak power (20 to 40 kw) and low duty cycle, 0.001 being typical. Nonambiguous range information is obtained by direct measurement of time of arrival of the return pulse and the range rate is determined by differentiation of the range data. Because the range rate estimation is based on averaging the differentiated range information over many samples of a relatively low PRF, the pulse radar has an inherent delay in providing the required range rate accuracy. Our analysis indicates that within the peak power limitations of 40 kw the specified range rate accuracy of 0.3 m/sec (3σ) cannot be achieved without exceeding the 2 sec maximum data delay specified for RCS braking.

The coherent pulse doppler radar is characterized by a relatively high duty cycle, 0.1 to 0.5 typically, and thus its peak power requirements are lower, i.e., 20 to 40 watts for the system under consideration. The range rate is determined nonambiguously by measuring the doppler shift of the main PRF line and the associated range rate accuracy and the read-out delays are within the specified limit. However, the doppler shifts and various oscillator instabilities necessitate PRF on the order of 100 kpps, or higher, to insure nonambiguous main line acquisition and tracking. The relatively high PRF limits the nonambiguous range to about 1.5 km (for 100 kpps), a range which is far below the minimum range of 19 km required for Mission III-B. Consequently, special techniques for resolving the range ambiguity, such as multiple PRFs with the Chinese remainder theorem algorithm and a separate tone ranging system have been considered.

The overall radar system design is addressed in Section 2.0 in terms of system requirements, passive target characteristics, active transponder characteristics, potential candidate systems, and the best radar operating frequency. Based on the system considerations, the non-coherent pulse and the coherent pulse doppler radar system designs are studied in detail in Section 3.0. Finally, the integrated radar/communi-cation system considerations are presented in Section 4.0. The primary

integrated system considerations are the combined system block diagrams, the filter requirements for the radar and communication channels, and an angle tracking design which is compatible with the radar signal and a PN spread spectrum communication signal.

2.0 SYSTEM CONSIDERATIONS

2.1 Requirements

The requirements for the rendezvous radar performance are determined primarily by the type of the mission to be accomplished. Table 1 summarizes these requirements.

As can be seen from this table, the most stringent requirements from the standpoint of angular search and the time allowed for the acquisition are those for Mission IIIB. For this mission, the rendezvous phase starts at a relatively short range and hence the time to maneuver to station keeping is limited.

The initial considerations were only for a passive mode for Mission III-B. However, because of the stringent requirements for this mission, the possibility of a cooperative mode for this mission are now being considered. Missions I and II involve the requirement for target acquisition at a maximum range of 560 km and thus they must depend on a cooperative, transponder-aided mode of operation. But, as indicated in Table 1, the acquisition time requirements for these two missions have now been relaxed.

2.2 Passive Target Characteristics

The exact characteristics of all passive targets to be encountered are difficult to predict but some modeling can be helpful in determining the bounds which may be encountered. The specific passive target model which has been analyzed is a two-point target having the following characteristics:

2-point scatterers
Separation = 18 meters (60 feet)
Rotation = 5°/second
Magnitude -- normalized to 1 m^2 Swerling Case I

The analysis of the two-point passive target model is of particular significance for the estimation of amplitude fluctuation (scintillation) and

Table 1. Rendezvous Radar Passive and Cooperative Mode Requirements

Parameter \ Target / Mission	Passive	Cooperative		
	IIIB	(IIIB)	I	II
Range				
Limits	19 km to 30 m	(14.8 km to 30 m)	560 km to 30 m	
Acquisition	19 m	(14.8 km)	560 km	
Accuracy	1% of R or 30 m	←	1% of R or 30 m	→
Bias (3 σ)	24 m	←	24 m	→
Range Rate				
Limits	$\pm$ 91 m/sec (-38 m/sec + 7.5 m/sec)	←	$\pm$ 91 m/sec	- - →
Accuracy (3 σ)	0.3 m/sec	← - - -	0.3 m/sec	→
Bias (3 σ)	0.3 m/sec	←	0.3 m/sec	→
Angle				
Search limits	90° x 90°	(90° x 90°)	10° x 10°	10° x 10°
Accuracy (3 σ)	0.573°	←	0.573°	→
Bias (3 σ)	3° max	←	3° max	→
Angle Rate				
Acquisition (3 σ)	$\pm$ 0.23°/sec	←	$\pm$ 0.23°/sec	→
Track (3 σ)	$\pm$ 5°/sec	($\pm$ 4°/sec)	$\pm$ 5°/sec	$\pm$ 5°/sec
Accuracy (3 σ)	0.008°/sec	←	0.008°/sec	→
Bias (3 σ)	0.008°/sec	←	0.008°/sec	→
Acquisition Time for $P_d = 0.99/P_{fa} = 10^{-8}$	1 min	(2 min max)	1 min ←	→ (Not critical 5 min now)

NOTE: Parameters in brackets ( ) indicate latest modifications or additions.

apparent angular displacement (glint) for the case of an extended target such as an Agena spacecraft. Acquisition reliability, as well as the accuracy of the subsequent range, range rate, and angle tracking, are affected by scintillation and glint.

The analysis of the two-point passive target model is detailed in Appendix A. In this appendix, the resulting radar cross section (RCS) of a two-point target is evaluated from two viewpoints. First, the RCS is evaluated from the point of view of amplitude scintillation with respect to the aspect angle. Second, the resultant movement of the RCS center versus range is determined with respect to the aspect angle and the relative magnitudes (gains) of the two points of the target.

Figure 1 shows the cross section distributions for two-point targets averaged over all aspect angles and normalized for $\bar{\sigma}$ of 1 m^2. The distributions indicate that the probability of a deep fade increases as the magnitude of σ_1 approaches that of σ_2, i.e., $a \rightarrow 1$. This is to be expected, because when the two contributing cross sections of a two-point target are equal they can, at certain aspect angles, cause a destructive interference which will make the combined return vanish. For the purpose of comparison, the cumulative probability of Swerling I mode with $\bar{\sigma}$ = 1 m^2 is also shown in Figure 1. It can be seen that the Swerling I amplitude scintillation model differs from that of the two-point target. Specifically, the Swerling I model is more pessimistic than that of the two-point target because it places more probability at smaller values of σ. One can conclude, therefore, that the Swerling I model is satisfactory for representing amplitude scintillations of most targets to be encountered during Orbiter rendezvous.

Target phase variation over signal bandwidth for a two-point target is shown by the curves of Figure 2. The parameter b in this case represents the relative amplitudes of the two targets and t_0 is the two-way time delay of the farther element with respect to the nearer element along the line of sight (LOS). From the phase shift curves, it is evident that for small and large values of b the slope of the phase is relatively constant

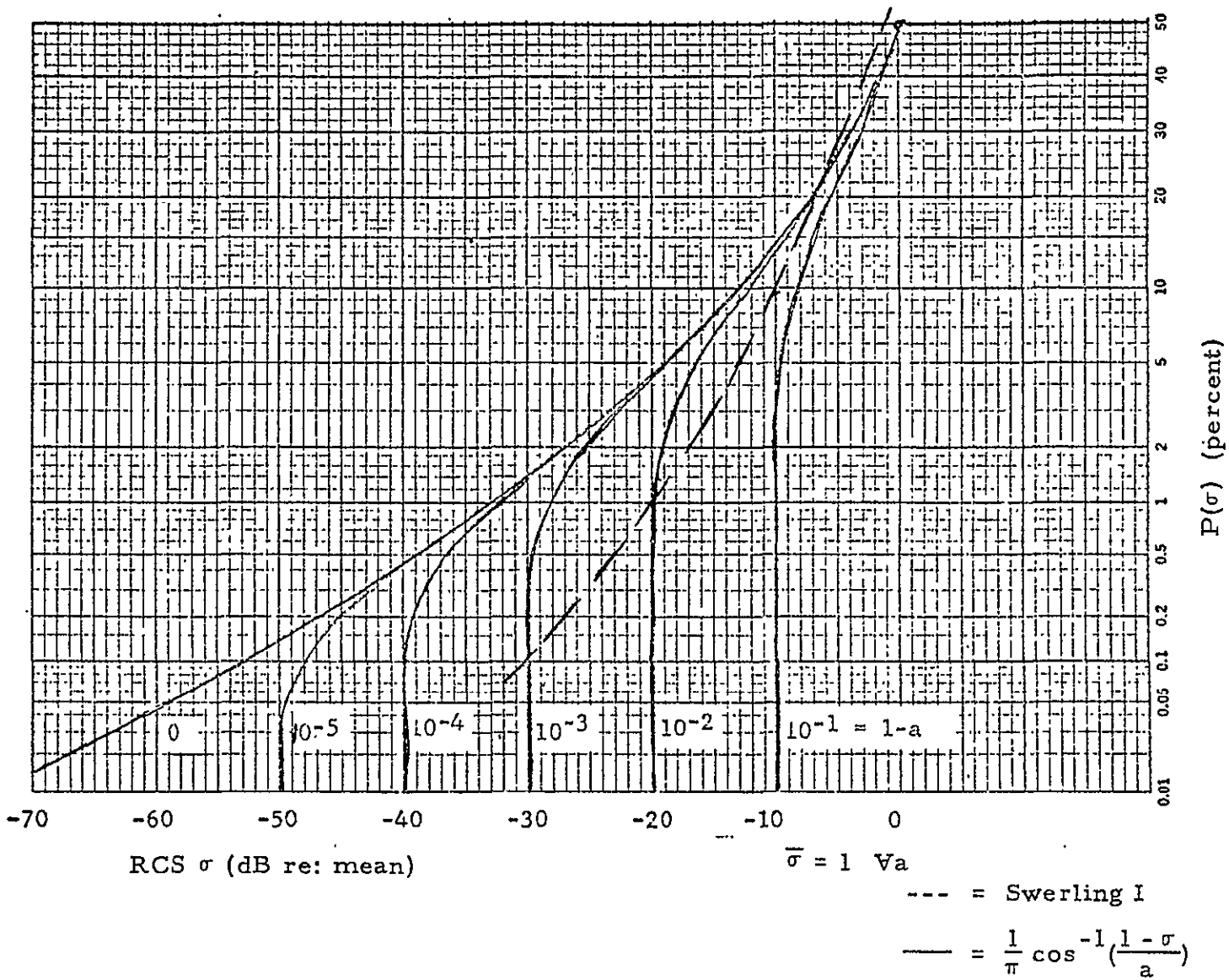

Figure 1. Cross Section Distribution for Two-Point Target

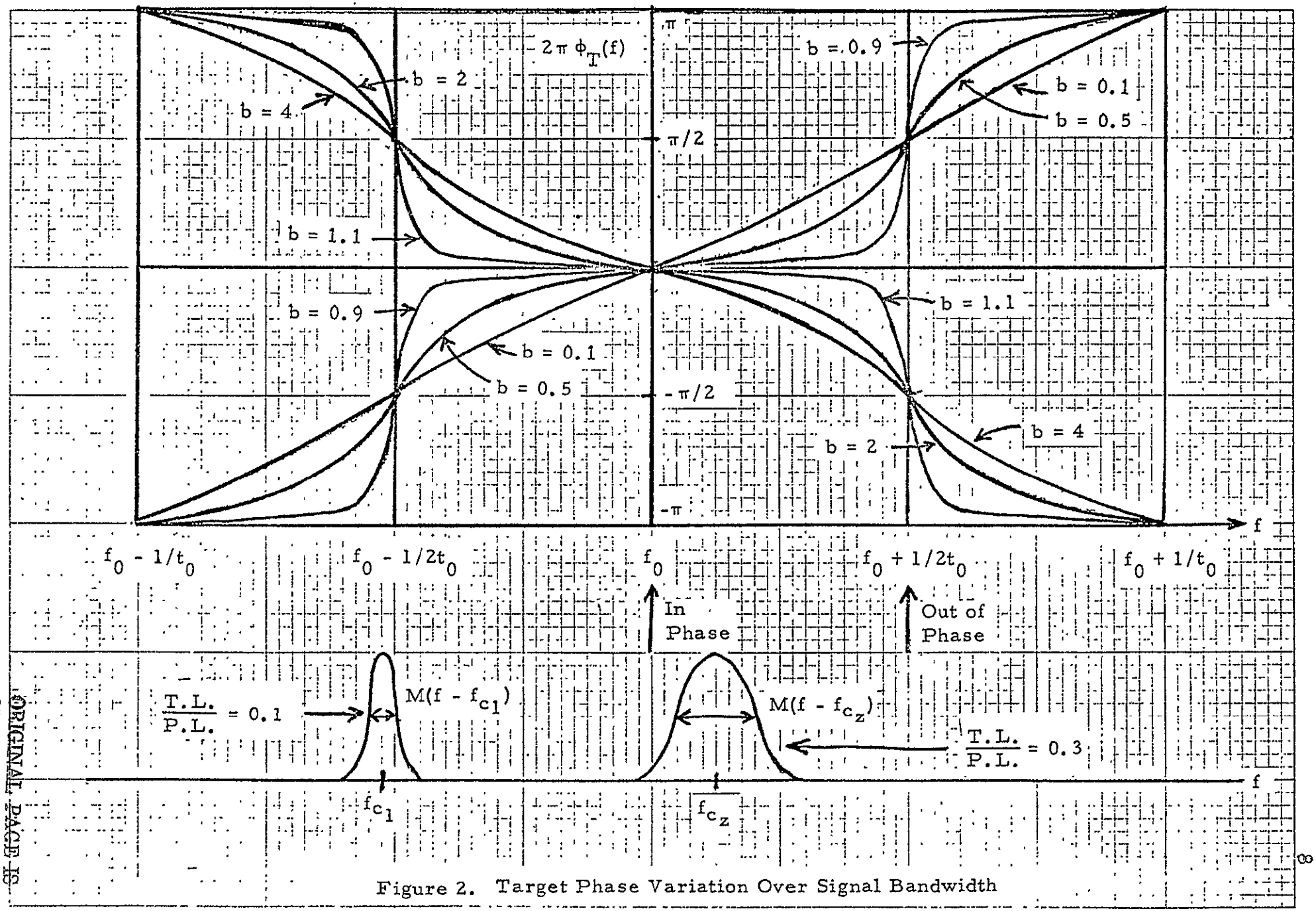

Figure 2. Target Phase Variation Over Signal Bandwidth

and therefore the radar return experiences a time shift but only relatively small envelope delay distribution.

Considering a specific example of an 18 meter target and the two points of the target colinear with the LOS (maximum t_0) the value of $1/t_0$ is 8.33 MHz. Thus, we see that if the signal frequency lies in the center region of the phase curve, i.e., between $f_0 - 1/2t_0$ and $f_0 + 1/2t_0$, a relatively wide band signal (say, 10 MHz wide) can be reflected with little envelope distortion even for values of b close to unity. In comparison, if the signal is centered at the frequencies where the phase curve experiences a maximum of phase change, considerable envelope delay distortion may take place when b is close to unity unless the signal bandwidth is narrow compared to $1/t_0$. The relative bandwidth of such "narrow-band" signals can be expressed in terms of the ratio of target length (TL) to pulse length (PL). Examples of such narrowband signals are also shown in Figure 2 for TL/PL ratios of 0.1 and 0.3.

Because the slope of the phase curve shown in Figure 2 corresponds to an apparent time delay, i.e., a range error, the radar returns from narrowband targets will experience a relative displacement in range as the function of the operating frequency and the relative amplitude ratio b. This range error is shown in Figure 3 as the function of b and $\omega_c t_0$. The significance of the curves in Figure 3 is that there are many cases where the indicated target range is well outside the physical extent of the target.

Thus, in the narrowband case, the area under the radar video pulse envelope is shifted in time and an early-late gate tracker will follow this shift. Similarly, an FM-CW ranging system, which measures range by the phase shift of the received FM modulation, will observe an erroneous time shift of the modulation.

The results shown in Figures 2 and 3 clearly demonstrate the advantages to be gained by use of frequency agility. For example, each new RF frequency will have an effect of choosing a point randomly between 0° and 360° in Figure 3. If a sufficient number of RF frequencies are employed

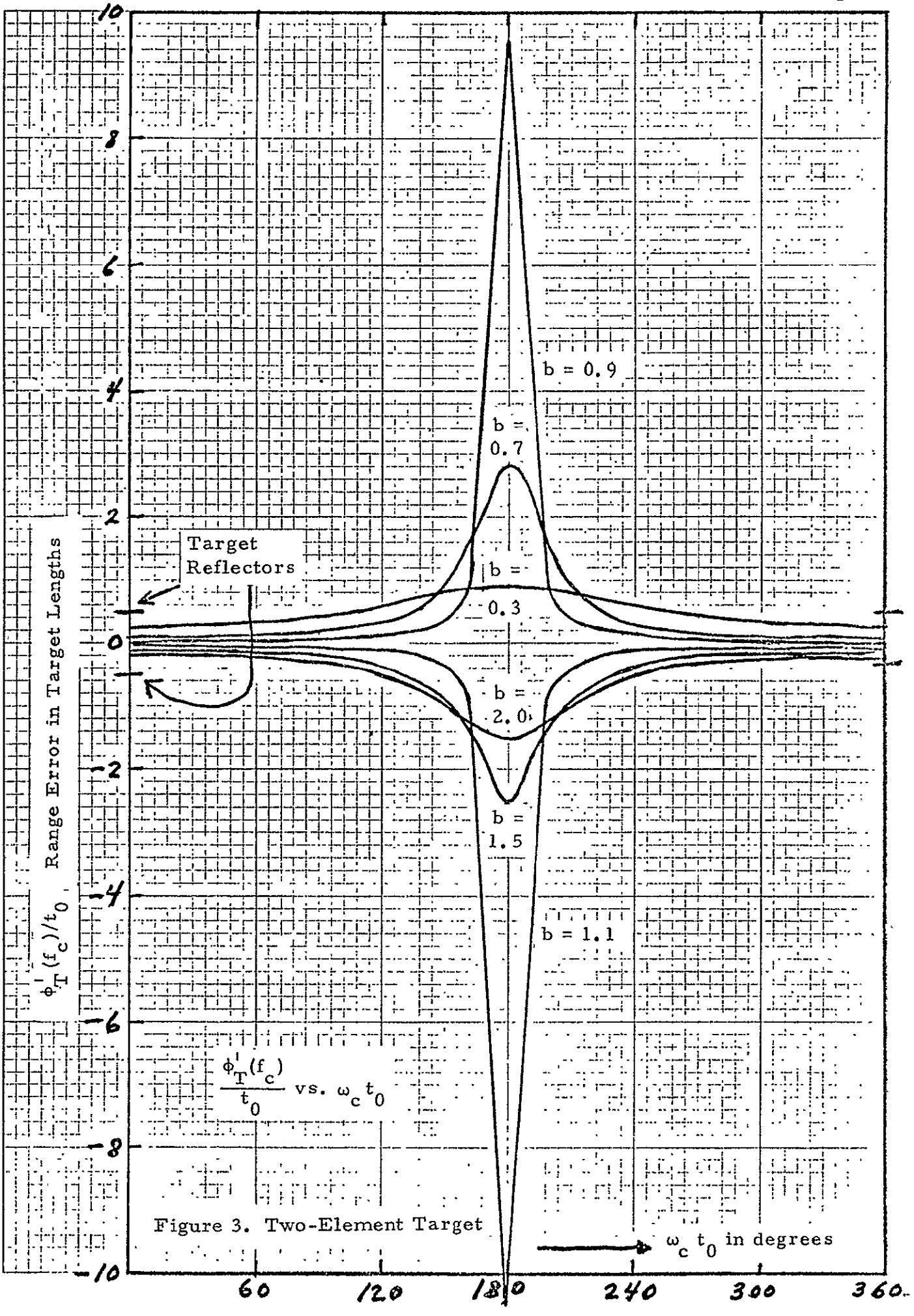

Figure 3. Two-Element Target

(say, 5 to 7), the resulting range error would be approximately the average value of the function shown in Figure 3.

The effect of frequency diversity on reducing the average value of range error, $E_c(t)$, and its variance about the mean is illustrated by the numbers in Table 2. For example, with b = 0.9, the maximum range error, as shown in Figure 3, is 9.5 target lengths, whereas the average error with a frequency diversity is only 1.11 times the target length. For an 18 meter target, typical frequency diversity shifts should be at least as large as $1/t_0$ ($\approx$ 10 MHz) to perform good averaging of curves in Figure 3, as well as to provide independent amplitude returns to reduce the effects of amplitude scintillation.

The results of the two-point target study indicate that such a target has more than sufficient versatility to model most ranging errors induced by target characteristics. Furthermore, the two-point target model permits modeling targets whose standard deviation in target position is either greater or smaller than the 0.35 L (L = target length) empirically derived value quoted on page 170 of Barton and Ward's Handbook of Radar Measurements. Consequently, we can proceed with applying the results of the two-point target analysis towards determining the ranging accuracy of the various candidate radar schemes.

2.3 Active Transponder Characteristics

In addition to the detection and tracking of the noncooperative, passive targets, certain Shuttle missions required acquisition and tracking of targets equipped with active, cooperative transponders. When in the cooperative mode the radar sensor must be able to acquire the targets at a maximum range of up to approximately 560 km (300 nmi). Although in general the cooperative mode alleviates many of the complications associated with the passive mode, such as excessive target scintillation and glint, and it also provides for reduction of the average power radiated by the sensor, the cooperative mode generates a requirement for radar/transponder compatibility. This requirement demands special consideration, particularly for

Table 2. Average and Standard Deviation Range Errors of a Two-Point Target Illuminated by a Frequency Diversity Signal

Relative Magnitude b	Average Range Error $E[t_e]^*$	RMS Range Error σ^*
0.1	0.50	0.074
0.3	0.51	0.24
0.5	0.53	0.45
0.7	0.59	0.83
0.9	1.01	2.70
1.1	-1.09	2.99
1.5	-0.57	0.74
2.0	-0.53	0.45
4.0	-0.51	0.19

*Values are in terms of target length.

the radars which have to operate in either one of the two modes.

When considering a beacon design, simplicity is of primary concern. Modulation used by the radar, however, places a bound on the simplicity of the system.

With a system which uses coherent tracking of the beacon return, such as pulse doppler or a tone ranging system, the beacon transmission takes place simultaneously with the reception of the radar signal. Thus, to prevent the transponder from going into oscillation, i.e., locking onto its own transmitter, a high degree of transmitter/receiver isolation is required. The most common method of providing such isolation, particularly with transponders which use a single* antenna, is to offset the beacon transmit frequency from the radar frequency by a certain amount, which is typically equal to the radar IF. Such offset not only provides for transmitter/receiver isolation at the beacon, but also permits a portion of the radar transmitter signal to be used as a local oscillator of the radar receiver. It must also be pointed out that a frequency offset in the beacon allows the radar receiver to discriminate between the skin return and the transponder reply. Generic configurations for a frequency offset radar and a transponder are shown in Figure 4.

With radar systems which utilize a low duty cycle, the transmission of the beacon RF pulse may be delayed until the reception of the interrogating pulse is terminated. This, in principle, may permit a single antenna beacon to reply at the radar transmit frequency but the receiver turn-off must be extremely good to prevent self-triggering and this implies complication of the beacon receiver design.

Figure 5 shows a block diagram for a single-frequency, coherent-pulse transponder. The salient features of such a transponder are also listed.

---

*Using separate antennas for transmitter and receiver requires physical antenna separation which may not be available on small satellites. For example, at 15 GHz isolation between two isotropic antennas separated by 1 meter is only 56 dB.

Figure 4. Frequency Offset Radar/Transponder

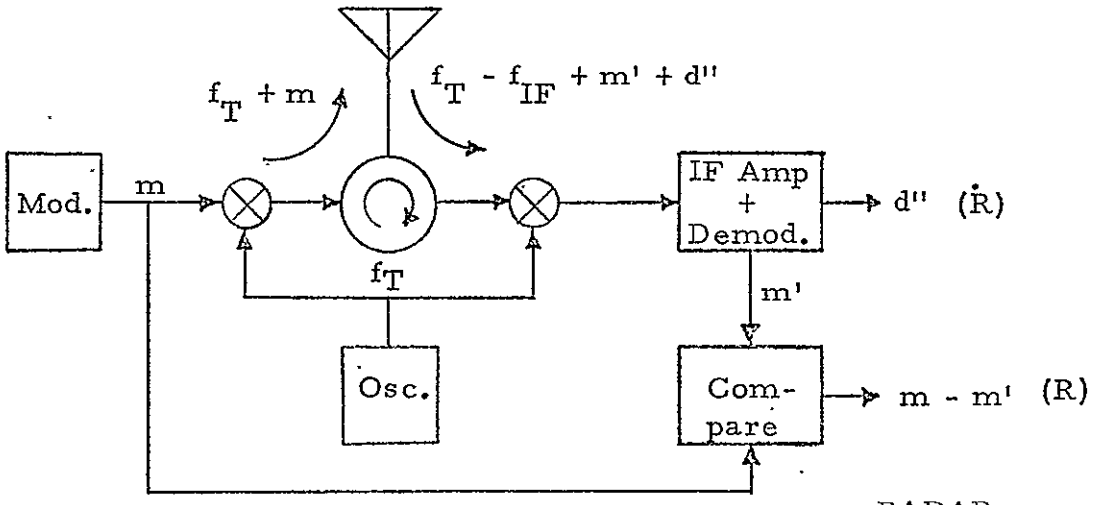

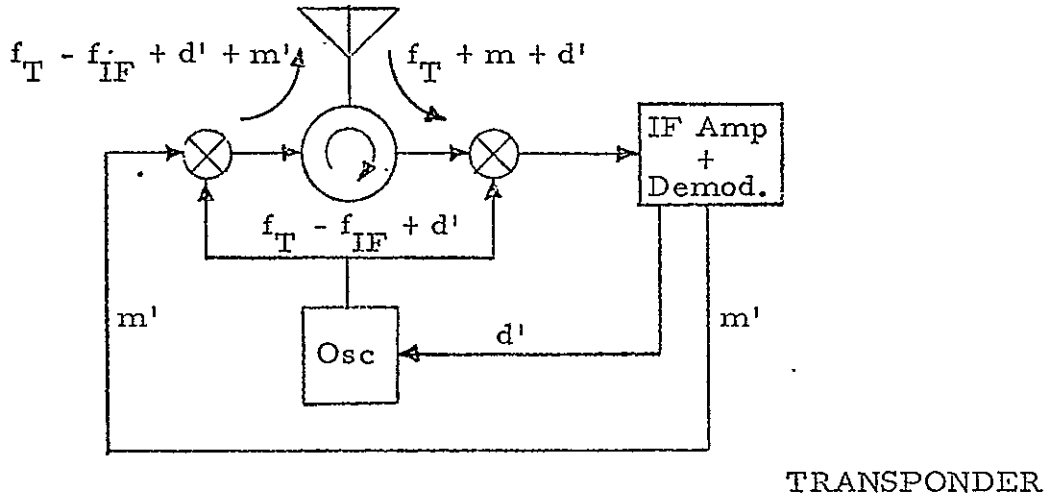

ADVANTAGES:

GOOD T_X/R_X ISOLATION

PROVEN TECHNIQUES

DISADVANTAGES:

COMPLEXITY

REQUIRES DELAY CALIBRATION AND CONTROL

(BIAS CONSIDERATIONS)

Figure 5. Single Frequency Coherent Pulse Transponder

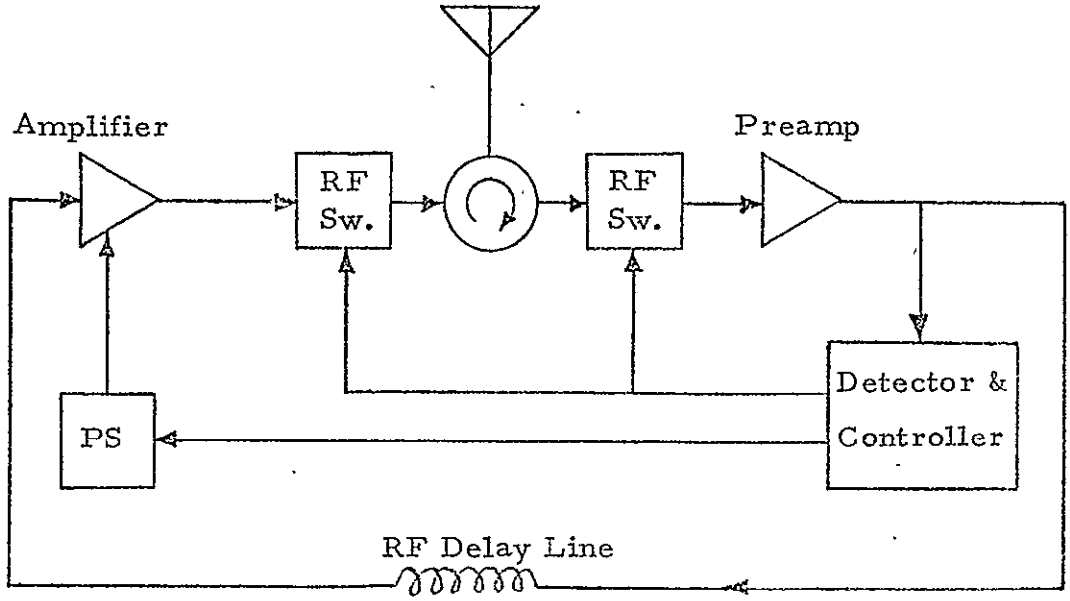

ADVANTAGES:

SINGLE FREQUENCY

SINGLE ANTENNA

COHERENT REPLY

DISADVANTAGES:

RELATIVE COMPLEXITY

DELAY LINE LIMITS PULSE DURATION

BULKY -- IF WG OR CABLE

LOSSY -- IF ACOUSTIC

REQUIRES DELAY CALIBRATION AND CONTROL

(BIAS CONSIDERATIONS)

REQUIRES GOOD SWITCHING

(FAST, HIGH ISOLATION, LOW INSERTION LOSS)

Another important factor which must be taken into account when considering operation with a cooperative transponder is the polarization alignment between the radar and transponder antennas. Because the physical alignment between the radar system and the transponder is random and it also varies with time, a circular polarization would be the best choice for both antennas. However, for best radar operation with passive targets, a linear polarization is indicated. Providing a dual polarization for the radar antenna complicates system design, particularly if one considers the requirement for a two-axis monopulse feed. Thus, a compromise solution, which is achieved at a nominal penalty of 3 dB in the cooperative mode, is to use linear polarization for the radar and circular polarization for the transponder antenna. The main advantage of this approach is the minimum complexity of the radar antenna.

The current emphasis on the integrated radar/communication system may provide the optimum polarization for the cooperative mode. Specifically, because the communication mode requires circular polarization, an antenna with a switchable feed is envisioned (linear/circular). Thus, when in the cooperative mode, the integrated system may take advantage of the available circular polarization.

2.4 Potential Candidate Systems

One of the initial tasks of this study was to provide block diagrams for several potential candidate radar systems and the associated transponders. The purpose of this task was to provide a basis for a qualitative assessment of the complexity of each candidate system and the subsequent quantitative analysis of the most likely candidates. The candidate systems to consider are:

1. Pulse radar
2. Pulse doppler radar for nonambiguous $\dot{R}$ determination
3. Pulse doppler radar with tone ranging
4. Pulse doppler radar with linear/stepped FM (chirp).

Block diagrams of the radar and the corresponding transponder for each of these candidate systems are presented in the following figures. Preceding each set of system block diagrams is a table that describes the block diagrams pointing out the salient features and the advantages and disadvantages of each candidate system.

2.5 Frequency Considerations

If the radar function is to be considered separately from the communication mode, the operating frequency may be anywhere from C to Ku band (i.e., 5 to 35 GHz), or even within a wider frequency span. Practical considerations, however, may limit the frequency selection to a narrow region, particularly if an integrated radar/communication system is to be taken as the ultimate goal. Thus, the baseline operating frequency for systems currently under consideration is 15 GHz. However, tradeoffs associated with operating at other frequencies are discussed in Appendix K.

Table 3. Pulse Radar System

RADAR

- FREQUENCY AGILITY FOR PASSIVE MODE
- FIXED FREQUENCY FOR COOPERATIVE MODE
- RANGE DERIVED BY SPLIT-GATE TRACKER
- RANGE RATE DERIVED FROM RANGE TRACKER
- ACCELEROMETER MAY BE USED TO AID RANGE RATE TRACKING
- POWER CONTROL AND T/R SWITCHING -- A PROBLEM AREA AT SHORT RANGES

TRANSPONDER

- RETURN FREQUENCY OFFSET PROVIDES DISCRIMINATION BETWEEN SKIN AND BEACON RETURNS AND IMPROVES TRANSMITTER/RECEIVER ISOLATION
- GOOD FREQUENCY STABILITY IS REQUIRED FOR TRANSPONDER TRANSMITTER AND LO TO MINIMIZE FREQUENCY UNCERTAINTIES, BUT COHERENCY IS NOT REQUIRED FOR $\dot{R}$ MEASUREMENT
- INTERROGATOR PRF AND PULSE WIDTH CHECKED PRIOR TO TRANSMISSION TO MINIMIZE FALSE RESPONSES

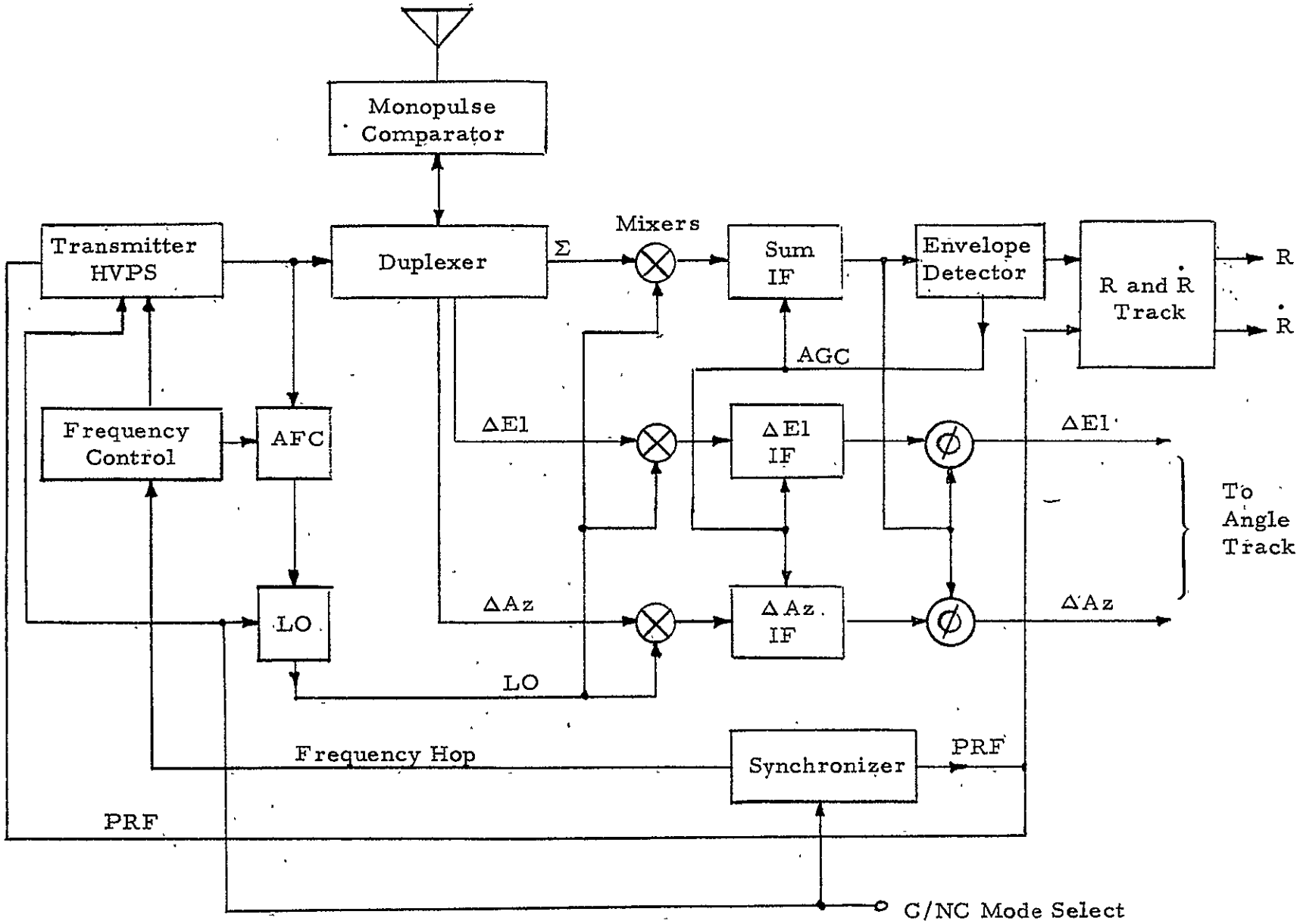

Figure 6. Pulse Radar Simplified Block Diagram

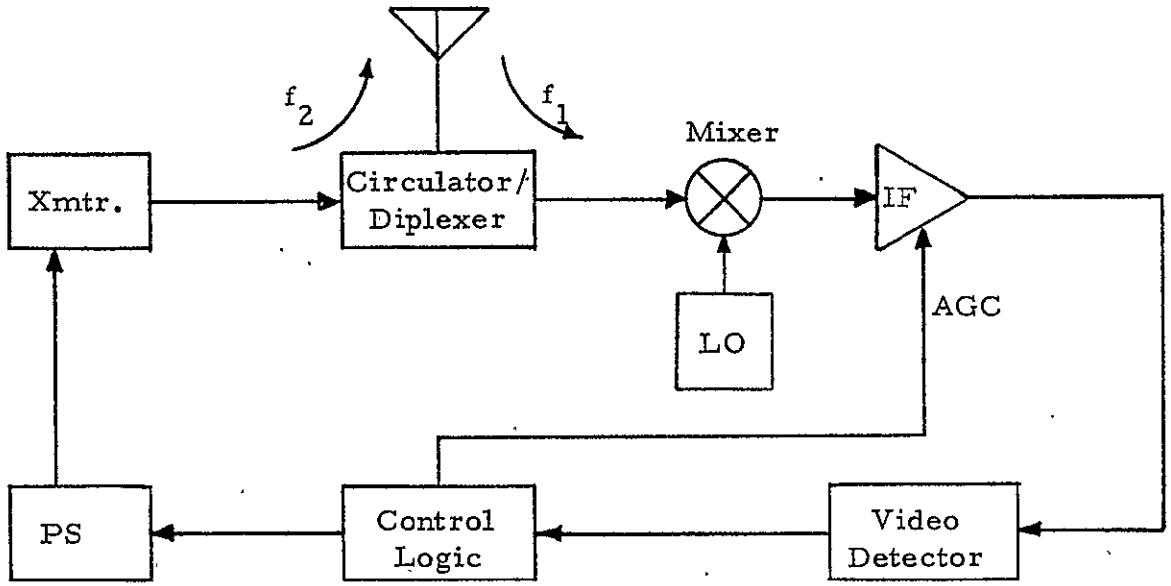

Figure 7. Pulse Radar Transponder Simplified Block Diagram

Table 4. Pulse Doppler Radar

RADAR

PASSIVE MODE

- NONAMBIGUOUS VELOCITY DETERMINATION WITH HIGH PRF
- PRF(S) SELECTED TO MINIMIZE ECLIPSING LOSS. MAY BE SWITCHED AFTER ACQUISITION
- HIGH DUTY CYCLE DURING ACQUISITION. MAY BE LOWERED AFTER ACQUISITION
- DOPPLER SHIFT PROVIDES RANGE RATE
- FREQUENCY DIVERSITY REQUIRED

COOPERATIVE MODE

- SAME AS PASSIVE MODE, EXCEPT FREQUENCY DIVERSITY NOT REQUIRED

TRANSPONDER

- PROVIDES COHERENT RETURN AT FREQUENCY OFFSET EQUAL TO RADAR IF
- TRANSPONDER PLL INSURES FREQUENCY STABILITY OF THE RETURN
- RETURN PULSE DURATION DETERMINED BY RECEIVED PULSES

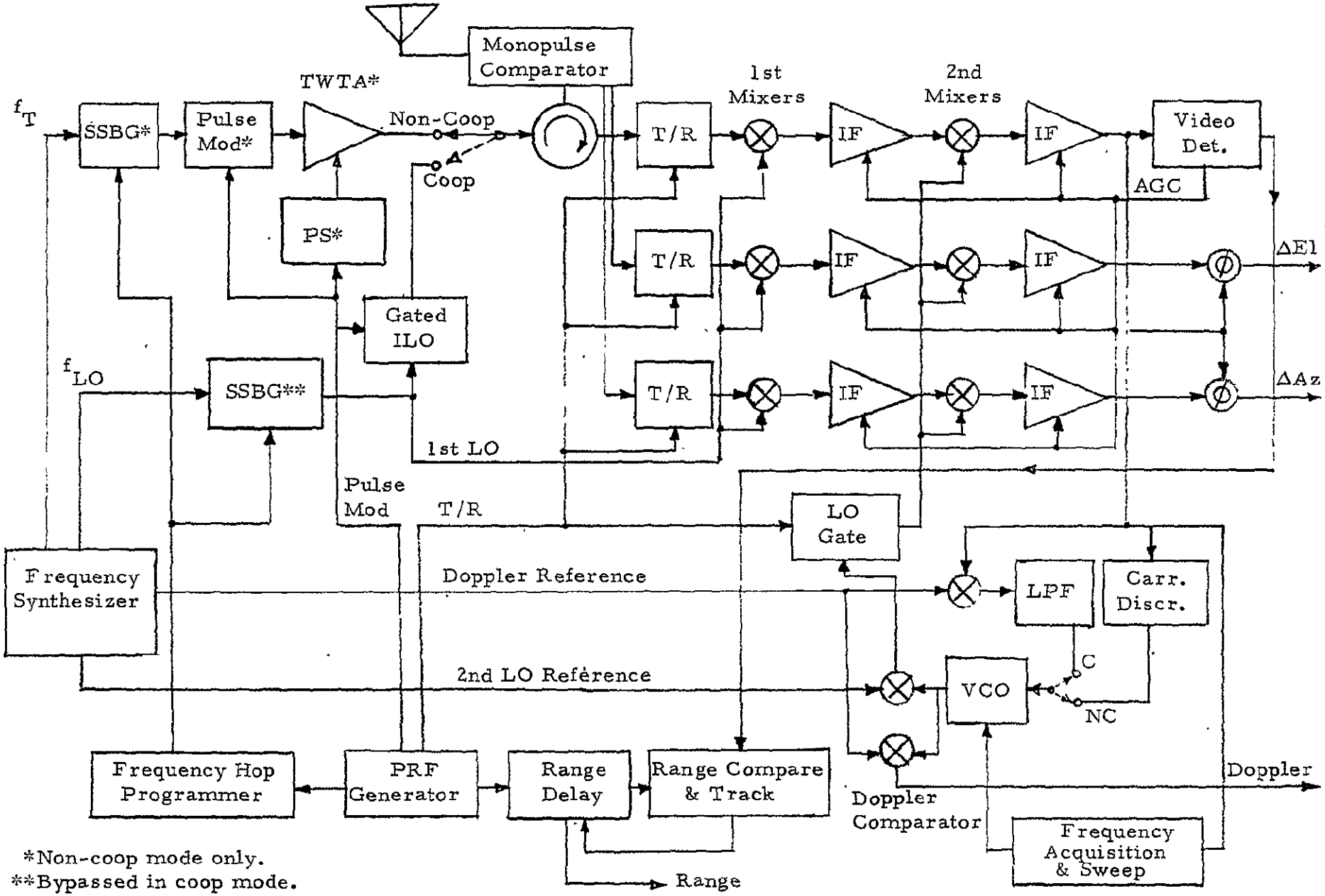

Figure 8. Pulse Doppler Radar (Nonambiguous Velocity Determination, Chinese Remainder Theorem, Pulsed Track Range)

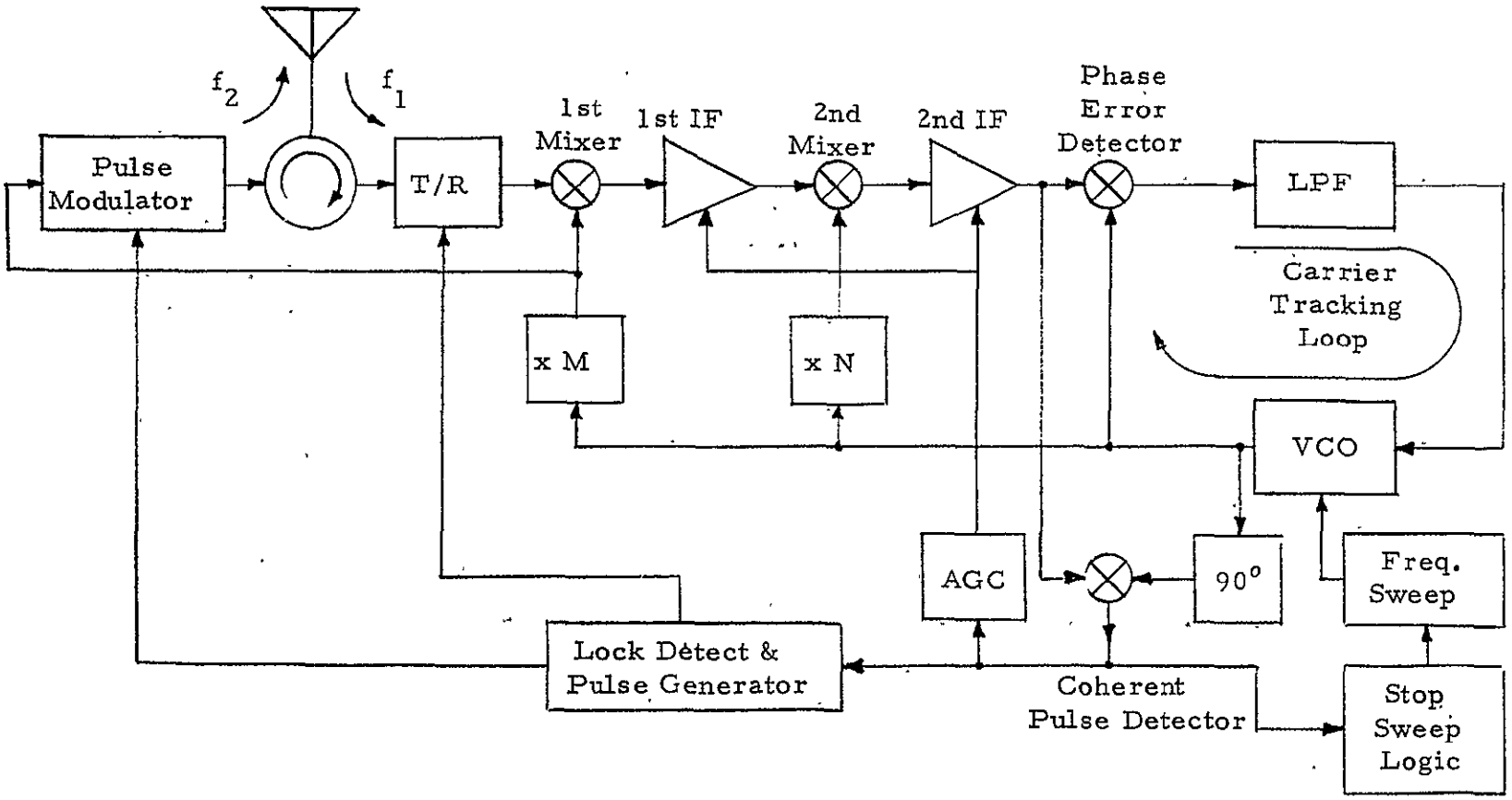

Figure 9. Pulse Doppler Radar Transponder Block Diagram (Coherent Operation)

Table 5. Pulse Doppler With Tone Ranging

RADAR

PASSIVE MODE

- PULSED OPERATION
- MULTIPLE PRF, HIGH DUTY CYCLE
- FREQUENCY DIVERSITY
- CENTER LINE TARGET ACQUISITION
- TONE MODULATION PROVIDES RANGE TRACKING
- DOPPLER SHIFT PROVIDES RANGE RATE

COOPERATIVE MODE

- CW OPERATION
- TONES MODULATION PROVIDES RANGE TRACKING
- DOPPLER SHIFT PROVIDES RANGE RATE
- FREQUENCY DIVERSITY NOT REQUIRED

TRANSPONDER

- PROVIDES COHERENT RETURN OF FREQUENCY OFFSET EQUAL TO RADAR IF
- TRANSPONDER PLL INSURES FREQUENCY STABILITY OF THE RETURN
- RANGING TONES ARE DEMODULATED AND RETRANSMITTED

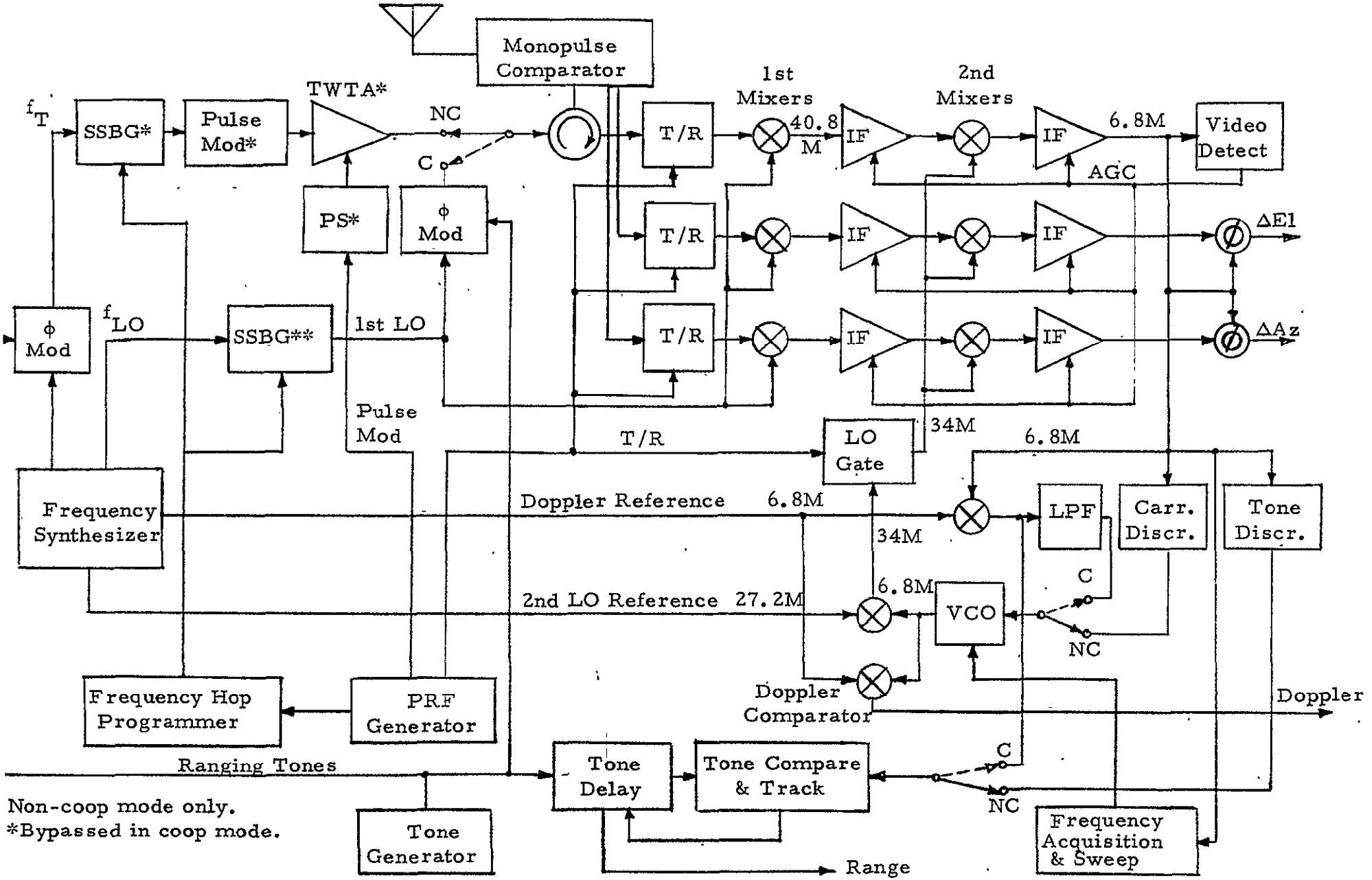

Figure 10. Pulse Doppler Radar with Tone Ranging (CW Track)

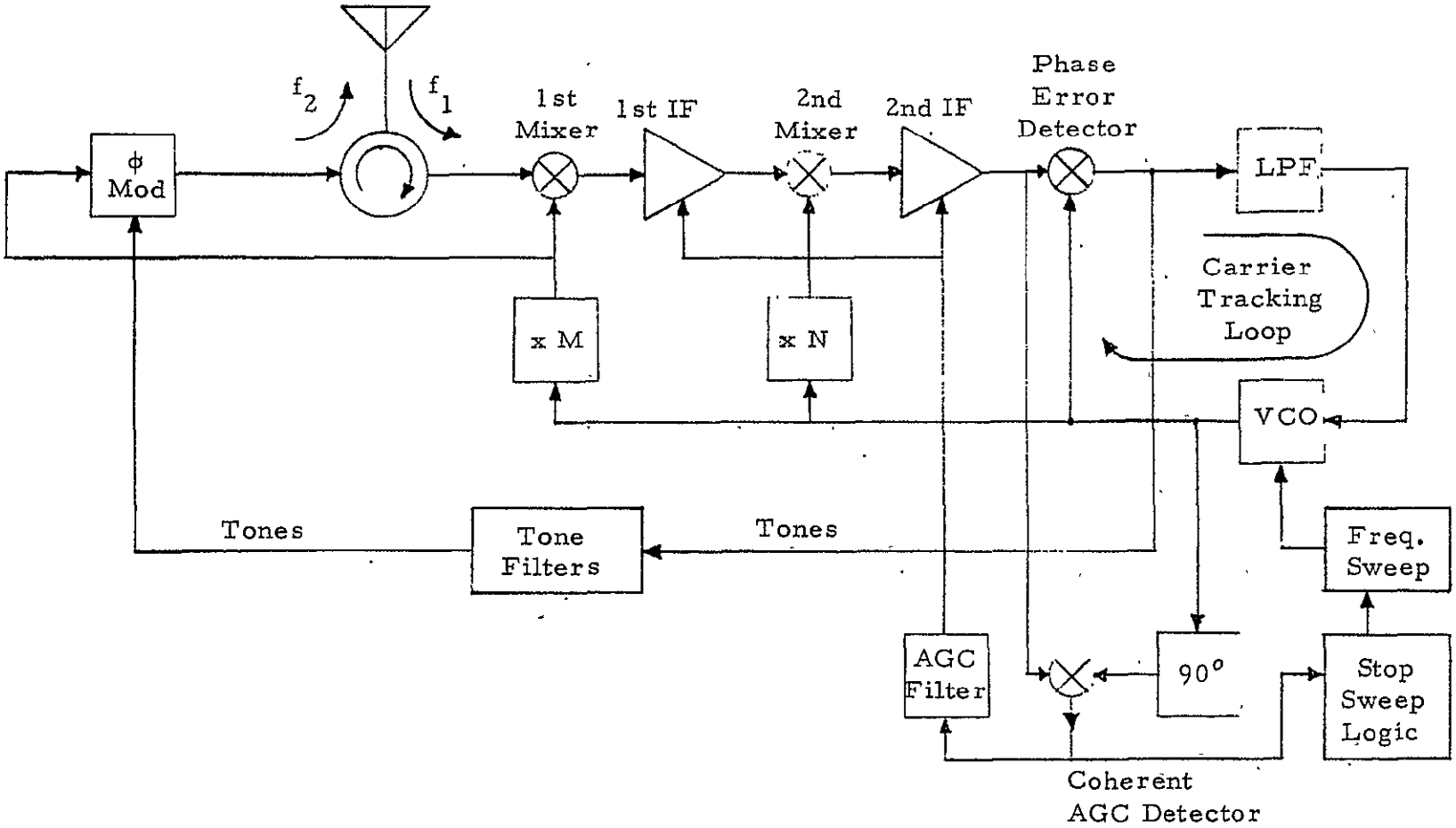

Figure 11. Tone Ranging Transponder Block Diagram (Coherent CW Operation)

Table 6. Linear FM (Chirp) or Stepped FM Pulse Radar

RADAR

- PROVIDES GOOD RANGE RESOLUTION WITH PEAK POWERS LOWER THAN CONVENTIONAL PULSE RADAR
- FREQUENCY WITHIN THE PULSE CHANGED EITHER LINEARLY OR IN STEPS
- FREQUENCY SPREAD DETERMINES RANGE RESOLUTION
- THREE CHANNEL COMPRESSION AND EQUALIZATION NETWORK REQUIRED FOR RADAR RECEIVER
- RANGE SIDELOBE CONTROL REQUIRED

TRANSPONDER

- RECEIVED PULSE RETRANSMITTAL WITHOUT ENVELOPE DETECTION
- RETRANSMISSION IS AT AN OFFSET FREQUENCY. THIS PROVIDES:
    - A) USE OF A SINGLE ANTENNA
    - B) SIMULTANEOUS RECEPTION AND TRANSMISSION
    - C) DISCRIMINATION AGAINST SKIN RETURN

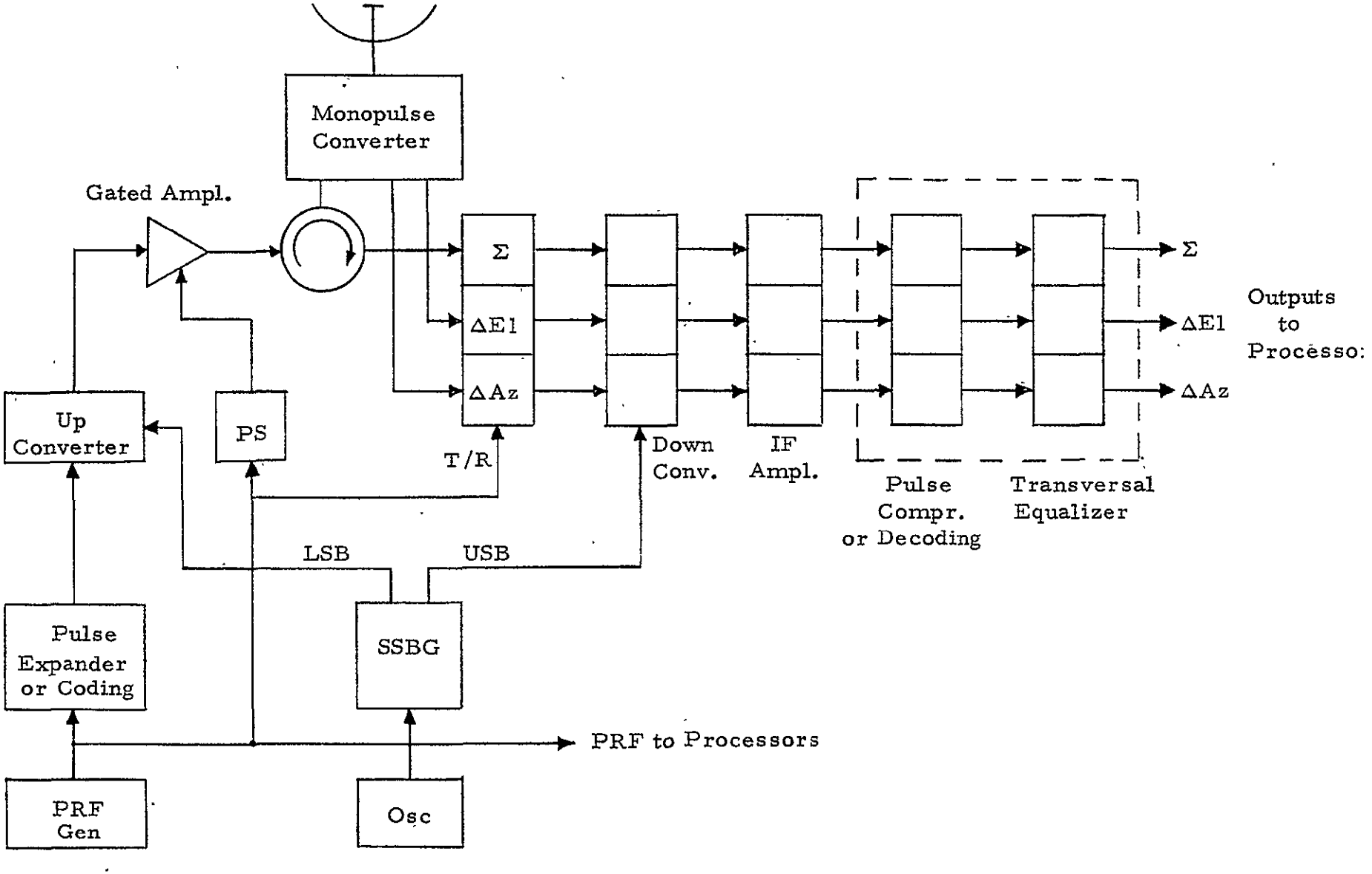

Figure 12. Three-Channel Monopulse Pulse Compression Radar (Generic Block Diagram)

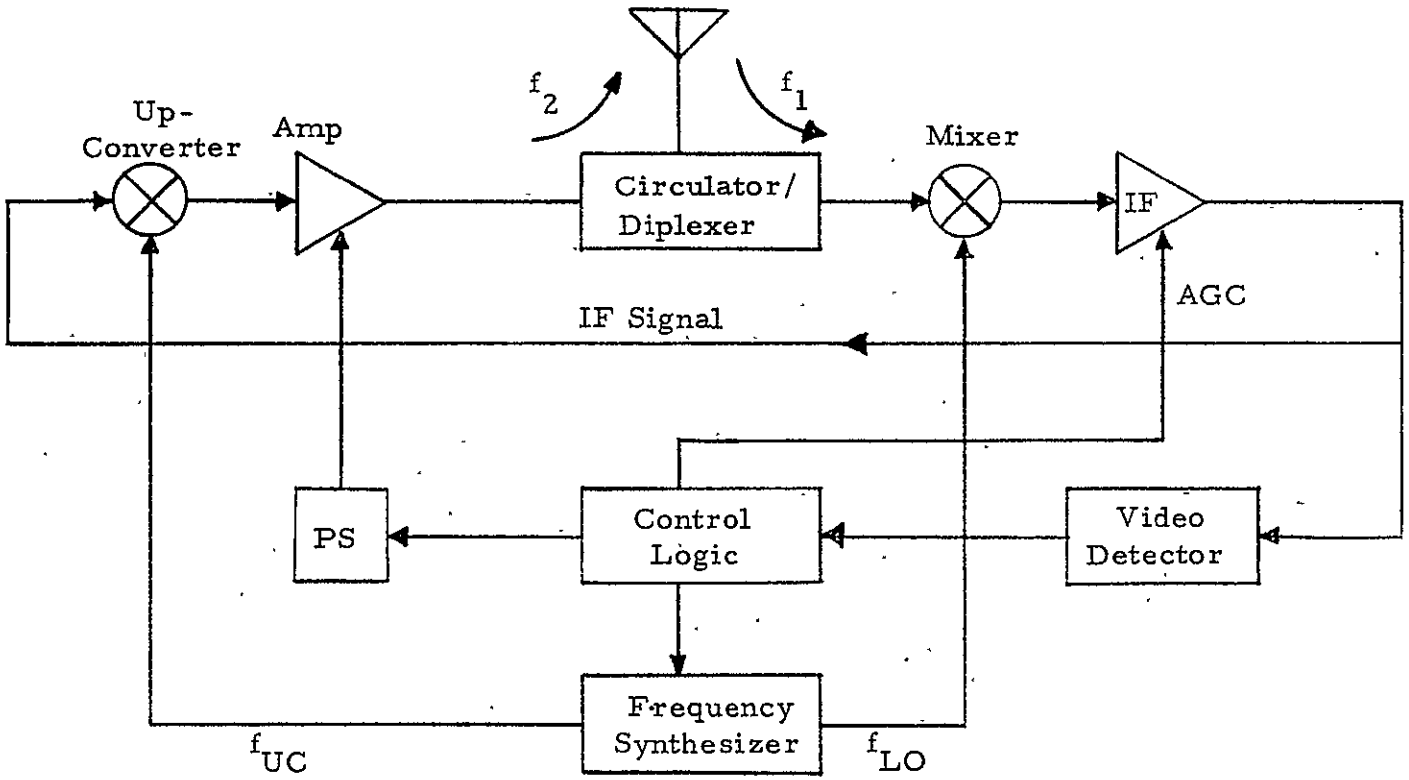

Figure 13. Linear (Chirp) or Stepped FM Pulse Radar Transponder

3.0 SPECIFIC CANDIDATE SYSTEMS

Out of the four candidate systems listed in the preceding section, the major effort was concentrated on the consideration of the pulse and the pulse doppler systems.

3.1 Pulse Radar System

The pulse radar system operates in a manner similar to an airborne-intercept (AI) radar. A high peak power, low duty cycle, noncoherent magnetron transmitter is used and a three-channel monopulse receiver provides signal detection and two-axis target tracking. The effects of the target cross section variations are reduced by employing frequency agility in the transmitter. Range is measured by a split-gate tracker, or equivalent, and the range rate is determined by differentiating the range.

Figure 6, in the preceding section, shows the simplified block diagram of the pulse radar system. The amplitude type monopulse converter provides three outputs, each applied to its own receiver channel. The outputs are, respectively, the sum (Σ), the elevation difference (ΔEl), and the azimuth difference (ΔAz). The sum channel provides both the AGC and the phase reference for the difference channels. The ΔAz and ΔEl receiver outputs are applied to the antenna steering servo loops which, for the purpose of simplicity, have been omitted from the block diagram.

The frequency diversity required for the noncooperative mode is provided by a frequency-agile magnetron. The selection of the magnetron tuning mechanism is an important factor because the automatic frequency control (AFC) usually operates over a limited range of frequency shifts and is generally designed to take care only of long-term frequency drifts. Thus, the device which frequency-tunes the magnetron must provide a signal which is related to the instantaneous frequency of the magnetron so that this signal can be used for supplying the first-order frequency correction to the AFC circuit. The residual frequency discrepancy at each transmitted frequency is then corrected by the AFC.

The typical parameters which have been baselined for the pulse radar in the noncooperative mode, skin tracking mode, are as follows:

Pulse Repetition Frequency (PRF)	2500 pps
Pulse Width	0.4 μsec
Duty Cycle	0.001
Peak Power	40 kw
Average Power	40 w
Frequency Diversity Spread	250 MHz (wider spreads are being considered)
Noise Figures	8 dB
System Losses	6-7 dB

These parameters, particularly the peak power level and pulse widths, are baselined to provide passive track target track initiation at a range of 19 km (10 nmi) with probability of detection of 0.99 and false alarm probability of 10^{-8}.

Additional considerations of pulse radar performance are given in Appendixes B, C, and D. In Appendix B the pulse radar is compared to a pulse doppler radar and it is shown that for the same acquisition performance the pulse radar requires higher average power as does the pulse doppler radar. Although Appendix C deals primarily with pulse doppler in the cooperative mode, some general considerations which apply to both modes are included. Specifically, a method for power control and short ranges is described. This method involves the use of two switches--one on electrically actuated, remotely controlled waveguide switch and the other a solid state, low power, "fast" switch. The proposed configuration for this switching is shown in Figure 3 of Appendix C. In part (a) of Figure 3 the waveguide switch is in the position which allows the full transmitter power to be delivered to the diplexer.

Because the power delivered to the diplexer in this case is about 40 kw, a conventional gas-type T/R provides the function of receiver isolation during the transmission. At short ranges, the full power is not

required and thus the microwave switch is placed into the position shown in part (b) of Figure 3. In this position the full power of the transmitter is delivered to a dummy load and thus the operation of the magnetron is not affected. A portion of the transmitter power is tapped by a coupler and delivered via a solid state switch to the duplexer. The duration of the transmitted pulse can thus be made as narrow as desired by gating on to the duplexer only a short segment of the magnetron's RF pulse output. Because the power level used in this mode may not be sufficient to trigger the T/R switch, a solid state switch may be used at the receiver input.

The operation of the two switches is then synchronized to provide the T/R function. Because the solid state switches are free of transients and have fast switching speeds (down to a few nanoseconds), a short pulse, reduced power operation can be provided with this technique at ranges down to the stationkeeping range of 30 meters.

In Appendix D the performance capability of various optional filters is determined for estimating range-rate from range measurements in a noncoherent pulse radar. The particular filters are the variable optimal $(\alpha_n, \beta_n, \gamma_n)$ filter for a second-order system and the variable optimal (α_n, β_n) filter for the first-order system. The range measurements are assumed to result from a split-gate tracker. At first the calculations were carried out using the assumption that the 3σ range measurement error at 10 nmi is 1% of the range, which implies σ_m (range) of approximately 200 feet. It is shown that, for this assumption, the performance of the optimal range-rate tracker does not meet the system specification of $\sigma_{\dot{R}} \leq 1/3$ ft/sec within 2 seconds smoothing time. The required smoothing times at 10 nmi for $\sigma_{\dot{R}} \leq 1/3$ ft/sec are 30.5 seconds for the second-order system and 12.1 seconds for the first-order system. It is also shown that, to meet the range-rate specifications for the Shuttle radar with a noncoherent pulse system, the range rate accuracy must be such that σ_m is less than approximately 14 feet for a first-order system.

Thus, an initial understanding has been obtained about the capability of noncoherent radar to track range rate. In many respects, the analysis of estimation of range rate for noncoherent radar as carried out in Appendix D was done so under relatively ideal conditions. For example, no target noise was taken into account, and no transient effects of the split-gate range tracker were accounted for as the result of target maneuverability.

On the other hand, however, the advantages that can be gained by the use of on-board-the-Shuttle accelerometers also have not been taken into account. This may provide a substantial improvement in performance, particularly in view of the fact that the primary limiting condition is the required smoothing times at 10 nmi in order to meet system specifications on range rate estimation.

In the cooperative mode, the pulse radar operates with a transponder whose simplified block diagram is shown in Figure 7. Because in this mode the transponder has to be acquired and tracked at a range of up to 560 km (300 nmi), the PRF of the radar is reduced to 250 pps which provides an unambiguous range of up to 600 km. The pulse width of the radar is also increased to a value which is from 1 to 4 microseconds. The frequency diversity, however, is not required and the radar transmitter frequency is set at a fixed value.

As shown in the block diagram, the transponder employs a super-heterodyne receiver to amplify and detect the Shuttle's radar signals. As the radar antenna beam illuminates the transponder's antenna, the detected radar pulses are applied to the control logic. When the level of the received signals exceeds a preset threshold, the logic circuitry verifies the PRF and the approximate pulse duration of the received signal and initiates the pulsing of the reply transmitter. The frequency of this transmitter is offset from that of the received radar signal by a fixed amount. Such offset provides for a better transmitter/receiver isolation within the transponder and thus alleviates the problem of self-triggering which could arise if the transponder were to reply directly at the frequency of the

interrogating radar. Also, at close ranges such frequency offset provides for discrimination between the skin and the transponded reply. The detailed description of the pulse doppler transponder, including the link budgets, is contained in Appendix C.

3.2 Pulse Doppler System

The salient feature of a pulse doppler radar system is an inherent capability to provide simultaneous measurements of range and range rate, with the particular advantage over the pulse radar being the accuracy of the range rate estimation. The latter feature is achieved by using a relatively high duty cycle, approximately 0.1 to 0.5, as compared to a typical duty cycle of 0.001 for the pulse radar. The high duty cycle, in conjunction with coherent transmission and reception, allows one to measure the doppler shift of the center line of the pulsed carrier. The doppler shift is then converted directly into the measure of the range rate. Pulse envelope information is used to determine the range. With proper selection of system parameters, such as the pulse repetition rate (PRF), the pulse width and the duty cycle, nonambiguous and relatively accurate measurement of both the range and range rate can be performed. The detailed description of the pulse doppler radar operations is contained in Appendixes B, E, and F.

In Appendix B the optimization of a Ku-band radar is performed with an emphasis on the integrated radar/communication system. It is shown that the coherent pulse doppler radar can operate within all non-cooperative search mode specifications with a peak transmitted power of less than 20 watts, providing at least a 3 dB design margin with respect to the 40 to 50 watt CW power required for the communication mode. The question of circular vs. linear polarization choice is addressed. It is shown that, if circular polarization is used for the passive mode, frequency diversity definitely must be used. This is not a limitation, however, since the frequency diversity may be required anyway to reduce glint effects in the angle track mode. The advantages of linear polarization

for the skin tracking mode are summarized.

Appendix F contains a discussion of target acquisition in the passive mode. The material presented there is primarily of reference nature since it does not include performance optimization included in the data of Appendix B.

Appendix E deals with the cooperative mode of operation. A pulse doppler radar system in the cooperative mode is shown in Figure 1 of Appendix E. A frequency synthesizer provides signals to both the transmitter and receiver. In the noncooperative mode the transmitter drive signal is frequency hopped to reduce the effects of passive target scintillation. To maintain constant the IF, the frequency of the receiver's first LO is hopped in synchronism. Single sideband generators provide for this hopping. In the cooperative mode, where frequency hopping is not required, the transmitter drive frequency equals the first LO frequency because the transponder offsets the return frequency by the radar's IF. In both modes the transmitter drive and the power amplifier are pulsed to provide the required waveform and PRFs.

A three-channel monopulse, superheterodyne receiver is used for amplifying and detecting the radar return. The monopulse converter provides the sum and the two difference signals required for the angle tracking of the targets. Each of these signals is amplified by a separate receiver channel with the sum channel providing the reference for the detection of the other two.

During the initial acquisition, the antenna scans over the target's angular uncertainty region. When the antenna is on target, the receiver intercepts and amplifies the pulsed, doppler shifted return. The frequency of the center line is detected and the VCO is tuned to that frequency. The antenna scan is then terminated and the angle as well as center line tracking is initiated. The range acquisition and tracking are also initiated using multiple PRFs to resolve range ambiguity. In the passive mode a carrier discriminator maintains the VCO frequency on the return center line. In

the cooperative mode a phase-locked loop coherently tracks the center line.

The range information in both the passive and cooperative modes is obtained by processing out the range ambiguities caused by the use of multiple, high rate PRFs and the Chinese remainder theorem. Once the true range is determined, the range tracking uses only one PRF at a time with the PRF switching taking place when the target return approaches the transmit period, called eclipsing.

A modified version of this radar system is given in the addendum to Appendix E (Figure A-3). The block diagram is essentially the same as that just described with the addition of coherent detection of phase reversals in the cooperative mode. Coherent detection is used for two reasons: (1) to extract the ranging information from the phase-modulated transponder signal and (2) to avoid integration losses at low SNR which is characteristic of ranging information at the maximum acquisition range of 560 km.

The operation of the transponder can be understood by referring to Figure A-2 of the addendum to Appendix E. Initially, the frequency of the VCO is swept to cover the frequency uncertainties. When the radar center line is intercepted, the transponder's first LO is coherently locked to it with an offset equal to the transponder's first IF. This turns on an injection-locked CW oscillator, and a portion of the first LO signal is used to establish the coherency of this CW oscillator output whose power is about 200 mw.

To provide the waveform required for phase modulation of the CW reply, the envelope of the radar pulses is detected and integrated. The resulting waveform is then applied to the phase modulator which introduces 180° phase reversals into the CW output of the oscillator. These reversals occur in sync with the incoming radar pulses so they provide the necessary ranging information to the radar receiver.

The resultant 3σ accuracies for this system at the maximum range of 560 km are:

$$\text{Range} \leq 9.3 \text{ m}$$

$$\text{Range Rate} \leq 0.3 \text{ m/sec}$$

$$\text{Angle Track} \leq 0.0235^{\circ} \text{ (each axis)}$$

These assume a peak transmitted power of 40 watts ($P_{ave} \approx 4$ watts) for the radar and 200 mw CW for the transponder. The probability of coherent lock-up within one minute is better than 0.99 with false alarm times in excess of one hour.

4.0 INTEGRATION COMPATIBILITY

The concept of combining the Shuttle Orbiter's rendezvous radar and Ku-band communication subunits into one integrated system is appealing from many viewpoints and thus has been under consideration for quite some time. The feasibility of such integration is due to the fact that the radar and the communication functions do not occur simultaneously; consequently, time sharing some of the equipment between them seems possible. The requirements for the communication function are relatively well defined, being constrained by such factors as TDRS frequency assignments, link budgets, and data rate specifications. In comparison, optimizing the radar function involves a multitude of tradeoffs and assumptions, some of which are still under study. Nevertheless, sufficient information has been generated to date to permit block diagram designs for an integrated radar/communication system.

Ideally, the maximum degree of integration would be achieved with a radar design which permits all three major subunits--antenna, receiver, and transmitter--to be shared by both the radar and communication functions. It is clear that the antenna assembly and the receiver functions, which include monopulse tracking, can be shared provided that the radar operating frequency is close to the 13.8 GHz communication receive band Whether the transmitter unit can be shared will depend on the type of radar selected. The two extremes of the candidate radar designs are represented by noncoherent pulse radar and coherent pulse doppler radar. The pulse radar is characterized by high peak power, 20 to 40 kw, and low duty cycle, 0.001 being typical. Thus, a separate and switchable magnetron transmitter must be used for the radar function. On the other hand, the pulse doppler radar requires only 20 to 40 watts peak with a duty cycle in the 0.1 to 0.5 range, so all that needs to be done is to pulse the communication system's TWTA.

4.1 System Description

4.1.1 Pulse Radar/Communication System

The detailed descriptions of these integrated radar/communication systems is given in Appendix G. The functional block diagram for non-coherent pulse radar is shown in Figure 1 of that appendix. As mentioned above, separate transmitter tubes must be used for the two functions. A frequency agile magnetron is a logical candidate for the radar transmitter while a TWTA is appropriate for the communication transmitter. To minimize RF losses, both transmitters are located within the deployed assembly. Depending on the mode, their outputs are selected by a remotely controlled waveguide switch.

Automatic frequency control (AFC) is required in the radar mode for two reasons: (1) to reduce the effects of the magnetron's long-term frequency drifts, and (2) to vary the LO's frequency in step with the frequency hopped radar transmitter output during the passive mode. Note that the AFC circuit is located within the gimbaled antenna assembly. This is consistent with the design philosophy of limiting the Ku-band interfaces between the deployed and the gimbaled assembly to the transmitter output rotary joints only.

To provide for maximum receiver commonality, the operating frequency of the radar is made approximately equal to the 13.8 GHz nominal frequency of the communication receive signal. As shown, the monopulse bridge provides the Σ, the ΔAz, and the ΔEl channel outputs. However, because the Σ receive channel is shared with the transmit channel, it is supplied to the receiver input via a circulator. Also, as discussed in section 4.2, additional isolation must be provided by a 13.8 GHz filter to keep the 15 GHz communication transmit signal from saturating the Σ channel in the communication mode when CW transmission and reception occur simultaneously. In the radar mode all three channels are protected by the T/R switches which prevent overloading of the receivers with spikes and residual leakages during the transmission of the high power radar pulse.

The first mixers for both the radar and the communication functions are located on the gimbaled assembly. Thus, after the first conversion to IF, which for a Ku-band system may be 300 to 1000 MHz, the three monopulse signals are preamplified and supplied to the deployed assembly via a set of cable wraps. The question of whether to use a paramp in the radar Σ-channel is open because the answer depends on the frequency allocation of the radar function. If the radar frequency is close to the communication receive frequency, an improvement in the radar Σ-channel noise figures can be realized with a paramp.

After conversion to the first IF, the Σ-channel and the Δ-channels can be shared by the radar and the communication functions. The only difference may be in the bandwidth of the IF filters required for each of these modes. Specifically, for the radar mode the final bandwidth may be from 1 to 10 MHz, while for the communication mode the bandwidth prior to despreading may be from 30 to 40 MHz. The output of the Σ-channel is applied either to the communication despreader or to the radar processor. In the radar mode, target acquisition is declared when this output exceeds a preset threshold. Antenna scan is then terminated and tracking is initiated. For range tracking a split-gate tracker is used. The output of this tracker is applied to a processor which performs an optimal estimation of range and range rate.

The Σ-channel is also used to generate the ΔAz and ΔEl error signals. These error signals are first applied to video filters and, in the radar mode, these signals are then range-gated and applied to the boxcar detectors. These outputs are then applied to the angle tracking electronics subunit which smooths the error data and supplies angle correction commands to the antenna servos. In the communication mode, the signal is continuous so the outputs of the video filters are applied directly to the angle tracking electronics subunit.

4.1.2 Pulse Doppler Radar/Communication System

Figure 2 of Appendix G shows the block diagram for an integrated pulse doppler radar/communication system. The TWTA which is used for the communication signal transmission is also used for the radar transmission; however, for radar it is pulsed at a rate and interval determined by the PRF and the duty cycle. Since it is assumed that the radar frequency is close to the communication receive frequency of 13.8 GHz, the 15 GHz communication transmit filter is bypassed in the radar mode. The peak output of the transmitter is 20 to 50 watts.

In the passive radar mode the transmitter frequency diversity is provided by a single sideband generator. In the cooperative mode the transponder offsets the frequency of the return signal by an amount equal to the radar's first IF. Thus, the transmit and first LO signals are the same.

For this system the receiver front end is the same as described for the pulse radar system. However, additional receiver protection is provided by turning off the LO drive to all three first mixers during the transmission of the radar pulse. To protect the receiver from the 15 GHz transmit signal leakage during the communication function, filters are included in all three receiver channels. This is further explained in the next section. Because the transmit signal and the LO signals are derived from a coherent synthesizer, the AFC is not required for the pulse doppler radar. In the passive mode when frequency diversity is required, the first LO signal is stepped in synchronism with the transmitter signal. A single sideband generator can be used for this purpose. In the cooperative mode, the first LO frequency is the same as that of the transmitter.

In the passive tracking mode, the target signal is detected by a bank of doppler filters. When the signal in one of the filters exceeds a preset threshold, the angular search is terminated and the frequency tracking commences. A discriminator and a VCO are used to perform tracking since the coherency of the return signal may be destroyed by target characteristics.

The output of the VCO is compared against a fixed reference and the frequency difference provides the estimate of range rate.

In the cooperative mode the transponder return is coherent and a phase-locked loop is used to acquire and track the frequency of the reply. The range acquisition is performed by cycling the PRFs through several values to resolve the range ambiguity caused by the high values of the PRFs used by the pulse doppler radar. Because of the presence of a strong center line component, the angle tracking can be performed directly on this component without resorting to range gating. Similar to the pulse radar, the channel provides the reference signal to the phase detectors which coherently recovers the amplitude and the polarity of the two Δ-channel error signals. The errors are lowpass filtered and applied to the angle tracking electronics unit which keeps the radar antenna pointed at the target.

4.2 Filtering Requirements

The RF filtering considerations for an integrated Ku-band radar/communication system are determined primarily by the requirements for minimizing the transmitter-to-receiver interference in the communication mode. In the communication mode the transmitter supplies about +47 dBm (50 watts) of CW power to the antenna, while the received signal is about -100 dBm. The approximate frequencies of the transmitter and receiver are 15 GHz and 13.8 GHz, respectively. Figure 2a of Appendix H shows the transmitter and receiver spectra. The two types of transmit signal components which are deleterious to receiver operation are: (1) transmit signal components which fall within the receiver bandwidth and (2) transmit signal components which, although outside the receive band, are of sufficient level to saturate the Σ and Δ channels of the receiver.

In the passive mode, both the pulse and pulse doppler radars utilize frequency diversity to eliminate scintillation effects. Figure 5 of Appendix H shows the radar spectrum. Since this spectrum is about 250 MHz wide while the communication received spectrum is only about 30 MHz wide, the input filter bandwidth is determined by the radar requirements. Figure 2b

of Appendix H shows the hypothetical transmit and receive filter characteristics.

4.3 Angle Tracking Compatibility with Communications Mode

For angle tracking, i.e., antenna pointing, a coherent amplitude comparison monopulse tracking system is proposed. Appendixes I and J verify that angle tracking of the TDRS PN spread communication signal received by the Orbiter can be carried out directly on the unspread wideband waveform. This significantly simplifies the acquisition sequence performed by the communication receiver. Appendix I assumes that there are paramps in both the sum and difference channels. It shows that, using a noncoherent AGC for normalization and a coherent amplitude detector for angle error information (Figure 1), the RMS angle tracking error due to receiver front-end noise is about 10^{-3} degrees. This is well below any anticipated system requirement with ample safety margin.

Appendix J extends these results to include the following cases:

1. The paramp is absent in all channels,
2. The paramp is present in the sum channel only,
3. PN sequence despreading is present in all channels,
4. The angle tracking is carried out on the wideband spread signal.

For all combinations of the above cases, it is shown that the RMS tracking error due to thermal noise is less than 10^{-2} degrees (see Figure 4 of Appendix J). Thus, these errors are well below any anticipated system requirement.

5.0 CONCLUSION

Many of the investigations required for a rendezvous radar system design and an integrated radar/communication system design have been presented in this report. Based on these investigations, system block diagrams have been presented and system parameters have been optimized for the noncoherent pulse and coherent pulse-doppler radar modulation types. Both cooperative (transponder) and passive radar operation were presented including the optimization of the corresponding transponder design for the cooperative mode of operation.

APPENDIX A

RADAR CROSS SECTION ERRORS INDUCED BY A TWO-POINT TARGET

RADAR CROSS SECTION ERRORS INDUCED BY A TWO-POINT TARGET

C. L. Weber

I. Introduction

The total Radar Cross Section (RCS) of a two point target is determined from two different points of view. First, the RCS is evaluated from the point of view of determining scintillation (amplitude) variations with respect to aspect angle. Second, the resultant RCS center versus range is determined with respect to aspect angle and the relative gains of the two points of the target.

Particular emphasis is placed on a two point target whose points are separated by 18 meters. The arithmetic sum of the RCS of the two points is assumed to be

$$\sigma = 1m^2 .$$

Finally the effect of frequency diversity is taken into account at the S, X, and Ku band frequency ranges.

II. Two-Point Target Scintillation Effects

The configuration of a two-point target is shown in Figure 1. The phase difference between the signal return from point 1 and point 2 is given by

$$\psi = 2d(\sin\theta)\frac{2\pi}{\lambda} = \frac{4\pi df \sin\theta}{c} \qquad (1)$$

where d and θ are shown in Fig. 1. λ is carrier wavelength, f is carrier frequency, and c is the speed of the E & M wave (3×10^8 m/sec).

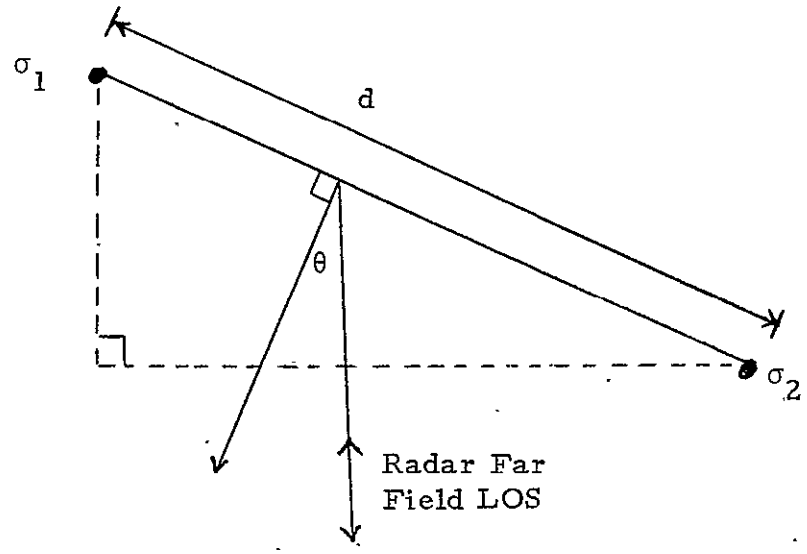

Figure 1. Two-Point Target Configuration.

The total RCS for the two point target is the vector sum of the individual cross sections, namely

$$\sigma = \left| \sqrt{\sigma_1} + \sqrt{\sigma_2}\, e^{j\psi} \right|^2 \tag{2}$$

where (as shown in [1])

σ_1 is the RCS of point 1 and σ_2 is the RCS of point 2. We parameterize σ_1 and σ_2 as follows:

$$\sigma_1 = \tfrac{1}{2} + \frac{\sqrt{1-a^2}}{2} \qquad 0 \le a \le 1$$

$$\sigma_2 = \tfrac{1}{2} - \frac{\sqrt{1-a^2}}{2} \qquad 0 \le a \le 1 \tag{3}$$

Then $\sigma_1 + \sigma_2 = 1m^2$ for all values of a.

Substituting (1) and (3) into (2) and performing the algebraic simplification yields

$$\sigma = 1 + a \cos\left[\frac{4\pi df \sin\theta}{c}\right] \tag{4}$$

When a = 1, so that $\sigma_1 = \sigma_2 = \frac{1}{2}$, then

$$\sigma = 2 \cos^2 \left[\frac{2\pi df \sin \theta}{c} \right] \tag{5}$$

Equation (5) is plotted in Figure 2 which is taken from DiFranco and Rubin [3], page 28. In Figure 2, $\sigma_1 = 1$, $\sigma_2 = 1$, $\sigma_0 = \sigma_1 + \sigma_2 = 2$, and σ_r in the Figure 2 is σ in (5). The number of lobes in the resultant RCS, L, is 8 times the factor d/λ, i.e.,

$$L = 8 \frac{d}{\lambda} \tag{6}$$

Therefore, in Fig. 2a, where $d = \lambda$, there are 8 lobes, 16 lobes in 2b and 32 lobes in 2c when $d = 4\lambda$.

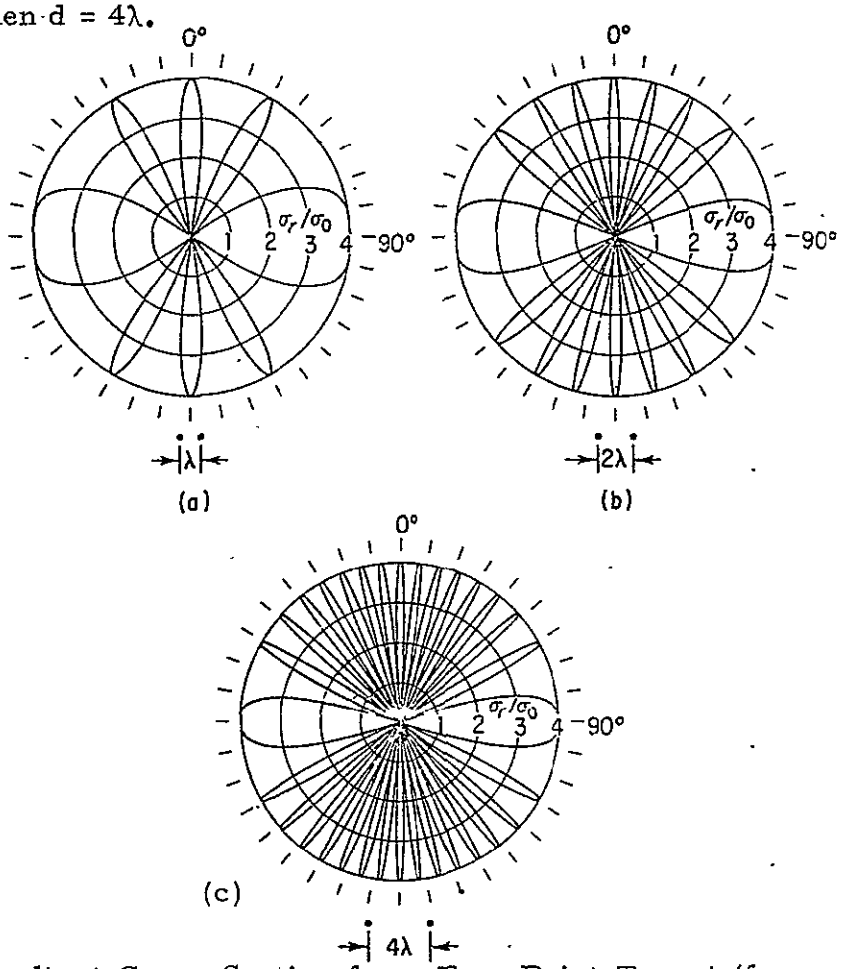

Figure 2. Resultant Cross Section for a Two-Point Target (from page 28 of [3]).

In the example we are using for Shuttle

$$d = 18 \text{ meters}$$

At

S-Band, $f = 2$ GHz, $\lambda = .15$m

X-Band, $f = 10$ GHz, $\lambda = .03$m

Ku-Band, $f = 15$ GHz, $\lambda = .02$m

Then the number of lobes for the $d = 18$ meter target is

$L = 960$ for S-Band

$L = 4800$ for X-Band

$L = 7200$ for Ku-Band

There is therefore very rapid variation in the resultant RCS with respect to aspect angle.

Also note that when $\sigma_1 = \sigma_2$, there are complete nulls in the RCS, as shown in Figure 2. This is not the case when $\sigma_1 \neq \sigma_2$.

The effectiveness of frequency agility can be determined by noting what frequency shift is required to obtain at least a 90^o phase shift in the argument of (5). Hence

$$\frac{2\pi d(\Delta f) \sin \theta}{c} \geq \frac{\pi}{2} \tag{6}$$

or equivalently

$$\Delta f \geq \frac{c}{4d_0} \tag{7}$$

where $d_0 = d \sin \theta$. If $d_0 = 0.75$ meter, for example,

$$\Delta f \geq 10 \text{ MHz} \tag{8}$$

Typically frequency agility hops are of the order of 50 to 75 MHz, which is more than sufficient to obtain statistically independent target RCS returns.

Probability Density Function

The probability density function of RCS is dependent on the choice of probability distribution of target aspect. We assume that the target is uniformly oriented in three dimensions so that, in spherical coordinates

$$p(\theta, \varphi) d\theta d\varphi = \frac{\cos \theta \, d\theta d\varphi}{4\pi} \tag{9}$$

$$-\frac{\pi}{2} \leq \theta \leq \frac{\pi}{2}, \quad 0 \leq \varphi \leq 2\pi$$

Integrating out φ,

$$p(\theta) = \frac{\cos \theta}{2}, \quad -\frac{\pi}{2} \leq \theta \leq \frac{\pi}{2} \tag{10}$$

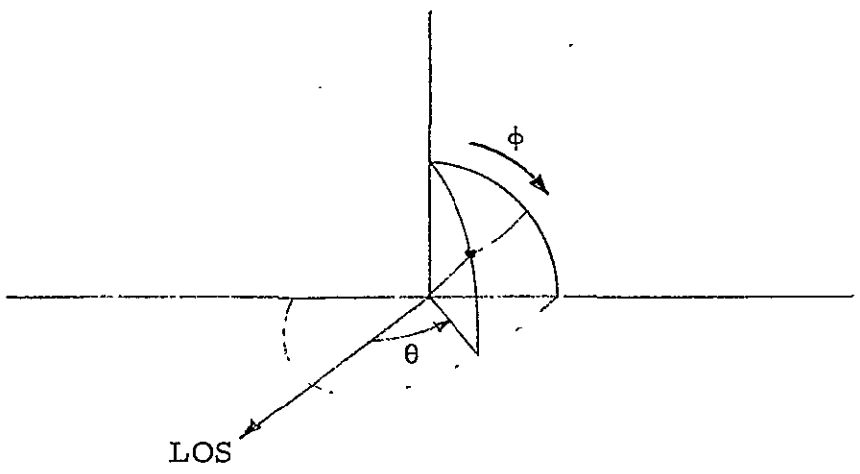

Figure 3. Uniform Target Orientation.

If θ is distributed as given in (10), then $\epsilon = \sin\theta$ is uniformly distributed between (-1, 1). Hence, ψ, in (1), is uniformly distributed between $\pm 4\pi fd/c$.

If df/c is an integer (i.e., if d is an integral number of quarter wavelengths), the pdf is the same as that of an endless $2\cos^2$ function. If not an integer, there is some additional fractional cycle of the sinusoid that distracts the pdf. If we restrict our attention, however, to targets with d equal to many wavelengths (which is the case in our example), insignificant error is introduced by ignoring the contribution of the odd fractional cycle. In that case we can equivalently say (when $a = 1$)

$$p(\sigma) = p(\tfrac{\psi}{2}) \left|\frac{d(\psi/2)}{d\sigma}\right| , \quad 0 \le \frac{\psi}{2} \le \frac{\pi}{2}$$

$$= \frac{2}{\pi} \frac{1}{2\sin\psi}$$

$$= \frac{1}{\pi\sqrt{1-(\sigma-1)^2}}, \quad 0 \le \sigma \le 2 , \quad a = 1 . \tag{11}$$

Integration of this pdf gives the cumulative distribution function

$$P(\sigma) = \frac{1}{\pi}\cos^{-1}(1-\sigma), \quad a = 1, \quad 0 \le \sigma \le 2. \tag{12}$$

If the two-point target has $\sigma_1 \neq \sigma_2$, i.e. $a \neq 1$, then by similar arguments

$$p(\sigma) = \frac{1}{\pi\sqrt{a^2-(\sigma-1)^2}} , \quad 1-a \le \sigma \le 1+a \tag{13}$$

and

$$P(\sigma) = \frac{1}{\pi} \cos^{-1}\left(\frac{1-\sigma}{a}\right), \quad 1-a \leq \sigma \leq 1+a \tag{14}$$

This distribution is plotted in Figure 4. (taken from [2].) It shows how the probability of a deep fade increases substantially as $\sigma_1 \rightarrow \sigma_2$ $(a \rightarrow 1)$.

The dotted line in Figure 4 is the cumulative probability of the Swerling I target model with $\bar{\sigma} = 1$ m. It is noted that the Swerling I amplitude scintillation model does vary differently from that of the two-point target. The Swerling I is more pessimistic than that of the two-point target since it places more probability at smaller values of σ. The Swerling I amplitude scintillation model is thus considered a satisfactory model.

III. Resultant RCS Center vs. Range

In this section we consider the resultant RCS center vs. Range variation due to changes in the target aspect. This can be termed target-generated range errors.

Complex targets cause scintillation in the range coordinate of a radar which is similar to angular scintillation or glint [7-10]. We shall consider primarily narrowband radar signal formats. For the narrowband case, the range scintillation is an erroneous delay of the modulating function regardless of the type of modulation such as FM, pulse doppler, etc.

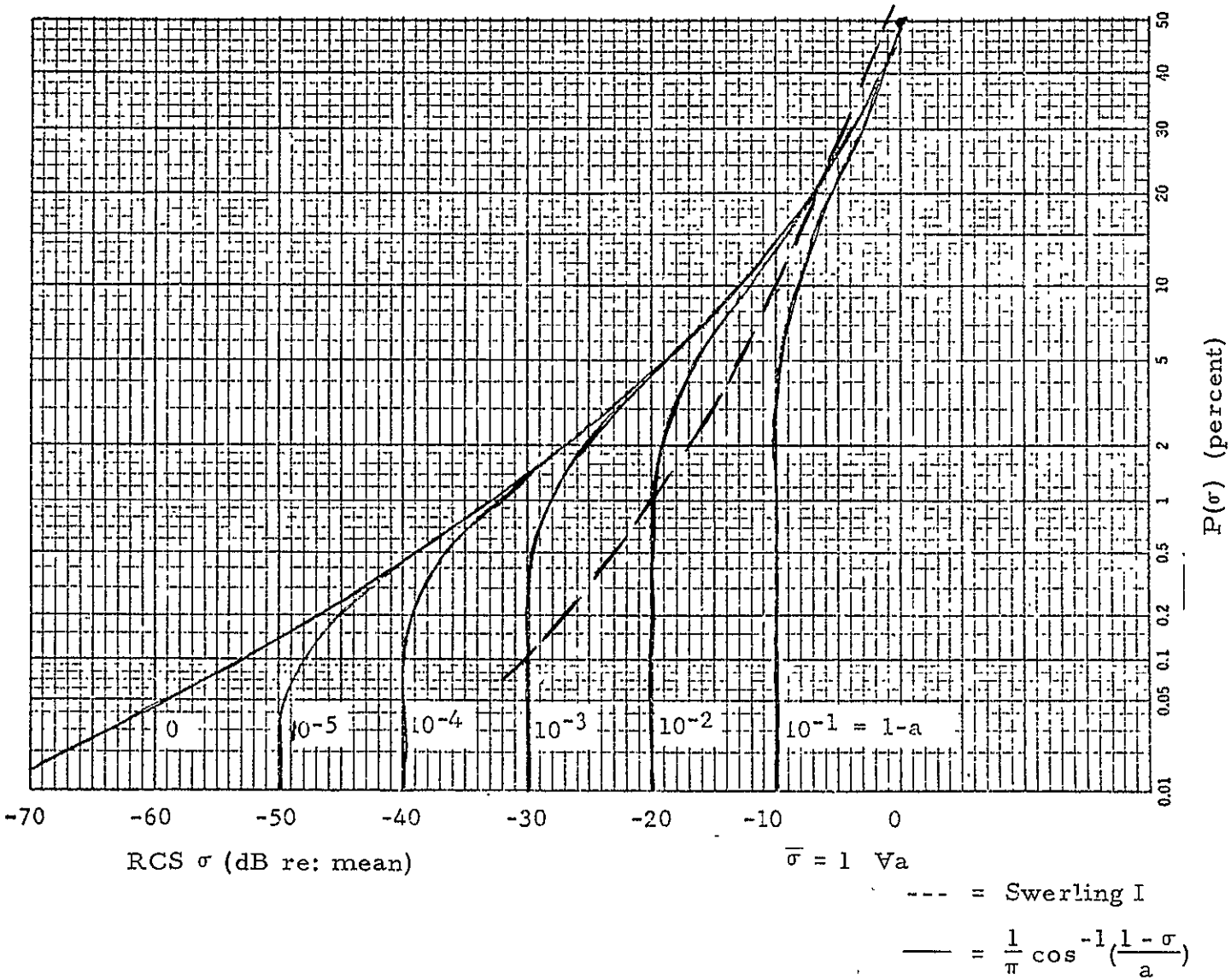

Figure 4. Cross Section Distribution for Two-Point Target

We consider first the narrowband case. By narrowband, we mean a pulse which is long compared to the target length. For the 18 meter target, the time to transverse the length of the target twice is given by

$$t_0 = \frac{2L}{c} = 120 \text{ nsec} \tag{15}$$

Radars with pulse lengths as short as 1 usec would still be considered narrowband with respect to 120 nsec.

It will be shown that the two point target can generate false range information which cannot be distinguished from true target range. The reduction of this range via frequency agility will then be considered. We first consider a one-point target.

3.1 One Point Target Considerations

In a manner similar to that developed in [4], let the transmitted signal, s(t), be given by

$$s(t) = m(t)e^{j\omega_c t} \tag{16}$$

where m(t) is the modulating waveform and $f_c = \omega_c/(2\pi)$ is the rF carrier frequency. For the most part we shall consider the effects of one pulse. If the Fourier transform of m(t) is M(f), then the Fourier transform of s(t) can be written as

$$S(f) \triangleq \mathcal{F}\{s(t)\} = M(f-f_c) \tag{17}$$

Consider now how the spectrum is changed when the transmitted signal is delayed in the time domain which is the case for a point source target. The Fourier transform of $s(t-t_d)$, where t_d is the total time delay between transmit and receive, is

$$\mathcal{F}\{s(t-t_d)\} = M(f-f_c)\exp(-j2\pi ft_d)$$
$$= M(f-f_c)\exp[-j\varphi_d(f)] \qquad (18)$$

where we have set

$$\varphi_d(f) = 2\pi ft_d \qquad (19)$$

for the one-point target. In a radar environment $t_d = 2R/c$ where R is the range to the point target. In (19), note that when a signal is delayed in time by t_d, each frequency component is shifted in phase by an amount $2\pi ft_d$. Equivalently, the phase variation is a linear function of frequency, and the slope of the phase variation is proportional to the time delay t_d.

Therefore, a linear phase shift versus frequency throughout the spectrum will appear in the Fourier transform of any undistorted time-shifted signal. Finally note that this phase variation due to time delay appears as a function in the frequency domain, which directly multiplies the spectrum of the original signal, as shown in (18).

3.2 Two-Point Target Considerations

The geometry of the two-point target for ranging is shown in Figure 5. The relative amplitude, b, is the ratio of the nearer reflector to the

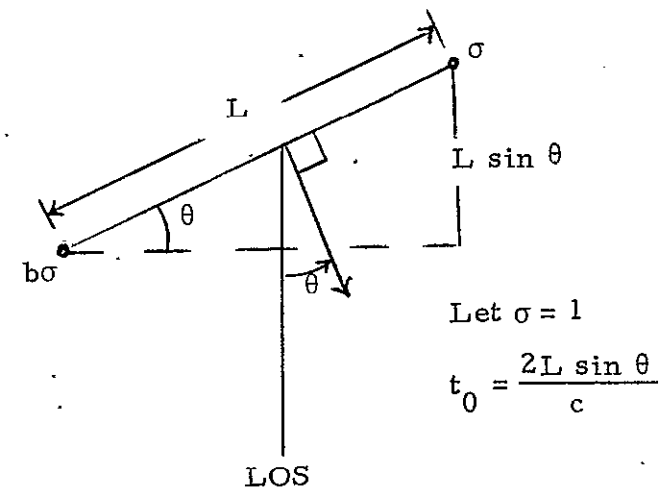

Figure 5. Two-Point Geometry for Target Ranging.

amplitude of the farther reflector. The relative-phase, φ_R, is the two-way radial target length, measured along the LOS at the carrier frequency. It is given by

$$\varphi_R = \frac{(2)(2\pi)}{\lambda_c} L \sin \theta = \frac{2\omega_c L \sin \theta}{c} \tag{20}$$

where the parameters are as designated in Figure 5, and λ_c is the wavelength of the rF. In Figure 5,

$$t_0 = \frac{2L \sin \theta}{c} \tag{21}$$

is the two-way time delay of the farther element with respect to the nearer element along the LOS. Let us establish a coordinate system along the LOS, measuring relative time from the midpoint of the target. The signal waveform, relative to the center of the target is given by

$$s(t) = bm\left(t + \frac{t_0}{2}\right) \exp\left[j\omega_c \left(t + \frac{t_0}{2}\right)\right] + m\left(t - \frac{t_0}{2}\right) \exp\left[j\omega_c\left(t - \frac{t_0}{2}\right)\right] \quad (22)$$

The Fourier transform of s(t) in (22) is given by

$$s(f) = \mathcal{F}\{s(t)\} = M(f-f_c)A(f)\exp\left[-j\varphi_T(f)\right] \quad (23)$$

where

$$A(f) = \left[1 + b^2 + 2b\cos(2\pi f t_0)\right]^{\frac{1}{2}} \quad (24)$$

and

$$\varphi_T(f) = \tan\left\{\frac{(1-b)\sin(\pi f t_0)}{(1+b)\cos(\pi f t_0)}\right\} \quad (25)$$

Hence, S(f) is the product of the transform of the modulating signal, $M(f-f_c)$, an amplitude factor, A(f), and a phase variation, $-\varphi_T(f)$. The amplitude and phase variations are a function of the target only. The overall phase has the term $-j2\pi f t_d$ added which represents the true time delay to the target. The phase, $-\varphi_T(f)$ represents the error about the true range.

If the amplitude is constant, and the phase $\varphi_T(f)$ is linear in frequency, the inverse Fourier transform would be a time-shifted undistorted version of the transmitted signal. The magnitude of the error in time shift is given by the slope of $\varphi_T(f)$ versus frequency.

Although the amplitude is not constant and $\varphi_T(f)$ is not linear for the two-element target when observed over a wide frequency region, a narrowband radar will observe only a small portion of the amplitude and phase functions. Within this small segment, the amplitude, A(f),

will be essentially constant and the phase $\varphi_T(f)$ versus frequency will be essentially linear. Consequently, the radar sees what appears like the echo from a one-point target. This can be demonstrated by considering a Taylor series of $\varphi_T(f)$ about some carrier frequency f_0, namely

$$\varphi_T(f) = \varphi_T(f_0) + \varphi'_T(f_0)(f-f_0) + \frac{\varphi''_T(f_0)}{2}(f-f_0)^2 + \cdots \tag{26}$$

Under the above assumption that $\varphi_T(f)$ is essentially linear over the region of interest, the higher order terms of the series can be omitted, and

$$\varphi_T(f) \approx \varphi_T(f_0) + \varphi'_T(f_0)(f-f_0), \tag{27}$$

Also, since A(f) is essentially constant over the region of interest, it also may be replaced by $A(f_0)$, so that for narrowband radar, (23) is approximately given by

$$S(f) \approx A(f_c)\exp\{-j[\varphi_T(f_c)-f_0\varphi'_T(f_c)]\}\exp\left\{j2\pi f\left[\frac{\varphi'_T(f_c)}{2\pi}\right]\right\}M(f-f_c) \tag{28}$$

Taking the inverse Fourier transform

$$s(t-t_e) = A(f_c)\exp\{-j[\varphi_T(f_c) - f_c\varphi'_T(f_c)]\}m\left(t - \frac{\varphi'_T(f_c)}{2\pi}\right) \tag{29}$$

Thus, the return signal in the narrowband case is a time shifted version of the transmitted signal, with an additional attenuation given by $A(f_c)$, and an error in time of arrival given by

$$t_e = \frac{\varphi_T'(f_c)}{2\pi} \tag{30}$$

The error in the time shift is therefore given by the derivative of $\varphi_T'(f_c)$ divided by 2π (the 2π factor disappears if this development is carried out in radians rather than Hertz).

The narrowband case is defined as signals whose pulse length is long compared to the target length, expressed by t_0. The signal return is approximately undistorted. This is shown in Figure 6. The phase $2\pi\varphi_T(f)$ is plotted for various values of b versus frequency, where f_0 is chosen so that $f_0 t_0$ is an integer. For an 18 meter target at $\theta = 90^\circ$

$$(t_0)^{-1} = 8.33 \text{ MHz} \quad . \tag{31}$$

In Figure 6 for small and large values of b, the slope of the phase is relatively constant. For values of b near 1, there is significant variation of the phase versus frequency. Superimposed at the bottom of Figure 6 is a Gaussian shaped pulse in the frequency domain for the cases of Target Length to Pulse Length (T.L./P.L.) equal to 0.1 and 0.3. The center frequencies of the pulses, f_{c_1} and f_{c_2} are arbitrarily chosen. For a T.L./P.L. of 0.3, the signal is still considered narrowband. One can see that for most carrier frequencies and values of t_0, the slope of $\varphi_T(f)$ is relatively constant over the bandwidth of the pulse. We can therefore conclude that for narrowband radar signals, there will be negligible signal distortion of the returned pulse from a wide variety of two-point targets.

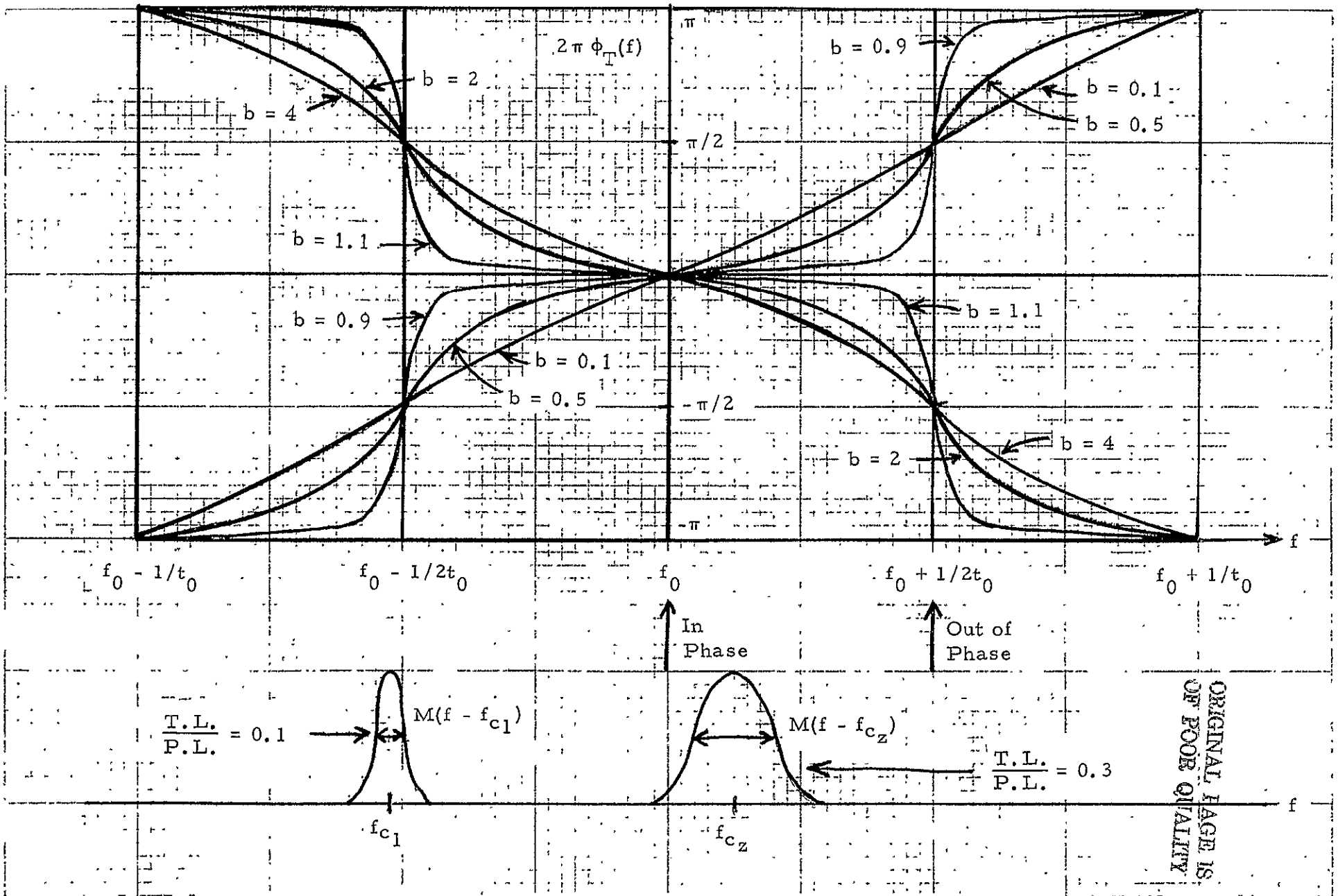

Figure 6. Target Phase Variation Over Signal Bandwidth

It should be noted that a two-point target is a relatively severe target from this point of view. If more complex targets would be considered, the distortion for narrowband radar signals would not be expected to be any greater than the amount indicated here for the two-point target.

From these comments, it is seen that for narrowband signals, the spectrum is essentially the same as the time shifted single-point target. The only difference here being that there will be an error in the time delay. The magnitude of the time delay error, t_e, is given in (30). When the differentiation in (30) is carried out and evaluated at $f=f_c$, we obtain that

$$t_e = \frac{\varphi_T'(f_c)}{2\pi} = \left(\frac{t_0}{2}\right)\left[\frac{1 - b^2}{1 + b^2 + 2b\cos(2\pi f_c t_0)}\right] \qquad (32)$$

where $2\pi f_c t_0 = \omega_c t_0$ is the relative phase of the two returns.

In Figure 7, t_e/t_0 is plotted versus $\omega_c t_0$ for various values of relative amplitude b. The results show that there are many cases where the indicated target range is well outside the physical extent of the target. Thus, in the narrowband signal case, the area under the video curve is shifted in time and an early-late gate tracker will follow this shift. Similarly, an FM-CW ranging system, which measures range by the phase shift of the received FM modulation, will observe an erroneous time shift of the modulation.

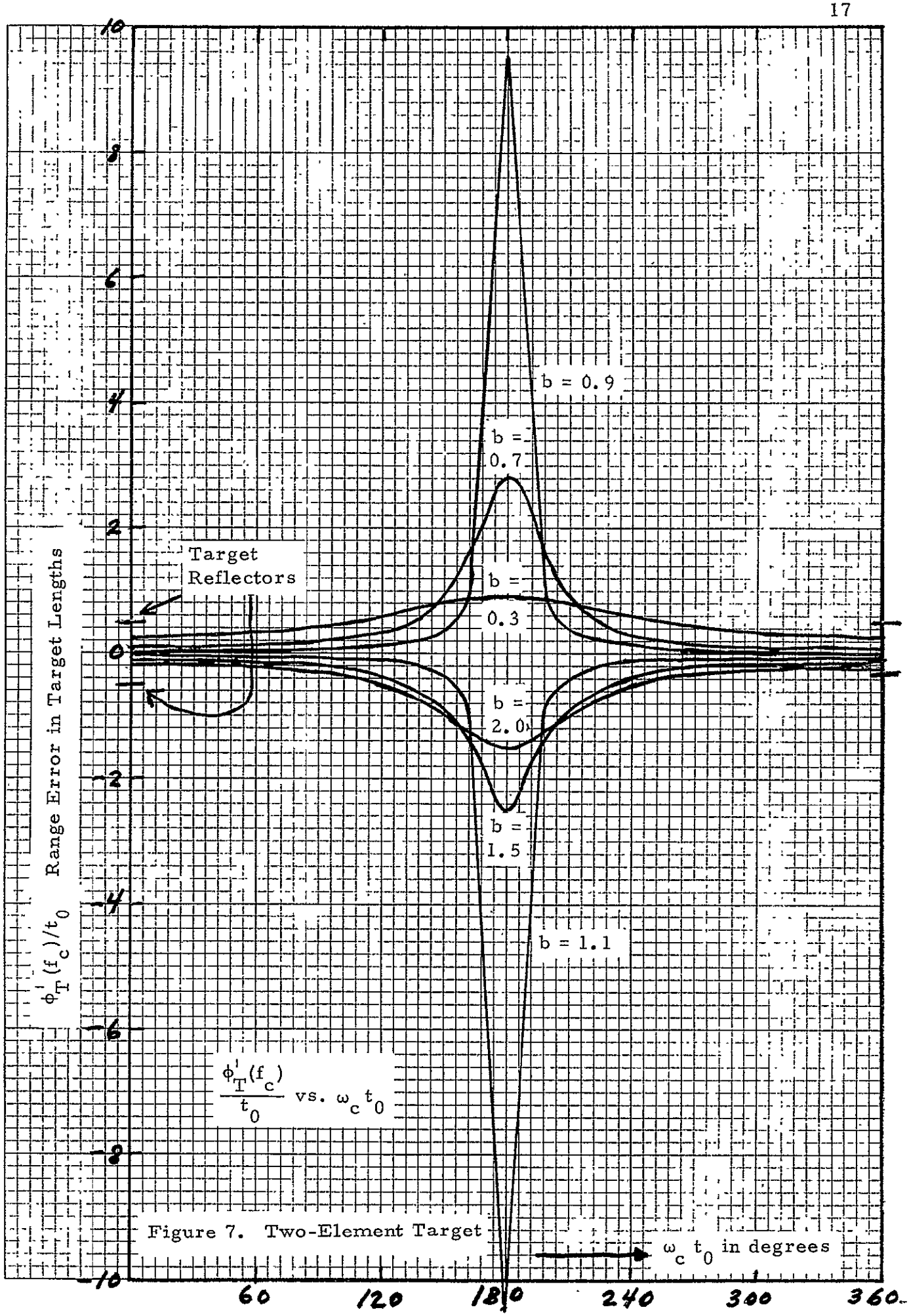

Figure 7. Two-Element Target

This error, as a function of spacing or relative phase between reflectors, is essentially the same as in the angle-glint case. The difference is that the range of errors is proportional to the range separation (L sin θ) of the sources, while the angle error is proportional to the angular separation of the two sources (L cos θ). This basic result also holds for a multiple point target.

3.3 The Effect of Frequency Agility

The effect of ranging errors due to target orientation can be substantially reduced by the use of frequency agility. Each new rF frequency will have the effect of choosing a point randomly between $(0, 360^0)$ in Figure 7. If a sufficient number of rF frequencies are employed (e.g. 5-7), the resulting range error would be approximately the average value of the function in Figure 7. These average values are tabulated in Table I, where for example, at b = 0.9, the maximum range error is 9.5 times the target length, whereas the average is only 1.11 times the target length. Frequency diversity has the additional advantage of substantially reducing the variance about the mean. Typical frequency shifts would need to be at least as large as that corresponding to $1/t_0$ ($\approx$10 MHz). It is therefore possible to easily choose a set of rF frequency shifts to satisfy the requirements of performing the average of the curves in Figure 7, as well as provide independent amplitude returns to reduce the effects of amplitude scintillation.

Also in Table I is shown the standard deviation about the mean, where the target orientation is assumed to be uniformly distributed.

TABLE I

Average Range and Standard Deviation in Target Lengths

b =	$E[t_e]$ =	σ_r =
0.1	0.50	0.074
0.3	0.51	.24
0.5	0.53	.45
0.7	0.59	.83
0.9	1.01	2.70
1.1	-1.09	2.99
1.5	-0.57	0.74
2.0	-0.53	0.45
4.0	-0.51	0.19

The results are given in target lengths. Certain empirical data is reported in the Barton and Ward Handbook, p. 170 wherein it is quoted that the standard deviation is approximately 0.35 times the target length. In terms of a two-point target this corresponds to a choice of b of approximately 0.4 or approximately 2.5. The two-point target model has the versatility therefore of modeling targets whose standard deviation in target position is greater or less than the empirical data quoted by the Barton and Ward handbook. The handbook does not address the important question that the average value can be significantly removed from the geometric center of the target.

REFERENCES

1. F. E. Nathanson, Radar Design Principles, McGraw-Hill, 1969.

2. D. P. Tice, "The Effect of Frequency Agility on the Radar Detectability of Spacecraft," Westinghouse Report, Baltimore, Maryland, Sept. 1973.

3. J. V. Di Franco and W. L. Rubin, Radar Detection, Prentice-Hall, 1968.

4. D. C. Cross and J. E. Evans, "Target Generated Range Errors," IEEE 1975 International Radar Conference, Arlington, Virginia, April 1975.

5. R. Stefanick, "Preliminary Target Modeling for Shuttle Rendezvous Application," NASA-JSC, January, 1975.

6. J. W. Crispin and K. M. Siegel, Methods of Radar Cross-Section Analysis, Academic Press, 1968.

7. R. B. Muchmore, "Aircraft Scintillation Spectra," IRE-AP, March 1960, pp. 201-212.

8. R. H. Belano and I. Pfeffer, "The Effects of AGC on Radar Tracking Noise," Proc. IRE, Vol. 44, pp. 801-810, June, 1956.

9. J. H. Dunn and D. D. Howard, "The Effects of AGC Performance on the Tracking Accuracy of Monopulse Radar Systems," Proc. IRE, Vol. 47, March, 1959, pp. 430-435.

10. J. H. Dunn, D. D. Howard, and A. M. King, "Phenomena of Scintillation Noise in Radar Tracking Systems," Proc. IRE, Vol. 47, pp. 855-863, May 1959.

APPENDIX B

OPTIMIZATION OF PROPOSED RADAR FOR THE INTEGRATED KU-BAND RADAR-COMMUNICATION SYSTEM

I. Introduction

In Figure 1 is a block diagram of a center line coherent pulsed doppler radar (ICW) operating in the search mode. In this implementation, the design is carried out to maximize the number of components which can be used both in the radar and comm subsystems of the shuttle Ku-band communication systems. In this design the radar center frequency is located close to the comm receive frequency. Inspection of Figure 1 shows the components that are used in both the radar and comm Ku-band operation. The comm system operates through the TDRS and cannot operate simultaneously with the rendezvous radar. In determining the performance of this system, several system parameters are varied: Number of scans, number of RF frequencies used in frequency diversity, and choice of polarization. Several optimizations have also been carried out.

The comm receiver employs an uncooled paramp. The radar receiver in this implementation uses the same paramp, which has a noise figure of about 3 dB, as compared to the balanced diode mixer (see Figure 1) of $F \approx 8$ dB. The balanced diode mixer is not as sensitive to large inputs as the uncooled paramp. The T/R switch may have to be used as an attenuator at shorter ranges, or the XTMR power reduced to protect the targets being tracked.

The paramp shown in Figure 1 is the only such device in this configuration of the integrated radar-comm system. The paramp

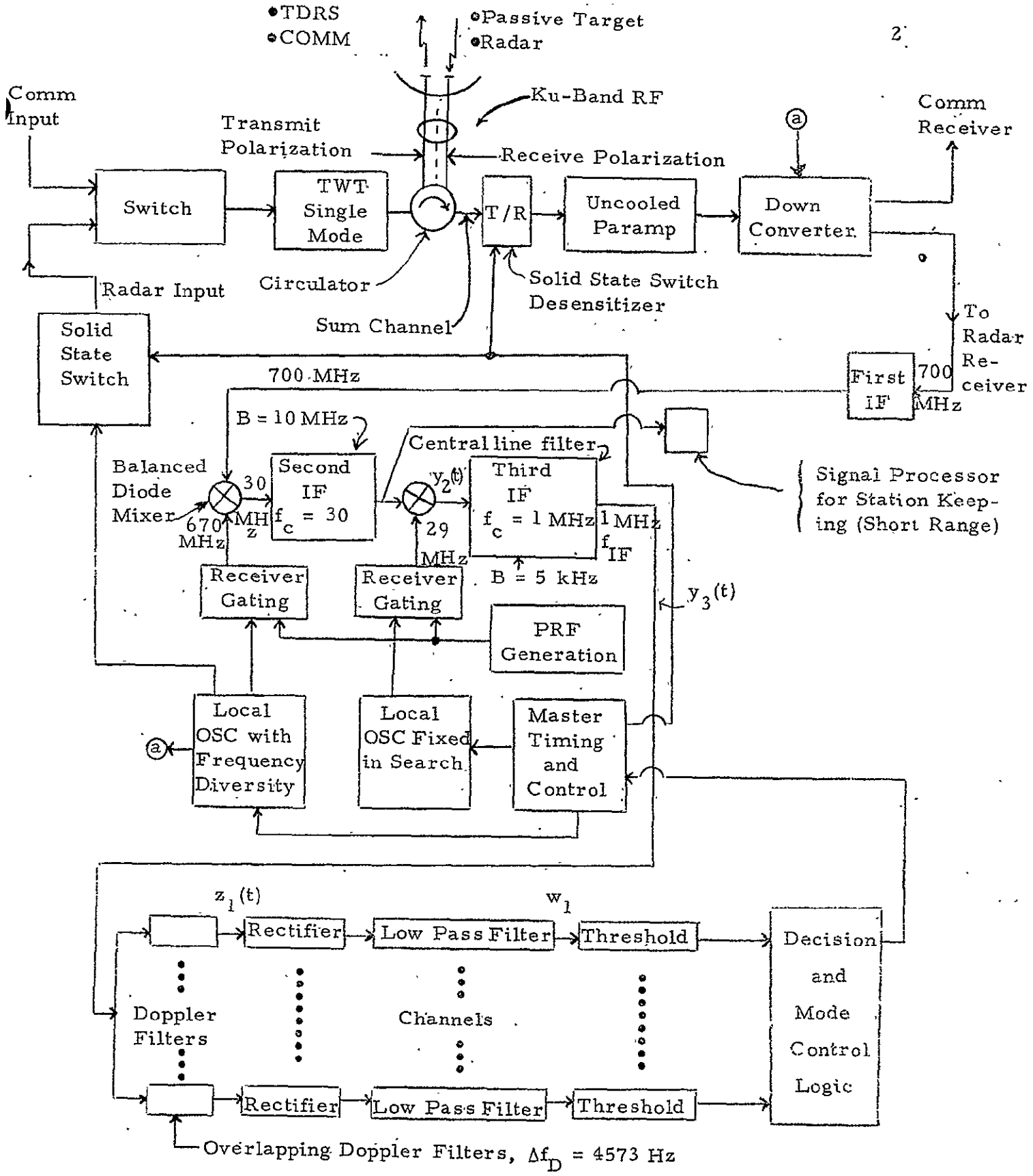

Figure 1. Center Line Pulsed Doppler Radar Receiver in Search Mode Where Radar Frequency is Close to the Comm Receive Frequency.

is located in the sum channel of the monopulse horn output. It is anticipated that a paramp receiver amplifier will not be required in the two difference channels, because of the long time constant in the angle tracking loops, thereby providing sufficient smoothing to obtain sufficiently high signal-to-noise ratio. The sum and difference channels will then have unequal gains. These can be monitored and taken into account in the subsequent signal processing. This will be the subject of a future report.

In section II, specific considerations are presented for each of the integrated components. In section III the detailed performance computations are described. A comparison is made with the noncoherent pulsed radar in section IV. In the last section, some comments are made concerning the signal processor for station keeping at short range.

II. Considerations for the Integrated Components

A. Uncooled Paramp - Ku-Band

1) A noise figure of 2-3 dB at 15 GHz as compared to a noise figure of 8 dB for the balanced diode mixer at 15 GHz (ref. Skolnik, [5, Ch. 5]).

2) The uncooled paramp (and single mode TWT transmitter amplifier) are essentially not off-the-shelf items that are space qualified. The technology is there, however, which for these components in this frequency band is the best that can be expected at this point in time.

3) The bandwidth of an uncooled paramp in the Ku-band is approximately 500 MHz. This is more than sufficient bandwidth to be used as the low noise front end RF amplifier for both radar and comm, provided the radar frequency is close to or equal to the comm receive frequency. This is the case whether or not frequency diversity is employed by the radar. This places the radar frequency in the TDRS band. This should not produce any problems since the radar and Ku-band comm to the TDRS can never be operating simultaneously.

4) When the noise figure is as low as 2-3 db for the RF amplifier of the receiver, it may be necessary to take into account the noise temperature of the antenna. When the balanced diode mixer is the first RF component, then $F \approx 8$ dB, and $T_s \approx 1540^{\circ}K$, so that the antenna temperature can be neglected. For the

uncooled paramp with F ≈ 3 dB, then $T_{paramp} \approx 290^{o}K$, and the antenna temperature could be significant. To date, we are not aware of an approximate noise temperature being specified for the antenna.

B. Single-Mode TWT Transmitter Amplifier

1) Single cathode, thereby employing a simpler power supply and support equipment and probably less weight overall.

2) With a single cathode, the radar is peak power limited and the comm is average power limited.

3) By comparison, the dual-mode TWT could be considered with two cathodes, one for radar and one for comm. Both systems would then be average power limited and the radar could transmit a much higher peak power. This implementation requires a dual power supply and more support equipment.

C. Frequency Diversity

In most cases, under the assumption of a Swerling I target model, it will be possible to maintain performance requirements without employing frequency diversity in the search mode of radar operation. In view of the following comments, however, some frequency diversity is going to be required.

1) The glint effects at short ranges will be sufficient so that angle tracking will not be able to be maintained within specifications without frequency diversity. Frequency diversity is very effective in reducing those glint effects.

2) The class of targets that are anticipated remains unknown. To offset the deep fades in RCS of many targets at a fixed frequency as a function of aspect angle, frequency diversity should be employed. In the performance section of this report, we consider the effect of frequency diversity for 2, 3, and 5 frequencies.

3) There are guard spaces in the TDRS spectrum which could be used by the Ku-band radar with frequency diversity. Whether they are used, or if the radar frequencies are placed on the edge of the TDRS band, the performance will be essentially unchanged so long as the bandwidth of the TDRS (comm) spectrum and that of the radar remain within the bandwidth of the paramp. Otherwise separate RF receiver amplifiers will have to be employed, thereby reducing the commonality of the integrated system.

4) The width of the frequency spacing must be considered. This is discussed in [8-9]. In summary, for a two point target with an orientation as shown in Figure 2, if the shift in frequencies of two adjacent frequencies in a frequency diversity radar is such that at one frequency the returns add, and at the other they cancel, then

$$\Delta f_c = \frac{c}{4D \cos \alpha} \qquad (1)$$

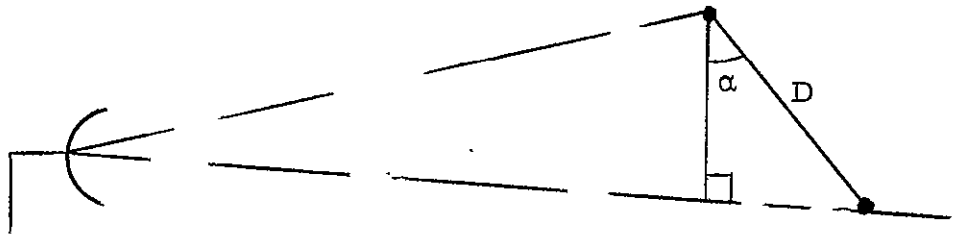

Figure 2. Two Point Target Orientation.

In (1), c is the speed of light and D and α are as defined in Fig. 2.

A couple of examples are:

D cos α Meters	Δf MHz
1	75
10	7.5
100	0.75

The guard spaces in the TDRS spectrum are separated by approximately 70 MHz. Therefore if D cos α is as small as 1 meter, frequency diversity with a Δf_c of 70 MHz would remove the nulls in the RCS.

8) A typical target for Shuttle is the Agena, although a wide variety of target sizes and shapes is anticipated.

9) The RCS of $\overline{\sigma} = 1\ m^2$ assumes a linear polarization.

10) Scintillation occurs slowly with one frequency. This may cause problems, but is overcome by more than one RF frequency.

D. Oscillator Stability

The choice of bandwidth of the doppler filters must take into account the short term stabilities of the oscillators that are to be used. Reference [1-3] discuss oscillator stability, wherein it is pointed out that in the Ku-band oscillators exist with a frequency spread of:

RMS Percent Bandwidth:

1 part in 10^{10} in .001 sec

1 part in 10^{12} in 1 sec

This is negligibly small with respect to the doppler frequency shifts that are anticipated and is therefore not taken into account henceforth.

E. Polarization

1) For most radars, linear polarization is used because it is easier to implement and has more desirable target RCS characteristics.

2) Satellites and deep space communication systems mostly use circular polarization in order to overcome the effects of the Faraday rotation in the terrestrial ionosphere. TDRS is no exception, as it transmits and receives RCP. It actually is an elliptically shaped polarization.

3) A basic problem in the choice of a receiver polarization for the radar is that there will always be an orthogonal polarization to which it is blind. A radar could independently receive two polarizations, such as horizontal and vertical simultaneously, in order to receive all the echo energy. These could not be added coherently, however.

4) In general measurements show that with linear polarization, the radar skin tracking echo signal is dominantly the same polarization as the transmitter polarization, and the cross-polarized component caused by depolarization due to the complex shaped target is typically 7-20 dB lower [5, 8], depending on the aspect angle.

5) With circular polarization, for any one sense of transmitter polarization, the echo signal is typically equally divided between RCP and LCP. The opposite sense dominates somewhat for typical aircraft-type targets [5, 8].

6) The total echo signal returned from a target is very dependent on its orientation, i.e., a dipole.

7) If the Ku-band comm receiver is linearly polarized it would nominally suffer a 3 dB polarization loss, since the TDRS is circularly polarized. Since the TDRS is elliptically polarized, the worst case loss is 4.4 dB, 3 dB because it is circular and an additional 1.4 dB when on the smaller axis of the elliptical polarization.

We conclude the comm must therefore be circular in polarization since the comm does not have the safety margin to withstand an additional 4 dB loss. The comm polarization loss with a circularly polarized horn is 0.5 dB, which accounts for the difference between the elliptical wave and the circular horn.

8) The performance computations in this report are carried out for both a linearly and circularly polarized horn. With linear polarization, the polarization loss is assumed negligible. With the circularly polarized horn, the polarization loss is set at 4 dB which is considered a representative worst case.

9) Independent of which polarization is employed, there exist targets and target orientations where the polarization loss is infinite. On the average however, linear polarization is certainly the more satisfactory choice.

10) With linear polarization for the radar and circular polarization for the comm then a dual feed is required which requires more hardware. There then is an insertion loss due to the dual feed as well as a drop in antenna gain because both feeds cannot be exactly at the focal point of the antenna. The drop in antenna gain is expected to not be more than 1 dB.

11) Autonetics is developing a dual polarization single feed horn system with both linear and circular polarization capability.* If such a horn can be space qualified, and if the polarization switching is electromagnetic (mechanical polarization switching runs the risk of getting stuck in one mode or inbetween), then a linear polarization for the radar is certainly the recommended choice. Such a dual horn must also have the monopulse capability.

*Ref. B. McQuillan at Rockwell.

There are other dual horn developments in progress. The antenna and insertion losses are expected to be similar to those quoted above.

12) The RCS of an object in general depends on:

i) Frequency of incident radiation.

ii) Polarization of XTMR.

iii) Polarization of RCVR.

iv) Target orientation.

v) Material of the target.

III. Performance Computations

Many of the parameters used in this performance evaluation have been previously specified or previously justified in [7].

The scan coverage is $40^{\circ} \times 40^{\circ}$.

The total time to illuminate the volume is 60 sec.

Allowance for scan reversal = 20%

Therefore, total scan time $\triangleq T_T = 48$ sec.

Time per complete scan = $T_s \triangleq T_T/K$ where K is the number of scans.

We consider K = 1, 2, and 3 scans. We use the notation in Addendum A on antenna scan patterns. The optimal scan overlap, based on the analysis performed in Addendum A is

$$\Delta_s = 0.4 \quad (40\%)$$

The number of scan lines/scan, N_s is

$$N_s \triangleq \frac{A_{EL}}{\theta_B[1-\Delta_s]} = \frac{40^{\circ}}{2.76^{\circ}(1-0.4)} = 24 . \qquad (2)$$

Table I summarizes additional antenna scan parameters based on a scan overlap of 40%. In Table I,

T_L = time per scan line.

V_s = antenna scan velocity in degrees/sec.

t_d = spatial dwell time along antenna boresight.

$\tilde{t}_d$ = spatial dwell time along edge of nonoverlapping portion of the scan coverage as shown in Figure A-3 in Addendum A.

TABLE I

ANTENNA SCAN PARAMETERS

	K = 1	K = 2	K = 3
T_s	48 sec	24 sec	16 sec
T_L	2 sec	1 sec	.667 sec
V_s	20 deg/sec	40 deg/sec	60 deg/sec
t_d	138 msec	69 msec	46 msec
$\tilde{t}_d$	110.4 msec	55.2 msec	36.8 msec

This is the worst case dwell time. It is this dwell time that is maximized in Addendum A, and is the dwell time which will be used in the ensuing computations.

With 3 scans, the antenna velocity, V_s, is relatively high. The comparison does however indicate the trade-off with number of scans.

Scan Alignment Loss. Under the assumption of a worst position target location, there exists a worst case scan alignment loss (see Addendum A) given by

$$S.A.L. = \left(\frac{\sin[(\theta'_B/2)(1-\Delta_s)]}{[(\theta'_B/2)(1-\Delta_s)]}\right)^2 \Bigg|_{\Delta_s=0.4} = .7882 = -1.03 \text{ dB} \tag{3}$$

where $\theta'_B/2$ is defined as the angle where $(\sin\theta/\theta)^2 = \frac{1}{2}$, namely

$$[\sin\theta/\theta]^2 \Big|_{\theta'_B/2} = \tfrac{1}{2} \tag{4}$$

This results in

$$\theta'_B/2 = 1.3915 \text{ radians} = 79.727 \text{ deg.} \qquad (5)$$

This is the scan alignment loss each way, so that the total scan alignment loss is 2.06 dB. The computations are based on the expressions in Addendum A.

Lateral Scan Loss. The lateral scan loss along the worst case path of the target across the antenna pattern is

$$\text{L.S.L.} = \int_0^{\tilde{\theta}_B/2} \left[\frac{\sin\left(\frac{(\theta'_B/2)}{(\theta_B/2)}\,\theta\right)}{\left(\frac{(\theta'_B/2)}{(\theta_B/2)}\right)} \right]^2 \frac{d\theta}{\tilde{\theta}_B/2} \qquad (6)$$

where $\tilde{\theta}_B = \theta_B \sqrt{\Delta_s(2-\Delta_s)}$ is pictorially shown in Figure A-3. The lateral scan loss is computed to be

$$\text{L.S.L.} = 0.8747 = -0.58 \text{ dB}$$

on transmit and receive. The total L.S.L. is 1.16 dB.

Doppler Filter Loss. There will be in general some loss due to the fact the received tone from the target is not in the center of one of the Doppler filters. We again assume worst case, and assume the received signal is midway between the two adjacent filters, as shown in Figure 3. Assuming a first order filter, the signal loss is given by

$$|H(f)|^2 = \frac{1}{1 + \left(\frac{f}{f_{3\,dB}}\right)^2} \Bigg|_{f=f_{3\,dB}/2} = \frac{4}{5} = -0.97 \text{ dB} \qquad (7)$$

Duty Factor. Based on the optimization performed in [7], the optimal choice of transmitter duty factor, under the peak power limited assumption, is

$$d_t = 0.625. \tag{8}$$

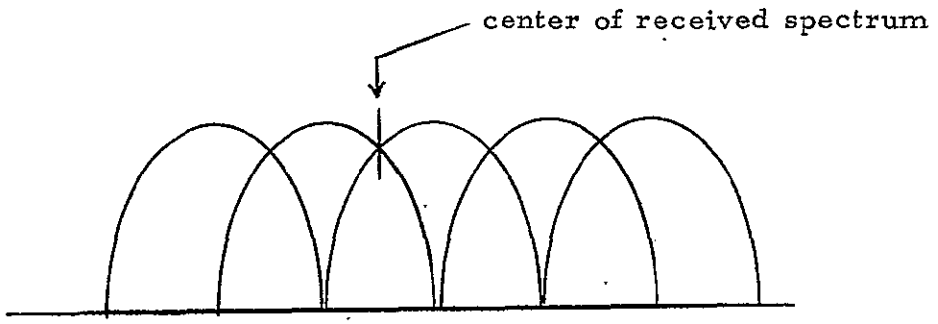

Figure 3. Bank of Doppler Filters.

Probability of Detection. The cumulative probability of detection is specified at $P_c = 0.99$. Using the approximation

$$P_c = 1 - (1-P_d)^K \tag{9}$$

the probability of detection per scan, P_d, is given by

for one scan $K = 1$ $P_d = 0.99$

for two scans $K = 2$ $P_d = 0.90$

for three scans $K = 3$ $P_d = 0.785$

Doppler Filters. The doppler filters must span a range of

$$\Delta f_d = 4574 \text{ Hz}$$

Based on a 100% overlap, the number of doppler filters required is given by

$$N_d = \Delta f_d / f_{3\,dB} \tag{10}$$

where $f_{3\,dB}$ is the one-sided 3 dB filter bandwidth. The two-sided 3 dB bandwidth is

$$B_d = 2f_{3\,dB} + f_{OSC} \tag{11}$$

where by f_{OSC} is meant the increase in doppler bandwidth due to any short term oscillator instabilities. Since all of the oscillators are assumed to be locked together, i.e. all coherently related, all frequencies will drift together, As a result no stability problem is anticipated, as was commented on in the last section. The 29 MHz oscillator may be a free running oscillator, but that is at a sufficiently low frequency, that stability problems will not arise since a 1 Hz stability is only one part in 30×10^6.

In Table II, for each choice of number of scans, and number of frequencies in the frequency diversity, the number of doppler filters, their bandwidth, and the frequency dwell time t_f are listed. The frequency dwell time was chosen so that each frequency is used once during each spatial dwell time, where we are using the spatial dwell time at the edge of the nonoverlapping position of the scan coverage.

In Table II, the first number after N_f is the number of doppler filters required. The second number is the next larger number which is equal to 2 raised to an integer power. This is the number of doppler filters which would be built if a digital implementation is employed.

TABLE II

DOPPLER FILTER PARAMETERS

	Frequency Diversity			
	1 Freq.	2 Freq.	3 Freq.	5 Freq.
K = 1 $\tilde{t}_d$ = 110msec	t_f = 110 msec $f_{3\,dB}$ = 9.05 Hz B_d = 20 Hz N_f = 505/512	t_f = 55 msec $f_{3\,dB}$ = 18.2 Hz B_d = 40 Hz N_f = 254/256	t_f = 37 msec $f_{3\,dB}$ = 27.3 Hz B_d = 60 Hz N_f = 168/256	t_f = 22 msec $f_{3\,dB}$ = 45.6 Hz B_d = 95 Hz N_f = 101/128
K = 2 $\tilde{t}_d$ = 55msec	t_f = 55 msec $f_{3\,dB}$ = 18.2 Hz B_d = 40 Hz N_f = 254/256	t_f = 27.5 msec $f_{3\,dB}$ = 36.4 Hz B_d = 75 Hz N_f = 126/128	t_f = 18.3 msec $f_{3\,dB}$ = 55 Hz B_d = 115 Hz N_f = 84/128	t_f = 11 msec $f_{3\,dB}$ = 91 Hz B_d = 190 Hz N_f = 50/64
K = 3 $\tilde{t}_d$ = 37msec	t_f = 37 msec $f_{3\,dB}$ = 27.3 Hz B_d = 60 Hz N_f = 168/256	t_f = 19 msec $f_{3\,dB}$ = 54 Hz B_d = 115 Hz N_f = 85/128	t_f = 12 msec $f_{3\,dB}$ = 82 Hz B_d = 170 Hz N_f = 56/64	t_f = 7.4 msec $f_{3\,dB}$ = 135 Hz B_d = 280 Hz N_f = 34/64

False Alarm Probability. The false alarm rate is to be no more than one per hour. The false alarm probability is approximately given by

$$F.A.P. = \alpha = 1/N_d$$

where $$N_d = 3600 N_f / \tilde{t}_d \qquad (12)$$

is the total number of dwells per hour. Table III gives the false alarm probability and approximate false alarm number as a function of the number of RF frequencies.

TABLE III

FALSE ALARM PROBABILITY

No. of RF Frequencies	α = F.A.P.	False Alarm Number
1	6×10^{-8}	$n' \approx 10^7$
2	1.2×10^{-7}	$n' \approx 6 \times 10^6$
3	1.8×10^{-7}	$n' \approx 4 \times 10^6$
5	3×10^{-7}	$n' \approx 2 \times 10^6$

Eclipsing Loss. From [7], the average eclipsing loss for $d_t = 0.625$ is

$$\overline{E.L.} = 0.18 = 7.45 \text{ dB} \qquad (13)$$

Choices of sets of PRF's whose eclipsing loss is approximately 7.5 dB in the range of 8-12 N. Mi. have been found.

Frequency Diversity Gain. In order to obtain a measure of the improvement in performance as the result of increasing the number of scans and the number of RF frequencies, the required peak-signal-energy-to-noise-spectral-density, $\overline{R}_p$, is shown in Table IV, along with the amount of improvement. In Table IV,

$$\overline{R}_p \triangleq \frac{2\overline{A}^2 \mathcal{E}_p}{N_0} \tag{14}$$

where $\overline{A}^2$ is assumed 1. The values are taken from [6]. The values in Table IV assume that a coherence time can be maintained equal to the spatial dwell time. These values also assume an ideal receiver.

System Performance. The required average power under a variety of conditions is determined. The radar equation is

$$\overline{R}_p = \frac{2\overline{A}^2 \mathcal{E}_p}{N_0'} = \frac{[G^2 \overline{\sigma} \lambda^2][2d_t^2][P_p \tau_t p]}{[(4\pi)^3 R^4][kT_s d_r][L]} \tag{15}$$

where the parameter definitions and values are as follows:

G = antenna gain = 35.4 dB

$\overline{\sigma}$ = average radar cross section = $1m^2$ = 0 dB

λ = (for 15 GHz) = 0.02 m = -16.99 dB

$$[G^2 \overline{\sigma} \lambda^2] = \underline{36.82 \text{ dB}} \tag{16}$$

d_t = transmitter duty factor = 0.625

$$[2d_t^2] = \underline{-1.07 \text{ dB}} \tag{17}$$

$(4\pi)^3 = 1984.4 = 32.98$ dB

R = 11 N.Mi. = 20,383 m

$$[(4\pi)^3 R^4] = \underline{205.4 \text{ dB}} \tag{18}$$

TABLE IV

FREQUENCY DIVERSITY GAIN
ΔR_p = NET GAIN PER PULSE

	1 Freq.	2 Freq.	3 Freq.	6 Freq.
K = 1 one scan	$P_d = 0.99$ $n' \approx 10^7$ swerling I N = 1 $\overline{R}_p = 36.5$ dB $\Delta R_p = 0$	$P_d = 0.99$ $n' \approx 6 \times 10^6$ swerling II N = 2 $\overline{R}_p = 24$ dB $\Delta R_p = 9.5$ dB	$P_d = 0.99$ $n' \approx 4 \times 10^6$ swerling II N = 3 $\overline{R}_p = 19.7$ dB $\Delta R_p = 12.0$ dB	$P_d = 0.99$ $n' \approx 2 \times 10^6$ swerling II N = 6 $\overline{R}_p = 14.5$ dB $\Delta R_p = 14.2$ dB
K = 2 two scans	$P_d = 0.90$ $n' \approx 10^7$ swerling I N = 1 $\overline{R}_p = 24$ dB $\Delta R_p = 0$	$P_d = 0.90$ $n' \approx 6 \times 10^6$ swerling II N = 2 $\overline{R}_p = 18.5$ dB $\Delta R_p = 2.3$ dB	$P_d = 0.90$ $n' \approx 4 \times 10^6$ swerling II N = 3 $\overline{R}_p = 15.7$ dB $\Delta R_p = 3.5$ dB	$P_d = 0.90$ $n' \approx 2 \times 10^6$ swerling II N = 6 $\overline{R}_p = 12$ dB $\Delta R_p = 4.2$ dB
K = 3 three scans	$P_d = 0.785$ $n' \approx 10^7$ swerling I N = 1 $\overline{R}_p = 21.3$ dB $\Delta R_p = 0$	$P_d = 0.785$ $n' \approx 6 \times 10^6$ swerling II N = 2 $\overline{R}_p = 16.3$ dB $\Delta R_p = 2$ dB	$P_d = 0.785$ $n' \approx 4 \times 10^6$ swerling II N = 3 $\overline{R}_p = 14$ dB $\Delta R_p = 2.5$ dB	$P_d = 0.785$ $n' \approx 2 \times 10^6$ swerling II N = 6 $\overline{R}_p = 10.7$ dB $\Delta R_p = 2.8$ dB

Eleven nautical miles is chosen instead of 12, since the lock-up time for range tones in a coherent radar is negligible with respect to one minute.

$$N_0 = kT_s, \quad N_0' = N_0 d_r \tag{19}$$

where

$d_r = 1 - d_t$ = receiver duty factor = 0.375 = -4.26 dB

k = Boltzman's constant = 1.38×10^{-23} joules/$^\circ$K = -228.6 dB

T_s = system noise temperature.

In determining the system noise temperature, we consider an M-component cascade

$$T_s = T_a + \sum_{i=1}^{M} T_{ei}/G_i \tag{20}$$

where

T_a = antenna noise temperature

T_{ei} = effective input noise temperature of the i^{th} component

G_i = available gain of the system between its input terminals and the input terminals of the i^{th} cascaded component.

If we set

T_r = transmission line noise temp with losses L_i, then

we simplify (20) to

$$T_s = T_a + T_{paramp} + T_r L_r \tag{21}$$

The noise figure of the paramp is approximately 3 dB. Therefore

$$T_{paramp} = (F-1)T_0 \approx 290^{\circ}K \tag{22}$$

where $T_0 = 290^{\circ}$.

The antenna noise temperature can be determined by noting first that the noise temperature of an idealized antenna (lossless, no earth-directed sidelobes) at 15 GHz, and with an antenna beam elevation angle of 90° (i.e. pointed skyward) is approximately [see [5], page 2-31, 2-32]

$$T'_a = 7^{\circ}K \tag{23}$$

A beam elevation angle of 90° was chosen because the shuttle's motion is such that it is pointing skyward most of the time, particularly during the initial detection operation of targets, that is it approaches targets from below.

The approximation suggested in [5] to transform ideal antenna noise temperature to one with losses is

$$T_a = 0.876T'_a + 36 \tag{24}$$

Upon substitution $T_a = 42^{\circ}K$. This assumes no additional Galactic noise. If an additional $23^{\circ}K$ is inserted to account for the transmission line losses in (21), then

$$T_s = 42^{\circ}K + 290^{\circ}K + 25^{\circ}K = 355^{\circ}K = 25.5 \text{ dB} \tag{25}$$

Then

$$N_0 = \underline{-207.36 \text{ dB}} \tag{26}$$

Losses. The RF losses from cables antenna-port, switches, VSWR mismatches, insertion losses, etc., have been set at 3.5 dB. Of these the insertion loss of approximately 1.5 dB is considered to be the largest. We list the losses as follows:

RF Losses	3.5 dB
p = Polarization {circular	4 dB
p = Polarization {linear	0 dB
L.S.L. = Lateral Scan Loss	1.16 dB
S.A.L. - Scan Alignment Loss	2.06 dB
E.L. = Average eclipsing Loss ($d_t = 0.625$)	7.45 dB
Doppler Mismatch	0.97 dB
Additional Post Detection Integration Loss	1.0 dB
Total Losses {Linear =	16.14 dB = L
Total Losses {Circular =	20.14 dB

Denoting the losses under the linear polarization assumption as L, and the polarization loss as p, then (15) can be written as

$$P_p = \overline{R}_p\Big|_{dB} - \tau_t\Big|_{dB} - p\Big|_{dB} - 21.57 \qquad (27)$$

where

P_p is the peak power per pulse

τ_t is the RF frequency dwell time after the center line filter at the input to the detector

p is the polarization loss.

In Table V, the required average power and peak power are tabulated for K = 1, 2, 3 scans, and 1, 2, 3 and 6 RF frequencies. Ref. [6] has performance curves for 6 pulses, and not 5. It is anticipated that the difference between 6 and 5 is not very great, so that the trade-off that is being shown is clearly established.

Let us assume that the average power requirement of the comm is approximately 40 watts, and that the peak power of the radar (in the coherent system) is not to exceed the comm requirement. It then becomes clear which cases qualify by inspection of Table V. For linear polarization, the choices are greater. It is clear that circular polarization cannot be used unless at least three frequencies of diversity are used, and five frequencies will not provide a substantial safety margin. With circular polarization and five frequencies of diversity, either one scan or two scans will provide a satisfactory design. With linear polarization, it would be possible to eliminate frequency diversity in the search mode. Because of the necessity of frequency diversity for angle tracking, frequency diversity with three frequencies is proposed. This provides over 3 dB of safety margin regardless of the number of scans chosen.

In some of the cases, the required peak power as a function of the number of scans has a minimum value at K=2 scans.

The optimal choice of number of scans is dependent on the choice of frequency diversity and vice versa. The optimal choice of the combination is case 4, namely, one scan and five frequencies of diversity. In order to obtain some system simplicity, if the number of frequencies

TABLE V

POWER REQUIREMENTS FOR COHERENT PULSED
DOPPLER CENTER LINE RADAR

Case	Number of Scans	Number of RF Freq.	Polarization	R dB	$\bar{R}_p$ dB	Freq Dwell Time τ_t msec	τ_t dB	P_p dB	P_p Watts	P_{avg} Watts
1	1	1	L	0	36.5	110	- 9.59	24.52	283.1	177
2	1	2	L	0	24	55	-12.60	15.03	31.8	19.9
3	1	3	L	0	19.7	37	-14.32	12.45	17.6	11.0
4*	1	5 (6)	L	0	14.5	22	-16.58	9.51	8.9	5.6
5	2	1	L	0	24	55	-12.60	15.03	31.8	19.9
6	2	2	L	0	18.5	27.5	-15.61	12.54	17.9	11.2
7	2	3	L	0	15.7	18.3	-17.38	11.51	14.2	8.8
8*	2	5 (6)	L	0	12	11	-19.59	10.02	10	6.3
9	3	1	L	0	21.3	37	-14.32	14.05	25.4	15.9
10	3	2	L	0	16.3	19	-17.21	11.94	15.6	9.8
11	3	3	L	0	14	12	-19.21	11.64	14.6	9.1
12*	3	5 (6)	L	0	10.7	7.4	-21.31	10.44	11.1	6.9
13	1	1	C	4	36.5	110	- 9.59	28.52	711.	445.
14	1	2	C	4	24	55	-12.60	19.03	80.	50.
15	1	3	C	4	19.7	37	-14.32	16.45	44.2	27.6
16*	1	5 (6)	C	4	14.5	22	-16.58	13.51	22.4	14.0
17	2	1	C	4	24	55	-12.60	19.03	80.	50.0
18	2	2	C	4	18.5	27.5	-15.61	16.54	45.1	28.2
19	2	3	C	4	15.7	18.3	-17.38	15.51	35.6	22.2
20*	2	5 (6)	C	4	12	11	-19.59	14.02	25.2	15.8
21	3	1	C	4	21.3	37	-14.32	18.05	64.8	39.9
22	3	2	C	4	16.3	19	-17.21	15.94	39.3	24.6
23	3	3	C	4	14	12	-19.21	15.64	36.6	22.9
24*	3	5 (6)	C	4	10.7	7.4	-21.31	14.44	27.8	17.4

*Calculation based on six individual RF frequencies.

of diversity is reduced to three, then the optimal choice is two scans.

One can see, however, that there is not an extensive variation in the peak power requirement over all of the cases listed above, and any of these would make a satisfactory design.

If a low PRF is used so that eclipsing loss is essentially eliminated in the range of 10-15 nautical miles, then a safety margin of over 7 dB can be gained. When this is the case, there is the probability of detecting the incorrect line in the coherent spectrum. If the transition from detection to tracking can be smoothly carried out, however, then that may be the most satisfactory implementation of the coherent radar.

IV. Noncoherent Ku-Band Pulsed Radar in the Search Mode

In this section, we consider the performance of a noncoherent Ku-band pulsed radar in the search mode of operation. As many of the system parameters as possible are kept the same as in the previous sections so as to provide a satisfactory comparison.

We shall consider frequency diversity and a fluctuating Swerling I target, as in the previous section. When considering frequency diversity with a pulsed radar, the question arises as to the method of obtaining the necessary frequency agility. There are at least three methods:

i) Mechanical Spin Tuning. This is old technology and much too slow for the kind of frequency diversity required.

ii) Voltage-Tunable Magnetron. The bandwidth is attainable by this method but this method is power limited as a pulsed radar. It is more commonly used in CW radars.

iii) Injection Locking. This method consists of priming the magnetron at a given frequency, then pulsing it. This will provide the necessary frequency diversity, but it is very inefficient.

These methods are discussed in Skolnik [5, Ch. 7]. The present-day methods of attaining a 3 percent bandwidth frequency diversity for a pulsed radar are presently being investigated. There is the additional consideration of insuring that the paramp has adequate protection from the magnetron both in the transmit and receive mode of operation.

In Table VI, the parameters of the pulse radar are listed. The 3 dB IF bandwidth is chosen as the reciprocal of the pulse width.

TABLE VI

PULSE RADAR PARAMETERS

Pulse width	0.4 μsec
IF bandwidth	2.5 MHz
PRF	2500/sec
Pulse repetition time	400 μsec
Transmitter duty factor	0.001

In Addendum B, we analyze the performance of the noncoherent pulse radar and arrive at the following results:

Case A: $K = 1$ scan, $\lambda = 1.00$, $\lambda = 0$ dB

Case B: $K = 2$ scans, $\lambda = 1.18$, $\lambda = 0.72$ dB

Case C: $K = 3$ scans, $\lambda = 1.29$, $\lambda = 1.11$ dB

where

$$\lambda \triangleq \frac{P_{pr}}{\sigma_n^2} \quad . \tag{28}$$

In (28), P_{pr} is the peak received signal power at the input to the detector, and

$$\sigma_n^2 = \frac{N_o B_{if}}{2} \tag{29}$$

is the average noise power; $N_o = k T_s$ is the noise spectral density, and B_{if} is the IF bandwidth.

The radar equation that is used to determine the required transmitter peak power is

$$\lambda = \frac{P_{pr}}{\sigma_n^2} = \frac{\left[G^2 \bar{\sigma} \lambda^2\right] P_p \; p \; G_D}{\left[(4\pi)^3 R^4\right]\left[\frac{k T_s B_{if}}{2}\right] L \; L_F} \quad , \tag{30}$$

where the parameters are as previously described with the additions that

G_D is the gain due to frequency diversity

L_F is the loss due to the fluctuating target.

From the previous section, the consistent values are:

$$\left[G^2 \bar{\sigma} \lambda^2\right] = 36.82 \text{ dB} \quad . \tag{31}$$

The range is now set at 12 nautical miles because of the time required to establish range rate estimates from range estimates in the noncoherent system.

With R = 12 n.mi.,

$$(4\pi)^3 R^4 = 206.86 \text{ dB} \tag{32}$$

$$B_{if} = 2.5 \text{ MHz} = 63.98 \text{ dB}$$

$$k T_s = -203.1 \text{ dB}$$

$$\frac{k T_s B_{if}}{2} = -142.1 \text{ dB} \quad . \tag{33}$$

Losses

RF	3.5 dB
L.S.L.	1.16
S.A.L.	2.06
Receiver mismatch	1.00
Total losses	7.72 dB

Upon substitution into (30), the peak power (in dB) is given by

$$P_p = \lambda + L_F - G_D - p + 35.64 \quad . \tag{34}$$

The values for frequency diversity gain are listed in Table IV. The fluctuating target loss is essentially independent of the number of pulses integrated, but very dependent on the probability of detection per scan. The values are taken from DiFranco and Rubin [6] and are shown in Table VII.

In Table VII, the cases are numbered in the same way as in Table V. For a given case number, the number of scans, the number of RF frequencies of diversity, the polarization, and the frequency dwell time are the same in both Table V and Table VII.

Comparison of Tables V and VII shows that the average power requirement for the coherent radar is uniformly better than for the noncoherent radar, but not by a great margin for the cases of most interest. The coherent system has a larger number of components integrated with the comm than does the noncoherent. The magnetron XTMR must also have its necessary accessories such as power supply and cooling equipment, which also would not be integrated with the comm. It is therefore anticipated that the total weight of the radar/comm will be less with the coherent radar.

For all of these reasons, the coherent radar appears the more satisfactory choice and is therefore our recommendation. In the discussion at the end of section III, several satisfactory cases are shown

TABLE VII

POWER REQUIREMENTS FOR NONCOHERENT PULSED RADAR

Case	N Number of Pulses/ Frequency	Net Frequency Diversity Gain G_D, dB	Fluctuating Target Loss L_F, dB	λ	λ dB	Polarization p dB	P_p dB	P_p kw	P_{avg} w
1	275	0	17.8	1.0	0	0	53.44	220	220
2	137	9.5	17.8	1.0	0	0	43.94	24.7	24.7
3	92	12.	17.8	1.0	0	0	41.44	13.9	13.9
4	55	14.2	17.8	1.0	0	0	39.24	8.4	8.4
5	137	0	8.5	1.18	0.72	0	44.86	30.6	30.6
6	68	2.3	8.5	1.18	0.72	0	42.56	18.0	18.0
7	45	3.5	8.5	1.18	0.72	0	41.36	13.7	13.7
8	27	4.2	8.5	1.18	0.72	0	40.7	11.6	11.6
9	92	0	5.2	1.29	1.11	0	41.95	15.7	15.7
10	47	2	5.2	1.29	1.11	0	39.95	9.9	9.9
11	30	2.5	5.2	1.29	1.11	0	39.45	8.8	8.8
12	18	2.8	5.2	1.29	1.11	0	39.15	8.2	8.2
13	275	0	17.8	1.0	0	4	57.44	554.	554.
14	137	9.5	17.8	1.0	0	4	47.94	62.2	62.2
15	92	12.0	17.8	1.0	0	4	45.44	35	35
16	55	14.2	17.8	1.0	0	4	43.24	21.1	21.1
17	137	0	8.5	1.18	0.72	4	48.86	76.9	76.9
18	68	2.3	8.5	1.18	0.72	4	46.56	45.3	45.3
19	45	3.5	8.5	1.18	0.72	4	45.36	34.4	34.4
20	27	4.2	8.5	1.18	0.72	4	44.7	29.5	29.5
21	92	0	5.2	1.29	1.11	4	45.95	39.4	39.4
22	47	2	5.2	1.29	1.11	4	43.95	24.8	24.8
23	30	2.5	5.2	1.29	1.11	4	43.45	22.1	22.1
24	18	2.8	5.2	1.29	1.11	4	43.15	20.6	20.6

to provide satisfactory operation with a safety margin of near 6 dB with respect to an average power requirement of 40 watts for comm.

V. Short Range Considerations

In this section, a sequence of comments are presented concerning the operation of the radar at short range in station keeping.

1. To protect the paramp, the T/R switch may have to be partially engaged at short ranges. In addition, in order to protect the targets, the TWT will need to be reduced in power or bypassed. The latter will in all likelihood be the most satisfactory approach.

2. The scintillation and glint at short ranges will be very large. Therefore, frequency diversity will virtually be a requirement in order to substantially reduce these effects at short ranges.

3. At short ranges, station keeping may be more effectively performed via Doppler frequency instead of range. One of the reasons for this is the ratio of target size to range becomes so large that the definition of range and the capacity of measuring range comes into doubt. If this is the case, a coherent radar with Doppler tracking capability will be the more acceptable approach.

4. Approximately, the far field of an antenna starts at

$$R_{FF} \approx 2d^2/\lambda$$

where d is the diameter of the antenna. For a 20" dish,

$$R_{FF} \approx 25.8 \text{ m} = 85 \text{ feet.}$$

Station keeping at 100 feet is therefore close to the edge of the far field of the antenna.

ADDENDUM A

OPTIMAL CHOICE OF ANTENNA SCAN OVERLAP

In this appendix we consider the optimum choice of antenna scan overlap for a pencil beam antenna. Three different optimization criteria are considered which will be described in the sequel. The optimal choice of scan overlap is dependent on the optimization criterion used, but is independent of the size of the scan average, the total search time, and the antenna 3 dB beamwidth.

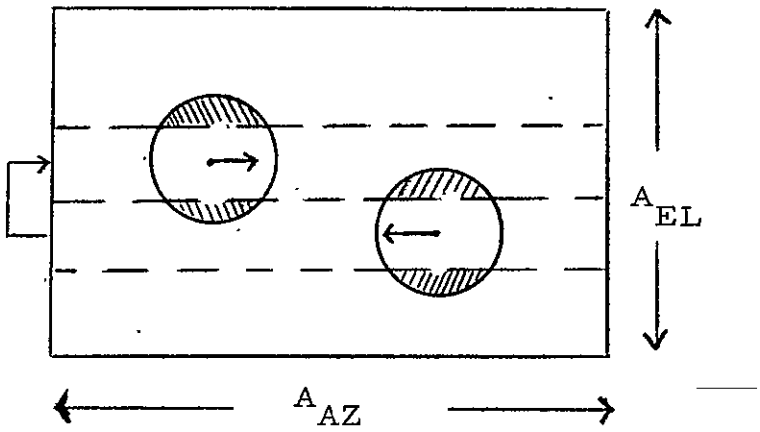

Figure A-1. Region of Scan Coverage and Indication of Scan Overlap.

We define the following:

$A_{AZ} \triangleq$ azimuth scan coverage in radians,

$A_{EL} \triangleq$ elevation scan coverage in radians,

$\theta_B \triangleq$ 3 dB antenna beamwidth in radians,

$T_T \triangleq$ total time to scan the entire column

$K \triangleq$ number of scans of the entire volume in the allotted time.

$T_s \triangleq \frac{T_T}{K}$ = time for each total scan.

In our example, the observation time is 60 sec, 20% of which is designated as set aside for scan reversal. Therefore $T_T = 48$ sec. Also, the antenna beamwidth is specified as $\theta_B = 2.76$ degrees = .04817 radians [4].

The scan overlap is defined as Δ_s, as shown in Figure A-2. When $\Delta_s = 0$, there is no scan overlap and when $\Delta_s = 1$, there is 100% scan overlap. Then we define

$$N_s \triangleq \text{number of scan lines/scan}$$

$$= \frac{A_{EL}}{\theta_B[1-\Delta_s]} \tag{A-1}$$

where horizontal scan lines are assumed. Also

$$T_L \triangleq \text{time per scan line} = \frac{T_s}{N_s}$$

$$V_s \triangleq \text{velocity of the scan} = \frac{A_{AZ}}{T_L}$$

We shall consider two different dwell times, one through the antenna boresight, and one through the edge of the nonoverlapping portion of

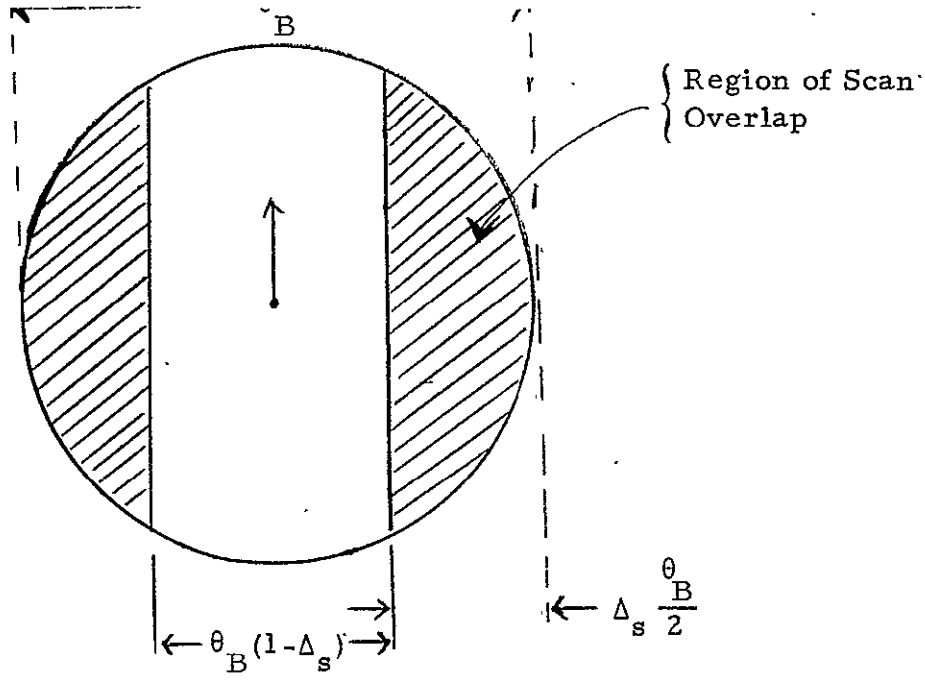

Figure A-2. Definition of Scan Overlap, $0 \leq \Delta_r \leq 1$.

the scan coverage as shown in Fig. A-3. We designate these dwell times as t_d and $\tilde{t}_d$ respectively. Then

$$t_d \triangleq \theta_B / V_s \tag{A-2}$$

and

$$\tilde{t}_d \triangleq \tilde{\theta}_B / V_s \tag{A-3}$$

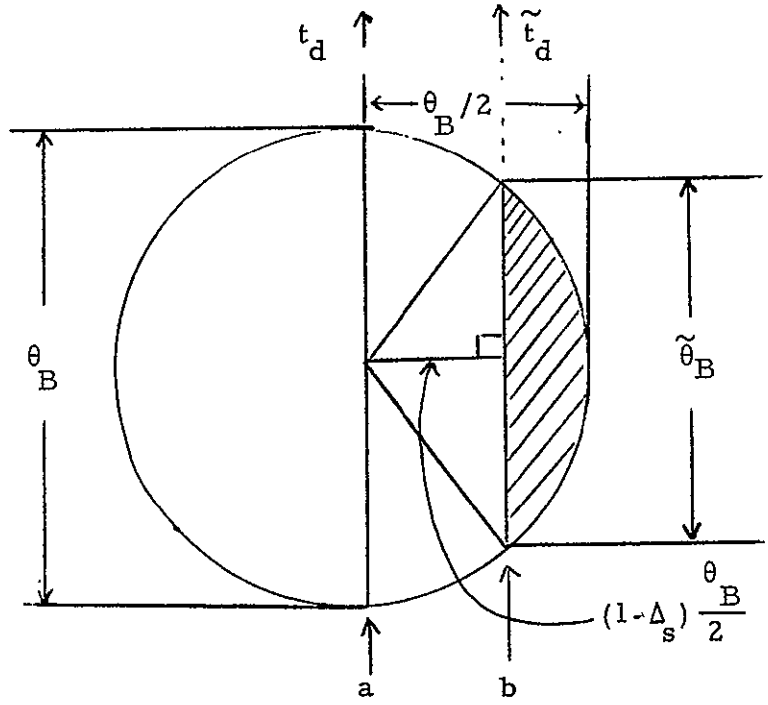

Figure A-3. Dwell Times.

where $\tilde{\theta}_B = \theta_B\sqrt{\Delta_s(2-\Delta_s)}$. The dwell time at boresight can be expressed as

$$t_d = \frac{\theta_B T_L}{A_{AZ}} = \frac{\theta_B T_s}{A_{AZ} N_s} = \frac{\theta_B^2 T_T(1-\Delta_s)}{A_{AZ} A_{EL} K} \tag{A-4}$$

In K scans, the total dwell time at boresight is

$$Kt_d = \frac{\theta_B^2 T_T(1-\Delta_s)}{A_{AZ} A_{EL}} \tag{A-5}$$

For the dwell time at the edge of the nonoverlapping coverage of the antenna beam, we have

$$\tilde{t}_d = \frac{\theta_B\sqrt{\Delta_s(2-\Delta_s)}}{A_{AZ}/T_L} = \frac{\theta_B^2(1-\Delta_s)\sqrt{\Delta_s(2-\Delta_s)}\, T_T}{A_{AZ} A_{EL} K} \tag{A-6}$$

The total dwell time in K scans in $K\tilde{t}_d$.

The first optimal choice of the scan overlap factor, Δ_s, is based on maximizing the total energy through the center of the antenna beam. This is marked as path "a" in Figure A-3. This corresponds to maximizing the dwell time when the target moves across the center of the beam. Under this criterion therefore, (not the most desirable optimization criterion) $\Delta_s = 0$, which can be seen by inspection of (A-5).

The second optimal choice of scan overlap is based on maximizing the received energy under the assumption that the target passes through the edge of the nonoverlapping portion of the scan coverage. This is marked as path "b" in Figure A-3.

The average power along this path is reduced by the factor

$$\left[\frac{\sin\left(\frac{\theta'_B/2}{\theta_B/2}\,\theta\right)}{\left(\frac{\theta'_B/2}{\theta_B/2}\,\theta\right)}\right]^2\Bigg|_{\theta=(1-\Delta_s)\theta_B/2} = \left[\frac{\sin(\theta'_B/2)(1-\Delta_s)}{(\theta'_B/2)(1-\Delta_s)}\right]^2 \tag{A-7}$$

by being on the edge of the nonoverlapped portion of the spectrum. The angle θ'_B is defined in radians as the angle such that

$$\left(\frac{\sin\theta}{\theta}\right)^2\Bigg|_{\theta=\theta'_B/2} = \tfrac{1}{2} \tag{A-8}$$

The power averaged along path b is then given by

$$\int_0^{\tilde{\theta}_B/2}\left[\frac{\sin\left(\frac{(\theta'_B/2)}{(\theta_B/2)}\,\theta\right)}{\frac{(\theta'_B/2)}{(\theta_B/2)}\,\theta}\right]^2 \frac{d\theta}{\tilde{\theta}_B/2} \tag{A-9}$$

The actual average power is the product of (A-9) and (A-7) which becomes

$$\tilde{P}_{avg} = \left[\frac{\sin[(\theta'_B/2)(1-\Delta_s)]}{(\theta'_B/2)(1-\Delta_s)}\right]^2 \int_0^{\sqrt{\Delta_s(2-\Delta_s)}}\left[\frac{\sin[(\theta'_B/2)\gamma]}{(\theta'_B/2)\gamma}\right]^2 \frac{d\gamma}{\sqrt{\Delta_s(2-\Delta_s)}} \tag{A-10}$$

The energy received in K scans is

$$\mathcal{E}_2 \triangleq K\tilde{t}_d\,\tilde{P}_{avg}$$

$$= \left[\frac{\theta_B^2 T_T(1-\Delta_s)\sqrt{\Delta_s(2-\Delta_s)}}{A_{AZ}A_{EL}}\right]\left[\frac{\sin[(\theta'_B/2)(1-\Delta_s)]}{(\theta'_B/2)(1-\Delta_s)}\right]^2 \int_0^{\sqrt{\Delta_s(2-\Delta_s)}} \frac{\sin(\theta'_B\gamma/2)}{(\theta'_B\gamma/2)} \frac{d\gamma}{\sqrt{\Delta_s(2-\Delta_s)}} \tag{A-11}$$

which can be slightly simplified to give

$$\overline{\delta}_2 = \left[\frac{\theta_B^2 T_T}{A_{AZ} A_{EL}}\right]\left\{(1-\Delta_s)\left[\frac{\sin[(\theta'_B/2)(1-\Delta_s)]}{(\theta'_B/2)(1-\Delta_s)}\right]^2 \int_0^{\sqrt{\Delta_s(2-\Delta_s)}} \left[\frac{\sin(\theta'_B\gamma/2)}{(\theta'_B\gamma/2)}\right]^2 d\gamma\right\} \qquad 0 \le \Delta_s \le 1 \qquad \text{(A-12)}$$

We see that

$$\lim_{\Delta_s \to 0} \delta_2 = \lim_{\Delta_s \to 1} \delta_2 = 0$$

Observation of (A-12) indicates that optimal setting of scan overlap is independent of θ_B, T_T, A_{AZ}, and A_{EL}. A plot of the factor in { } in (A-12) is shown in Figure A-4, from which it can be seen that the optimal choices of Δ_s under this second optimization criterion is

$$\boxed{\Delta_s\Big|_{opt} = 0.40} \qquad \text{(A-13)}$$

This appears to be the most desirable optimization criterion to use. It is the maxi-min approach, since it maximizes the energy return when the target is located in the most undesirable position.

The third optimal choice for Δ_s is to base the choice on maximizing the average energy over the entire region of nonoverlapping scan coverage. The average power per scan in this case is given by

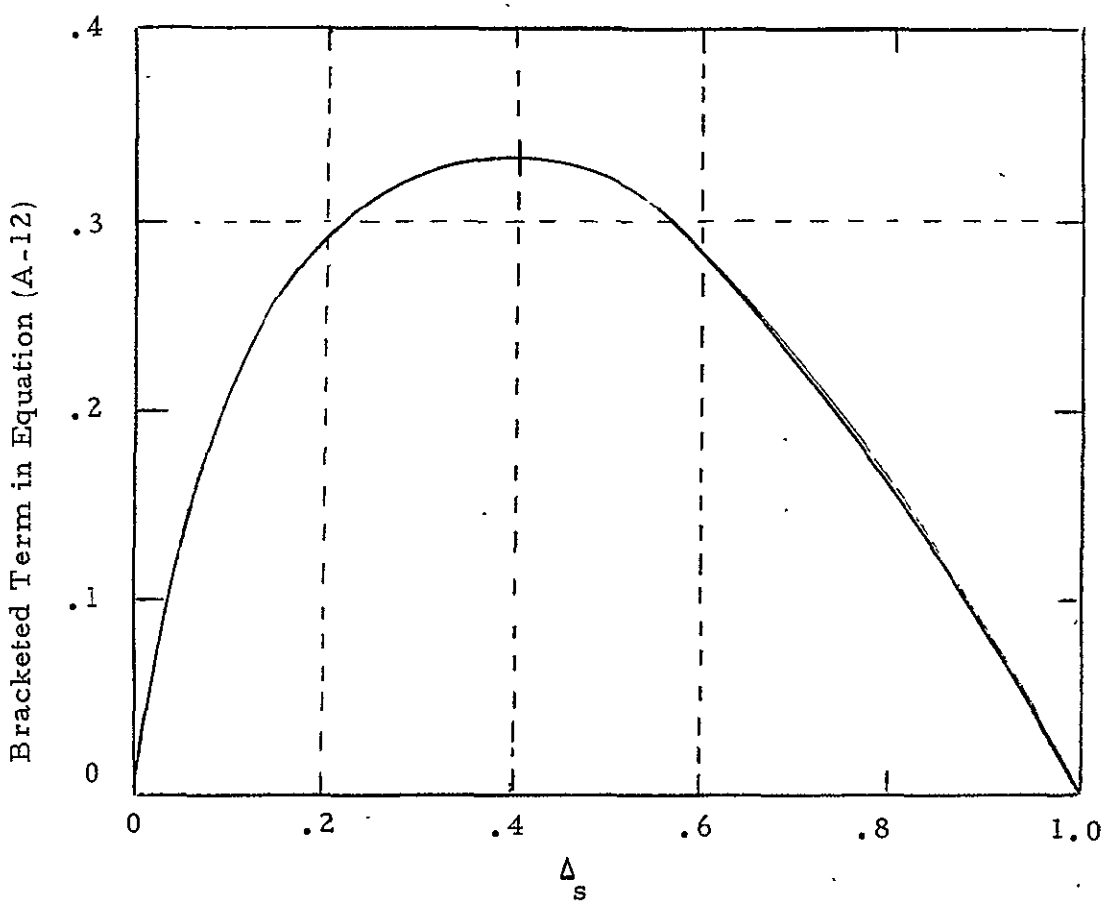

Figure A-4. Plot of Factor in Brackets in (A-12).

$$\overline{P}_{avg_3} = \underbrace{\int_0^{(1-\Delta_s)\theta'_B/2} \frac{dx(\sin x/x)^2}{(1-\Delta_s)\frac{\theta'_B}{2}} \frac{\int_0^{\sqrt{(\theta'_B/2)^2-x}} \frac{dy(\sin y/y)^2}{y}}{\sqrt{\left(\frac{\theta'_B}{2}\right)^2 - x^2}}}_{\text{average power}} \underbrace{\frac{\sqrt{\left(\frac{\theta'_B}{2}\right) - x^2}}{\theta'_B/2}}_{\substack{\text{fraction of} \\ \text{center line} \\ \text{dwell time}}} \qquad \text{(A-14)}$$

The energy received over the entire observation is given by

$$\mathcal{E}_3 = \overline{P}_{avg} Kt_d \qquad \text{(A-15)}$$

where we have multiplied by the boresight dwell time Kt_d. The energy can be expressed as

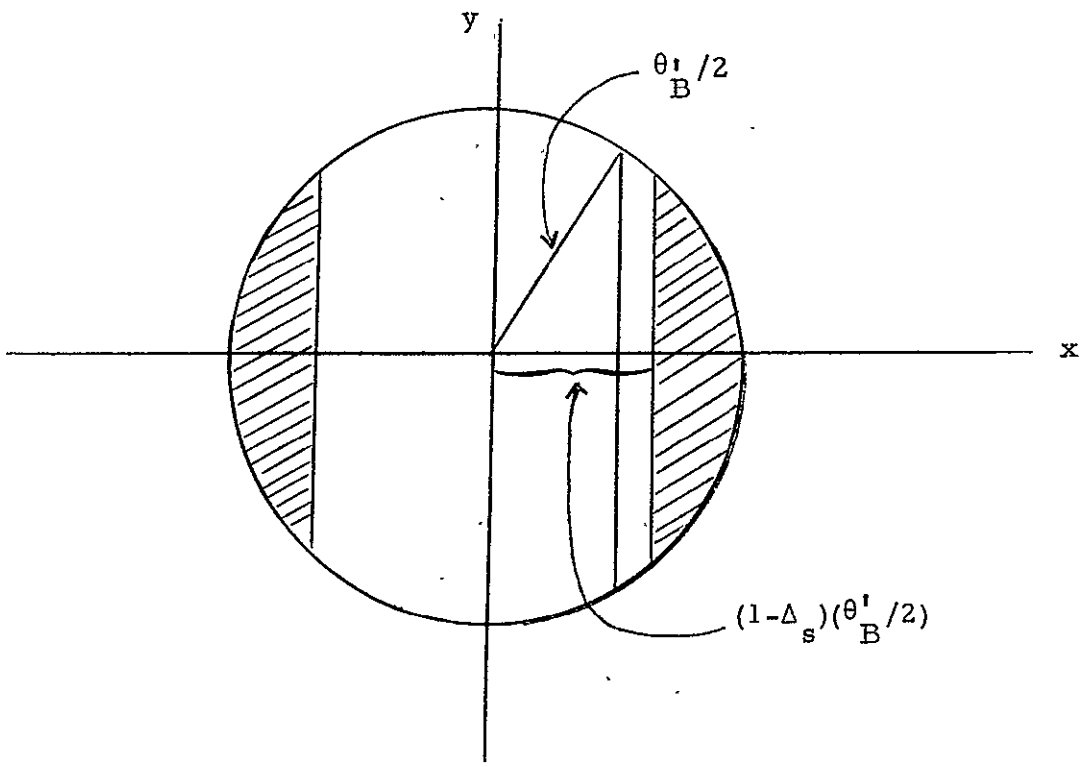

Figure A-5. Region for Third Optimization Criterion.

$$\delta_3 = \left[\frac{\theta_B^2 T_T}{A_{AZ} A_{EL}}\right]\left\{\frac{1}{(\theta'_B/2)^2}\int_0^{(1-\Delta_s)(\theta'_B/2)} dx(\sin x/x)^2 \int_0^{\sqrt{(\theta'_B/2)^2-x^2}} dy(\sin y/y)^2\right\}$$

This optimization is similar to that for δ_1. From (A-16) it is seen that the optimum choice of Δ_s is given by

$$\Delta_s\Big|_{opt_3} = 0$$

for the third optimization criterion.

The recommended choice of scan overlap is to employ the second optimization criterion and choose the scan overlap to $\Delta_s = 0.40$. This is the choice of Δ_s which is used in the body of the report for all of the required power computations.

In our example

$$A_{EL} = A_{AZ} = 40^{o} = .698 \text{ radians}$$

$$\theta_{B} = 2.76^{o} = .048 \text{ radians}$$

The optimization carried out in this appendix is similar to a "Beam Overlapping Optimization Study" recently performed at NASA-JSC, wherein the conclusion was that a 30% overlap was the optimal choice to maximize the minimum received energy over the total dwell time. The definitions and concept of scan overlap differ somewhat from that presented in this report.

ADDENDUM B

PERFORMANCE ANALYSIS OF NONCOHERENT PULSE RADAR

There appears to be no exact analytical method for determining the performance of a typical suboptimal pulse radar detector such as shown in Figure B-1. The input is $y_2(t)$ which is also shown on Figure 1. The front end of the receiver up to $y_2(t)$ could be the same for both a coherent and a noncoherent receiver, provided the gating is appropriately altered. The method employed here is similar to that used for the suboptimal coherent receiver in Appendix D of [7], and [12].

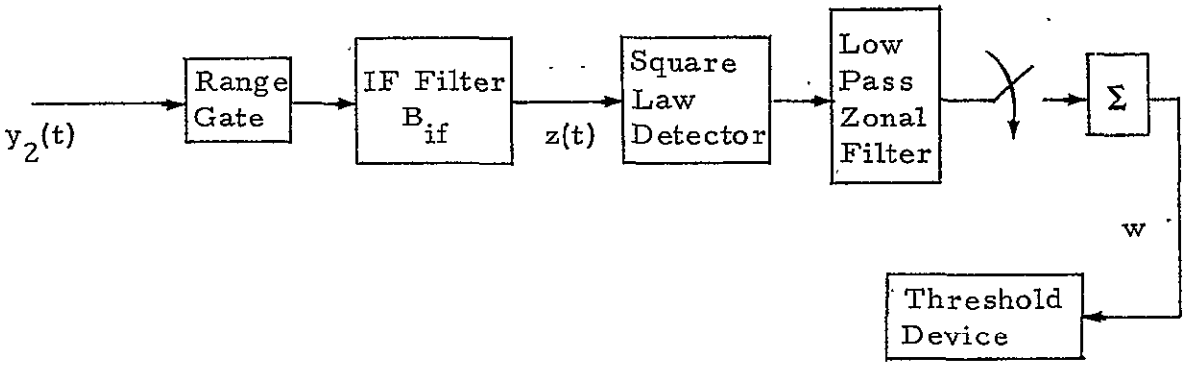

Figure B.1. Typical Suboptimal Pulse Radar Detector

We shall simplify the analysis by assuming that the improvement due to frequency diversity and the loss due to the fluctuations of the target for the suboptimal system are approximately the same as for the ideal optimal system. We therefore examine the receiver in Figure B.1 for a nonfluctuating target in the absence of frequency diversity.

We shall assume that the low pass filter usually used for integration can be replaced by a sampler and summer as shown in Figure B.1.

The sampling rate for the sampler is equal to the PRF, namely, 2500 samples/second. When a nonfluctuating signal pulse is present, the received waveform during the pulse time is

$$z(t) = \sqrt{2 P_{pr}} \sin(\omega_0 t + \theta_0) + n_f(t) \tag{B-1}$$

where

$$n_f(t) = \sqrt{2}\, n_s(t) \sin(\omega_0 t + \theta_0) + \sqrt{2}\, n_c(t) \cos(\omega_0 t + \theta_0) . \tag{B-2}$$

In (B-1) and (B-2),

i) P_{pr} is the received peak signal power,

ii) $n_c(t)$ and $n_s(t)$ are independent identically distributed Gaussian random processes, whose spectrum is dictated by the shape of the preceding IF filter.

The autocorrelation function and spectral density of $n_f(t)$ are given by

$$\begin{aligned} R_n(\tau) &= 2 R_L(\tau) \cos \omega_0 \tau \\ &= 2 (N_0 B_{if}/2) \sin(\pi B_{if}/2) \Big/ (\pi B_{if}/2) \end{aligned} \tag{B-3}$$

and

$$S_n(f) \equiv S_L(f - f_0) + S_L(f + f_0) , \tag{B-4}$$

respectively, where $R_L(\tau)$ and $S_L(f)$ are the autocorrelation and spectral density of $n_c(t)$ and $n_s(t)$. If the IF filter in Figure B-1 is ideal, then $S_L(f)$ is as shown in Figure B-2.

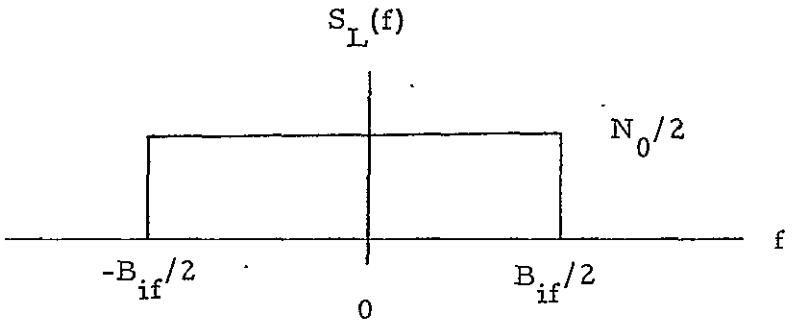

Figure B-2. Spectral Density of $n_c(t)$ and $n_s(t)$

Following a procedure similar to Appendix D of [7], we note that, over one spatial dwell time,

$$W = \sum_{j=1}^{J} \left(\sqrt{P_{pr}} + n_{s_j}\right)^2 + \left(n_{c_j}\right)^2 \qquad \text{(B-5)}$$

where $n_{s_j} = n_s(t_j)$ and $n_{c_j} = n_c(t_j)$. The time sampling interval is 400 μsec, so that the $\{n_{s_j}\}$ and $\{n_{c_j}\}$ are independent Gaussian random variables.

We consider three cases, which correspond to sets of cases in Table V:

Case A	Case B	Case C
One scan	Two scans	Three scans
$P_d = 0.99$	$P_d = 0.90$	$P_d = 0.785$
$\tilde{t}_d = 110$ msec	$\tilde{t}_d = 55$ msec	$\tilde{t}_d = 37$ msec
$J = 275$ samples	$J = 137$ samples	$J = 92$ samples

From page (D-7) in [7], the design equation becomes

$$E[w|s+n] = E[w|n] + \sigma_{w|n}\,\mathrm{erfc}^{-1}(FAP) + \sigma_{w|s+n}\,\mathrm{erfc}^{-1}(1 - P_d) \qquad \text{(B-6)}$$

where

$$E(w|n) = 2J\sigma_n^2 \tag{B-7}$$

$$E(w|s+n) = J(P_{pr} + 2\sigma_n^2) \tag{B-8}$$

$$\sigma_{w|n}^2 = 4J\sigma_n^4 \tag{B-9}$$

$$\sigma_{w|s+n}^2 = 4J\sigma_n^4(1 + P_{pr}/\sigma_n^2) \ . \tag{B-10}$$

Upon substitution of (B-7) through (B-10) into (B-6), and simplifying, we have

$$\sqrt{J}\,(P_{pr}/\sigma_n^2) = 2\left\{a + b\left[1 + (P_{pr}/\sigma_n^2)\right]^{1/2}\right\} \tag{B-11}$$

or, equivalently,

$$\boxed{(J/4)\lambda^2 - (\sqrt{J}\,a + b^2)\lambda + (a^2 - b^2) = 0} \tag{B-12}$$

where

$$\lambda \triangleq (P_{pr}/\sigma_n^2) \ , \tag{B-13}$$

$$a \triangleq \text{erfc}^{-1}(FAP) \ , \tag{B-14}$$

and

$$b \triangleq \text{erfc}^{-1}(1 - P_d) \ . \tag{B-15}$$

The values of a and b for Cases A, B, and C are given in Table B-1. These are the values of required received signal-to-noise ratios that are used in the computations in Section IV.

Case	FAP	a = $\text{erfc}^{-1}(\text{FAP})$	P_d	b = $\text{erfc}^{-1}(1 - P_d)$	λ	λ_{dB}
A	3×10^{-7}	5	0.99	2.33	1.00	0
B	3×10^{-7}	5	0.9	1.28	1.18	0.72
C	3×10^{-7}	5	0.785	0.79	1.29	1.11

TABLE B-1

REQUIRED RECEIVED SIGNAL-TO-NOISE RATIOS
FOR NONCOHERENT PULSED RADAR

REFERENCES

1. D. B. Leeson and G. F. Johnson, "Short-Term Stability for a Doppler Radar: Requirements, Measurements, and Techniques," Proc. IEEE, February, 1966.

2. M. J. Mum, "The Meaning and Measurement of Spectral Purity," Motorola Report, Communications Division, Chicago.

3. W. B. Offutt, "A Review of Circular Polarization as a Means of Precipitation Clutter Suppression and Examples," Proc. of NEC, Vol. XI, October, 1955.

4. W. F. McQuillan, A. W. Bologna, and D. M. Calabrese, "Rendezvous Radar for Space Shuttle Orbiter Vehicle," Proc. of International Telemetry Conf., Los Angeles, October, 1974.

5. M. I. Skolnik. Radar Handbook. McGraw-Hill, 1970.

6. J. V. DiFranco and W. L. Rubin. Radar Detection. Prentice-Hall, 1968.

7. C. L. Weber, "Analysis of a Center Line Pulsed Doppler Radar Operating in the Search Mode," Appendix F of this report.

8. F. E. Nathanson. Radar Design Principles. McGraw-Hill, 1969.

9. C. L. Weber, "Radar Cross Section Errors Induced by a Two Point Target," Appendix A of this report.

10. J. Omura and T. Kailath, "Some Useful Probability Distributions," Stanford Electronics Laboratory Technical Report No. 7056-6, September, 1965.

11. D. P. Tice, "The Effect of Frequency Agility on the Radar Detectability of Spacecraft," Westinghouse Electric Corporation, Baltimore, Maryland, September, 1973.

12. C. L. Weber. Elements of Detection and Signal Design. McGraw-Hill, 1968.

APPENDIX C

SHUTTLE PULSE RADAR/TRANSPONDER CONFIGURATIONS AND PRELIMINARY PERFORMANCE ESTIMATES FOR THE COOPERATIVE MODE

1.0 INTRODUCTION

One of the requirements for the Shuttle radar sensor is the operation with a cooperative target, i.e., the target which carries an active transponder. The use of a transponder permits the acquisition and track initiation of a cooperative target at a maximum range of up to 557 km (300 nm). Furthermore, a relatively steady reply from a cooperative transponder alleviates the problems caused by scintillation and glint associated with most of the passive targets. Unfortunately, not all of the targets can be equipped with transponders and the optimization of the radar function for the uncooperative mode still remains one of the major objectives of this study program. Consequently, when considering the candidate radars and the corresponding transponders, one must keep in mind the fact that the radar configuration for the cooperative mode must have a high degree of compatibility with the configuration selected for the passive, noncooperative mode.

So far, the candidate sensor configurations have included the following types of radar systems:

1. pulse radar,
2. pulse doppler radar,
3. pulse doppler with tone ranging,

and 4. pulse radar with linear (chirp) or stepped FM.

It is the purpose of this report to describe the block diagrams for the pulse radar and transponder and to point out the switchovers required between the passive and the active modes. Preliminary performance estimates for the cooperative mode of the pulse radar system are presented. A technique for reducing radar transmitter power at short ranges is also described.

2.0 PULSE RADAR SYSTEM

2.1 Noncooperative Mode

The pulse radar system has been considered to date as a baseline system against which all other candidates have been compared. In the noncooperative mode, this system operates in a manner similar to the airborne-intercept (AI) radar. A high peak power, low duty cycle, noncoherent magnetron transmitter is used and a three-channel monopulse receiver provides signal detection and two-axis target tracking. The effects of target cross section variations are reduced by employing frequency agility in the transmitter. Range is measured by a split-gate tracker, or equivalent, and the range rate is determined by differentiating the range.

The target angle search and acquisition have been analyzed for this radar in the noncooperative mode and the required parameter estimates have been documented.* The question of obtaining the required range rate accuracy by range differentiation is still open and such techniques as accelerometer-aided $\alpha\beta\gamma$ trackers are being considered.

Figure 1 shows the simplified block diagram of the pulse radar system. The amplitude type monopulse converter provides three outputs, each applied to its own receiver channel. The outputs are, respectively, the sum (Σ), the elevation difference (ΔEl), and the azimuth difference (ΔAz). The sum channel provides both the AGC and the phase reference for the difference channels. The ΔAz and ΔEl receiver outputs are applied to the antenna steering servo loops which for the purpose of simplicity have been omitted from the block diagram.

The frequency diversity required for the noncooperative mode is provided by a frequency-agile magnetron. The selection of the magnetron tuning mechanism is an important factor because the automatic

---

*W. F. McQuillan, A. W. Bologna, and D. M. Calabrese, "Rendezvous Radar for Space Shuttle Orbiter Vehicle," ITC Proceedings, 1975.

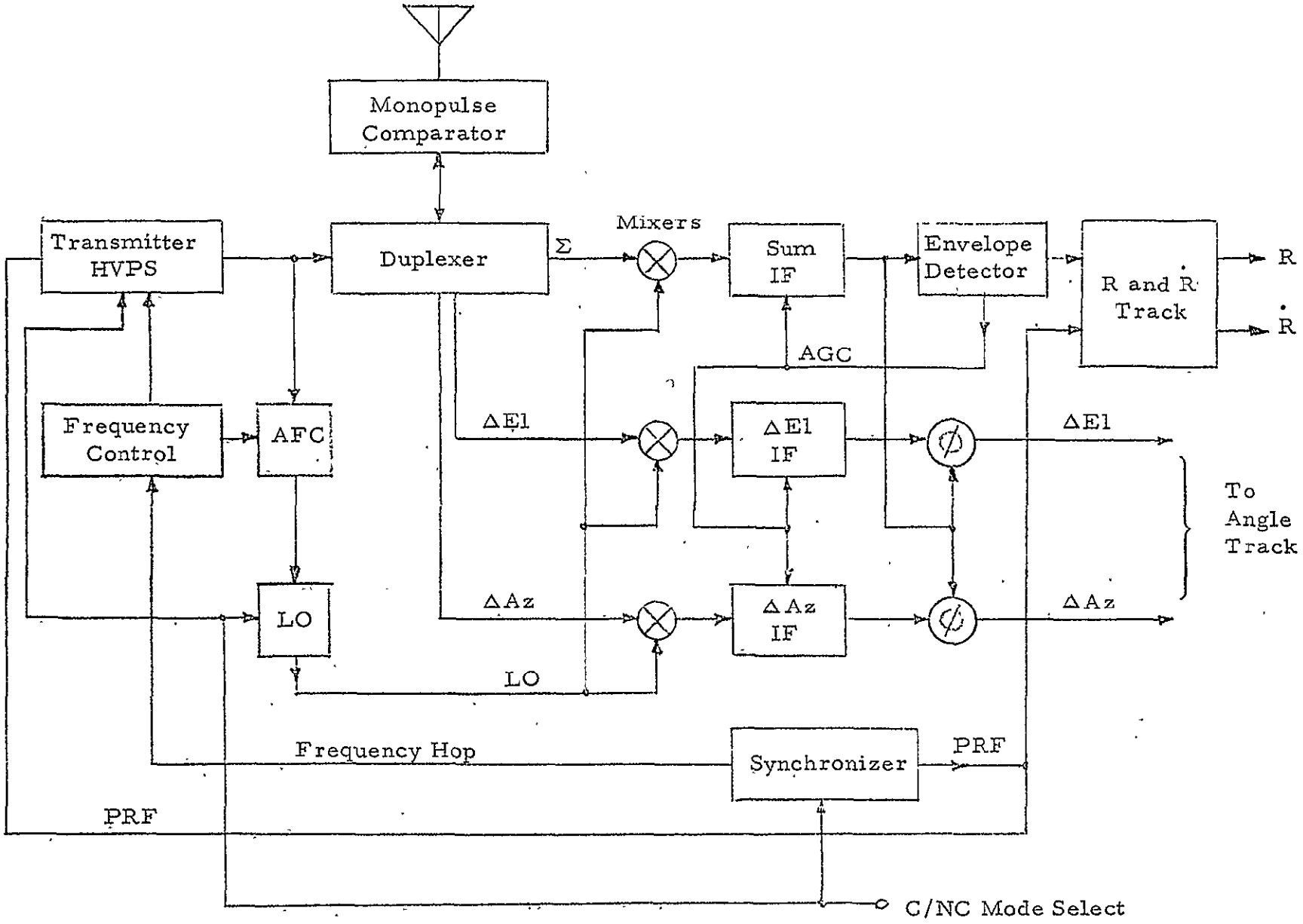

Fig. 1. PULSE RADAR SIMPLIFIED BLOCK DIAGRAM

frequency control (AFC) usually operates over a limited range of frequency shifts and is generally designed to take care only of long-term frequency drifts. Consequently, the device which frequency-tunes the magnetron must provide a signal which is related to the instantaneous frequency of the magnetron so that this signal can be used for supplying the first order frequency correction to the AFC circuit. The residual frequency discrepancy at each transmitter frequency is then corrected by the AFC. Furthermore, once the frequency tuning is discontinued and the system is put into the cooperative mode, the tuning device must return the center frequency of the magnetron to a value which is within the frequency acquisition range of the transponder.

Because most of the existing frequency agile magnetrons employ electro-mechanical devices for frequency readout, the question of readout accuracy and space qualification of both the tuning device and the magnetron itself is an important one and requires further investigation. The typical parameters which have been baselined for the pulse radar in the noncooperative, skin tracking mode are as follows:

Pulse Repetition Rate (PRF)	2500 pps
Pulse Width	0.4 microseconds
Duty Cycle	0.001
Peak Power	40 kw
Average Power	40 w
Frequency Diversity Spread	250 MHz (up to 800 MHz is being considered)
Noise Figure	8 dB
System Losses	6-7 dB

It must be pointed out that these parameters, particularly the peak power levels and pulse widths, are baselined to provide a passive target track initiation at a range of 19 km (10 nmi) with probability of detection of 0.99 and false alarm probability of 10^{-8}. As the range to the target decreases and eventually reaches the stationkeeping range of 30 meters, the high peak power level may present a twofold problem: (1) excessive irradiation

level of the target and (2) switching transients associated with a gas-type T/R device. Because the power level of the magnetron cannot be controlled directly, alternate techniques such as diverting the magnetron output into a dummy load and using only a fraction of the available power are being considered. A possible configuration for this technique is described in Section 2.3.

2.2 Cooperative Mode

2.2.1 Angular Search and Dwell Time Considerations for the Cooperative Mode

Before we discuss the various features of the candidate radars and the transponders for the cooperative mode, let us consider the angular acquisition of a target in this mode. The specification requires that a cooperative target be acquired at a maximum range of 557 km (300 nmi) and that both the angular and range acquisition be completed within one minute after the radar has been designated to the expected target direction. Unlike some of the passive modes of operation, where the target position is unknown within a relatively large scan volume, we will assume that in the cooperative mode the target direction is known with an accuracy which is better than the designation accuracy of the radar antenna. Thus, we will base our reasoning on the assumption that it is the radar antenna designation accuracy that determines the scan volume in the cooperative mode. From the data available to us so far, we make the following assumptions:

Antenna 3 dB beamwidth:	$\theta_B = 2.8$ (20" dish, $f_0 = 15$ GHz)
Azimuth designation uncertainty:	$A_{AZ} = \pm 3^0 (3\sigma)$
Elevation designation uncertainty:	$A_{EL} = \pm 3^0 (3\sigma)$
Scan overlap:	$S_0 = 30\%$
Allowance for scan reversal:	$S_1 = 20\%$

Based on an assumption of a raster scan, the number of horizontal lines is therefore

$$\text{Number of Horizontal Lines} = \frac{A_{EL}}{(1 - S_0)\theta_B} = \frac{6^0}{(1 - 0.3)\, 2.8^0}$$

$$= 3.06 \cong 3 \text{ lines} . \qquad (1)$$

Assuming that two scans will be made in 60 seconds, time per scan line is then

$$\text{Time per scan line} = \frac{30}{3} = 10 \text{ sec} . \qquad (2)$$

The corresponding scan speed is

$$\text{Scan Speed} = \frac{A_{AZ}}{10 \text{ sec}} (1 + 0.2) = \frac{6^0}{10 \text{ sec}} (1.2) = 0.72^0/\text{sec} \qquad (3)$$

where 0.2 represents the 20% time required for scan reversals.

The dwell time per beamwidth, t_d, i.e., the time a given point in space is illuminated by the antenna inside its 3 dB beamwidth, plays an important role in establishing the probability and the accuracy of target acquisition. For the parameters assumed, this time is given by

$$t_d = \frac{\theta_B}{\text{Scan Speed}} = \frac{2.8^0}{0.72^0/\text{sec}} = 3.9 \text{ or} \approx 4 \text{ seconds} . \qquad (4)$$

It may be noted that, for any particular radar system and a corresponding transponder, trade-offs exist between the scan speed, the scan overlap, the dwell time and the probability of detection. However, because these trade-offs may provide only a secord-order type of optimization, we will use the 4 seconds dwell time as a baseline number for generating the preliminary estimates of candidate system performance. But, if new findings pertaining to antenna designation accuracy, antenna beamwidth, and antenna scan pattern reveal that assumptions other than those used above pertain, the dwell time can easily be recomputed.

2.2.2 Transponder Configuration

In the cooperative mode, the pulse radar operates with a transponder whose simplified block diagram is shown in Figure 2. Because in this mode the transponder has to be acquired and tracked at a range of up to 557 km (300 nmi), the PRF of the radar is reduced to 250 pps which provides an unambiguous range of up to 600 km. The pulse width of the radar is also increased to a value which is from 1 to 4 microseconds. The frequency diversity, however, is not required and the radar transmitter frequency is set at a fixed value.

As shown in the block diagram, the transponder employs a superheterodyne receiver to amplify and detect the Shuttle's radar signals. The superheterodyne receiver is required in this case to provide reliable detection of the radar signals whose level, as shown later in the power budget, is below the -40 to -50 dBm detection capability of the video detector receivers. As the radar antenna beam illuminates the transponder's antenna, the detected radar pulses are applied to the control logic. When the level of received signals exceeds a preset threshold, the logic circuitry verifies the PRF and the approximate pulse duration of the received signal and initiates the pulsing of the reply transmitter. The frequency of this transmitter is offset from that of the received radar signal by a fixed amount. Such offset provides for a better transmitter/receiver isolation within the transponder and thus alleviates the problem of self-triggering which could arise if the transponder were to reply directly at the frequency of the interrogating radar. Although the frequency offset of the transponder's reply requires a change in the local oscillator frequency of the radar receiver, this requirement is not considered to be a major problem.

While for the pulse radar system and its transponder, pulse-to-pulse frequency stability and phase coherence are not required, the radar and the transponder IF bandwidth place limitations on the long-term frequency drifts which can be tolerated. In the noncooperative mode, the

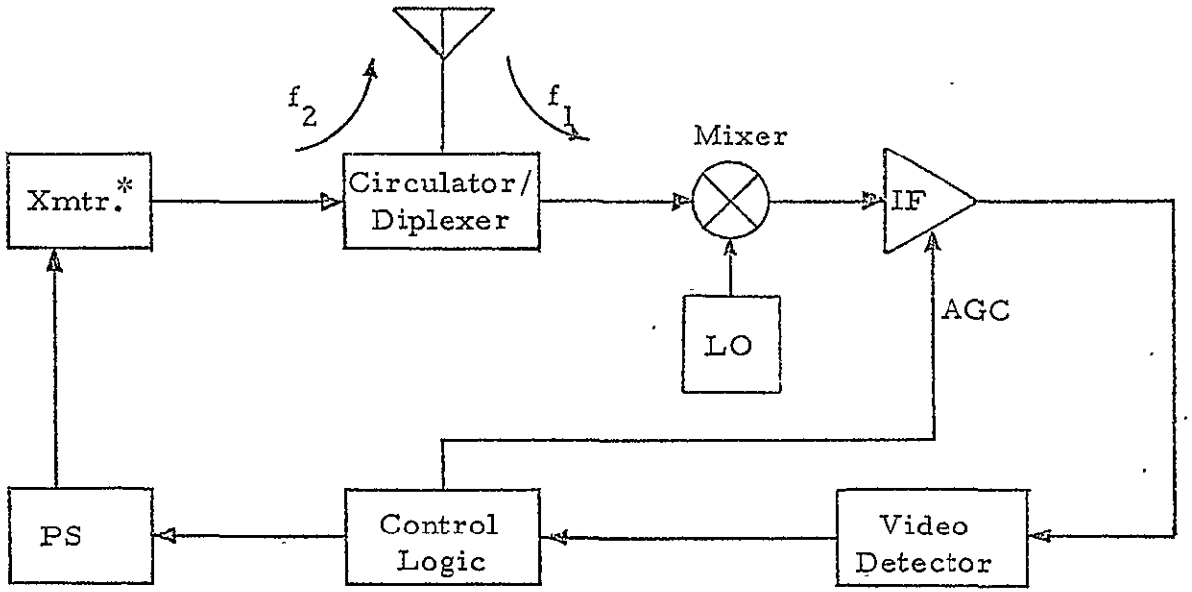

* May employ priming for frequency stability

Fig. 2. PULSE RADAR TRANSPONDER SIMPLIFIED BLOCK DIAGRAM

AFC takes care of long-term frequency drifts and thus maintains a relatively constant IF. For the cooperative mode, however, the absolute frequency drift in the radar transmitter frequency must be minimized to preclude the requirement for a frequency search at the beacon. Presently, we assume that by judicious design, the radar transmitter frequency in the cooperative mode can be maintained within 10 MHz over the range of expected operating conditions. Thus, for subsequent power budget calculations we use 10 MHz as the 3 dB bandwidth for the transponder receiver.

At the transponder, we may improve frequency stability of the reply by "priming" the transmitter, which may be either a beacon magnetron or an LSA oscillator, by a small amount of an RF power derived from a crystal controlled source. Thus, if we assume nominal stability, $\pm 1 \times 10^{-5}$, which allows for crystal aging and a wide degree of environmental changes, the expected frequency drift of a primed beacon transmitter may be kept within a $\pm$150 kHz limit. This permits us to assume that the radar bandwidth may be as narrow as 250-300 kHz to match the maximum beacon reply pulse width of 4 microseconds. For the preliminary power budget calculations, however, we will assume that the beacon transponder reply pulse width is 1 microsecond and the 3 dB bandwidth of the radar receiver is 1 MHz. The small mismatch resulting from this assumption is accounted for by the inclusion of a 1.0 dB loss into the 6.7 dB total loss estimate* for the pulse radar system.

The automatic gain control (AGC) must be applied to the transponder receiver to prevent overloading as the target approaches the radar. The AGC may have to be controlled by transponder receiver noise in conjunction with a threshold circuit to prevent transponder actuation by the sidelobes of the searching radar's antenna pattern. The detailed function of the transponder AGC cannot be established, however, until the final values of radar antenna sidelobes are defined.

---

*W. McQuillan et al., op. cit.

2.2.3 Radar to Beacon Link Power Budget

Table 1 gives the preliminary estimates for the radar-to-beacon link power budget at the maximum acquisition range of 557 km. This budget is based on the assumption that the peak power radiated by the radar in the cooperative mode is the same as that in the noncooperative mode, i.e., the peak power is 40 kw. Radar pulse width of one microsecond is assumed, but for the reasons explained earlier, the beacon receiver bandwidth is assumed to be 10 MHz. Beacon antenna aperture magnitude is based on a 0 dB gain at 15 GHz, which may be typical of a wide beamwidth antenna. Also, because the electromagnetic alignment between radar and transponder antennas is random and varies with time, circular polarization is assumed for the transponder antenna and linear for the radar antenna. This polarization difference introduces a nominal 3 dB loss for the cooperative mode, but allows the radar antenna to have only a linear polarization which is optimum for working in the noncooperative, skin tracking mode. An additional 3 dB RF loss is included to account for loss in a solid state T/R switch and a limiter which may be included in the receiver channel of the antenna. Presently, this value may be considered as nominal and it may be re-evaluated as a more detailed design of the transponder is worked out.

The important result of the radar-to-beacon link power budget shown in Table 1 is the relatively high (approximately +30 dB) value of peak signal-to-noise (SNR) ratio. This SNR provides sufficient safety margin for the radar to beacon link. It also implies that beacon transmitter triggering jitter will be relatively low.

2.2.4 Beacon to Radar Link Power Budget

Table 2 shows the preliminary estimates for the beacon-to-radar link power budget. The peak radiated power for the beacon transmitter is assumed to be 100 watts which is typical for small beacon magnetrons or solid state LSA devices. The radar antenna aperture

TABLE 1

RADAR TO BEACON LINK POWER BUDGET (PULSE RADAR)

$$P_r(B) = \frac{P_t G_t A_b L_b}{4\pi R^2} \qquad \text{Assume } f_0 = 15 \text{ GHz}$$

where $P_r(B)$ = Peak received power (at beacon)

P_t = Peak transmitted radar power

G_t = Radar antenna gain

A_b = Beacon antenna aperture

L_b = Beacon antenna losses

R = Range

Term	Units	Gain (dB)	Loss (dB)	Comments
P_t	40 kw	46 dBw		P_{ave} = 40 w for 0.001 duty cycle
G_t		35.4		λ = 0.02 m
$1/4\pi$			-11	
$1/R^2$	557 km		-115	
A_b	3.2×10^{-5} m^2		-45	0 dB gain at 15 GHz
L_b			-6	3 dB RF loss 3 dB polarization loss
		+81.4 dBw	-177 dB	

$P_r(B)$ = +81.4 dBw - 177 dB = <u>-95.6 dBw</u>

For beacon NF = 8 dB and BW = 10 MHz beacon noise:

N_b = -144 dBw + 8 dB + 10 dB = <u>-126 dBw</u>

$\frac{P_r(B)}{N_b}$ = -95.6 dBw - (-126 dBw) = <u>+30.4 dB</u> = Peak S/N per pulse

TABLE 2

BEACON TO RADAR LINK POWER BUDGET (PULSE RADAR)

$$P_r(R) = \frac{P_b G_b L_p L_r A_r}{4\pi R^2} \qquad \text{Assume } f_0 = 15 \text{ GHz}$$

where $P_r(R)$ = Peak received power (at radar)

P_b = Peak transmitted beacon power

G_b = Beacon antenna gain

L_p = Polarization losses

L_r = Radar system losses

A_r = Radar antenna aperture

R = Range

Term	Units	Gain (dB)	Loss (dB)	Comments
P_b	100 w	20 dbw		P_{ave} = 0.1 w for 0.001 duty cycle
G_b		0		
$1/4\pi$			-11	
$1/R^2$	557 km		-115	
L_p			-3	
L_r			-6.7	(W. F. McQuillan et al.)
A_r	0.11 m^2		-9.6	35.4 dB at 15 GHz
		20 dbw	-145.3 dB	

$P_r(R)$ = +20 dbw - 145.3 dB = <u>-125.3 dBw</u>

For radar NF = 8 dB and BW = 1 MHz radar noise:

N_r = -144 dBw + 8 dB = <u>-136 dBw</u>

$\frac{P_r(R)}{N_r}$ = -125.3 dBw - (-136 dBw) = <u>+10.7 dB</u> = Peak S/N per pulse

is based on 35.4 dB gain at 15 GHz. Beacon pulse duration of one microsecond is postulated and it is assumed that radar receiver bandwidth is 1 MHz. The 6.7 dB system loss is based on an estimate given in the reference.* This estimate includes a 1 dB loss for IF bandwidth mismatch. It must be also noted that, to insure beacon reception within the 1 MHz bandwidth, the radar local oscillator may have to be disconnected from the AFC loop and a stable crystal controlled LO driver substituted for the cooperative mode. Such switching will prevent the LO frequency from drifting with the magnetron frequency which, as was assumed earlier, may vary over a 10 MHz range.

The beacon to radar link budget indicates that the signal-to-noise ratio at the radar is approximately +10 dB as compared to approximately +30 dB at the transponder receiver. This implies that the random range error will be determined primarily by the SNR at the radar. As shown in the next section, this is not a limitation for beacon acquisition and subsequent range tracking accuracy. The range rate estimation by range differentiation, however, may require smoothing times which will result in lag times in excess of the 2 seconds specification. This problem also exists with the noncooperative, skin tracking mode and, thus, as was mentioned earlier, an accelerometer-aided $\alpha\beta\gamma$ tracker may have to be used for both modes. An alternative for the cooperative mode would be to increase the beacon power, but this does not appear to be an efficient approach when compared with range rate tracker optimization.

2.2.5 Transponder Acquisition and Range/Range Rate Tracking Performance Estimates

During the initial acquisition the radar antenna will search through the uncertainty volume and for the duration of the dwell time it will illuminate the transponder for each of the two consecutive scans. The approximate number of pulses received by beacon during this time will

---

*McQuillan et al., op. cit.

be

$$\text{Number of pulses per dwell time} = t_d \times \text{PRF} = 4 \text{ secs} \times 250 \text{ pps}$$

$$= 1000 \text{ pulses} \quad . \tag{5}$$

With a +30 dB SNR at the transponder, it will take only a few pulses to actuate the beacon transmitter. Thus, the radar receiver will intercept transponder replies during an early portion of the dwell time. With an SNR of +10.7 dB, only about 4 pulses* have to be integrated to provide probability of detection, P_D, of 0.95 consistent with a false alarm of 10^{-12}. If two consecutive 4-pulse groups are used for detection, P_D becomes

$$P_D = 1 - (1 - 0.95)^2 = 0.9975 \quad . \tag{6}$$

Consequently, it appears that the probability of beacon detection is not a problem and that such detection will most likely occur during the first of the two scans.

After the detection of the transponder signal the range and angle acquisitions take place. The time required to complete these acquisitions and to initiate the range and angle tracks will depend on the mechanization and the bandwidth of the respective loops, as well as the initial offsets, but it is assumed that the total time to initiate track in both the range and angle will be less than 10 seconds.

Once the range tracking of the transponder is initiated the rms timing error of the output of the range track is defined as:

$$\sigma_t \cong \frac{\tau}{2\sqrt{(S/N)_1 \, n}} \tag{7}$$

where

---

*M. Skolnik, Radar Handbook, Figure 8, page 2-21.

σ_t = timing uncertainty

τ = pulse width

$(S/N)_1$ = signal-to-noise ratio per pulse

n = number of pulses integrated .

In our case, τ = 1 microsecond, $(S/N)_1$ = 10.7 dB or a ratio of ≈ 12, and n $\approx$ PRF/range tracker bandwidth. With PRF = 250 pps and an assumed range tracker bandwidth of approximately 2.5 Hz, the value for n is approximately 100. Thus,

$$\sigma_t = \frac{1.0}{2\sqrt{(12)(100)}} \cong 0.014 \text{ microsecond.} \tag{8}$$

The rms range error is consequently

$$\sigma_r = \frac{c}{2}\sigma_t = 150 \text{ m/}\mu\text{sec} \times 0.014 \ \mu\text{sec} = 2.11 \text{ meters.} \tag{9}$$

This accuracy is well within the 30 m specification for ranges over 9 km.

Consider now the smoothing time required of a simple range differentiation type of range estimator. The smoothing time required is

$$t_s = \frac{\sqrt{2}\,\sigma_r}{\sigma_{\dot{R}}} \tag{10}$$

where $\sigma_{\dot{R}}$ is the required accuracy, which in our case is 0.1 m/sec. Thus

$$t_s = \frac{\sqrt{2}\ (2.11)}{(0.1)} = 29.7 \text{ seconds.} \tag{11}$$

The lag time, t_D, is then

$$t_D = \frac{29.7 \text{ sec}}{2} = 14.8 \text{ sec} . \tag{12}$$

As seen from the calculation above, the lag time exceeds the specified recovery time of 2 seconds. A "brute force" approach would be to increase transponder power and to narrow the transponder pulse width to improve the range measurement accuracy, but this approach not only complicates the beacon design, it also may be ineffective if one considers that a limit may be set on the range measurement accuracy by the instrumentation errors* of the radar system itself. Thus, it appears that a most promising approach towards improving the accuracy of the range rate readout and reduction of the recovery time for the pulse radar system lies in the exploration of better tracker implementations such as the aforementioned accelerometer-aided $\alpha\beta\gamma$ tracker. Improved tracker implementation will aid not only the cooperative mode but the noncooperative mode as well.

2.3 Short Range Power Control

As was mentioned in Section 2.1, the high peak power of the radar system at close ranges in the passive mode is undesirable from both the standpoint of excessive target illuminations and switching transients associated with a gas-type T/R device. The same considerations apply to the cooperative mode. A method for reducing the radiated transmitter power and eliminating T/R tube transients for short range operation is shown in Figure 3. The method involves the use of two switches--one an electrically actuated, remotely controlled waveguide switch and the other a solid state, low power, "fast" switch. In part (a) of Figure 3 the waveguide switch is in the position which allows the full transmitter power to be delivered to the duplexer. Because the power delivered to the duplexer in this case is about 40 kw, a conventional gas-type T/R provides the function of receiver isolation during the transmission.

At short ranges the full power is not required and thus the microwave switch is placed into the position shown in part (b) of Figure 3.

---

*The instrumentation error estimates will be determined as part of the detailed pulse radar system design.

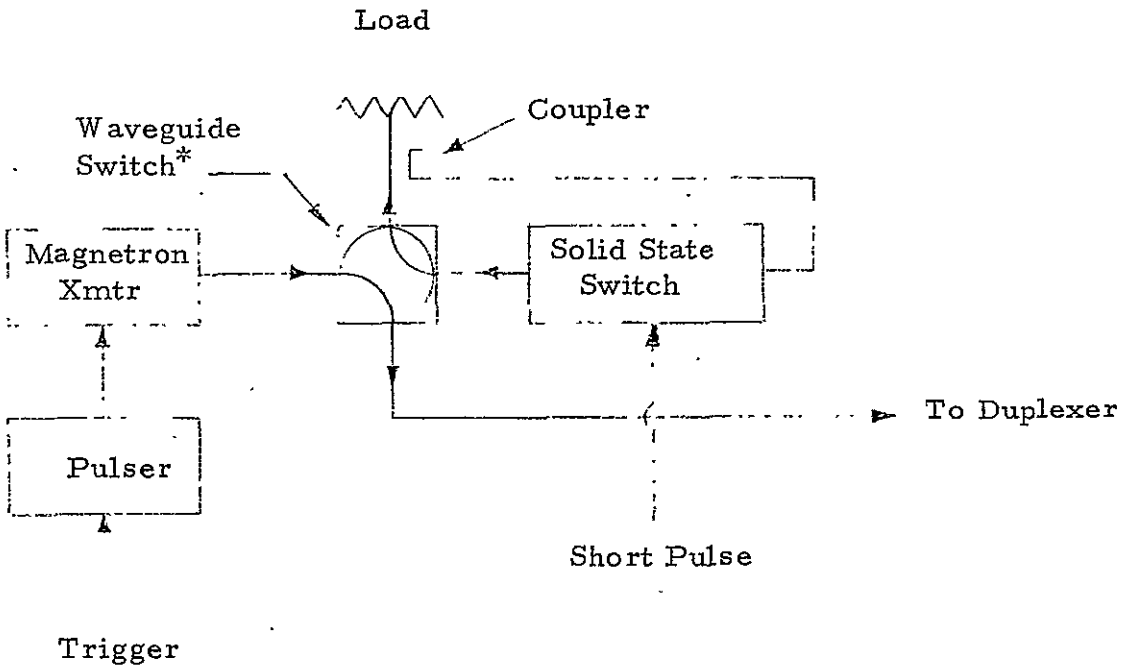

(a) Full Power Mode

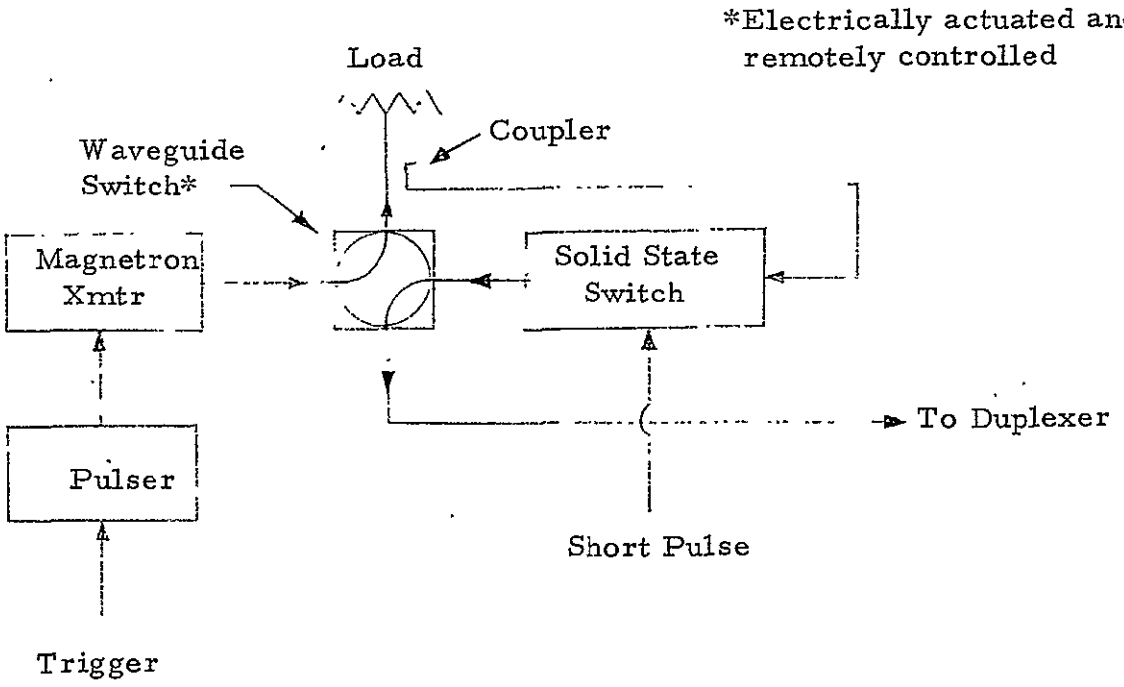

(b) Reduced Power Mode

Figure 3. Remotely Controlled Waveguide Switch Provides for Selection of Either (a) Full or (b) Reduced Transmitter Output Modes

In this position the full power of the transmitter is delivered to a dummy load and thus the magnetron operation is not affected. A portion of the transmitter power, however, is tapped by a coupler and delivered via a solid state switch to the duplexer. The duration of the transmitted pulse can now be made as narrow as desired by gating on to the duplexer only a short segment of the magnetron's RF pulse output. Because the power level used for this mode is not sufficient to trigger the T/R switch, a similar solid state switch (not shown) is used in the receiver path of the duplexer. The operation of the two solid state switches is synchronized to provide the T/R function. Because the solid state switches are free of transients and have fast switching speeds (down to a few nanoseconds), a short pulse, reduced power operation can be provided with this technique at ranges down to the stationkeeping range of 30 meters.

3.0 CONCLUSIONS

The cooperative mode transponder configuration has been established for the pulse radar. This configuration provides a pulsed reply at a frequency offset from that of the interrogating radar. Maintaining good frequency stabilities at both the radar and the transponder is important to preclude a frequency search employed at both ends. Preliminary link power budgets indicate that a good signal margin exists at the beacon receiver but at the radar end smoothing times in excess of 2 seconds are required to maintain the specified range rate accuracy of 0.1 m/sec with the presently assumed beacon parameters. This condition, however, applies only to the SNR at the maximum acquisition range of 557 km and a simple range-differentiation range rate tracker. Increasing beacon power and narrowing the beacon pulse appears undesirable, but is not ruled out. Alternately, an improved accelerometer-aided $\alpha\beta\gamma$ tracker will be considered for reduction of excessive range rate lag times. A simple method for radar power control has been worked out and looks promising enough to warrant further detailed consideration.

APPENDIX D

THE ESTIMATION OF RANGE RATE FOR NONCOHERENT RADAR

I. Introduction

The performance capability of various estimators of range rate which obtain noisy information from a split-gate range tracker is considered. In the analysis of the range-rate estimator, we assume somewhat ideal conditions. In Section II, however, we discuss the items which would have to be taken into account if a complete evaluation of range-rate estimation were to be conducted.

The environment under which the $\dot{R}$ estimator is to function is roughly described as follows. During the approach phase towards eventual rendezvous with a target, there will be a sequence of deacceleration burns spaced 50-60 sec apart. The length of each burn will be random (since it is manually controlled to maintain $\dot{R}$ to within prescribed values), but it is anticipated that the average length of each burn will be 10-20 sec.

The performance specs for the range tracker and range-rate estimator are:

a) $3\sigma_{\dot{r}}$ for range-rate is ± 1 ft/sec so that $\sigma_{\dot{r}}$ for range-rate is $\pm\frac{1}{3}$ ft/sec.

b) After a burn has been completed, a 2-sec period for smoothing (recovery) is allowed, after which the $\dot{R}$ estimate must again be within the specs of (a) above. There is no $\dot{R}$ estimation requirement during a burn.

c) 3σ for range is 1% of range at large ranges. At the maximum range of 10 N. Mi., $3\sigma_r = 608$ ft. so that $\sigma_r = 203$ ft.

In the next section we consider various items pertaining to the performance of the split-gate range tracker. The output will be a sequence of noisy range estimates, which the estimator of range rate can filter to provide smoothed estimates of range as well as range-rate. This is developed in Section III under somewhat ideal conditions, namely:

i) There is no target glint.

ii) During and immediately after a burn, the split-gate range tracker has zero recovery time.

iii) The range estimates from the split-gate range tracker consist of the sum of the true range value and white noise (i.e., a sequence of statistically independent identically distributed zero mean random variables).

II. Split-Gate Range Tracking

Most practical range tracking systems employ the split-gate tracker. We shall assume this is the range tracking device that is being employed, the output of which is the input to the $\dot{R}$ estimator.

The ideal performance of range tracking devices and the standard deviation of the error of the split-gate range tracker are discussed in [1-3].

In most cases, best overall results are obtained when the IF filter, with bandwidth B, is approximately matched to the pulse spectrum, so that

$$1 < B_T < 2 \qquad (1)$$

where τ is the pulse width of the noncoherent radar. In addition, the gate width τ_g is matched to the pulse width, i.e.,

$$\tau < \tau_g < 2\tau \tag{2}$$

This is reasonably close to the condition of correlation processing, which provides optimal performance.

Under these conditions for the split-gate tracker, the standard deviation of the range timing error, σ_t, is approximately given by

$$\sigma_t = \frac{\tau}{2.5\sqrt{2S/N}} \tag{3}$$

where

S = average signal power $= E_s/\tau$

E_s = the signal energy per pulse

$N = N_0 B$ = average noise power in the IF bandwidth

and

N_0 = one-sided noise spectral density.

his provides a very accurate measure of performance for $B\tau \approx 1.4$ and $\tau_g/\tau \approx 1.4$, and also within the vicinity of these products. These are also the optimal designs for a split-gate tracker. The corresponding standard deviation in range is

$$\sigma_{\Delta R} = (C/2)\sigma_{\Delta t} \tag{4}$$

An analysis of the split gate tracker is given in Barton [1, pp. 356-365] wherein the above conclusions are reached.

The split-gate tracker is an optimal tracking device in the sense that it provides the maximum likelihood estimate of the time delay between transmission and reception of a signal [4]. The performance of the split-gate tracker when only broad-band noise is taken into account was discussed in the above paragraphs, and in [1-2]. What is also important, particularly when the range tracker is to be followed by a range-rate estimator, is the transient errors due to sudden changes in velocity. As in a phase-locked loop, the transient response depends upon both the input transient assumed and the choice of loop filter.

For example, based upon a linearized analysis, a ramp in velocity will have steady state bias in the estimate when the loop filter is a perfect integrator, but the steady state bias will be reduced to zero when the loop filter is of the form

$$F(p) = \frac{1 + ap}{p^2} \tag{5}$$

In either case as well as in any loop filter, there is a transient response when sudden changes in velocity occur. The length of the transient response (or the settling time) is dependent on the size of the sudden change in velocity, and the peak value of the transient response is directly proportional to the size of the step in velocity. All of these factors need to be taken into account when choosing the loop filter for the split-gate tracker as well as the analysis and design of the range-rate estimator.

When there is a significant dynamic range, as is anticipated in this application, the effects of AGC and limiting on the performance of the split-gate tracker need to be taken into account.

Until recently all analyses of split-gate trackers (delay-lock loops) have been approximate. A more precise analysis has recently been carried out [5-7], but not in a radar environment. The results are such, however, that they can be extended to the radar range tracking problem.

2.1 Target Noise

There is the significant problem of taking into account target noise. Target noise may be considered as composed of three components: angle glint, amplitude scintillation, and range glint. The vast majority of target noise literature, among which are the following [8-18], addresses angle glint and amplitude scintillation. There is little literature on range glint. Howard and Lewis [22] have measured range glint from one aircraft target and obtained a probability density function from the empirical data similar to that shown in Figure 1. The data was collected for a nose view only.

For this one target and this one aspect angle, it should be noted that the apparent range deviation exceeds the physical limits of the target a much smaller fraction of the time than does the apparent angle in angle glint noise. By fitting a Gaussian curve to the empirical data in Figure 1 in such a way that it has the same probability of

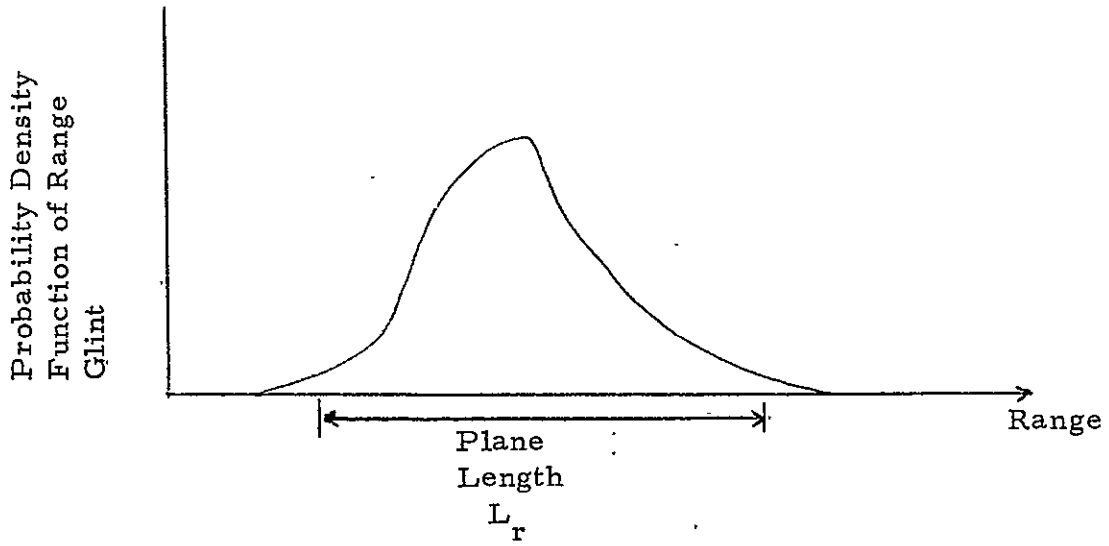

Figure 1. Distribution of Range Glint Noise for One Aircraft for a Nose-On View.

exceeding the physical limits of the target (about fifteen percent), we find that the standard deviation is given by

$$\sigma_r = 0.35\, L_r \tag{6}$$

This appears to be a satisfactory model. The consistency among targets and aspect angles is not immediately clear.

2.2 Power Spectral Densities and Correlation Functions

For the purposes of tracking range and estimating range rate, what is equally important is the power spectral density of the signal which has been subjected to range glint. For this, consider a uniform target rotation of a simple line target about the vertical axis. It is shown by Muchmore [9], that the power spectral density of the received signal is

$$S(f) = \frac{cg^2}{2f_0\Omega_a}, \quad f_0 - f_m \leq f \leq f_0 + f_m \tag{7}$$

where

f_0 = RF frequency

Ω_a = angular rotation rate

c = speed of light

g = target intensity parameter

and

$$f_m = \frac{f_0 L\Omega_a}{c} = \frac{L\Omega_0}{\lambda} \quad \text{(one-sided)} \tag{8}$$

where L is the length of the simple line target. The spectrum of the envelope of a square law detector with the above spectrum as the input would be

$$S_E(f) = C\frac{1}{f_m}\left(1 - \frac{f}{2f_m}\right), \quad |f| \leq f_m \tag{9}$$

This agrees with the spectral shapes used in [19-21].

If the intensity distribution of the target return elements is altered (e.g., Gaussian or Markovian), the correlation of power spectral densities will be significantly altered.

In general, the spectral density of the sequence of samples at the input to the split-gate range tracker is dependent upon the intensity distribution of the elements of the target and whether a linear or square law envelope detector is employed in the noncoherent radar receiver. A thorough analysis must take into account all of the

various possibilities indicated in this section.

III. Range-Rate Measurement Using Non-Coherent Pulsed Radar

3.1 (α, β) and (α, β, γ) Filters

Initially we consider the range rate measurement accuracy problem by a non-coherent pulsed radar both in the frequency and the time domains. With regard to the former, it is concluded to be non-feasible. More than one method exists, however, with respect to the latter using only position (range) data. Specifically, equations are developed for the mean-square smoothing errors in range rate (as well as range and radial acceleration) for first order and second order systems using variable (α, β) and (α, β, γ) filters, respectively. The pertinent equations are expressed in terms of the time interval between successive range measurements, (i.e., 1/PRF), total smoothing time, and range measurement error variance. These equations serve the purpose of getting a quick assessment of the possible accuracy attainable during the tracking mode and under ideal conditions; the results are deemed to be somewhat inferior to the corresponding error attainable using a Kalman filter routine which, in fact, should be at least recommended for the acquisition mode. A more complete discussion on the trade-offs between the variable (α, β, γ) implementation versus the state-variable Kalman filter implementation will be given in a later section of this report.

3.2 Frequency Domain Measurement

The range rate (radial velocity) of a target can be measured, in principle, via the doppler shift with respect to the transmitted frequency. In order to detect moving targets with a non-coherent airborne pulsed radar, one possible conventional scheme which is sometimes used is to make reference to the neighboring clutter returns. Such "clutter referenced" radar essentially establishes the zero doppler reference from the averaged doppler of the incremental clutter returns provided the latter are of sufficient magnitude. In the present application, the radar has to acquire the moving satellite in (clutter free) space thus rendering the non-coherent doppler measurement technique ineffective.

3.3 Time Domain Measurement

When the dynamics of the target are known, various filtering operations (least squares, fixed and variable (α, β), state variable Kalman filtering) can be applied, each of which has its own advantages and drawbacks in terms of memory and computational requirements, accuracies, and various more subtle trade-offs involving target dynamics, PRF rate, total smoothing time, and detection probability. In the sequel, we will derive the mean square smoothing errors for both first and second order systems using "optimum" variable (α, β) and (α, β, γ) filters. It can be shown that under certain usual assumptions the variable (α, β, γ) smoothing is equivalent to the n-point least

squares method in terms of errors due to measurement noise. We will not prove this statement here. However, its performance will be compared with that obtained with the state variable Kalman filtering approach in a later section of this report. The inferiority of the fixed (α, β) filter in comparison with the state-variable approach is well known and thus will not be addressed further.

3.4 Errors Due to Measurement Noise - Second Order Case, α, β, γ Filters

a. Recursive Solution

Assuming the vehicle does indeed follow a second degree law (i.e., the true value of radial acceleration is non-zero), the one-step prediction and smoothing equations for second order tracking using the variable (α, β, γ) filter can be written respectively as follows:

One Step Prediction Equations

$$\begin{aligned}
\hat{R}_P(n) &= \hat{R}_S(n-1) + \hat{\dot{R}}_S(n-1)(\Delta T) + \tfrac{1}{2}\hat{\ddot{R}}_S(n-1)(\Delta T)^2 \\
\hat{\dot{R}}_P(n) &= \hat{\dot{R}}_S(n-1) + \hat{\ddot{R}}_S(n-1)(\Delta T) \\
\hat{\ddot{R}}_P(n) &= \hat{\ddot{R}}_S(n-1)
\end{aligned} \tag{10}$$

Smoothing Equations

$$\begin{aligned}
\hat{R}_S(n) &= \hat{R}_P(n) + \alpha_n(R(n) - \hat{R}_P(n)) \\
\hat{\dot{R}}_S(n) &= \hat{\dot{R}}_P(n) + \frac{\beta_n}{(\Delta T)}\,(R(n) - \hat{R}_P(n)) \\
\hat{\ddot{R}}_S(n) &= \hat{\ddot{R}}_P(n) + \frac{\gamma_n}{(\Delta T)^2}\,(R(n) - \hat{R}_P(n))
\end{aligned} \tag{11}$$

for $n = 1, 2, \ldots$

where ΔT = time between successive measurements, i.e., $1/(PRF)$

$R(n) = n^{th}$ range measurement = actual range + noise (from output of split-gate range tracker)

P => prediction

S => smoothing

$\dot{R}$ = range rate or radial velocity

$\ddot{R}$ = radial acceleration

$(\hat{\ })$ = an estimated (predicted or smoothed) value.

From (10) and (11), the following mean-square prediction and smoothing errors are obtained (assuming successive measurement errors are independent with zero means the variance of the n^{th} measurement = σ_n^2). A horizontal bar denotes an ensemble average.

One Step Prediction Error Averages

Variances

$$\overline{\epsilon(\hat{R}_P(n))^2} = \overline{\epsilon(\hat{R}_S(n-1))^2} + 2(\Delta T)\overline{\epsilon(\hat{R}_S(n-1))\epsilon(\hat{\dot{R}}_S(n-1))} + (\Delta T)^2\overline{\epsilon(\hat{\dot{R}}(n-1))^2} + (\Delta T)^2\overline{\epsilon(\hat{R}_S(n-1))\epsilon(\hat{\ddot{R}}_S(n-1))} + (\Delta T)^3\overline{\epsilon(\hat{\dot{R}}_S(n-1))\epsilon(\hat{R}_S(n-1))} + \tfrac{1}{4}(\Delta T)^4\overline{\epsilon(\hat{\ddot{R}}_S(n-1))^2}$$

$$\overline{\epsilon(\hat{\dot{R}}_P(n))^2} = \overline{\epsilon(\hat{\dot{R}}_S(n-1))^2} + 2(\Delta T)\overline{\epsilon(\hat{\dot{R}}_S(n-1))\epsilon(\hat{\ddot{R}}_S(n-1))} + (\Delta T)^2\overline{\epsilon(\hat{\ddot{R}}_S(n-1))}$$

$$\overline{\epsilon(\hat{\ddot{R}}_P(n))^2} = \overline{\epsilon(\hat{\ddot{R}}_S(n-1))^2} \qquad (12)$$

Covariances

$$\overline{\epsilon(\hat{R}_P(n))\epsilon(\dot{\hat{R}}_P(n))} = \overline{\epsilon(\hat{R}_S(n-1))\epsilon(\dot{\hat{R}}_S(n-1))} + (\Delta T)\left[\overline{\epsilon(\dot{\hat{R}}_S(n-1))^2} + \overline{\epsilon(\hat{R}_S(n-1))\epsilon(\ddot{\hat{R}}(n-1))}\right] + \frac{3}{2}(\Delta T)^2\overline{\epsilon(\dot{\hat{R}}_S(n-1))\epsilon(\ddot{\hat{R}}_S(n-1))} + \tfrac{1}{2}(\Delta T)^3\overline{\epsilon(\ddot{\hat{R}}_S(n-1))^2}$$

$$\overline{\epsilon(\hat{R}_P(n))\epsilon(\ddot{\hat{R}}_P(n))} = \overline{\epsilon(\hat{R}_S(n-1))\epsilon(\ddot{\hat{R}}_S(n-1))} + (\Delta T)\overline{\epsilon(\dot{\hat{R}}_S(n-1))\epsilon(\ddot{\hat{R}}_S(n-1))} + \tfrac{1}{2}(\Delta T)^2\overline{\epsilon(\ddot{\hat{R}}_S(n-1))^2}$$

$$\overline{\epsilon(\dot{\hat{R}}_P(n))\epsilon(\hat{R}_P(n))} = \overline{\epsilon(\dot{\hat{R}}(n-1))\epsilon(\ddot{\hat{R}}_S(n-1))} + (\Delta T)\overline{\epsilon(\ddot{\hat{R}}_S(n-1))^2} \qquad (13)$$

Smoothing Error Averages

Variances

$$\overline{\epsilon(\hat{R}_S(n))^2} = \overline{\epsilon(\hat{R}_P(n))^2} - 2\alpha_n\overline{\epsilon(\hat{R}_P(n))^2} + \alpha_n^2(\sigma_n^2 + \overline{\epsilon(\hat{R}_P(n))^2})$$

$$\overline{\epsilon(\dot{\hat{R}}_S(n))^2} = \overline{\epsilon(\dot{\hat{R}}_P(n))^2} - \frac{2\beta_n}{(\Delta T)}\overline{\epsilon(\hat{R}_P(n))\epsilon(\dot{\hat{R}}_P(n))} + \frac{\beta_n^2}{(\Delta T)^2}(\sigma_n^2 + \overline{\epsilon(\hat{R}_P(n))^2})$$

$$\overline{\epsilon(\ddot{\hat{R}}_S(n))^2} = \overline{\epsilon(\ddot{\hat{R}}_P(n))^2} - \frac{2\gamma_n}{(\Delta T)^2}\overline{\epsilon(\hat{R}_P(n))\epsilon(\ddot{\hat{R}}_P(n))} + \frac{\gamma_n^2}{(\Delta T)^4}(\sigma_n^2 + \overline{\epsilon(\hat{R}_P(n))^2}) \qquad (14)$$

Covariances

$$\overline{\epsilon(\hat{R}_S(n))\epsilon(\dot{\hat{R}}_S(n))} = \overline{\epsilon(\hat{R}_P(n))\epsilon(\dot{\hat{R}}_P(n))} - \alpha_n\overline{\epsilon(\hat{R}_P(n))\epsilon(\dot{\hat{R}}_P(n))} - \frac{\beta_n}{(\Delta T)}\overline{\epsilon(\hat{R}_P(n))^2} + \frac{\alpha_n\beta_n}{(\Delta T)}(\sigma_n^2 + \overline{\epsilon(\hat{R}_P(n))^2})$$

$$\overline{\epsilon(\hat{R}_S(n))\epsilon(\ddot{\hat{R}}_S(n))} = \overline{\epsilon(\hat{R}_P(n))\epsilon(\ddot{\hat{R}}_P(n))} - \alpha_n\overline{\epsilon(\dot{\hat{R}}_P(n))\epsilon(\ddot{\hat{R}}_P(n))} - \frac{\gamma_n}{(\Delta T)^2}\overline{\epsilon(\hat{R}_P(n))^2} + \frac{\alpha_n\gamma_n}{(\Delta T)^2}(\sigma_n^2 + \overline{\epsilon(\hat{R}_P(n))^2})$$

$$\overline{\epsilon(\hat{\dot{R}}_S(n))\epsilon(\hat{\ddot{R}}_S(n))} = \overline{\epsilon(\hat{\dot{R}}_P(n))\epsilon(\hat{\ddot{R}}_P(n))} - \frac{\beta_n}{(\Delta T)}\overline{\epsilon(\hat{R}_P(n))\epsilon(\hat{\ddot{R}}_P(n))}$$

$$- \frac{\gamma_n}{(\Delta T)^2}\overline{\epsilon(\hat{R}_P(n))\epsilon(\hat{\dot{R}}_P(n))} + \frac{\beta_n\gamma_n}{(\Delta T)^3}(\sigma_n^2 + \overline{\epsilon(\hat{R}_P(n))^2}) \tag{15}$$

The recursive equations of (12) and (14) constitute the computational basis for second order variable (α, β, γ) smoothing. They can also be used to demonstrate the main theoretical results. The first three equations in (14) can be used to obtain the so-called countdown values of (α, β, γ) as functions of the mean-square prediction errors. By taking derivatives of these equations with respect to α, β, and γ, respectively, and setting the results to zero, we obtain the following set of values which minimize the mean square smoothing errors $\overline{\epsilon(\hat{R}_S(n))^2}$, $\overline{\epsilon(\hat{\dot{R}}_S(n))^2}$, and $\epsilon(\hat{\dot{R}}_S(n))^2$, at the n^{th} measurement:

$$\alpha_n = \frac{\overline{\epsilon(\hat{R}_P(n))^2}}{\sigma_n^2 + \overline{\epsilon(\hat{R}_P(n))^2}}$$

$$\beta_n = (\Delta T)\frac{\overline{\epsilon R_P(n)\epsilon\dot{R}_P(n)}}{\sigma_n^2 + \overline{\epsilon R_P^2(n)}} = (\Delta T)\frac{\overline{\epsilon(\hat{R}_P(n))\epsilon(\hat{\dot{R}}_P(n))}}{\sigma_n^2 + \overline{\epsilon(\hat{R}_P(n))^2}}$$

$$\gamma_n = (\Delta T)^2\frac{\overline{\epsilon R_P(n)\epsilon\ddot{R}_P(n)}}{\sigma_n^2 + \overline{\epsilon R_P^2(n)}} = (\Delta T)^2\frac{\overline{\epsilon(\hat{R}_P(n))\epsilon(\hat{\ddot{R}}_P(n)}}{\sigma_n^2 + \overline{\epsilon(\hat{R}_P(n))^2}} \tag{16}$$

The same set of equations can also be used to establish the so-called steady-state values of α, β and γ by prescribing the desired "goal values" for the respective smoothing errors and then solving for α, β and γ in terms of these goal values and mean square prediction errors. The details of this algebraic exercise will not be shown since it is not exactly germane to our main concern.

In actual implementation, the computational cycle starts with the specification of the mean square smoothing errors which, together with the time difference ΔT since last measurement, will yield the mean square (MS) prediction errors using (12). The appropriate values of α, β, γ are then calculated from (16) for the countdown phase or from the pertinent equation (not derived but mentioned above) for the steady state case. Using these calculated α, β, γ values and the MS prediction errors, the new MS smoothing errors can be computed from (14). The cycle thus repeats itself. The complexity of such a recursive implementation is rather obvious. In the sequel, we shall present an explicit set of equations that characterize the weighting coefficients $(\alpha_n, \beta_n, \gamma_n)$ and MS errors in terms of n (the number of range measurements) which yield a simple implementation as well as establish theoretical closed form solution for the errors. For the case of no missed measurements (i.e., detection probability equals one or ΔT is identical between any two successive measurements), and identical range measurement errors from the split-gate range tracker, i.e., $\sigma_n^2 = \sigma_{n-1}^2$ for all n, these results are equivalent to those derived earlier

in their recursive form. Indeed, they can be viewed as algebraic solutions to the recursive relations established earlier under such hypotheses.

b. Algebraic Solution

For purposes of clarity and compactness, the results will be presented in forms of theorems.

Theorem A. If no range measurement is missed, and the RMS error for such successive measurement is equal to σ_n^2 for all n, the smoothing errors and the associated variable weighting coefficients at time = $n\Delta T$ are given by:

Variances

$$\overline{\epsilon(\hat{R}_S(n))^2} = \frac{9n^2-9n+b}{n(n+1)(n+2)} \sigma_m^2, \quad n = 3,4,\ldots$$

$$\overline{\epsilon(\hat{\dot{R}}_S(n))^2} = \frac{192n^2 - 360\,n + 132}{n(n+1)(n+2)(n-1)(n-2)} \frac{\sigma_m^2}{(\Delta T)^2}$$

$$\overline{\epsilon(\hat{\ddot{R}}_S(n))^2} = \frac{720}{n(n^2-1)(n^2-4)} \frac{\sigma_m^2}{(\Delta T)^4} \tag{17}$$

Covariances

$$\overline{\epsilon(\hat{R}_S(n))\epsilon(\hat{\dot{R}}_S(n))} = \frac{18(2n-1)}{n(n+1)(n+2)} \frac{\sigma_m}{\Delta T}$$

$$\overline{\epsilon(\hat{R}_S(n))\epsilon(\hat{\ddot{R}}_S(n))} = \frac{60}{n(n+1)(n+2)} \frac{\sigma_m^2}{(\Delta T)^2}$$

$$\overline{\epsilon(\hat{\dot{R}}_S(n))\epsilon(\hat{\ddot{R}}_S(n))} = \frac{360}{n(n+1)(n^2-4)} \frac{\sigma_m^3}{(\Delta T)^3} \tag{18}$$

and Coefficients

$$\alpha_n = \frac{9n^2-9n+6}{n(n+1)(n+2)}$$

$$\beta_n = \frac{36n-18}{n(n+1)(n+2)}$$

$$\gamma_n = \frac{60}{n(n+1)(n+2)} \tag{19}$$

where

σ_m^2 = measurement error variance for all n

n = total number of measurements.

Proof: Equation (17) is proved by induction. Assume it is valid for (n-1), using these values in (12), the following MS prediction errors at time = $n\Delta T$ are obtained:

Prediction Error Variances

$$\overline{\epsilon(\hat{R}_p(n))^2} = \frac{9n^2+9n+6}{(n-1)(n-2)(n-3)}\ \sigma_m^2$$

$$\overline{\epsilon(\dot{\hat{R}}_p(n))^2} = \frac{192n^2-24n-36}{n(n^2-1)(n-2)(n-3)}\ \frac{\sigma_m^2}{(\Delta T)^2}$$

$$\overline{\epsilon(\ddot{\hat{R}}_p(n))^2} = \frac{720}{n(n^2-1)(n-2)(n-3)}\ \frac{\sigma_m^2}{(\Delta T)^4} \tag{20}$$

Prediction Error Covariances

$$\overline{\epsilon(\hat{R}_p(n))\epsilon(\dot{\hat{R}}_p(n))} = \frac{18(2n-1)}{(n-1)(n-2)(n-3)}\ \frac{\sigma_m}{\Delta T}$$

$$\overline{\epsilon(\dot{R}_p(n))\epsilon(\ddot{\hat{R}}_p(n))} = \frac{60}{(n-1)(n-2)(n-3)}\ \frac{\sigma_m^2}{(\Delta T)^2}$$

$$\overline{\epsilon(\dot{\hat{R}}_p(n))\epsilon(\dddot{\hat{R}}_p(n))} = \frac{360}{(n^2-1)(n-2)(n-3)}\ \frac{\sigma_m^3}{(\Delta T)^3} \tag{21}$$

Substituting the above values into (16), we obtain the countdown weighting coefficients of (19). Substituting (19) into (14) gives the desired values of (17). This completes the induction proof. Q.E.D.

It is important to realize that second order tracking does not start until the third measurement (n-3), since at least three points are required to obtain the acceleration components.

If the same MS errors as in (17) are to be maintained for succeeding measurements after the first n "countdowns", then the following theorem prevails.

Theorem B. The MS smoothing errors in (17) can be maintained subsequent to the n^{th} measurement by using the following "steady-state" weighting coefficients for all computations after the n^{th} measurement:

$$\alpha_{SS} = \frac{12(n^2+1)}{(n+1)(n+2)(n+3)}$$

$$\beta_{SS} = \frac{60n}{(n+1)(n+2)(n+3)}$$

$$\gamma_{SS} = \frac{120}{(n+1)(n+2)(n+3)} \qquad (22)$$

Proof: Assume the MS smoothing errors of (17) at the n^{th} measurement; application of (12) yields the MS prediction errors at time $(n+1)\Delta T$ as in (20) with n replaced by (n+1). Using these values along with (22) into (14), the resulting MS smoothing errors at time $(n+1)\Delta T$ are identical to the corresponding ones at time $n\Delta T$ as given by (17). This establishes the theorem. Q.E.D.

The previous two theorems provide, respectively, the approximate means of explicitly estimating pertinent MS errors of a second order system and the "freezing" of such errors once certain predetermined goals are reached for a system with sufficiently high detection probability.

3.5 First Order Case, α-β Filter

a. Errors Due to Measurement Noise

Assuming the vehicle does indeed follow a first degree law (i.e., its radial acceleration is identically equal to zero), the prediction and smoothing equations for first order tracking using variable (α, β) filter are as follows:

$$\begin{aligned} \hat{R}_P(n) &= \hat{R}_S(n-1) + \hat{\dot{R}}_S(n-1)(\Delta T) \\ \hat{\dot{R}}_P(n) &= \hat{\dot{R}}_S(n-1) \end{aligned} \tag{23}$$

$$\begin{aligned} \hat{R}_S(n) &= \hat{R}_P(n) + \alpha_n (R(n) - \hat{R}_P(n)) \\ \hat{\dot{R}}_S(n) &= \hat{\dot{R}}_P(n) + \frac{\beta_n}{\Delta T} (R(n) - \hat{R}_P(n)) \end{aligned} \tag{24}$$

As was done in the previous section on second order systems, identical arguments and analyses lead to the following results for the first order system under the assumptions that only measurement noises are of concern and no range measurement is missed (i.e., identical time interval between successive range measurements).

Theorem C (Counterpart of A). For a first order system, the smoothing errors and the associated countdown smoothing parameters at time = $n\Delta T$ are given by:

$$\overline{\epsilon(\hat{R}_S(n))^2} = \frac{4n-2}{n(n+1)}\,\sigma_m^2$$

$$\overline{\epsilon(\hat{\dot{R}}_S(n))^2} = \frac{12}{n(n^2-1)}\,\frac{\sigma_m^2}{(\Delta T)^2}$$

$$\overline{\epsilon(\hat{R}_S(n))\epsilon(\hat{\dot{R}}_S(n))} = \frac{6}{n(n+1)}\,\frac{\sigma_m^2}{\Delta T} \qquad (25)$$

and

$$\alpha_n = \frac{4n-2}{n(n+1)}$$

$$\beta_n = \frac{6}{n(n+1)} \qquad (26)$$

Theorem D (Counterpart of B). The MS smoothing errors in (25) can be maintained subsequent to the n^{th} range measurement by using the "steady-state" smoothing parameters given below:

$$\alpha_{SS} = \frac{6n}{(n+1)(n+2)}$$

$$\beta_{SS} = \frac{12}{(n+1)(n+2)} \qquad (27)$$

b. Errors Due to Maneuver

An acceleration in a first order system constitutes a simple maneuver. Assume the non-existence of measurement errors; the measured value of range at time = $n\Delta T$ is given by:

$$R(n) = \frac{A}{2}\,n^2(\Delta T)^2 \qquad (28)$$

and the true range rate at the same time is:

$$\dot{R}(n) = An(\Delta T) \qquad (29)$$

where

A = radial acceleration

Using the tracking equations (23) and (24) together with the following definitions of errors due to maneuver:

$$\begin{aligned} \epsilon_P(n) &= \hat{R}_P(n) - R(n) \\ \epsilon_S(n) &= \hat{R}_S(n) - R(n) \\ \epsilon_V(n) &= \hat{\dot{R}}_S(n) - \dot{R}(n) \end{aligned} \tag{30}$$

a set of difference equations for the three errors can be established. If it is assumed that n is sufficiently large that steady-state operation is in effect (i.e., each of the three above errors is independent of n), then the following "steady-state" errors due to simple maneuver are obtained:

$$\begin{aligned} \epsilon_P(n) &= -\frac{A(\Delta T)^2}{\beta_n} \\ \epsilon_S(n) &= -\frac{A(\Delta T)^2}{\beta_n}(1-\alpha_n) \\ \epsilon_V(n) &= -A(\Delta T)\frac{\alpha_n}{\beta_n} - \frac{1}{2} \end{aligned} \tag{31}$$

Substituting the steady-state values of α_n and β_n from (27) in (31), the following is obtained:

$$\begin{aligned} \epsilon_P(n) &= -A\frac{(n+1)(n+2)}{12}(\Delta T)^2 \\ \epsilon_S(n) &= -A\frac{(n-1)(n-2)}{12}(\Delta T)^2 \\ \epsilon_V(n) &= -A\frac{(n-1)}{2}(\Delta T) \end{aligned} \tag{32}$$

Recall that these errors are the result of a simple maneuver in the absence of measurement errors.

3.6 Numerical Evaluation Examples

Since the main interest here is the range rate errors, only the second equation of (17) and (25) and the third equation of (32) will be evaluated. For $n \gg 1$, the following approximate equations can be used:

$$\sigma_{\dot{R}}^2 = \frac{192}{n^3} \frac{\sigma_m^2}{(\Delta T)^2} \quad (2^{nd} \text{ order range rate } \underline{\text{smoothing variance}} \text{ due to measurement noise}) \tag{33}$$

$$\sigma_{\dot{R}}^2 = \frac{12}{n^3} \frac{\sigma_m^2}{(\Delta T)^2} \quad (1^{st} \text{ order range rate } \underline{\text{smoothing variance}} \text{ due to measurement noise}) \tag{34}$$

$$\epsilon_V(n) = -\frac{A}{2} n(\Delta T) \quad (1^{st} \text{ order range rate tracking error due to simple maneuver}) \tag{35}$$

It is interesting to note that the difference in range rate smoothing errors between a second order system and a first order one is an exact factor of 4 (factor of 16 in variance). With respect to a 2.5 kHz PRF system ($\Delta T = 4 \times 10^{-4}$ sec) with range measurement error of 100 feet and 203 feet (1 sigma), the following tables summarize the required smoothing times as a function of the specified range rate accuracy ($\sigma_{\dot{R}}$).

In Table I, the results for the second order system are listed. Recall that $\sigma_m = 203$ ft. is the present spec at 10 N. Mi. The present spec for $\dot{R}$ is $\sigma_{\dot{R}} = 1/3$ ft/sec. It can be seen that the corresponding

σ_m = standard deviation of range measurement

$\sigma_{\dot{R}}$ = standard deviation of range rate estimate

$n\Delta T$ = required smoothing time

σ_m (ft.)	$\sigma_{\dot{R}}$ (ft/sec)	$n\Delta T$ (sec)
203	1	14.7
203	0.5	23.3
203	1/3	30.5
203	0.1	68.1
100	1	9.2
100	0.5	14.5
100	1/3	19.1
100	0.1	42.5

Table I. Second Order System - Equation 33.

smoothing time is 30.5 sec. If σ_m is maintained at 100 feet, then the required smoothing time can be reduced to 19.1 sec.

The corresponding values for a first order system are shown in Table II, wherein it is seen that the required smoothing times are 12.1 sec and 7.6 sec, respectively. It appears that a second order system is inferior to a first order. Recall, however, that the first order system assumes that the acceleration is identically zero. The range rate errors that build up during a burn where a first order system is used are shown in Table III, under the assumption of no

σ_m (ft)	$\sigma_{\dot{R}}$ (ft/sec)	$n\Delta T$ (sec)
203	1	5.8
203	0.5	9.3
203	1/3	12.1
203	0.1	27.0
100	1	3.6
100	0.5	5.8
100	1/3	7.6
100	0.1	16.9

Table II. First Order System (Equation 34).

A^2 ft/sec^2	$n(\Delta T)$ = Burn Time (sec)	$\sigma_{\dot{R}}$ (ft/sec)
1	10	5
0.85	10	4.25
0.5	10	2.5
0.33	10	1.65
1	20	10
0.85	20	8.5
0.5	20	5
0.33	20	3.3

Table III. First Order System (Equation 25) Tracking Error Due to Simple Maneuver.

range error and no system noise.

Since there is no $\dot{R}$ estimation requirement when a burn is taking place, the question is: how fast will the first order system recover after a burn when the initial $\dot{R}$ error is as given in Table III. It will be significantly greater than the values in Table II, all of which are way out of the system spec of "recovery in 2 sec after a burn."

Note, however, that the preceding calculations were carried out using the assumption that σ_m(range) is approximately 1% of 10 N.Mi., which implies $\sigma_m \cong 200$ feet. Calculations were also carried out for $\sigma_m = 100$. We therefore included the calculations for σ_m which are required to meet or exceed system specifications. These are shown in Table IV.

σ_m (ft)	$\sigma_{\dot{R}}$ (ft/sec)	($n\Delta T$) sec
13.6	1/3	2
4.81	1/3	1
1.70	1/3	0.5
0.43	1/3	0.2

$n\Delta T$ = required smoothing time

$\sigma_{\dot{R}}$ = 1/3 ft/sec = system specification

σ_m = required standard deviation of range tracker

Table IV. First Order System Showing Required Standard Deviation of the Range Tracker

From Table IV it is evident that, to meet and to exceed the required range-rate measurement specifications, the range measurement accuracy σ_m must be less than approximately 14 feet. Whether such accuracies can be achieved at 10 N. Mi. with a non-coherent pulse radar with an average power constraint of 40 watts should be studied further.

These further considerations are of particular importance because the results provided in this report were derived under an assumption of ideal conditions. When additional degradation characteristics are accounted for, the required smoothing times can be expected to increase.

IV. Discussion - Conclusion

We make the following comments.

1) In the development of the previous section, primary emphasis has been placed upon the assessment of performance rather than details in implementation. The latter is a relatively easy task once the particular filter algorithm has been chosen.

2) The representation for range rate error used by Rockwell's report entitled "Support to Alternate Passive Target Rendezvous Sensor Study" is approximately equal (for a large number of range measurement points) to the one obtained in Section III equation (25) of this report with optimal variable (α_n, β_n) filter for a constant velocity target. With respect to a non-zero acceleration target, this simple implementation is clearly not adequate due to the cumulative effect of target maneuver error. For the first order system, the total range-rate error (in variance) can be closely approximated by the sum of

the variances due to measurement noise and that due to maneuver (non-zero constant acceleration).

3) Under the assumptions of statistically independent range measurements which are characterized by zero mean Gaussian errors, and that the target dynamics can be characterized by a constant acceleration model, then the following three filters are equivalent in terms of filtering errors due to measurement noise.

i) The classical n-point least squares filter,

ii) The optimal variable $(\alpha_n, \beta_n, \gamma_n)$ filter,

iii) The Kalman filter.

The equivalence is essentially shown in the literature in references [25, 28, 29, 30]. We cannot expect to improve our results, therefore, by the use of any of the other filters listed above.

4) Since the dynamics of the relative range between the target and radar can be adequately modeled by a constant acceleration model (allowing the possibility of being equal to zero), then the recursive filter employing optimal variable $(\alpha_n, \beta_n, \gamma_n)$ coefficients is preferred over the Kalman filter implementation. This is because of the savings in computer requirements (storage and computation time) by a factor of at least 2 or 3 realized by the former over the latter (see [25]).

In addition, under the assumptions of constant range measurement error (i.e., the variances of successive range measurements are invariant with respect to range) and there is a constant time interval

between any two successive measurements, a set of algebraic equations can be established for the variable $(\alpha_n, \beta_n, \gamma_n)$ filter coefficients (thus the successive gain) to allow "table look up" computation (e.g., a ROM) rather than the time consuming recursive calculation.

5) When the statistics of the data and measurement noise are Gaussianly distributed, linear estimates are globally optimal estimates. We have restricted attention to linear estimates, and therefore have developed the globally optimal filters for Gaussian statistics. Under these assumptions, any "adaptive" or "hybrid" algorithm will not be fruitful.

6) If the range dynamics can be modeled a priori as a function of range (i.e., knowledge of when a burn occurs exists, a priori), then the optimal filter to be used is a variable (α_n, β_n) filter over the no burn region, and an $(\alpha_n, \beta_n, \gamma_n)$ filter while the burn is in effect. This would minimize the required smoothing times, and not allow range-rate errors to accumulate due to target maneuverability. If the burn is to be modeled as a random process rather than a constant, then the use of the Kalman filter renders an optimal solution in terms of error at the expense of more extensive computational requirements.

7) All of the smoothing times presented in the previous section were developed and computed under relatively ideal conditions. When realistic items of Section II are taken into account (among which are transients in the split-gate range tracker, target noise, and target

maneuverability), the required smoothing time in all cases can be expected to substantially increase.

We conclude, therefore, that the optimal signal processing of range measurements cannot provide satisfactory range-rate estimates, even under relatively ideal conditions, when $\sigma_m \geq 100$ feet. On the other hand, Table IV shows the required range accuracies to meet range-rate measurement specifications.

REFERENCES

1. D. K. Barton, Radar System Analysis, Prentice-Hall, 1964.

2. C. L. Weber, "Feasibility of a Skin-Tracking Radar for the Space Shuttle Mission Re-Entry Portion of Mission," Axiomatix Report No. 7405-1, May, 1974.

3. M. I. Skolnik, "Theoretical Accuracy of Radar Measurements," IRE Trans. on Aeronautical and Navigational Electronics, Vol. ANE-7, No. 4, Dec. 1960, pp. 123-129.

4. J. J. Spilker, Jr., and D. T. Magill, "The Delay-Lock Discriminator - An Optimum Tracking Device," Proc. of IRE, Sept. 1961, pp. 1403-1416.

5. H. Meyr, "Nonlinear Analysis of Correlation Tracking Systems Using Renewal Theory," Univ. of So. Cal. Electronic Sciences Lab. Report No. USCEE 468, Feb. 1974.

6. H. Meyr, "Delay Measurement Using Stochastic Signals by Cross-Correlation Techniques," Univ. of So. Cal. Elec. Sci. Lab, Report No. USCEE 474, July, 1974.

7. W. T. Gill, "A Comparison of Delay-Lock Tracking Loop Implementations," IEEE Trans. on Aerospa ce and Elec. Sys., Vol. AES-2, July 1966, pp. 415-425.

8. R. H. DeLano, "A Theory of Target Glint or Angular Scintillation in Radar Tracking," Proc. IRE, Vol. 41, pp. 1778-1784, Dec. 1953.

9. R. B. Muchmore, "Aircraft Scintillation Spectra," IRE Trans. on Antennas and Propagation, Vol. AP-8, pp. 201-212, March, 1960.

10. R. H. Delano and Irwin Pfeffer, "The Effect of AGC on Range Tracking Noise," Proc. of IRE, June 1956, pp. 801-810.

11. J. H. Dunn and D. D. Howard, "The Effects of Automatic Gain Control Performance on the Tracking Accuracy of Monopulse Radar Systems," Proc. of IRE, March 1959, pp. 430-435.

12. J. H. Dunn, D. D. Howard, and A. M. King, "Phenomena of Scintillation Noise in Radar-Tracking Systems," Proc. of IRE, Vol. 47, May, 1959, pp. 855-863.

13. D. D. Howard, "Radar Target Angular Scintillation in Tracking and Guidance Systems Based on Echo Signal Phase Front Distortion," Proc. of National Electronics Conference, 1959, pp. 840-849.

14. J. E. Lindsay, "Angular Glint and the Moving, Rotating, Complex Radar Target," IEEE Trans. on Aerospace and Elec. Sys., Vol. AES-4, No. 2, March 1968, pp. 164-173.

15. J. H. Dunn and D. D. Howard, "Radar Target Amplitude, Angle, and Doppler Scintillation from Analysis of the Echo Signal Propagating in Space," IEEE Trans. on Microwave Theory and Tech., Vol. MTT-16, No. 9, Sept. 1968, pp. 715-728.

16. R. J. Sims and E. R. Graf, "The Reduction of Radar Glint by Diversity Techniques," IEEE Trans. on Antennas and Propagation, Vol. AP-19, No. 4, July 1971, pp. 462-468.

17. R. A. Scholtz, "On the Joint Density Signal Amplitude and Glint," Hughes Aircraft Co., Report 2143.31/6, 12 June 1972.

18. R. A. Scholtz, "Estimating Target Angle in Glint Situations," Hughes Aircraft Co. Report 2143.31/16, 26 July 1972.

19. D. K. Barton and H. R. Ward, Handbook of Radar Measurement, Prentice-Hall, 1969.

20. L. E. Matson, "Shuttle Radar, Effect of Radar Glint Error on Range Rate Data," RCA Report T/S-2-LEM-151, 31 May 1974.

21. L. E. Matson, "Shuttle Radar, Range Rate Processor Implementation for Noncoherent Pulse Radar," RCA Report T/S-2-LEM, 152, 11 June, 1974.

22. D. D. Howard and B. L. Lewis, "Tracking Radar External Range Noise Measurements and Analysis," Naval Res. Lab. Report 4602 (Aug. 31, 1955).

23. J. C. Axford, "Use of Adaptive Filter to Estimate Range Rate on Shuttle," NASA-JSC, Report No. CG4-73M-69, 17 Dec. 1973.

24. R. A. Singer, "Estimating Optimal Tracking Filter Performance for Manned Maneuvering Targets," IEEE Trans. Aerospace and Elec. Sys., Vol. AES-6, No. 4, July 1970, pp. 473-483.

25. R. A. Singer and K. W. Behuke, "Real-Time Tracking Filter Evaluation and Selection for Tactical Applications," IEEE Trans. on Aerospace and Elec. Sys., Vol. AES-7, No. 1, Jan. 1971, pp. 100-110.

26. A. J. Kanguck, "Transient Response of Tracking Filters with Randomly Interrupted Data," IEEE Trans. on Aerospace and Elec. Sys., Vol. AES-6, No. 3, May 1970, pp. 313-323.

27. C. Grubin, "An Interpretation of α, β Filters," Hughes Aircraft Co. Report 21 43.10/189, 19 Aug. 1970.

28. B. L. Marks, "Adjustment Pulses for Automatic Tracking," Royal Aircraft Establishment, Ministry of Aviation, London Tech. Note Math. 79, Nov. 1961.

29. H. W. Sorenson, "Kalman Filtering Techniques," in Advances in Control Systems, edited by C. T. Leondes, Vol. 3, 1966.

30. R. S. Bucy and D. D. Joseph, Filtering for Stochastic Processes with Appl. to Guidance, Wiley, 1968.

31. M. Aoki, Optimization of Stochastic Systems, Academic Press, 1967.

32. N. E. Nahi, Estimation Theory and Applications, Wiley, 1970.

APPENDIX E

SHUTTLE PULSE DOPPLER RADAR/TRANSPONDER SYSTEM FOR NONAMBIGUOUS RANGE AND RANGE RATE DETERMINATION

SUMMARY

This report presents a preliminary design analysis of a pulse doppler radar/transponder system for Shuttle rendezvous functions. The system analyzed provides for nonambiguous and simultaneous range and range rate tracking consistent with the specifications placed on the cooperative mode of operation. The salient features of the system are: (1) coherent tracking of the transponder reply, (2) multiple PRFs for range ambiguity resolution, (3) high PRF values (120 to 180 kHz) for resolution of doppler shifts and system frequency instabilities, and (4) eclipse-free range tracking. The peak transmitted power of 40 watts is assumed for both the radar and the transponder with the average power being about 3 to 4 watts for both.

The resultant 3σ accuracies at the maximum range of 560 km are:

$$\text{Range} \leq 1.2 \text{ meters}$$
$$\text{Range Rate} \leq 0.3 \text{ meters/sec}$$
$$\text{Angle Track} \leq 0.0235 \text{ (each axis)}.$$

The probability of the radar/transponder coherent lock-up within one minute is better than 0.99 with false alarm times in excess of one hour for both the radar and the transponder.

1.0 INTRODUCTION

The requirement for 0.1 m/sec range rate accuracy within 2 seconds lag time during the RCS braking places stringent demands on the implementation of the range rate estimator for the Shuttle pulse radar. Although special consideration is being given to the (α, β) and (α, β, γ) trackers, as well as accelerometer-aided tracking, radar configurations other than the baseline noncoherent pulse radar are being considered to meet the specified range and range rate requirements. One of such alternate configurations is a pulse doppler radar which provides nonambiguous range and range rate data for both the cooperative and noncooperative modes.

The salient feature of a pulse doppler radar system is an inherent capability to provide simultaneous measurements of range and range rate, with the particular advantage over the pulse radar being the accuracy of the range rate estimation. The latter feature is achieved by using a relatively high duty cycle, approximately 0.1 to 0.5, as compared to a typical duty cycle of 0.001 used for pulse radars. The high duty cycle, in conjunction with coherent transmission and reception, allows one to measure the doppler shift of the center line of the pulsed carrier. The doppler shift is then converted directly into the measure of the range rate. Pulse envelope information is used to determine the range. With proper selection of system parameters, such as the pulse repetition rate (PRF), the pulse width and the duty cycle, nonambiguous and relatively accurate measurement of both the range and range rate can be performed. Special techniques such as multiple PRF's, centerline tracking, etc., must be used, however, to achieve the desired goals.

A preliminary configuration for such a radar and a compatible transponder (beacon) are described in this report, along with the performance estimates for the cooperative mode. A nominal operating

frequency of 15 GHz is used for these baseline estimates. The performance estimates for the skin tracking, noncooperative mode are relegated to a later date when the full significance of the recently completed two-point target analysis is evaluated.

2.0 PULSE DOPPLER RADAR/TRANSPONDER SYSTEM

2.1 Block Diagram Descriptions

To provide a better understanding of the design philosophy which is discussed in the subsequent sections of this report, brief descriptions of both the radar sensor and the transponder block diagrams are presented first.

2.1.1 Radar Sensor Block Diagram

Figure 1 shows the block diagram for a pulse doppler radar which can be used with either the noncooperative or the cooperative (transponder) targets. However, because this report is devoted primarily to the design considerations for the cooperative mode, only a minimal description of the noncooperative (skin tracking) mode is provided.

As shown in the figure, a frequency synthesizer provides signals to both the transmitter and the receiver portion of the radar. All these signals are derived from a common crystal-controlled oscillator and thus are coherent. In the noncooperative mode, the transmitter drive signal is frequency hopped to reduce the effects of passive target scintillation. To maintain constant intermediate frequency (IF), the frequency of the receiver's first local oscillator is hopped in synchronism with the transmitted signal. Single sideband generators (SSBG) provide the frequency hopping of both the transmitter drive and the receiver's first LO signals. In the cooperative mode the frequency hopping is not required and the SSBGs are bypassed. Also, because in the cooperative mode the transponder offsets the return frequency by the radar's IF, the transmitter drive frequency is the same as that of the first LO.

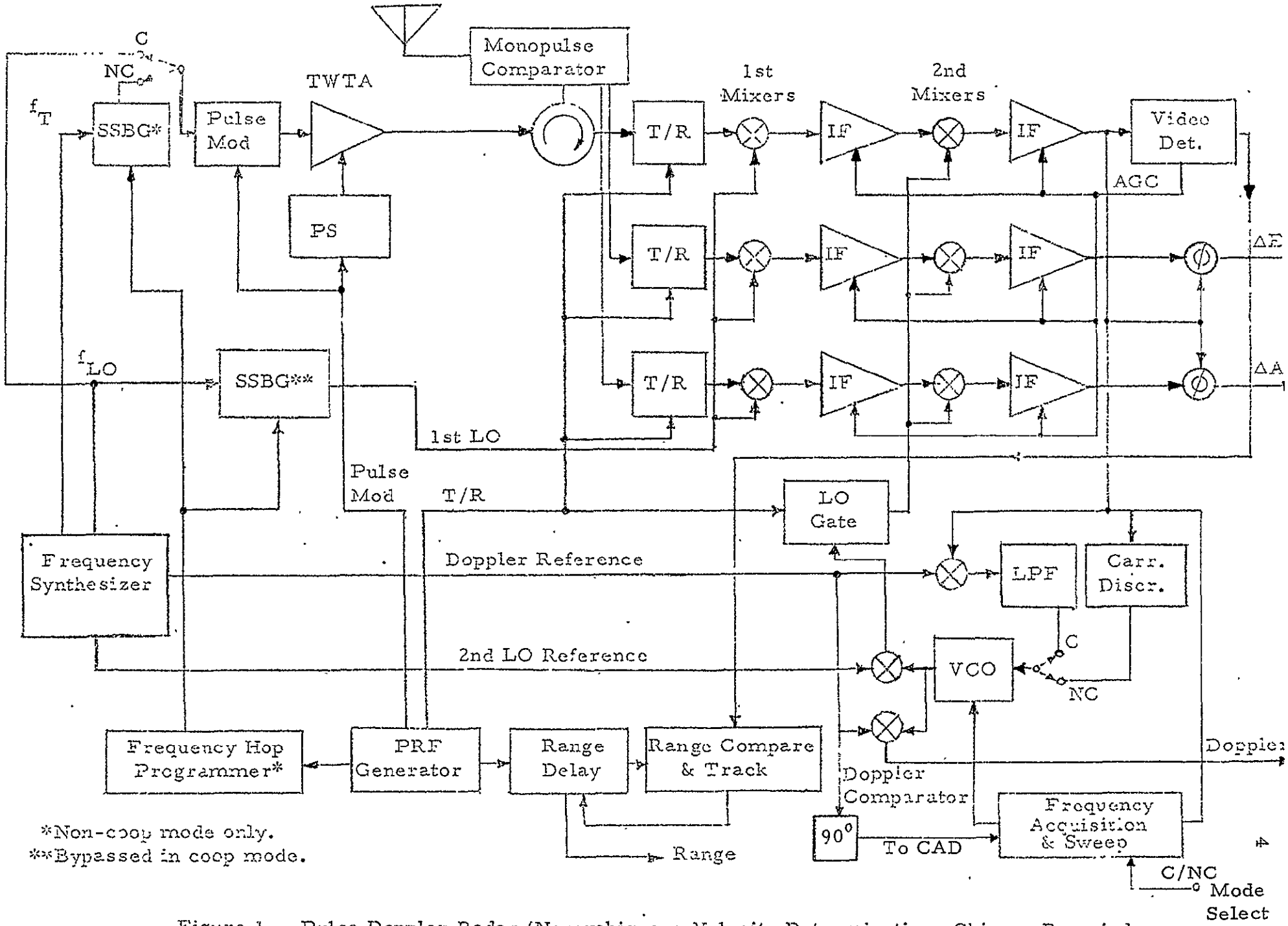

Figure 1. Pulse Doppler Radar (Nonambiguous Velocity Determination, Chinese Remainder Theorem, Pulsed Track Range)

In both modes (coop and noncoop), the transmitter RF drive and the power amplifier are pulsed to provide the required transmitter waveforms and pulse repetition rates. Although the gating of the transmitter drive alone could accomplish this function, turning off the transmitter tube prevents the transmitter noise from interfering with the target returns which arrive during the receive period.

Because of the relatively high PRFs used (tens of kilohertz) a gridded TWTA is preferred for the transmitter to reduce the complexity of the power supply/modulator unit. Preliminary estimates indicate, however, that a peak power on the order of 20 to 40 watts may be sufficient for both the cooperative and the passive target modes, and thus a possibility of using a high power solid state switch for TWTA output gating is not ruled out. Such gating may replace the function of the grid if a gridded tube is not available at the desired operating frequency.

A three-channel monopulse, superheterodyne receiver is used for amplifying and detecting the radar return in both the passive and cooperative modes. As shown, the monopulse converter provides the sum (Σ) and the two differences (ΔAz and ΔEl) signals required for the angle tracking of the targets. Each of these signals is amplified by a separate receiver channel with the Σ-channel providing the reference for the detection of the ΔAz and ΔEl signals.

On-off switching of the three receiver inputs provides receiver protection during the transmit period. An alternate technique (not shown) is to turn off the LO inputs to first mixers of all three channels. The advantage of the latter technique is that it eliminates the insertion loss of the T/R switches. Additional receiver isolation may be achieved by turning off the second LO and also by providing IF gating.

Although for the purpose of clarity, a dual-conversion, three-channel receiver is shown in Figure 1, the actual final configuration may require triple conversion to provide the necessary gain. Furthermore, techniques for multiplexing the difference channels may also be used in the final configuration for the purpose of reducing the number of receiver channels required to achieve two-axis monopulse angle tracking.

During the initial acquisition, the antenna scans over the target's angular uncertainty region. When the antenna is on target, the receiver intercepts and amplifies the pulsed, doppler shifted returns. The frequency of the doppler shifted center line is thus detected and the VCO is tuned to that frequency. The antenna scan is then terminated and the angle, as well as center line tracking, are initiated. The range acquisition and tracking are also initiated using a technique which involves multiple PRFs to resolve range ambiguity.

Because in the passive mode the coherency of the radar return may be destroyed by target errors and by frequency hopping, a carrier discriminator is used to maintain the VCO frequency on the center line of the return. In the cooperative mode the transponder provides a coherent return and thus the VCO becomes a part of a phase-locked loop (PLL) which coherently tracks the doppler-shifted center line.

In the receiver configuration shown, the doppler shift is "tracked out" at the second mixers by combining the VCO output with the "2nd LO reference" signal. The result is a second LO signal which includes the doppler shift. Thus, when either a coherent or a noncoherent frequency track is established the input to the second IF amplifiers has virtually no doppler shift. The VCO output frequency, however, includes this shift. Consequently, by comparing the VCO output with a known stable reference, the doppler shift, which is proportional to the range rate, is detected and measured.

The range information in both the passive and cooperative modes is obtained by processing out the range ambiguities caused by use of multiple, high rate PRFs. During the initial range acquisition, the radar may be cycled through several PRFs and the nonambiguous range determined by use of the Chinese remainder theorem.* Once the true range is determined, the range tracking may involve only one PRF at a time with

---

*M. Skolnik, Radar Handbook, pp. 19-13 to 19-16.

the PRF switching taking place when the target return approaches the transmit period, i.e., the condition known as eclipsing. Because after the initial acquisition the target is tracked in true range, the switching of the PRF does not introduce any transients. Thus, an eclipse-free tracking can continue indefinitely to within the pulse width.*

2.1.2 Transponder Configuration

Figure 2 shows the block diagram of the pulse doppler radar transponder. The transponder receives the signal at the radar frequency and provides a reply at the frequency which is offset by a value equal to the radar IF. Therefore, similar to the radar system in the cooperative mode, the first LO signal of the transponder is used to drive the transmitter.

Prior to the acquisition of the radar signal the transponder is "silent" and only its receiver is active. Because the actual frequency of the expected signal is not known, the LO frequency of the transponder is swept over the range of the frequency uncertainty. The sweep is performed by varying the frequency of a voltage controlled crystal oscillator (VCXO) whose output is multiplied to provide both the first and the second LO signals for the transponder's receiver. The rate and the width of the frequency sweep are determined by the considerations presented in sections 2.2 through 2.4.

As the radar antenna scans across the angular uncertainty region, a condition occurs when the transponder is within the beamwidth of the radar's antenna. During this condition, which is known as "dwell time," the transponder receiver locks on to the center line, i.e., the carrier line, of the pulsed radar signal. The lock is performed by a phase-locked loop (PLL) formed by the VCO and all the mixers to which the VCO supplies the LO signals. Of particular importance are the in-phase (I) and the quadrature (Q) phase detectors driven by the two orthogonal components

---

*Ibid., p. 19-17.

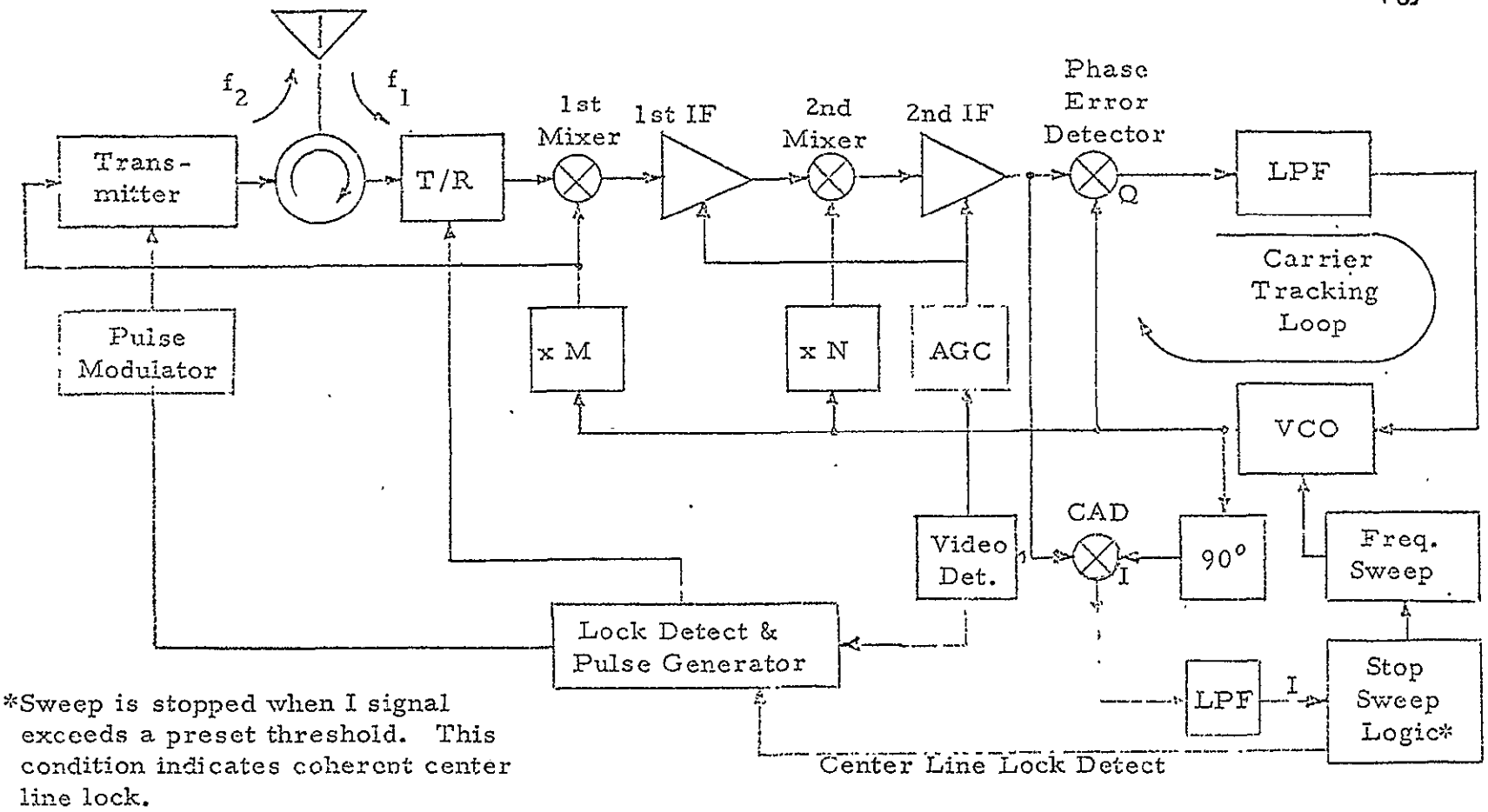

Figure 2. Pulse Doppler Radar Transponder Block Diagram (Coherent Operation)

of the VCO signal. When frequency and phase lock occur, the output of the in-phase detector is maximum and that of the quadrature detector is at its minimum. Thus, when the magnitude of the I signal exceeds a preset threshold, a lock condition is declared and the frequency sweep is terminated. Note that the I signal, which is generated by a coherent amplitude detector (CAD) is applied to the Stop Sweep Logic unit via a low-pass filter (LPF). This filter, plus the limited range of the VCO frequency sweep, prevent spurious lock-ups on spectral lines other than the carrier line.

Once the center line lock is detected the pulse generator initiates keying of the reply transmitter. In this report, it is assumed that the transmitter is a miniature magnetron* (20 to 100 watts peak output) which is primed by the LO signal to provide a coherent reply to the radar interrogator. The pulse duration and the rate of the transponder's replies are determined by the characteristics of the pulses received from the radar. Although the transponder replies at a frequency different from that of the received signal, a T/R switch is shown as included to prevent the receiver's first mixer from saturation.

2.2 Signal Design Considerations for the Active Mode

2.2.1 PRF Selection

Simultaneous and nonambiguous determination of both the range and the range rate generally imposes conflicting requirements on the selection of the PRF for a pulse doppler radar. The minimum theoretically acceptable PRF for nonambiguous range rate determination is twice the two-way doppler shift. Furthermore, with an active transponder the PRF may have to be increased beyond the theoretical minimum to accommodate

---

*Alternate candidates, such as small power TWTs or a pulsed solid state device, may be considered at a later date if it is established that acceptable performance can be obtained at the maximum acquisition range with smaller average transponder power than assumed here for the power link budgets.

drifts in the radar transmitter and the transponder's local oscillator frequencies.

For a 15 GHz (λ = 0.02 m) Ku-band radar, the doppler shift is determined by the closing and opening velocities of the target, which for the cooperative mode are ±91 m/seconds. Thus, the two-way doppler shift is

$$f_d = \pm\frac{2v}{\lambda} = \pm\frac{(2)(91)}{0.02} = \pm 9100 \text{ Hz} = \pm 9.1 \text{ kHz} . \qquad (1)$$

The corresponding minimum PRF (f_{rm}) for nonambiguous velocity (doppler) measurement is 18.2 kpps. The maximum nonambiguous range available (R_{max}) with this f_{rm} is

$$R_{max} = \frac{c}{2f_{rm}} = \frac{3\times10^5 \text{ km/sec}}{2\times1.82\times10^4} \cong 8.24 \text{ km } (4.45 \text{ nmi})$$

(c = velocity of light) . (2)

Because this R_{max} does not meet the requirements even for the passive target mode, which calls for target detection at 19 km, one must resort to use of more than one PRF.* However, before we consider the application of multiple PRFs, let us estimate what factors, other than the maximum doppler shift, determine the minimum usable PRF. For a practical system these factors will include the frequency drifts of various oscillators used in a system. Thus, in general, one can state that the minimum PRF (f_{rm}) must be

$$f_{rm} = 2(f_d + D_1 + D_2 + \ldots D_n) \qquad (3)$$

---

*M. Skolnik, op. cit., pp. 19-13 to 19-16.

where f_d is maximum doppler shift and D_n are the frequency drifts of various oscillators, including the PRF clock. It must be noted that although in some cases $+f_d \neq -f_d$ and that D_n's may add in a random fashion, the most conservative design approach is to use the maximum absolute value of each term within the brackets of equation (3). A case in point is a pulse doppler system which has to operate with an active transponder, such as a system described in this report. If we assume 15 GHz as the nominal system operating frequency, the major drift contributions will be due to the transmitter MOPA chain and due to local oscillators in the transponder. Considering typical stabilities available of the components and the maximum doppler shift due to relative velocities we can come up with the following tentative budget for a 15 GHz system:

Table 1. Major Sources of Frequency Uncertainty for a 15 GHz Pulse Doppler Radar/Transponder System

Source	Contribution	Assumption	Comments
Doppler shift	9.1 kHz	$\|91$ m/sec$\|$	Same for +V and -V
Radar MOPA Stability	1.5 kHz	$\|1 \times 10^{-7}\|$	Temperature compensated crystal oscillator (TCXO)
Transponder LO Drift	15.0 kHz	$\|1 \times 10^{-6}\|$	Voltage controlled crystal oscillator (VCXO)
Total ΔF =	25.6 kHz		

The frequency shift budget given in Table 1 indicates that the minimum PRF for the cooperative mode should be <u>at least</u> 52 kpps <u>prior</u> to radar/transponder frequency lock-up. After the frequency lock-up, the transponder instability is tracked out and the MOPA contribution is reduced by time averaging.

We now can proceed with the selection of multiple PRFs keeping in mind the fact that the implementation considerations limit such a number to a typical range from 2 to 5. First, we compute the radar time T_{max}

which will insure a maximum nonambiguous range that is in excess of the maximum specified range of approximately 560 km (300 nmi) for the cooperative mode. In the design example presented here, we arbitrarily assume, including a reasonable safety factor, that the maximum nonambiguous range for the cooperative mode is 1200 km. For this range, T_{max} is

$$T_{max} = \frac{2 R_{max}}{c} = \frac{(2)(1200 \text{ km})}{3 \times 10^5 \text{ km/sec}} = 8 \times 10^{-3} \text{ sec}$$

$$= 8 \text{ msec} . \qquad (4)$$

The next step is to apply the Chinese remainder theorem towards determining the "basic range time," τ, from T_{max} and a set of relatively prime numbers. These are related by the following expression:

$$\tau = \frac{T_{max}}{\prod_{k=1}^{K} n_k} \qquad (5)$$

where K = number of PRFs, and n_k = set of relatively prime numbers, such as N, N+1, N+2, etc.*

Practical considerations, such as hardware complexity and acquisition time limitations, dictate that the largest value of n_k should be limited to the range from about 8 to 50.** After considering various tradeoffs for our specific case we have tentatively selected four PRFs based on the following set of relatively prime numbers:

N = 9	N + 2 = 11
N + 1 = 10	N + 4 = 13 .

---

*C. L. Weber, "Analysis of a Center Line Pulsed Doppler Radar Operating in the Search Mode," Appendix F of this report.

**M. Skolnik, op. cit., p. 19-15.

Based on these numbers, the basic range time is:

$$\tau = \frac{T_{max}}{N(N+1)(N+2)(N+4)} = \frac{8 \times 10^{-3} \text{ sec}}{(9)(10)(11)(13)} = 0.62 \times 10^{-6} \text{ sec}$$

$$\approx 0.6 \ \mu\text{sec} . \qquad (6)$$

The four PRFs and their corresponding interpulse periods are then

$$f_1 = \frac{1}{(9)(0.62)10^{-6}} = 179 \text{ kpps} \qquad T_1 = \frac{1}{f_1} = 5.6 \ \mu\text{sec}$$

$$f_2 = \frac{1}{(10)(0.62)10^{-6}} = 161 \text{ kpps} \qquad T_2 = \frac{1}{f_2} = 6.2 \ \mu\text{sec}$$

$$f_3 = \frac{1}{(11)(0.62)10^{-6}} = 147 \text{ kpps} \qquad T_3 = \frac{1}{f_3} = 6.8 \ \mu\text{sec}$$

$$f_4 = \frac{1}{(13)(0.62)10^{-6}} = 124 \text{ kpps} \qquad T_4 = \frac{1}{f_4} = 8.1 \ \mu\text{sec}$$

These PRFs are considerably above the minimum value of 52 kpps, and thus provide adequate safety margin against any excessive frequency drifts. Yet their range is reasonably small so that it does not impose severe requirements on the modulator design.

2.2.2 Pulse Width and Duty Cycle Selection

Having selected the four PRFs (f_1 through f_4) and the corresponding interpulse periods (T_1 through T_4), we can address the question of selecting the pulse width and the corresponding duty cycle. If we were not concerned with the range measurement we could make the pulse width longer than the basic range time τ which, according to equation (6), is approximately 0.6 μsec. For a fixed transmitter peak output this would have placed more power into the center line, because the relationship between the peak power, P_r, and the center line power, P_c, is

$$P_c = P_r d^2 \tag{7}$$

where d is the duty cycle.

However, because we are concerned with the nonambiguous range measurement, as well as the accuracy of such measurement, we wish to keep the pulse width as narrow as possible, provided that the center line power is adequte to allow for the reliable acquisition of the center lines at both the transponder and the radar. As the subsequent power budgets indicate, we can meet this condition by allowing the pulse width to be as narrow as the basic range time τ of 0.6 μsec. With this pulse width, the lowest duty cycle will occur with the f_4 = 124 kpps, i.e., T_4 of 8.1 μsecs. The duty cycle in this case is 1/13 or 0.077. The P_c is then

$$P_c = P_r d^2 = P_r (0.077)^2 \cong 0.006\, P_r \ . \tag{8}$$

This corresponds to the center line power being about 22.3 dB below the peak power of either the beacon or the radar transmitter. With these assumptions, we proceed to work out the radar-to-beacon and the beacon-to-radar link power budgets.

2.3 Power Budgets

Because in this report we are considering the cooperative mode which involves a transponder (beacon), two power budgets have to be compiled to define the performance of the overall system. One budget defines the radar-to-beacon link and the other defines the beacon-to-radar link. Both of these budgets, however, are computed for the maximum range of 557 km and for parameters typical of a 15 GHz Ku-band system. Eclipsing loss is not taken into account since it is assumed that eclipse-free range tracking can be implemented by means of PRF switching.

2.3.1 Radar-to-Beacon Link

Table 2 shows the power budget for the radar-to-beacon link. It is assumed that the transmitter is capable of supplying to the antenna 40 watts of peak power and that the nominal radar antenna gain is 35.4 dB, a number which has been used in the past as the baseline gain of a 20-inch diameter, 4-horn, Cassegrain-fed dish. The beacon antenna loss of 6 dB includes the 3 dB polarization loss resulting from use of circular polarization for the beacon and linear polarization for the radar antennas.* A nominal 3 dB RF loss is also assumed for the T/R switch and a limiter which may be required to protect the receiver during the transmit cycle. This loss assumption may be re-evaluated as the details of the beacon design are worked out. The beacon antenna aperture is based on 0 dB gain at 15 GHz.

The 2 MHz beacon receiver bandwidth is determined by the 0.6 microseconds pulse width. Because of the crystal controlled MOPA chain at the receiver, the frequency drift is assumed to be negligible compared to this bandwidth (see data in Table 1). The assumption of 2 kHz two-sided noise bandwidth for the phase-lock loop at the beacon is based on the allowable sweep rates for searching over the frequency uncertainty region. This assumption is supported by calculations given in Section 2.4.

The results indicate that a reasonably high (+15 dB) SNR is available for PLL acquisition** of the center line. In comparison, the peak SNR per pulse may result in an excessive beacon transmitter triggering jitter which will have to be integrated out at the radar to achieve the required range accuracy. Such integration, however, may be quite feasible, since the fast PRFs used will provide many redundant returns which can be used for multiple pulse integration.

---

*Such polarization assignments simplify radar antenna design and still permit operation with random electromagnetic alignments of the two antennas.

**Typical acquisition threshold SNR for a PLL is +6dB.

Table 2. Radar-to-Beacon Link Power Budget (Pulse Doppler Radar)

$$P_r(B) = \frac{P_t G_t A_b L_b}{4\pi R^2} \qquad \text{Assume } f_0 = 15 \text{ GHz}$$

where $P_r(B)$ = Peak received power (at beacon)
P_t = Peak transmitted radar power
G_t = Radar antenna gain
A_b = Beacon antenna aperture
L_b = Beacon antenna losses
R = Range .

Term	Units	Gain (dB)	Loss (dB)	Comments
P_t	40 w	16 dBw		P_{ave} = 3.1 w for 0.077 duty cycle
G_t		35.4 dBw		λ = 0.02 m
$1/4\pi$			- 11	
$1/R^2$	557 km		-115	
A_b	3.2×10^{-5} m^2		- 45	0 dB gain at 15 GHz
L_b			- 6	3 dB RF loss; 3 dB polarization loss
		+51.4 dBw	-177 dB	

$P_r(B)$ = +51.4 dBw - 177 dB = -125.6 dBw

For beacon NF = 8 dB and BW = 2 MHz, beacon noise is:

$$N_b = -144 \text{ dBw} + 8 \text{ dB} + 3 \text{ dB} = -133 \text{ dBw}$$

$$\left(\frac{S}{N}\right)_P = \frac{P_r(B)}{N_b} = -125.6 \text{ dBw} - (-133 \text{ dBw}) = \underline{+7.4 \text{ dB}} = \text{Peak S/N per pulse}$$

$$\left(\frac{S}{N}\right)_{CL} = \left(\frac{S}{N}\right)_P \text{dB} + \left(\frac{BW}{2B_L}\right) \text{dB} - (d_{min}^2) \text{ dB}$$

$$= +7.4 \text{ dB} + 30 \text{ dB} - 22.3 \text{ dB} = \underline{+15.1 \text{ dB}} = \text{minimum center line S/N for } 2B_L^* = 2 \text{ kHz and } d_{min} = 0.077$$

*$B_L \equiv$ one-sided noise bandwidth of the PLL.

A certain amount of pulse integration may also be required at the beacon to reduce spurious transmitter triggering and missed pulses. With a 7.4 dB SNR and probability of detection of 0.9 per pulse, the false alarm rate is about 0.1.* This means that about one pulse out of ten received will not trigger the beacon transmitter and that about one pulse in an average period of several microseconds will be in a wrong time position. Although, as mentioned above, this may not be a problem at the receiver because of multi-pulse integration, spurious triggering of the beacon transmitter may place an excessive load on the modulator. Continuous integration of 3 to 10 pulses prior to triggering the beacon transmitter will virtually eliminate this problem. This integration, however, must be carried out in such a manner that no excessive time biases are introduced and that the range acquisition and tracking are not affected at the radar end.

2.3.2 Beacon-to-Radar Link

The beacon-to-radar link power budget is presented in Table 3. In estimating this budget we have assumed that the beacon transmitter power and the duty cycle are the same as that of the radar. Also, the noise figure and the IF bandwidths for pulse reception at the radar have been assumed to be the same as that of the beacon. Thus, if we were to use a 3 dB figure for radar system losses instead of 4 dB tentative assumptions, the peak and centerline power would have come out the same for both links. This, however, would not have been of significance because the radar system has potentially a better capability for signal processing than the transponder and thus any additional minor losses encountered due to relative complexity of the radar RF system can be compensated. The significant result is that the center line SNR is about 14 dB and thus a high probability of beacon acquisition can be obtained. The trade-offs pertaining to the acquisition sequence are discussed in section 2.4.

---

*M. Skolnik, op. cit., Figure 4, p. 2-19.

Table 3. Beacon-to-Radar Link Power Budget (Pulse Doppler Radar)

$$P_r(R) = \frac{P_b G_b L_p L_r A_r}{4\pi R^2}$$ Assume f_0 = 15 GHz

where $P_r(R)$ = Peak received power (at radar)

P_b = Peak transmitted beacon power

G_b = Beacon antenna gain

L_p = Polarization losses

L_r = Radar system losses

A_r = Radar antenna aperture

R = Range

Term	Units	Gain (dB)	Loss (dB)	Comments
P_b	40 w	16 dBw		P_{ave} = 3.1 w for 0.077 duty cycle
G_b		0		
$1/4\pi$			- 11	
$1/R^2$	557 km		-115	
L_p			- 3	
L_r			- 4	(Tentative assumption)
A_r	0.11 m^2		- 9.6	35.4 dB gain at 15 GHz
		16 dBw	-142.6 dB	

$P_r(R)$ = +16 dBw - 142.6 dB = -126.6 dBw

For radar NF = 8 dB and BW = 2 MHz, radar noise is:

$$N_r = -144 \text{ dBw} + 8 \text{ dB} + 3 \text{ dB} = -133 \text{ dBw}$$

$$\left(\frac{S}{N}\right)_P = \frac{P_r(R)}{N_r} = -126.6 \text{ dBw} - (-133 \text{ dBw}) = \underline{+6.4 \text{ dB}}$$ = peak S/N per pulse

$$\left(\frac{S}{N}\right)_{CL} = \left(\frac{S}{N}\right)_P \text{ dB} + \left(\frac{BW}{2B_L}\right) \text{ dB} - (d_{min}^2) \text{ dB}$$

For same parameters as beacon, i.e., $2B_L$ = 2 kHz and d_{min} = 0.077:

$$\left(\frac{S}{N}\right)_{CL} = +6.4 \text{ dB} + 30 \text{ dB} - 22.3 \text{ dB} = \underline{+14.1 \text{ dB}}$$ = minimum center line S/N

Because of the high PRF's used, the range accuracy of the pulse doppler system can be relatively good, even at the extreme range of about 560 km. For a single pulse SNR of 6.4 dB, the rms time error per pulse is, in the worst case,

$$\sigma_t = \frac{\tau}{\sqrt{(S/N)_1}} = \frac{0.62\ \mu\text{sec}}{\sqrt{4.35}} = \frac{0.62\ \mu\text{sec}}{2.1}$$

$$\cong 0.3\ \mu\text{sec} . \qquad (9)$$

The corresponding range error is

$$\sigma_r = 150\ \text{m}/\mu\text{sec} \times 0.3\ \mu\text{sec} = 45\ \text{meters} . \qquad (10)$$

This error is better than 0.01% of the maximum range of 560 km and, after multi-pulse integration available with high PRF, it can be reduced by an order of magnitude or more. The main concern is to insure that the device which estimates the true range from multiple ambiguous returns can perform its function and initiate the true range track without being limited by this error. This is one of the main reasons for assuming a relatively high average transponder reply power. If range and range rate accuracy requirements presently specified for the maximum acquisition range of 560 km are relaxed, lower peak and average beacon powers will be considered.

2.4 Acquisition Sequence

The acquisition sequence commences when the Shuttle navigation computer designates the radar antenna to the expected position of the cooperative target. The following events then take place:

1. The radar antenna is scanned over the angular uncertainty region.

2. During the time when the transponder is within the beamwidth of the radar's scanning antenna, the transponder receiver detects the radar signal and starts transmitting the replies.

3. The radar receiver detects the transponder replies and terminates antenna scan.

4. Angle, range, and range rate tracking are initiated by the radar.

Let us consider the details of this sequence.

2.4.1 Angular Search

The baseline procedure for acquiring the cooperative target was described in detail in an earlier report pertaining to the pulse radar.* It was determined that two scans, each limited to 30 seconds, will provide on-target dwell time of approximately 4 seconds per each scan. This dwell time is based on the antenna 3 dB beamwidth of 2.8 degrees, total uncertainty of 6 degrees by 6 degrees, a raster scan with 30% overlap and a scan reversal allowance of 20%. In the calculations that follow we will assume that the same parameters are applicable to the pulse doppler system and, thus, the on-target dwell time is 4 seconds.

2.4.2 Radar Acquisition and Reply Actuation

To conserve the power the transponder should activate its transmitter only after the detection of the radar signal. With a pulse doppler radar, which uses a coherent transmitter, two techniques are available for detection of the radar signal of the transponder. One technique is based on the detection of the center line (carrier) of the radar signal. The second technique utilizes a noncoherent detection of the radar pulses. In principle, both of these techniques can be used either sequentially or simultaneously for added reliability. Thus, in addition to describing both of these methods, we will also discuss the trade-offs involved in their use.

---

*S. Udalov, "Shuttle Pulse Radar/Transponder Configurations and Preliminary Performance Estimates for the Cooperative Mode," Appendix C of this report.

2.4.2.1 Center Line Acquisition

Consider first the center line acquisition. With this technique, the frequency of the VCXO, which provides all of the LO frequencies, is swept over a small range. This frequency deviation, when multiplied to the frequency of the first LO, covers the uncertainty range defined in Table 1. The rate at which this frequency uncertainty range can be swept is determined by the bandwidth of the carrier acquisition phase lock loop, signal-to-noise ratio and the probability of acquisition.

The maximum sweep rate which will provide 90% probability of acquisition is given by an empirical equation:*

$$\dot{\Delta}f_{max} \approx \left(1 - \frac{1}{\sqrt{SNR_L}}\right)(0.566)\, B_L^2 \qquad (11)$$

where $\dot{\Delta}f_{max}$ = maximum sweep rate

B_L = one side loop noise bandwidth

SNR_L = signal-to-noise ratio in $2B_L$.

From the power budget of Table 2, SNR_L = 15.1 dB (ratio of 32) for B_L = 1000 Hz. Thus,

$$\dot{\Delta}f_{max} \approx \left(1 - \frac{1}{\sqrt{32}}\right)(0.566)(1000)^2 \cong 0.466 \times 10^6 \text{ Hz/sec}$$

$$= 466 \text{ kHz/sec}. \qquad (12)$$

For an increased margin of safety it is advisable to sweep at a rate which is lower than the maximum rate indicated by equation (12). Let us assume a conservative rate of 100 kHz/sec and uncertainty range

---

*This is a modified version of equation 4-33, F. Gardner, Phaselock Techniques, p. 49. The modifications consist of conversion to Hz instead of radians and neglecting the effect of an amplitude limiter which may not be used in this system.

of ±50 kHz. This means that the sweep time will be one second. With a 4-second dwell time, it means that at least 4 sweeps will be available during one dwell time. Thus, for a single sweep probability of 0.9, the probability that the loop has acquired after four sweeps is

$$P_{Acq}(4) = 1 - \left[1 - P_{Acq}(1)\right]^4 = 0.9999 \quad . \tag{13}$$

When the acquisition takes place the output of the in-phase I detector, or CAD, reaches the amplitude of the center line component. This output is passed through a low pass filter and when the resultant DC voltage exceeds a preset threshold, the acquisition is detected. Because, as mentioned earlier, the detection of the center line acquisition can serve as the command to initiate transponder replies, the false alarm rate of this command must be low.

A trade-off exists between the bandwidth of the LPF, the available SNR, the probability of acquisition detection (P_D) and the false alarm rate (P_{fa}). If we assume that the LPF is a 2-pole Butterworth filter with a 3 dB bandwidth of 1000 Hz the required P_{fa} for one false alarm per hour is

$$P_{fa} \approx \frac{1}{(3600)(2)(1000)} = 0.14 \times 10^{-6} \text{ or } 1.4 \times 10^{-7} \quad . \tag{14}$$

Thus we can assume $P_{fa} = 10^{-7}$ criterion in calculating P_D. From curves in figure 4* for S/N = +15 dB, we obtain $P_D = 0.99$ for $P_{fa} = 10^{-7}$. These criteria provide for an acceptable performance. However, if we wish to improve the performance margin, we can narrow the LPF bandwidth to 500 Hz and thus increase S/N to about +18 dB. With 18 dB SNR, we can achieve $P_D = 0.999$ at P_{fa} of 10^{-14}. The response time for a 500 Hz LPF bandwidth is approximately 1 msec, which is twice the value for the 1000 Hz bandwidth case.

---

*M. Skolnik, op. cit., p. 2-13.

It is important to note that the 1 msec acquisition detection time is short compared to the time the swept signal spends in the 2 B_L interval. For the sweep rate of 100 kHz/sec and B_L = 1000 Hz, this time is 20 msec, thus providing adequate time for stopping the sweep. Because the decision times of the order of even a few milliseconds are short compared with the dwell time of 4 seconds, we conclude that we have adequate margin to satisfy all the detection and false alarm criteria required for radar detection and transponder actuation.

2.4.2.2 Radar Pulse Envelope Detection

Envelope detection and integration of the radar pulses is another technique which can be used for actuation of the transponder. The advantage of this technique is that it provides a check of the pulse width and the interrogation rate (PRF) before initiating a reply. The disadvantages are the relative complexity of the integration device, particularly if several PRFs are used, and the signal-to-noise ratio is low, thus requiring integration of many pulses.

Consider the requirements for our particular case which involves four PRFs. To insure one false alarm per hour, with a decision output available from either one of the four PRF integrators, the P_{fa} (per integrator) must be:

$$P_{fa} = \frac{1}{(3600)(4)(2 \times 10^6)} = 0.35 \times 10^{-10} \qquad (15)$$

(BW = 2 MHz)

With peak SNR of +7.4 dB per pulse, about 10 pulses must be integrated to obtain $P_D = 0.95$.* With two groups of 10 pulses each, the probability of detection can be increased to 0.9975.

Since the interpulse period corresponding to the lowest PRF (124 kpps) is about 8 microseconds, the "signal present" decision time

---

*M. Skolnik, op. cit., Figure 8, p. 2-21.

can be, including 2 groups of 10 pulses,

$$T_D = 8 \times 10^{-6} \times 2 \times 10 = 160 \times 10^{-6} \text{ sec or } 0.16 \text{ msec} . \quad (16)$$

This decision time may be longer if more pulses are integrated or if one integrates nonconsecutive groups. The order of magnitude of T_D then approaches that obtained with the center line detection.

Although some pulse integration may be required at the transponder to improve transmitter triggering stability, there appears to be little to be gained from using the radar pulse integration as the decision mechanism for reply initiation. On the other hand, pulse integration can be used as verification of radar signal reception after the center line has been acquired. The important trade-off lies between the complexity of a pulse integrator required at the transponder and the benefits to be gained from having pulse integration detection which provides reliability equivalent to that of a center line detector.

2.4.3 Transponder Acquisition

A few milliseconds after the transponder acquires the radar signal, its transmitter is turned on and the transponder replies begin to arrive at the radar. Now it is the radar's turn to detect these replies and to terminate the antenna scan. Again, similar to the radar acquisition, the detection of the transponder reply can be based on either the center line acquisition, the pulse envelope integration, or the combination of both.

2.4.3.1 Center Line Acquisition

For the center line acquisition, the frequency uncertainty is now reduced only to the two-way doppler shift which, as has been calculated earlier, is limited to about ±9.1 kHz. From Table 3, the center line SNR in $2B_L$ of 2 kHz is about +14 dB. Thus, we can use the frequency sweep technique similar to the one used in the transponder and obtain nearly similar acquisition performance. The sweep range in this case will be

limited to about ±10 kHz and with the sweep rate of 100 kHz/sec only 0.2 seconds will be required to make each sweep.

Furthermore, because the frequency uncertainty range is now reduced to only the two-way doppler shift we may consider widening the radar's phase lock loop bandwidth and thus allow the loop to acquire without sweeping. In general, the wider the loop bandwidth B_L the faster is the acquisition for a given frequency offset. But widening the loop decreases the signal-to-noise ratio. Thus, with finite SNR we can widen the loop only to a point where SNR_L is not less than 6 dB, a value which is considered a lower limit for acquisition without a priori knowledge of the frequency. With +14 dB SNR in $2B_L$ of 2 kHz we can increase B_L to about 6 kHz and still retain SNR_L of +6 dB. The ratio of maximum frequency offset to B_L is then approximately 1.5.

For SNR_L = +6 dB and $\Delta f/B_L = 1.5$, the probability of indicating lock* within 7 msec is 0.99. Thus, we see that acceptable center line acquisition performance can be obtained at the radar end without necessarily resorting to frequency search. However, SNR_L of 6 dB may not be sufficient to maintain lock for a long period of time and, thus, the B_L should be switched 1000 Hz after lock. Specifically, the average time to unlock is:**

$$T_{av} = \frac{1.06}{B_L} \exp\left[\pi (SNR)_L\right] \qquad (17)$$

where B_L and SNR_L are as defined earlier. For B_L = 6 kHz and SNR_L = 6 dB, T_{av} is approximately 50 seconds. Reducing the bandwidth to 1000 Hz after lock improves the SNR_L by a factor of 6 and T_{av} becomes 1.87×10^{22} years!

To determine the false alarm time with the non-sweeping phase lock method we consider the assumptions used for determining lock times.

---

*D. H. Hummels, "Some Simulations for the Time to Indicate Phase Lock," IEEE Transactions on Communications, Vol. COM-20, No. 1, February 1972, Figure 2, p. 42.

**F. Gardner, op. cit., p. 25.

These were based on LPF noise bandwidth equal to $0.1\,B_L$ and threshold corresponding to residual phase error of 0.5 radians.* Thus, the SNR in the LPF is 10 dB above that in $2B_L$ minus the loss due to $\cos^2(0.5\text{ rad})$ factor. In our case,

$$\text{SNR(LPF)} = 6\text{ dB} + 10\log_{10}\left(\frac{6000\text{ Hz}}{600\text{ Hz}}\right) + 10\log_{10}\cos^2(0.5\text{ rad})$$

$$= 6\text{ dB} + 10\text{ dB} - 1.1\text{ dB} = +14.9\text{ dB}\ . \qquad (18)$$

For $P_D = 0.99$, the P_{fa} is 10^{-7}. Thus, the false alarm time can be estimated:

$$t_{fa} = \frac{1}{2 \times 600\text{ Hz} \times P_{fa}} = \frac{10^7}{1200} = 8{,}333\text{ seconds or } 2.3\text{ hours}\ . \qquad (19)$$

This time exceeds the baseline specification of one false alarm per hour.

Thus, we have shown that at the radar end it is feasible, at least for the assumptions used, to provide center line lock without frequency sweep. However, if subsequent analysis indicates that additional safety margin is required at the radar end we may reconsider the use of frequency sweep over the doppler uncertainty range.

2.4.3.2 Range Acquisition

During the initial phase of range acquisition the radar PRFs are cycled over the four values and the position of the reply within the interpulse period of each PRF is determined. The nonambiguous range is then determined by solving the equation which defines the Chinese remainder theorem.

However, because of a relatively low signal-to-noise ratio per pulse (+6.4 dB from Table 3), integration of a number of pulses may be required to provide the accuracy required for reliable initiation of the range track. As was shown in equation (9) of section 2.3.2, the σ_t per pulse for SNR of +6.4 dB is about 0.3 microseconds. This value is

---

*D. H. Hummels, op. cit.

one-half of the 0.6 microsecond wide pulse. But for reliable tracking the maximum σ_t should be at least 1/6 of pulse width or less.* Thus, the number of pulses integrated for each search range cell must be:

$$n \geq \left(\frac{0.3\ \mu\text{sec}}{0.1\ \mu\text{sec}}\right)^2 \geq 9 \ . \tag{20}$$

After acquisition, when the nonambiguous range is determined and the range tracking begins in true range, the number of pulses integrated will be several orders of magnitude greater than that shown by equation (20).

During the acquisition, when several range cells have to be examined we may limit the number of pulses integrated to a value between 10 and 100. The maximum number of range cells to examine is required when the lowest PRF (124 kpps) is on. The number of basic range cells for this case is 12, but to provide for the intermediate positions, we require another set of overlapping cells. Thus, the total number of cells is approximately 25. With SNR = +6.4 dB to obtain $P_D = 0.95$ we have to integrate at least 14 pulses per range cell.** This corresponds to $P_{fa} = 10^{-12}$ per range gate. The false alarm time is then

$$t_{fa} = \frac{n\tau}{N P_{fa}} \tag{21}$$

where n = number of pulses integrated

τ = pulse width

N = number of range cells

P_{fa} = false alarm probability per cell .

Thus,

$$t_{fa} = \frac{(14)(0.6)(10^{-6})}{25 \times 10^{-12}} = 0.34 \times 10^6 \text{ sec}$$

$$= 3400 \times 10^2 \text{ sec or} \approx 94 \text{ hours.} \tag{22}$$

---

*Barton and Ward, Handbook of Radar Measurement, Section 8.2, p. 205.

**M. Skolnik, op. cit., Figure 8, p. 2-21.

If we integrate two groups of 14 pulses, the P_D becomes 0.9975 but the t_{fa} is still an order of magnitude above the baseline specification of 1 hour. Thus, we see that adequate range acquisition can be obtained within the framework of assumptions used.

2.5 Tracking Accuracy

Upon the completion of the acquisition cycle, tracking of the transponder reply is initiated. The expected tracking accuracies of the range, the velocity and the angle are discussed below.

2.5.1 Range Tracking Errors

2.5.1.1 Thermal Noise Error

The range tracking error due to the thermal noise term is expressed in time units as

$$\sigma_t \cong \frac{\tau}{\sqrt{(S/N)_1 \, n}} \tag{23}$$

where τ = pulse length

$(S/N)_1$ = peak SNR per pulse

and n = number of pulses integrated.

The number of pulses integrated is, in turn, defined as

$$n = f_r/\beta_{nr} \tag{24}$$

where f_r is the pulse repetition rate and β_{nr} is the noise bandwidth of the range tracking loop. In our case, at the acquisition range of approximately 560 km we have:

$(S/N)_1$ = 6.4 dB or a ratio of 4.3

τ = 0.6 microsecond

$f_r(\text{min})$ = 124 kpps .

If we assume β_{nr} of 10 Hz, we have at f_r(min) of 124 kpps:

$$n = \frac{124 \times 10^3}{10} = 1.24 \times 10^4 \tag{25}$$

and $$\sqrt{n} = \sqrt{1.24 \times 10^4} \cong 110 \ . \tag{26}$$

Thus,

$$\sigma_t = \frac{0.6 \ \mu sec}{110 \sqrt{4.3}} = \frac{0.6 \ \mu sec}{230} = 0.0026 \ \mu sec \tag{26}$$

and the corresponding rms range error is

$$\sigma_{rt} = \sigma_t \times 150 \ m/\mu sec = 0.39 \ meters \ . \tag{27}$$

This is an extremely good accuracy, but we must keep in mind the fact that we are assuming a relatively high transponder average power and our PRFs are also very high compared to the range tracking loop noise bandwidth.

2.5.1.2 Instrumentation Errors

2.5.1.2.1 Range Clock Error

Let us assume that a 10 MHz oscillator is used as a clock in the range counter and the range is measured to the nearest whole number of clock pulses. We then have Δ_r = 15 m, and the range error, assuming uniform distribution, is

$$\sigma_{rc} = \frac{15 \ m}{\sqrt{12} \ \sqrt{n}} = \frac{15 \ m}{(3.46)(110)} \cong 0.04 \ meters \ . \tag{28}$$

From (28) it is evident that the range clock error is an order of magnitude below the thermal noise error and thus does not limit the system accuracy at the extreme ranges. This is typical of most radar systems.

2.5.1.2.2 Bandpass Filter Time Delay Errors

Bandpass filtering of the pulse signal is used both at the beacon and at the radar. Such filtering introduces a delay bias. Although, in

principle, the major portion of this bias is fixed and thus can be calibrated out, some random component may remain due to variations of environmental conditions (temperature) and signal strength (AGC effects). Thus, a simplified calculation is made here to obtain a preliminary estimate for an order of magnitude of this error.

For the preliminary estimate, we assume that a 4-pole Butterworth filter 2 MHz wide (at 3 dB points) is used at the radar. The total envelope delay to the 50% step response amplitude for such a filter is about 0.223 microseconds.* If we assume that only 10% of this delay is random and it is uniformly distributed we obtain for an RMS range error:

$$\sigma_{rd} = \frac{(0.223\ \mu\text{sec})(150\ \text{m}/\mu\text{sec})(0.1)}{\sqrt{12}} = 0.97\ \text{meter} \quad . \tag{29}$$

The true nature of the randomness of this error is difficult to determine without going into the details of the circuit design, but the assumption used in (29) indicates that this error cannot be neglected, particularly for the short range operation. One must also keep in mind the fact that the transponder may also introduce an error of the same order of magnitude.

2.5.2 Velocity Tracking Accuracy

As has been stated earlier, the main reason for considering the pulse doppler radar system is the inherent capability of such a system to provide an unambiguous and highly accurate velocity, i.e., $\dot{R}$, readout. With a coherent transponder the frequency uncertainty of the return, after transponder/radar frequency lock-up is determined by the radar's MOPA stability and the signal-to-thermal noise ratio of the received signal. The widely used expression for time averaged frequency error is

---

*K. W. Henderson and W. H. Kautz, "Transient Response of Conventional Filters," IRE Trans. on Circuit Theory, December 1958, pp. 333-347.

$$\sigma_f = \frac{B_0}{\sqrt{2\,(S/N)_1\,n}} \tag{30}$$

where B_0 is the width of the spectral line and $(S/N)_1$, as well as n, is the same as defined for equation (23). In this case let us assume that the noise band of the frequency measuring device, β_{nf}, is 10 Hz and we therefore have the same n and $\sqrt{n}$ as for range error computation. In Table 1, MOPA frequency uncertainty is estimated at ±1.5 kHz (i.e., $\pm 1 \times 10^{-7}$ at 15 GHz). Thus, if we assume that this uncertainty is the primary factor in determining the spectral line width, we use B_0 = 3 kHz. Using equation (30) we calculate σ_f at the maximum acquisition range of 560 km:

$$\sigma_f = \frac{3000\ \text{Hz}}{110\sqrt{(2)(4.3)}} = 9.3\ \text{Hz} \ . \tag{31}$$

The corresponding range rate (velocity) error is

$$\sigma_{\dot{R}} = \sigma_f \frac{\lambda}{2} = \frac{(9.3)(0.02\,\text{m})}{2} = 0.093\ \text{m/sec} \tag{32}$$

and, consequently, $3\,\sigma_{\dot{r}} = 0.28$ m/sec < 0.3 m/sec, which means that the specified range rate accuracy can be achieved at the 560 km range.

It is important to point out that β_{nf} is not necessarily the bandwidth of the phase-lock loop, for it is questionable whether a phase-lock loop of such narrow bandwidth could track a carrier line of 3 kHz width. Thus, β_{nf} must be considered to be the bandwidth of some other frequency measuring device such as a counter, which performs the averaging function but does not have to perform the tracking.

It is also questionable whether the Ku-band carrier and the PRF lines will be smeared to a 3 kHz bandwidth. A more reasonable assumption is that the line widths will be an order of magnitude narrower (i.e., in the 100 to 300 Hz range) based on deriving the transmitter source from a crystal controlled reference.

Nevertheless, the calculations presented above indicate that, within the frame of the assumptions used, the pulse doppler radar/transponder system is capable of meeting the required range rate accuracy even at the maximum transponder acquisition range of 560 km.

2.5.3 Angle Tracking Accuracy

The angle error for each of the two angle tracking coordinates is expressed as:

$$\sigma_\theta = \frac{\theta_{3\ dB}}{K_m \sqrt{(S/N)_1 \ (f_r/\beta_{n\theta})}} \tag{33}$$

where $\theta_{3\ dB}$ = 3 dB antenna beamwidth

K_m = error slope for monopulse antenna (K_m = 1.57, typically)

$(S/N)_1$ = single pulse SNR

f_r = pulse repetition frequency

$\beta_{n\theta}$ = noise bandwidth of angle servo loop .

Assuming:

θ = 2.8 degrees

K_m = 1.57

$\beta_{n\theta}$ = 10 Hz

f_r = 124 kpps

$(S/N)_1$ = 6.4 dB or ratio of 4.3 ,

we obtain at the 560 km range, using $\sqrt{n}$ = 11.0

$$\sigma_\theta = \frac{2.8^0}{(1.57)(110)\sqrt{4.3}} = 0.0078^0 \text{ or } 3\sigma_\theta = 0.023^0. \tag{34}$$

This angle accuracy is about an order of magnitude better than the specified random error of 10 mr or 0.573^0. We conclude, therefore, that the

tracking error due to thermal noise is not a limiting factor within the framework of the assumptions used. Other factors, such as target rotation, may cause angular errors at close ranges even if one considers that a transponder is used. The transponder's antenna position may change, for example, as the target rotates at close ranges.

3.0 CONCLUSIONS

The preliminary analysis of a pulse doppler radar/transponder system indicates that the acquisition and tracking specifications can be met for the cooperative mode at the maximum range of 560 km. The results are favorable for the radar portion of the system because reliable radar signal acquisition at the transponder end can be achieved with peak power of about 40 watts and an average power on the order of 3 to 4 watts. These power requirements can be met at the radar end by a TWT amplifier which also must provide the bandwidth to permit frequency diversity during the passive mode. It must be noted that if a gridded TWTA capable of continuous operation at 40 watts is available the same TWT can be used also as a communication transmitter in an integrated radar/communication system.

At the transponder end a beacon type injection-locked magnetron can meet both the peak and average power requirements. However, because it is desirable to reduce the average power requirements for the transponder, other transmitter devices, possibly all solid state, should be considered for this type of system. Range accuracy may have to be sacrified, at least at the acquisition range, to allow use of the lower power devices. Latest information* indicates that, at ranges over 55 km (30 nmi), cooperative mode range accuracy requirements may be on the order of 100 meters. This may permit a use of a pulsed system which will place more power

---

*Shuttle Orbiter Ku-Band Radar/Communication Subsystems, Technical Status Presentation, RI/SD Document SSV75-28, 13-14 August, 1975.

into the center line by reducing the peak power and increasing the duty cycle. A reduction in average power may thus be achieved but then an eclipsing loss must be taken into account. With the present system, the eclipsing loss is virtually nonexistent because of accurate range track initiation at the maximum acquisition range of 560 km.

ADDENDUM TO APPENDIX E

METHOD FOR REDUCTION OF TRANSPONDER AVERAGE POWER REQUIREMENTS

In the preceding document, it was pointed out that lowering the average power of the beacon transmitter is desirable, and means for achieving this goal are being investigated. As the result of such investigation, an acceptable solution has been found and is recommended here.

The proposed method involves replacing the pulsed coherent transponder operation with a coherent CW reply which is bi-phase modulated in synchronism with the interrogating radar pulses. The received radar pulses and the transponder reply modulation are shown in Figure A-1.

We still assume that the parameters of the interrogating radar have not been changed. Therefore, the radar transmits 40-watt peak power pulses of about 0.6 microsecond duration at four switchable PRFs of 124, 147, 161, and 179 kpps, respectively.

At the output of the transponder receiver, these pulses have positive SN (+7.4 dB) and the center line component is sufficiently strong (+15.1 dB) for the receiver's carrier tracking loop to lock up during the available dwell time.

Transponder operation can be understood by referring to the block diagram of Figure A-2. Initially, the frequency of the VCO is swept so that the uncertainty range due to doppler shift and oscillator drifts is covered. When the center line of the doppler radar is intercepted, the transponder's first LO is coherently locked to the radar center line with an offset frequency equal to the transponder's first IF.

The lock detection circuit then turns on an injection-locked CW oscillator. A portion of the first LO signal is used to establish the coherency of the CW oscillator output. The output power of this oscillator is about 200 mw.

To provide the waveform required for phase modulation of the transponder CW reply, the envelope of the radar pulses is detected and

several samples of this envelope are integrated to provide a "cleaned up" modulation waveform. The resulting waveform is then as shown in part (a) of Figure A-1. This waveform is then applied to the phase modulator which introduces 180-degree phase reversals into the CW output of the injection-locked oscillator. Because these reversals occur in synchronism with the incoming radar pulses, they provide the necessary ranging information to the radar receiver.

The block diagram of the interrogating radar is shown in Figure A-3. This diagram is essentially the same as that described in previous reports with the exception of the addition of coherent detection of phase reversals in the cooperative mode. Coherent detection is used for two reasons: (1) to extract the ranging information from the phase-modulated transponder signal and (2) to avoid integration losses at low SNR which are now associated with the ranging information.

The operation of the radar receiver in the cooperative mode is otherwise unaltered. In other words, the VCO is searched until the center line of the transponder reply is detected. The VCO then tracks coherently the doppler shifted transponder reply and the doppler shift is extracted by comparing VCO frequency against a stable local reference. The ranging information is then recovered by a coherent amplitude detector (CAD) and the resulting pulses integrated to improve the tracking SNR. Initial range ambiguities are resolved by application of the Chinese remainder theorem algorithm.

The transponder-to-radar link budget corresponding to 200 mw CW transponder output is given in Table A-1. From this budget, we see that SNR of +13.4 dB, minimum, is available for the transponder center line acquisition. With this SNR, acquisition may be performed either without frequency sweep or with a sweep over a range determined only by the ±9.1 kHz maximum doppler uncertainty. The link budget also indicates that the SNR per pulse of ranging information is negative. But the subsequent analysis of range error, shown in Table A-2, indicates that because of relatively high PRFs used the ranging error is only 3.1 meters (1 σ) at 560 km. This is far in excess of the specifications.

τ = 0.6 microsecond
T = 5.6 to 8.1 microseconds

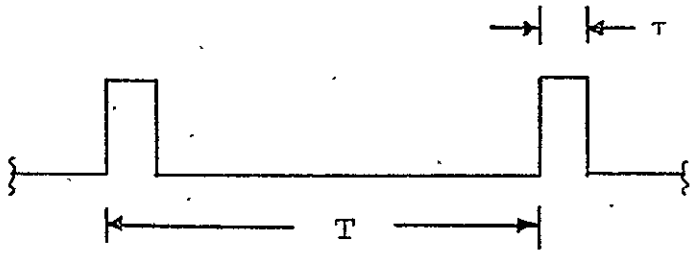

(a) Received and processed radar pulses (at transponder)

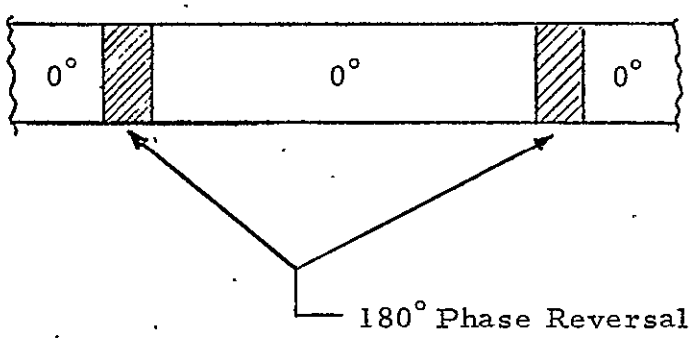

(b) Transponder reply RF phase modulation

Figure A-1. Transponder Reply RF Phase Modulation

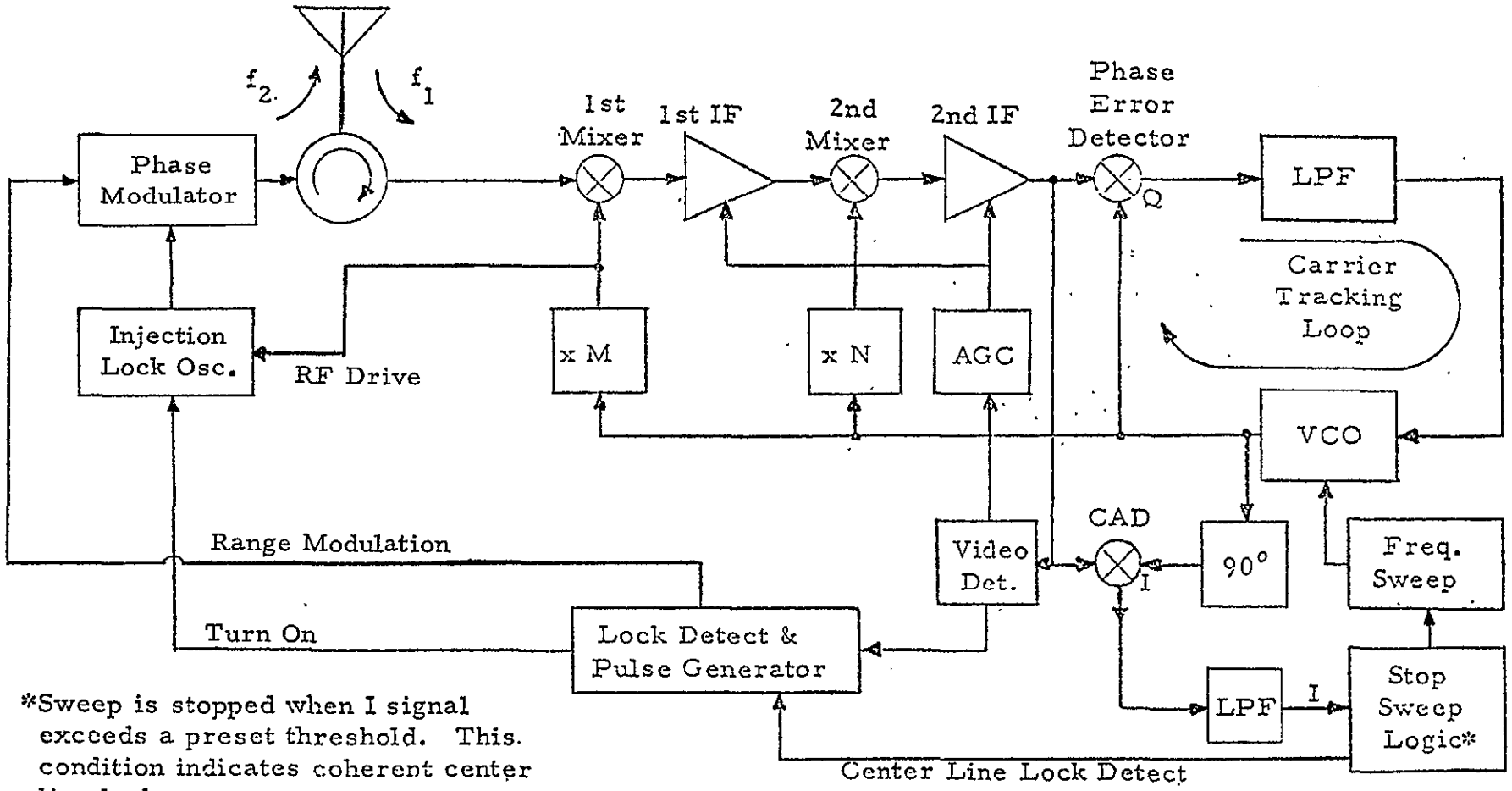

Figure A-2. Pulse Doppler Radar Transponder Block Diagram (Coherent Operation)

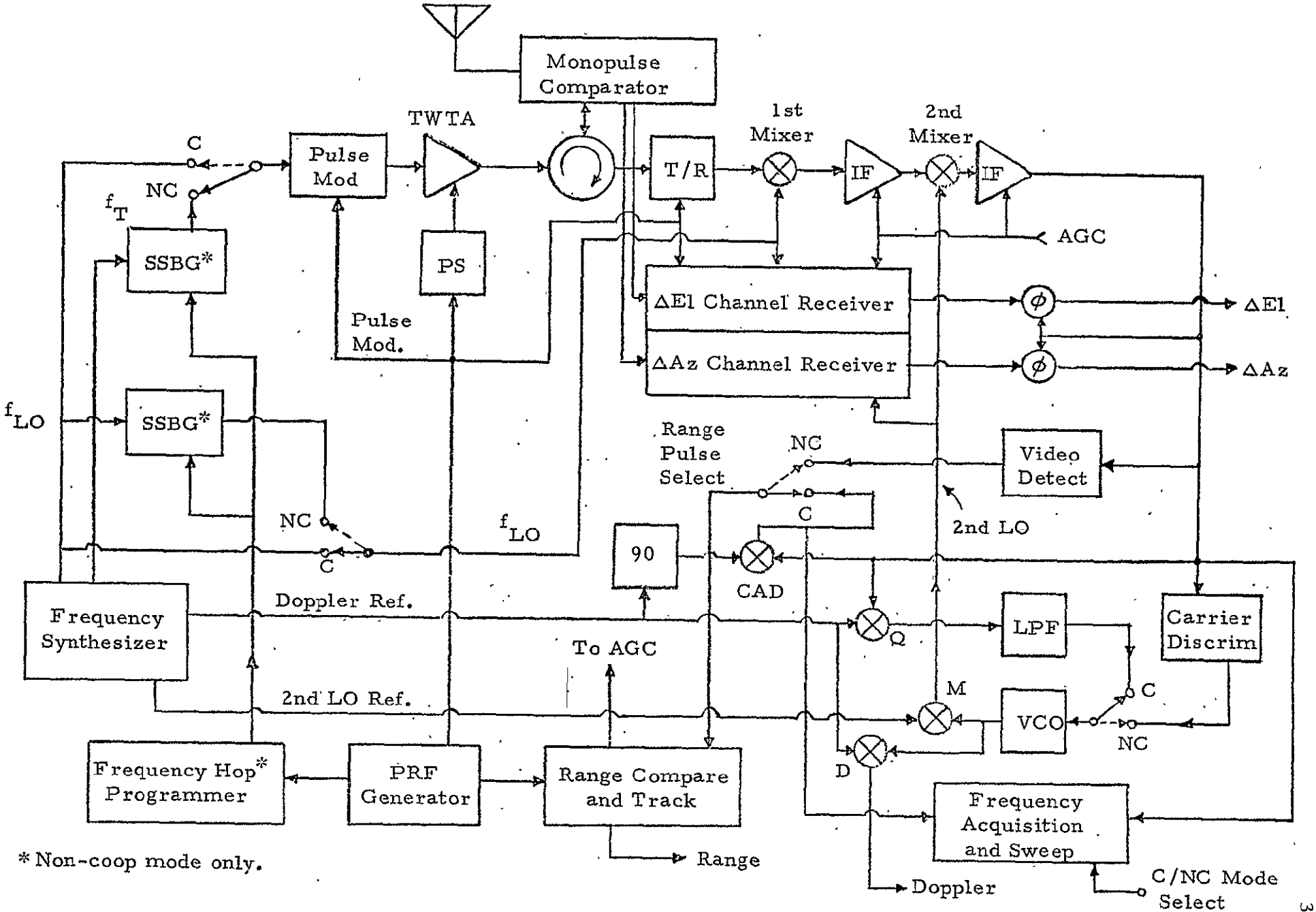

Figure A-3. Pulse Doppler Radar (Nonambiguous Velocity Determination, Chinese Remainder Pulse Track Range)

Table A-1. Transponder-to-Radar Link Power Budget (Pulse Doppler Radar)

$$P_r(R) = \frac{P_b G_b L_p L_r A_r}{4\pi R^2}$$

where

$P_r(R)$ = Power received at radar
P_b = Transponder RF power
G_b = Transponder antenna gain
L_p = Polarization losses
L_r = Radar system losses
A_r = Radar antenna aperture
R = Range

Term	Units	Gain (dB)	Loss (dB)		Comments
P_b	0.2 w	0 dBw	-7		CW power w/r to 1 watt
G_b		0			
$1/4\pi$			-11		
$1/R^2$	557 km		-115		
L_p			-3	(-0.5)	( ) Integrated system
L_r			-2	(-3.0)	
A_r	0.11 m^2		-9.6		
		0 dBw	-147.6	(-146.1)	

$$P_r(R) = 0 \text{ dBw} - 147.6 \text{ dB} = -147.6 \text{ dBw}$$

For radar NF = 8 dB and $2B_L$ = 2 kHz, radar noise is:

$$N_r(CL) = -174 \text{ dBw} + 8 \text{ dB} + 3 \text{ dB} = -163 \text{ dB}$$

$$(S/N)'_{CL} = -147.6 \text{ dBw} - (-163 \text{ dB}) = \underline{+15.4 \text{ dB}}$$

$$(S/N)_{CL} = (S/N)'_{CL} - L_{\text{duty cycle}} - L_{\text{eclips.}}$$

$$= +15.4 \text{ dB} - 1 \text{ dB} - 1 \text{ dB} = \underline{+13.4 \text{ dB}} \text{ min. (PRF} \cong 180 \text{ kpps)}$$

Range Data SNR for radar NF = 8 dB and BW = 2 MHz:

$$N_r(R) = -144 \text{ dBw} + 8 \text{ dB} + 3 \text{ dB} = -133 \text{ dBw}$$

$$(S/N)_1 = -147.6 \text{ dBw} - (-133 \text{ dBw}) = \underline{-14.6 \text{ dB}} \text{ peak S/N per pulse}$$

(Numeric value = .035)

Table A-2. Range Tracking Error - Thermal Noise

$$\sigma_t \cong \frac{\tau}{\sqrt{2\,(S/N)_1\, n}} = \frac{\tau}{\sqrt{2\,(S/N)_1\, f_r/\beta_{nr}}}$$

τ = pulse length = 0.6 microsecond

$(S/N)_1$ = SNR per pulse = -14.6 dB (0.035 numeric) at 560 km

f_r = PRF = 124 kpps (min)

β_{nr} = Noise BW of range tracking loop = 10 Hz

$n = f/\beta_{nr}$ = number of pulses integrated

$$= \frac{124 \times 10^3}{10} = 1.24 \times 10^4 \text{ or } \sqrt{n} \cong 110$$

$$\sigma_t = \frac{0.6\ \mu\text{sec}}{110\sqrt{(2)(0.035)}} = 0.021 \text{ microsecond}$$

$$\sigma_{rt} = \sigma_t \times 150\ \text{m}/\mu\text{sec} = (0.021)(150) \cong 3.1 \text{ meters}$$

APPENDIX F

ANALYSIS OF A CENTER LINE PULSED DOPPLER RADAR OPERATING IN THE SEARCH MODE

I. Radar Description

The transmitted waveform and receiver signal processing are different in the various modes of operation of a radar. We restrict attention in this presentation to the search mode of a particular coherent pulsed doppler radar. A simplified block diagram of the pulsed radar appears in Figure 1. In the search mode, the transmitted signal continuously cycles through 5 rF frequencies and 5 PRF's with a constant duty cycle as shown in Figure 2. The carrier component of the transmitted signal is coherent in all modes over the period of time that a given center frequency is employed, namely 12.5 msec. Target detection is performed on range rate information only; that is, there is no range detection via a bank of range gates.

The radar parameters which are common to all modes of operation are listed in Table I. The carrier component of the radiated signal is coherent implying that at all times the rf phase relative to that of a CW reference oscillator does not change. The coherence time is therefore equal to that of the dwell time at a particular rf frequency, namely 12.5 msec.

The PRF is one of 5 values. The choice of PRFs is discussed later and in the Appendices. The duty cycle of the transmitter is

$$d_t = 0.4$$

of each pulse repetition time, and the receiver is gated off during this time. The receiver duty cycle is

$$d_r = 0.6$$

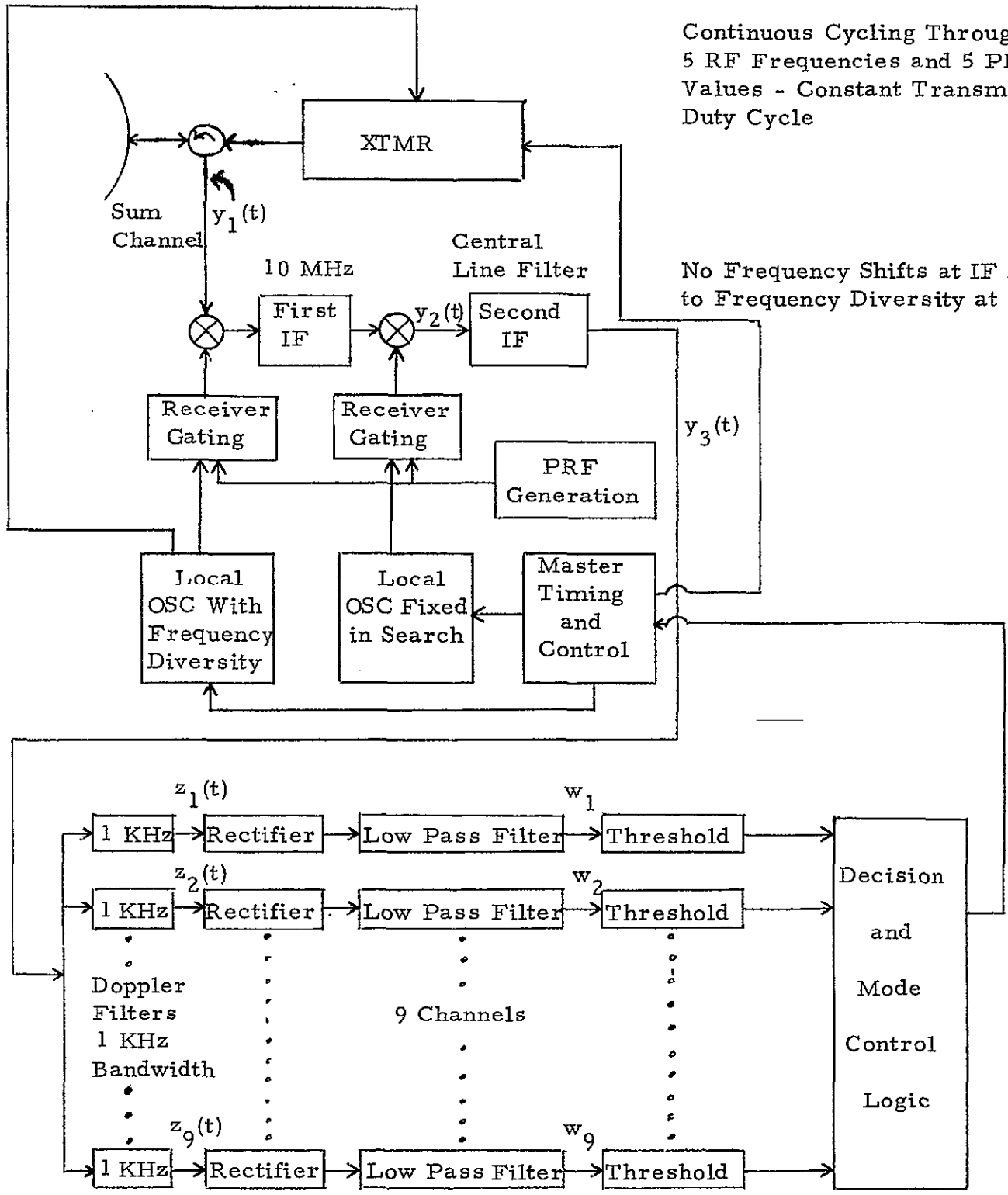

Figure 1. Center Line Pulsed Doppler Radar Receiver in Search Mode.

TABLE I

GENERAL RADAR PARAMETERS

Radar Classification	Center Line Coherent Pulsed Doppler Radar using a Medium PRF and a High Transmitter Duty Factor
Frequency	f_c = 15 GHz
Wavelength	λ = .02 m
Antenna Type	Cassegrain, 4-horn monopulse
Antenna Diameter	dia = 20"
Antenna Gain	G = 35.4 dB
Antenna Beamwidth	θ_B = 2.7 deg
Transmitter Duty Factor	d_t = 0.4
Receiver Duty Factor	d_r = 0.6
Noise Figure	F = 8 dB
Frequency Diversity	5 frequencies, sequentially switched, 50 MHz spacing, covering 200 MHz total
Pulse Repetition Frequencies	5 values

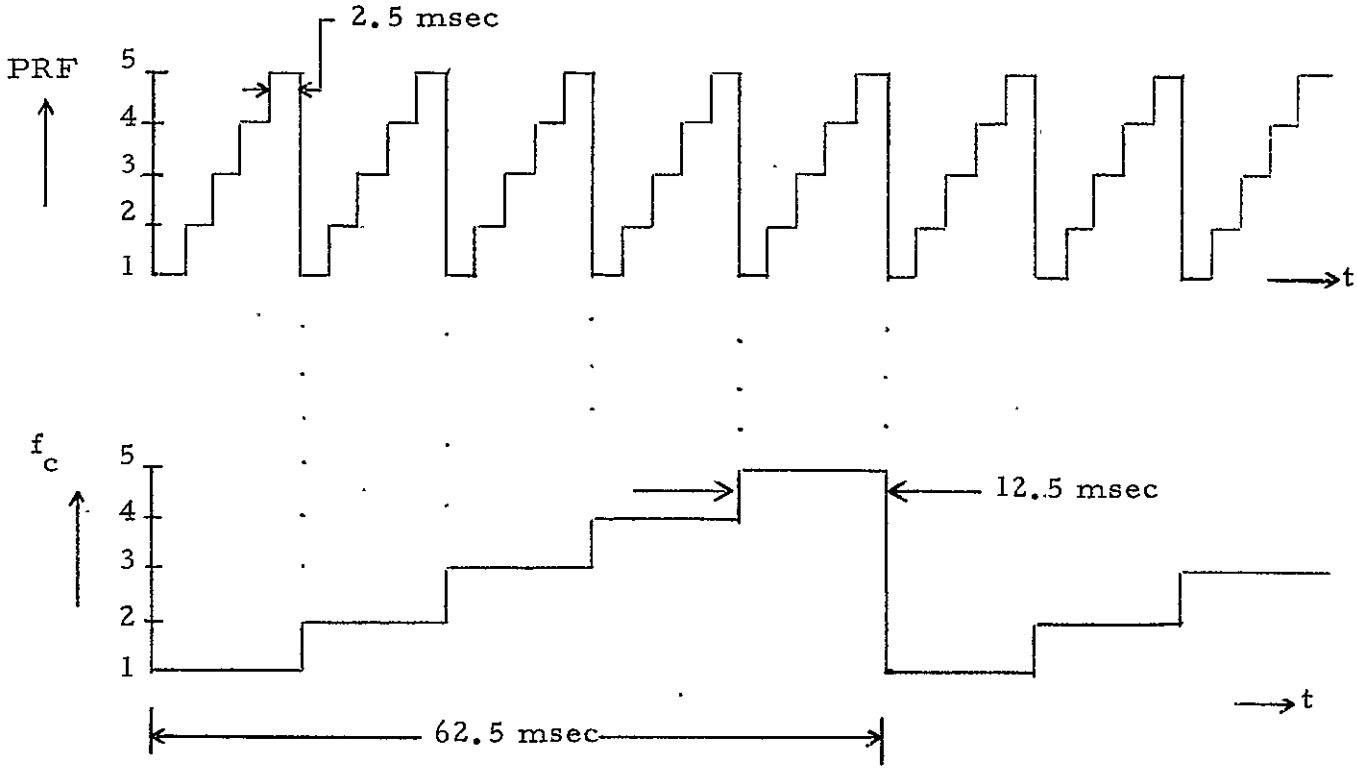

Figure 2. Time Schedule of RF Frequencies and PRF's

The variable PRF is provided to avoidblind ranges. This is important, even when detection is via Doppler frequencies only, so as to ensure sufficient energy return continuously.

As can be seen from Figure 1, the frequency of the first L.O. in the receiver is switched simultaneously with the transmitter, with the result that the signal at the IF does not change in frequency, except for the variation in Doppler frequency, which in our case is

$$\Delta f_D \approx 4.5 \text{ KHz}$$

This will be considered in more detail in the next section.

The first IF filter and amplifier, and the second IF mixer and filter (the center line filter) inputs are both gated. This provides isolation from the transmitter and eliminates the noise from being delivered by the receiver front end and first IF amp when the receiver is gated off at its input. The second IF filter is the center line filter; that is, it passes only the center line of the coherent radar waveform.

As shown in Figure 1 the output of the center line filter feeds a bank of Doppler filters which are designed with 100% overlap. This will be described in the next section. A detector is located at the output of each Doppler filter, which consists of an envelope detector, low pass filter (matched to the spacial dwell time, t_d = 80 msec), and a threshold comparison circuit. When any of the thresholds is exceeded, the search mode is terminated, and range acquisition and tracking is initiated.

Spectral Properties

The spectral properties of coherent pulse trains are summarized in Figures 3 and 4. When several PRF's are employed at the same rF, the pertinent spectral properties of the resulting waveform can be determined from the following. If the transmitter were turned on only for one PRF dwell time (2.5 msec), the spectrum of the received signal before the center line filter consists of lines spaced at f_{PRF} as shown in Figure 3. In the absence of eclipsing the detail between the lines for a small number of coherent pulses is shown in Figure 4. The power in the various lines are related by the normalized grating function

SPECTRAL PROPERTIES OF PULSE TRAINS

$$E_c(F) = \frac{N}{2}\left|P(F - F_0)\right|^2 \frac{1}{N}\left|\frac{\sin[\pi(F - F_0)NT]}{\sin[\pi(F - F_0)T]}\right|^2$$

$E_c(F)$: ENERGY SPECTRUM COHERENT PULSE TRAIN POSITIVE FREQUENCIES

$P(F - F_0)$: FOURIER TRANSFORM OF A SINGLE PULSE

$\triangleq C(F)$: NORMALIZED GRATING FUNCTION

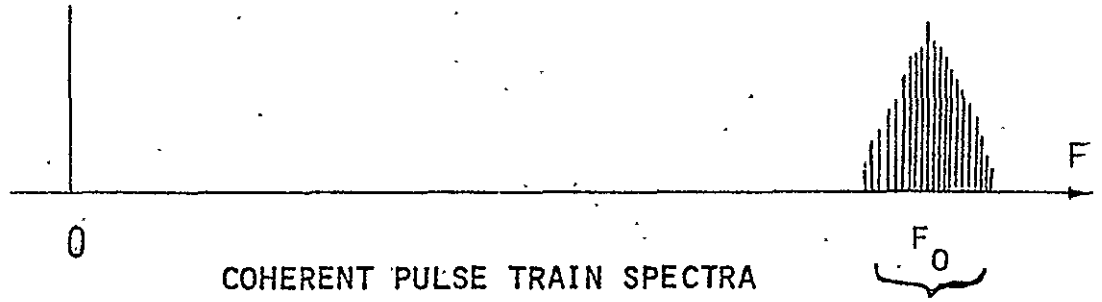

COHERENT PULSE TRAIN SPECTRA

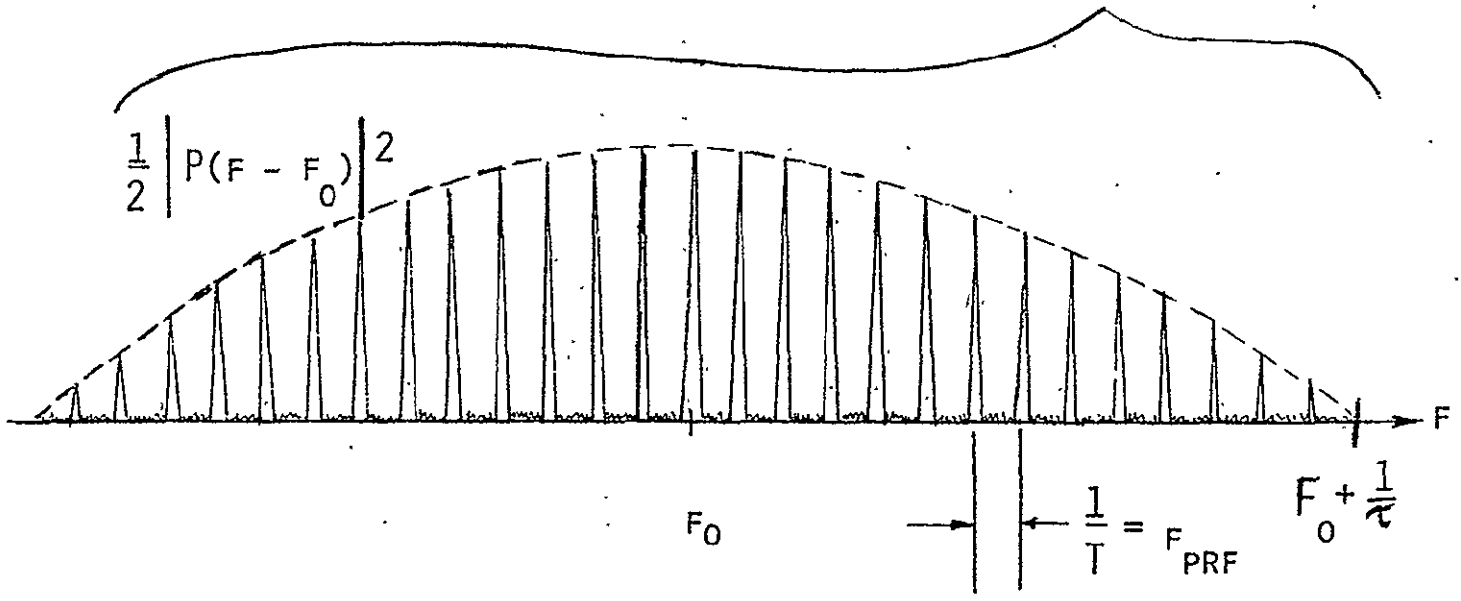

K = NUMBER OF LINES FROM CENTER TO FIRST CROSSOVER

$$= \frac{T}{\tau}_{PRF} = \frac{1}{D}$$

= [DUTY FACTOR]$^{-1}$

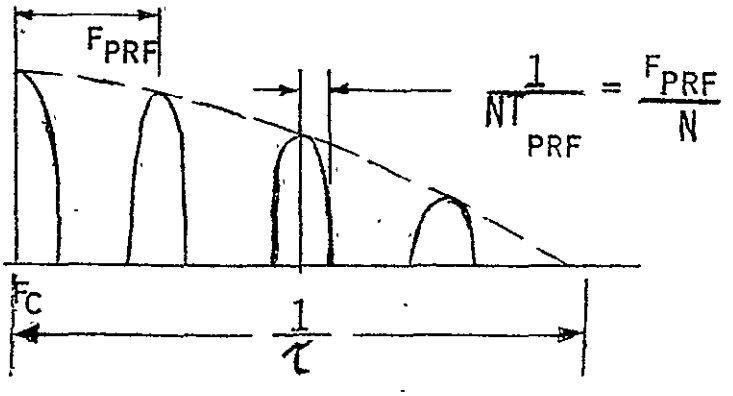

Figure 3.

N PULSE GRATING FUNCTION

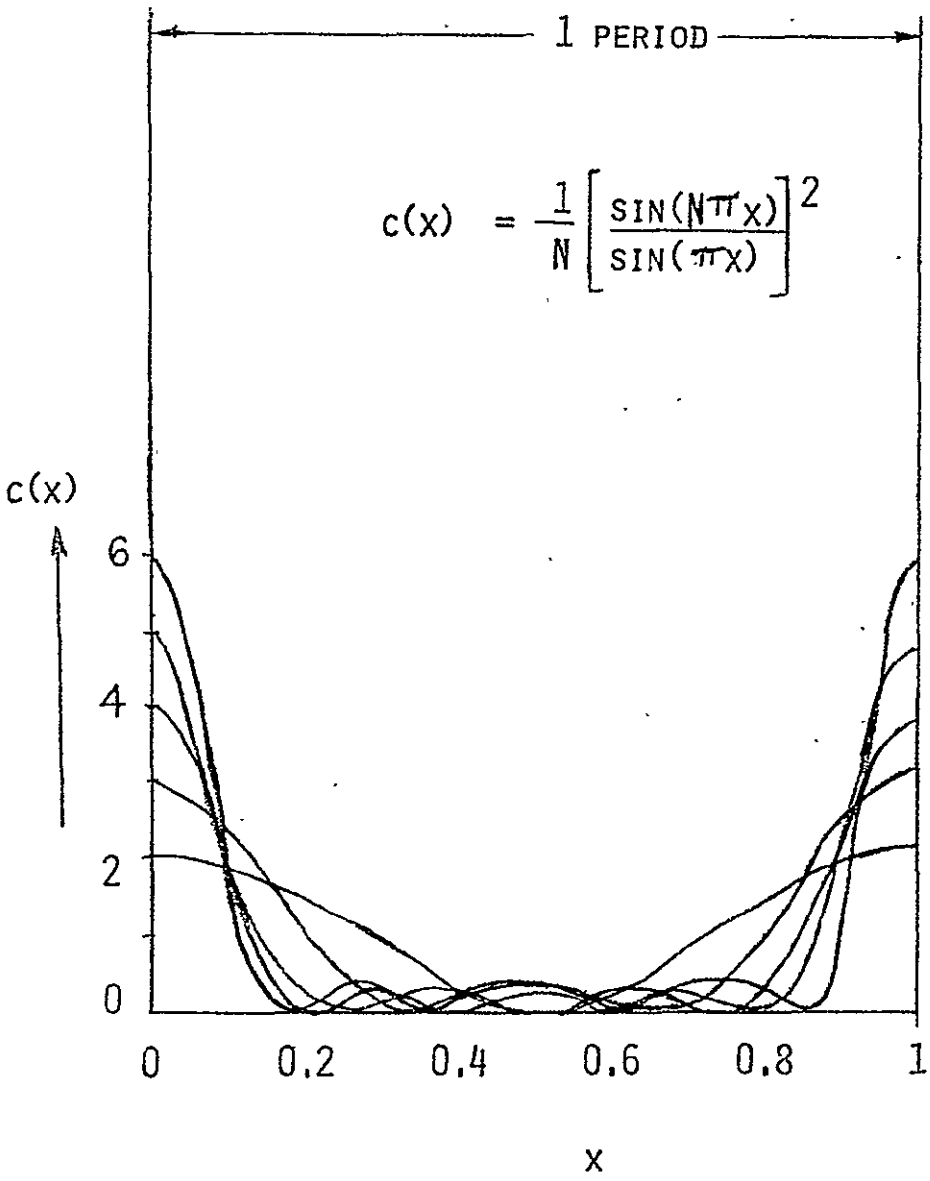

FIRST SIDELOBE LEVEL

N	LEVEL	DB DOWN
3	0.33	- 9.6
4	0.29	-11.4
5	0.31	-12.1
6	0.34	-12.5

Figure 4.

$$C_{(f)} \triangleq \frac{1}{N} \left[\frac{\sin[\pi(f-f_c)NT]}{\sin[\pi(f-f_c)T]} \right]^2$$

where

$$T = 1/f_{PRF}$$

and

N = number of pulses in the coherent pulse train .

The number of spectral lines in a coherent pulse train between the center line and the first null in C(f) is approximately given by the reciprocal of the transmitter duty cycle, i.e.

$$K \approx 1/d_t$$

The effects of eclipsing will be considered in the next section.

When additional PRF's are employed during the same rf frequency dwell, the rf phase is the same throughout. Because of the coherence over the entire rf frequency dwell, the spectrum in the individual PRF dwells reinforce each other in the center line. Therefore the one-sided spectral width of the center line is the reciprocal of the rf frequency dwell time. In our case this is 12.5 msec, so that this bandwidth is approximately 80 Hz. The noncentral spectral lines do not coherently add since the PRF's are different. As a result of this difference in PRF's the noncentral lines become more spread, resulting in "smeared sidebands." Since we are discussing a center line coherent radar, spectral properties of the noncentral lines are not of interest.

When the several rf frequency dwells in a single spacial dwell time are included, no further narrowing of the spectral width of the center line takes place, since the signal is not coherent from rf frequency to rf frequency. The maximum coherence time is 12.5 msec.

This discussion indicates that it would be possible to use more Doppler filters which are narrower in bandwidth, thereby reducing the required transmitter power. A bank of Doppler filters, each of 320 Hz bandwidt and 100% overlapped, would have the property that the center line spectrum would always have all its energy within one Doppler filter at all times. Some of the energy would also be in adjacent filters simultaneously.

It is anticipated that this choice will provide a more satisfactory design.

II. Search Mode Description

An enumeration of the search mode parameters is given in Table II. The requirement is that the target, which has radar cross section of $\bar{\sigma}$ = 1 square meter, be detected at a range of 10 nautical miles with a cumulative probability of detection of $P_c = 0.99$. One minute of scan time is allowed to carry out this requirement. This is the acquisition time. The target is assumed to be located in a volume of $40^\circ \times 40^\circ$, which is the scan coverage.

The maximum relative target range rate is specified as

$$\dot{R}_{max} = +100 \text{ ft/sec}$$

$$\dot{R}_{min} = -50 \text{ ft/sec}$$

Table II

SEARCH MODE PARAMETERS

P_c = Cumulative Probability of Detection

Requirement: $P_c = 0.99$

Acquisition Time = 60 sec

Acquired and Tracking at 10 NMI

Assume Two Scans:

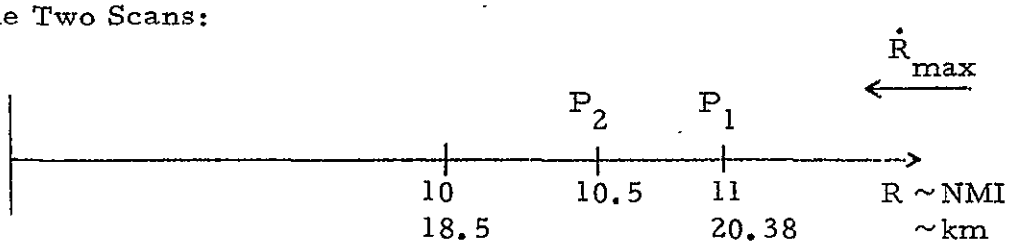

$\dot{R}_{max}$ = 100 ft/sec

$P_c = 1 - (1-P_1)(1-P_2)$

Assume $P_2 = P_1$ ⇒A Safety Factor of ≈0.4 dB

$P_d = 1 - [1-P_c]^{\frac{1}{2}} = 0.9$

Target Area = $\bar{\sigma} = 1\ m^2$

Target Model = Swerling Class 1

Target Range Rate: $\dot{R}_{max}$ = +100 ft/sec

$\dot{R}_{min}$ = -50 ft/sec

Scan Coverage = 40° x 40°

Scan Overlap = 30%

Allowance for Scan Reversal = 20%

Number of Scan Lines/Scan = 21

Time per Scan Line = 1.43 sec

Scan Speed = 33.6°/sec

TABLE II (Cont'd)

Dwell Time per Beamwidth = t_d = 80 msec = Spacial Dwell Time

Doppler Uncertainty Interval = f_d = 4573
(+3049 Hz - 1524 Hz)

Bandwidth of Doppler Filter = B_d = 1 KHz

Number of Doppler Filters = 9

Doppler Filter Arrangement

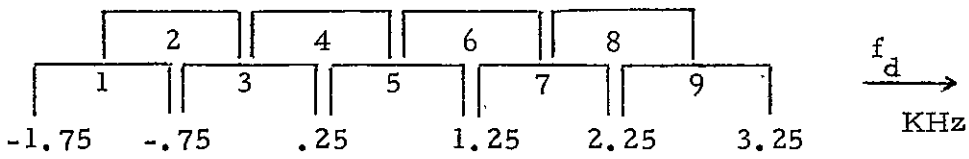

where positive implies an approaching target. If the target is at R_{max}, in one minute it will move approximately one nautical mile. If we assume two complete scans of the entire volume during the acquisition time, then the cumulative detection probability is

$$P_c = 1 - (1-P_1)(1 - P_2)$$

where

P_1 = Probability of Detection from a single observation at 11 Nautical miles

P_2 = Probability of Detection from a single observation at 10.5 nautical miles

The usual conservative simplification is to let

$$P_2 = P_1 = P_d$$

so that

$$P_d = 1 - (1-P_c)^{\frac{1}{2}} = 0.9$$

This corresponds to a safety factor of approximately 0.4 dB in average transmitted power. The design actually is required to detect (acquire) the target and be in the range tracking mode of operation by the time the target has reached a distance of 10 Na. Mi . No additional time has been provided to allow the range tracking subsystem to acquire, as the time for this lockup is expected to be negligible with respect to any significant change in range.

The dwell time in a given direction is calculated based on a given amount of time allowed for scan reversal and for a certain amount of scan overlap as shown in Figure 5.

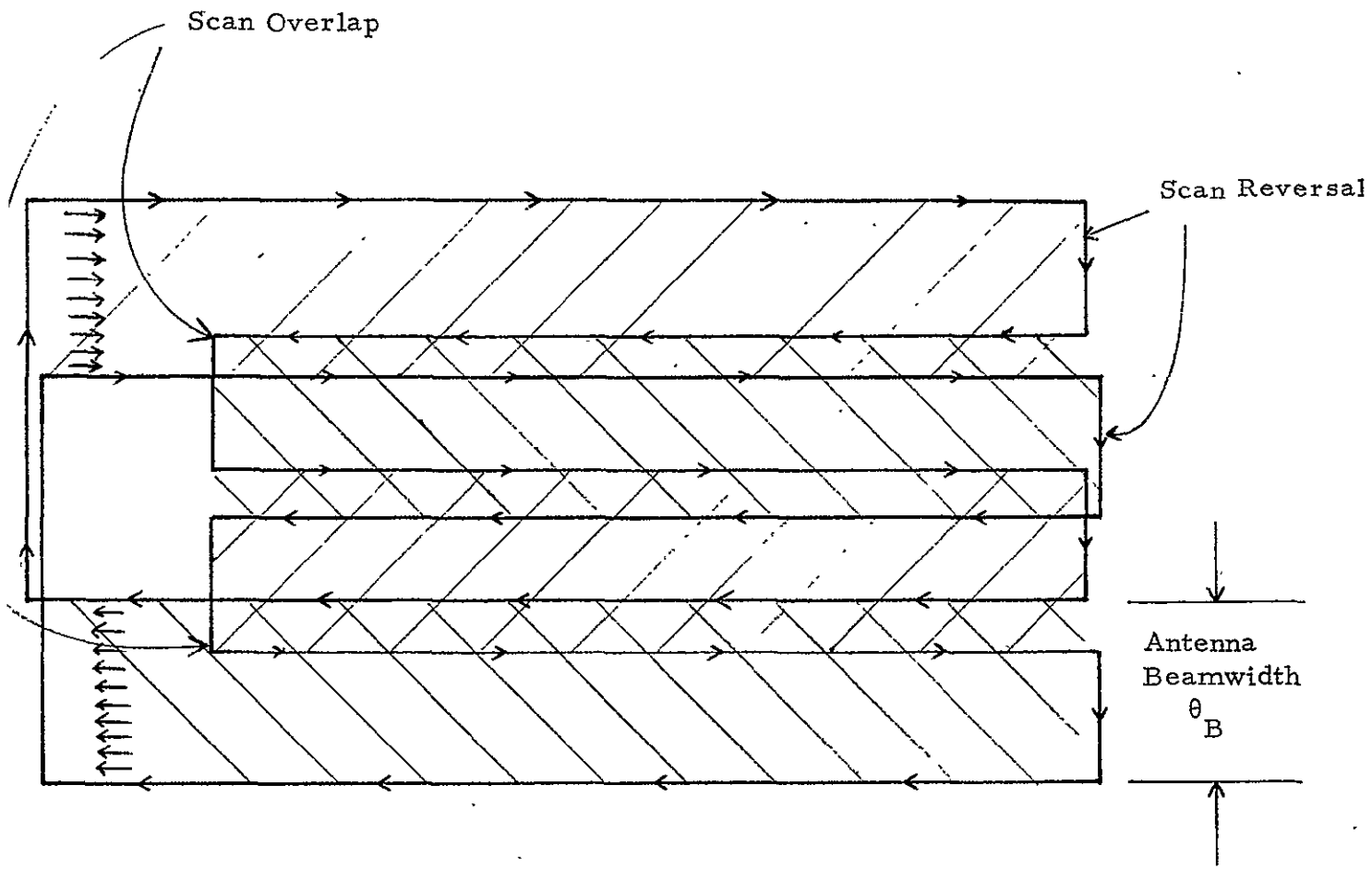

Figure 5. Typical Scan Pattern.

The total angular search area is A_θ in $(\text{deg})^2$, and

$$A_\theta = A_{AZ} A_{EL}$$

where

A_{AZ} = azimuth angle to be searched

A_{EL} = elevation angle to be searched

If the time for a single complete scan of the total volume is t_1, then the dwell time, t_d, is given by

$$\frac{A_\theta}{\theta_B^2} t_d = t_1$$

or

$$t_d = t_1 \theta_B^2 / A_\theta$$

This would be the case in the absence of scan overlap and without allowance for scan reversal. In this design we allow 20% of the total time for scan reversal, and specify a scan overlap of 30% as seen in Table II. Then the

Number of Horizontal Scan Lines

$$= \frac{A_{EL}}{[1-0.3]\theta_B} = 21.2 \approx 21$$

where the 0.3 designates the scan overlap. With two scans in 60 sec, or one in 30 sec, then the

$$\text{Time Per Scan Line} = \frac{30 \text{ sec}}{21} = 1.43 \text{ sec}$$

Hence the scan speed is given by

$$\text{Scan Speed} = \frac{A_{AZ}}{1.43 \text{ sec}} [1 + 0.2] = 33.6 \text{ deg/sec}$$

where the 0.2 designates the percent time specified for scan reversals.

The dwell time per beamwidth, t_d, (the time a given point in space is illuminated by the antenna inside its 3 dB beamwidth) is given by

$$t_d = \frac{\theta_B}{\text{Scan Speed}} = \frac{2.7^o}{33.6^o} = 80 \text{ msec}$$

A trade-off exists between the dwell time, the scan speed, the scan overlap and the probability of detection. In particular, if the scan overlap is reduced, the dwell time can be increased, but the target has a

higher probability of being on the skirts of the antenna pattern. This trade off has not been explored to determine the optimal choice of parameters to maximize the probability of detection, or equivalently, to maximize the average value of returned energy from the target. Such an optimization must be performed within the maximum allowed scan speed of the antenna, a physical constraint.

Doppler Filters

The total change in range rate is

$$\Delta\dot{R} = 150 \text{ fps}$$

so that the total doppler variation at 15 GHz is

$$\Delta f_d = \frac{2\Delta\dot{R}f_c}{c} = 4574 \text{ Hz}$$

The doppler filter arrangement is as shown in Table II where provision is made for 100% filter overlap. From the arrangement, it is seen that the number of doppler filters is 9.

False Alarm Probability

The false alarm rate is designated as 1/hour. The number of dwells per hour is given as

$$N_d = \frac{(3600 \text{ sec})(\text{No. Doppler Filters})}{t_d}$$

$$= \frac{(3600)(9)}{.080} = 4.05 \times 10^5$$

The false alarm probability for a given sample from a Doppler filter is

$$\alpha = \text{F.A.P.} = 1/N_d \approx 2.5 \times 10^{-6}$$

III. Antenna Position Losses

We consider two antenna position losses, the antenna lateral scan loss and the scan alignment loss. Then the effects of multiple PRF's and eclipsing loss are considered.

Antenna Lateral Scan Loss

The antenna lateral scan loss accounts for the fact that a target is not on the beam axis of the antenna pattern throughout the dwell time. The actual gain at a given instant is equal to the antenna gain corresponding to that point. The antenna lateral scan loss is the average loss over the ±3 dB portion of the pattern. This average gain is defined by

$$G_{avg} \triangleq \int_{-\theta'_B/2}^{\theta'_B/2} |F(\theta)|^2 \, \frac{d\theta}{\theta'_B}$$

where $\theta'_B/2$ is that value of θ such that $|F(\theta)|^2 = G(\theta) = \frac{1}{2}$ as shown in Figure 6. The normalized aperture power distribution is $G(\theta) = |F(\theta)|^2$. Common approximations for $|F(\theta)|^2$ that are used are

$$|F(\theta)|^2 = [(\sin\theta)/\theta]^2$$

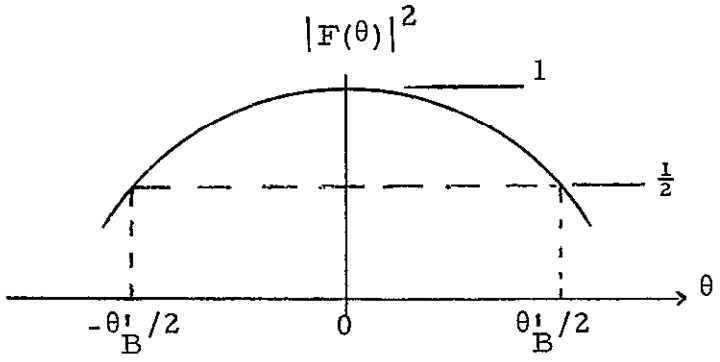

Figure 6. Typical Normalized Antenna Gain Pattern.

for a rectangular aperture and

$$|F(\theta)|^2 = [J_1(\theta)/\theta]^2$$

for a circular aperture, where $J_1(\cdot)$ is the Bessel function of order one. Within the 3 dB portions of the antenna pattern, the two $|F(\theta)|^2$ functions are essentially identical [2]. For computational simplicity, we use the $|F(\theta)|^2$ for the rectangular aperture, even though the antenna to be used in this radar has a circular aperture. By way of the rectangular aperture, we have

$$G_{avg} = \frac{1}{\theta'_B} \int_{-\theta'_B/2}^{\theta'_B/2} \left(\frac{\sin \theta}{\theta}\right)^2 d\theta$$

which is equal to -0.93 dB. The total lateral scan loss (transmit and receive) is therefore

$$L_{s\ell} = 1.86 \text{ dB}$$

Scan Alignment Loss

The scan alignment loss accounts for the fact that the beam axis may miss the target. Again, for simplicity, we employ a rectangular pattern, as indicated in Figure 7a, so that

$$G(\theta_{el}, \theta_{az}) \approx \left(\frac{\sin \theta_{el}}{\theta_{el}}\right)^2 \left(\frac{\sin \theta_{az}}{\theta_{az}}\right)^2$$

The scan alignment loss therefore weights the lateral scan loss by the factor $[(\sin \theta_{el})/\theta_{el}]^2$ where θ_{el} is the elevation angle by which the beam axis of the antenna misses the target. Averaging over the 3 dB beamwidth

of the antenna patterns, we conclude that the scan alignment loss contributes another 1.86 dB of loss, assuming there is no scan overlap of 30%. This is shown in Figure 5b where 15% of the overlap takes place on each end of the pattern. The additional loss due to scan alignment loss with a 30% scan overlap is

$$\int_{-\frac{35}{50}\frac{\theta'_B}{2}}^{\frac{35}{50}\frac{\theta'_B}{2}} \left(\frac{\sin\theta}{\theta}\right)^2 \frac{d\theta}{\theta'_B}$$

which is equal to 0.47 dB. Therefore the total scan alignment loss is

$$L_{SA} = 0.94 \text{ dB}$$

Multiple PRF's

The radar in this design has 5 PRF's. The criterion that is employed to choose a set of PRF's is either a) to ensure the determination of range unambiguously, or b) to minimize the eclipsing loss. In Addendum A of this presentation, we review the procedure for choosing a set of PRF's so as to ensure the unambiguous computation of range. In Addendum B, we address the question of the deterministic eclipsing loss as a function

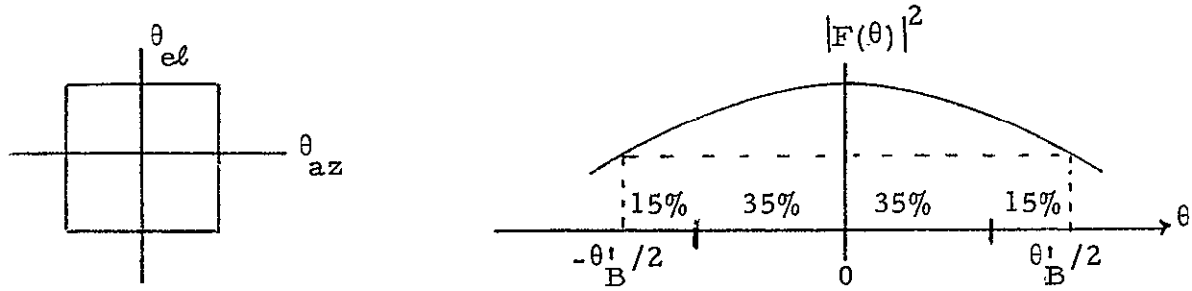

(a) Rectangular Pattern (b) Scan Overlap

Figure 7. Scan Alignment Losses

of range for various choices of PRF's. We then compare these results to the average eclipsing loss which we consider in the next section.

In the radar considered herein, the range tones are not transmitted during the search mode of operation. Detection is via velocity only, after which range tracking is initiated.

Eclipsing Loss

Because the receiver is gated off during the transmission time, targets received at this time are blanked, or eclipsed. With the high values of PRF commonly used, a target may be eclipsed several times in the range interval of interest. These eclipses occur at multiples of the maximum unambiguous range for that PRF.

The relationship between the received pulse, the receiver gating function and the eclipsed pulse after receiver gating are shown in Figure 8. The time between peaks is T_p which is the reciprocal of the

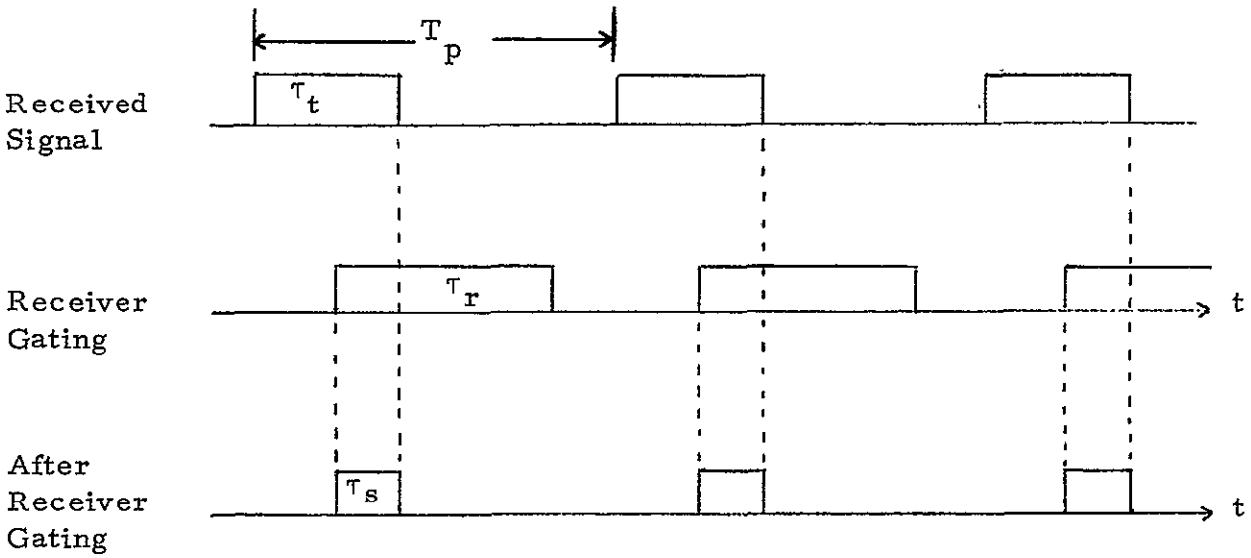

Figure 8. Relationship of Gated Signals

PRF. In addition to the transmitter duty cycle d_t and the receiver duty cycle d_r, we introduce d_s as the duty cycle of the signal after receiver gating. The characteristics of the transmitted signal are:

P_p = Peak Power (average power over the period that the transmitter is on)

$P_{avg} = P_p d_t$ = average power (averaged over all time)

$P_c = P_{avg} d_t = P_p d_t^2$ = the power in the center line of the coherent spectrum

These parameters are summarized in Table III. The center line power is a result of examining the first term in the Fourier series representation of the signal.

For a given set of parameters we calculate the <u>average eclipsing loss</u>. By average eclipsing loss is meant the time average over all ranges of the eclipsing loss in the center line of the received waveform.

After receiver gating the peak power is still P_p; there is no signal attenuation when the receiver gate is open. The average power after gating $\tilde{P}_{avg}$, is given by any of the following expressions

$$\tilde{P}_{avg} = P_p \frac{\tau_s}{T_p} = P_p d_s = P_{avg} d_t d_s$$

The center line power after receiver gating is

$$\tilde{P}_c = P_p d_s^2 = P_p d_t^2 \left(\frac{d_s}{d_t}\right)^2 = P_c \left(\frac{\tau_s}{\tau_t}\right)^2$$

TABLE III

ECLIPSING LOSS PARAMETERS

$T_p = 1/f_p$ = Time between peaks

d_t = Transmitted duty cycle

d_r = Receiver Duty Cycle

d_s = Duty cycle of signal after receiver gating

P_p = Peak Power

$P_{avg} = P_p d_t$ = Average power

$P_c = P_{avg} d_t = P_p d_t^2$ = Center line power

τ_t = Transmitted pulse width

τ_r = Receiver gate width

τ_s = Pulse width of signal after receiver gating

The eclipsing loss for a given set of parameters and a given range is therefore defined as

$$\text{E.L.} \triangleq \frac{\tilde{P}_c}{P_c} = \left(\frac{\tau_s}{\tau_t}\right)^2 = \left(\frac{d_s}{d_t}\right)^2$$

The average eclipsing loss is then given by the average value of the above, namely, <u>average eclipsing loss</u> is defined as

$$\text{AEL} \triangleq E\left(\frac{d_s}{d_t}\right)^2 = E\left(\frac{\tau_s}{\tau_t}\right)^2$$

These various values are summarized in Table IV. The value of the eclipsing loss for the average center line power is determined by calculating the area under the last curve in Figure 9, for $0 < d_t < 0.5$ in which provision is made for blanking periods between the transmitter

TABLE IV

New Peak Power = P_p (unchanged)

New Average Power = $P_p \frac{\tau_s}{T_p} = P_p d_s = P_{avg} d_t d_s$

New Center Line Power

$$= P_p d_s^2 = P_p d_t^2 \left(\frac{d_s}{d_t}\right)^2 = P_c \left(\frac{\tau_s}{\tau_t}\right)^2$$

Average Eclipsing Loss $\triangleq E\left[\frac{d_s}{d_t}\right]^2 = E\left[\frac{\tau_s}{\tau_t}\right]^2$

on-time and the receiver on-time. These have been designated τ_{B_1} and τ_{B_2}, but have been set equal to zero in the calculation. For $0 < d_t < 0.5$

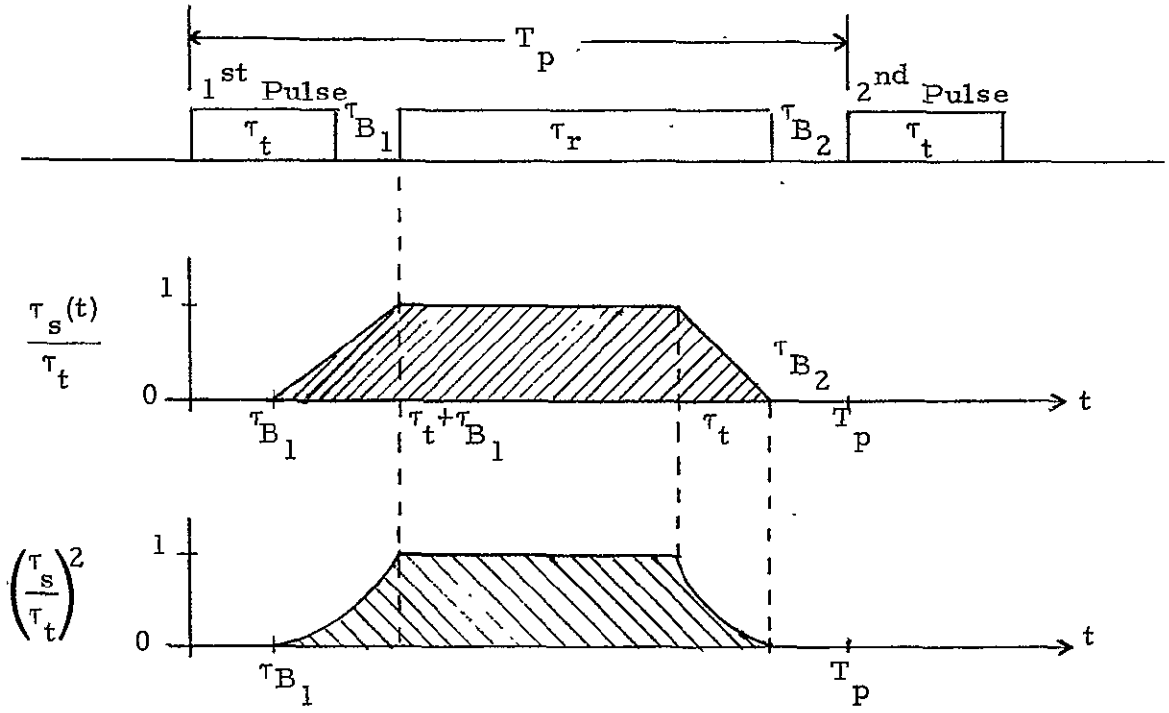

Figure 9. Calculation of Average Eclipsing Loss When $0 < d_t < 0.5$

$$E\left(\frac{\tau_s}{\tau_t}\right)^2 = \frac{(T_p - 2\tau_t - \tau_{B_1} - \tau_{B_2})}{T_p} + \frac{2}{T_p}\int_0^{T_t}\left(\frac{s}{\tau_t}\right)^2 ds$$

$$= 1 - \frac{4}{3}d_t \qquad 0 < d_t < 0.5$$

For $0.5 < d_t < 1$

$$E\left(\frac{\tau_s}{\tau_t}\right)^2 = \frac{1}{T_p}\left\{2\int_0^{T_p - \tau_t}\left(\frac{s}{\tau_t}\right)^2 ds + \left(\frac{T_p - \tau_t}{\tau_t}\right)^2 (2\tau_t - \tau_p)\right\}$$

$$= \frac{(1-d_t)^2}{3d_t^2}(4d_t - 1) \qquad 0.5 < d_t < 1$$

The calculation for $0.5 < d_t < 1$ reduces to determining the area under the curve squared in Figure 10. The results are shown in Figure 11. The average eclipsing loss is 0.466 or approximately 3.3 dB when $d_t = 0.4$.

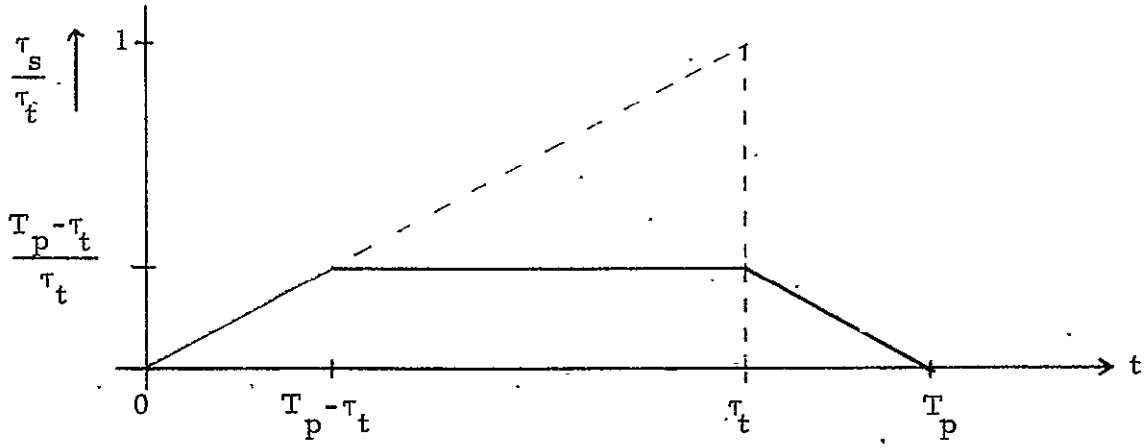

Figure 10. Calculation of Average Eclipsing Loss for $0.5 < d_t < 1$.

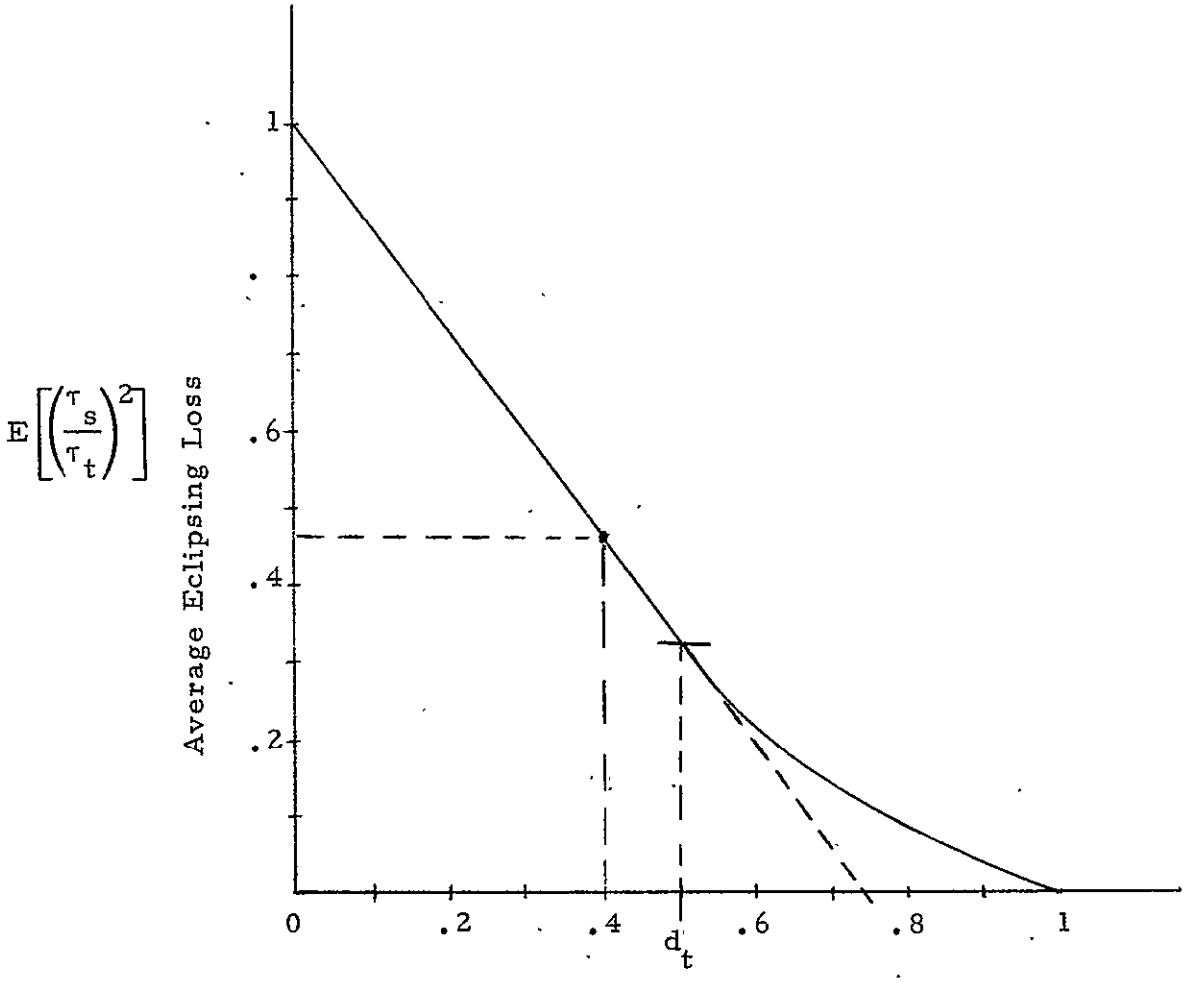

Figure 11. Average Eclipsing Loss vs Transmitter Duty Cycle

A simple optimization can be performed to choose that transmitter duty cycle which will maximize the signal-to-noise ratio at the input to the detector. We carry out this optimization under each of the two assumptions of a) fixed peak transmitted power and b) fixed average transmitted power.

Case a: Fixed peak transmitter power. The average power in the center line of the received signal is given by

$$\tilde{P}_c = P_p d_t^2 E\left(\frac{d_s}{d_t}\right)^2$$

and the average noise power is proportional to

$$\tilde{N}_0 = N_0(1-d_t)$$

Therefore for fixed peak power

$$\frac{\tilde{P}_c}{\tilde{N}_0} = \left(\frac{P_p}{N_0}\right) \frac{d_t^2 E\left(\frac{d_s}{d_t}\right)^2}{1-d_t}$$

Hence

$$\frac{\tilde{P}_c}{\tilde{N}_0} = \begin{cases} \left(\frac{P_p}{N_0}\right) \frac{d_t^2\left(1-\frac{4}{3}d_t\right)}{1-d_t}, & 0 < d_t < 0.5 \\ \left(\frac{P_p}{N_0}\right)\left(\frac{1-d_t}{3}\right)(4d_t-1), & 0.5 < d_t < 1 \end{cases}$$

It can be shown directly that this function reaches its maximum value at $d_t = 5/8$.

For a center line coherent radar with a transmitter having a fixed peak power constraint, the optimal choice of transmitter duty cycle is $d_t = 0.625$.

Case b: Fixed average transmitter power. The average power in the center line of the received case also can be written as

$$\tilde{P}_c = P_{avg}\, d_t E\left(\frac{d_s}{d_t}\right)^2$$

Hence

$$\frac{\tilde{P}_c}{\tilde{N}_0} = \begin{cases} \dfrac{P_{avg}}{N_0} \dfrac{d_t\left(1 - \frac{4}{3} d_t\right)}{1 - d_t}, & 0 < d_t < 0.5 \\ \dfrac{P_{avg}}{N_0} \dfrac{(1-d_t)}{3d_t} (4d_t - 1), & 0.5 < d_t < 1 \end{cases}$$

This function reaches its maximum value at $d_t = 0.5$. Therefore, for a center line coherent radar with a transmitter having a fixed average power constraint, the optimal choice of transmitter duty cycle is $d_t = 0.5$.

When employing a TWT with a high duty cycle, the limitation is going to be in average transmitted power. Therefore, based on physical limitations, case b is the more useful and a transmitter duty cycle of $d_t = 0.5$ would be the optimal choice.

IV. Performance

The measure of performance of the system is given by the transmitted power required to meet the probability of detection specifications that have been previously discussed. This is determined for a variety of cases. We first determine, however, the gain from employing frequency diversity.

Frequency Diversity Gain

The frequency diversity gain is determined under the assumption of an ideal optimal receiver. The gain that is obtained from employing frequency diversity in the center line suboptimal radar receiver is then assumed to be the same as that for the ideal receiver. Although no proof of this conjecture is presented nor available, simulations and empirical data point out that this is a very satisfactory assumption.

With frequency diversity, the amplitude of the received signal consists of a sequence of statistically independent random variables as we move from frequency to frequency. In this example the spatial dwell time is t_d = 80 msec and the frequency dwell time is 12.5 msec. As shown in Figure 12, there are 6.4 frequency dwells of the target during one spatial dwell time. The sixth frequency dwell is at the same frequency as the first and the seventh is at the same frequency as the second. The amplitude of the received signal during the sixth dwell is therefore not statistically

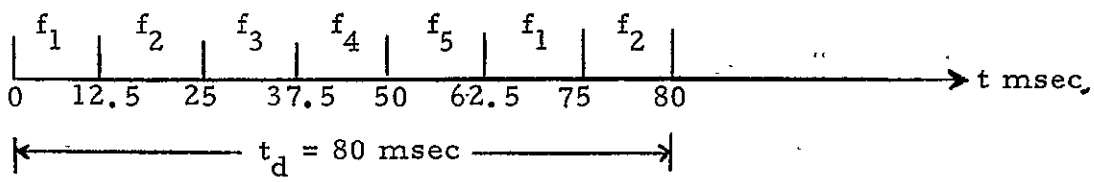

Figure 12. Frequency Change Over one Spatial Dwell Time.

independent from that of the first frequency dwell. In fact they are quite dependent, and could be assumed to be equal. We shall approximate the number of statistically independent frequency dwells by N = 6. This discards the received signal energy during the seventh frequency dwell and assumes the amplitude of the signal in the sixth dwell is statistically independent of the first dwell. These are offsetting simplifications of the analysis.

Based on this argument, with frequency diversity in the ideal receiver we have:

I) With Frequency Diversity

a) Swerling II, Noncoherent Waveform

b) $P_d = 0.9$

c) $n' = 10^6$, so that the FAP = $0.693/n' \approx 0.7 \times 10^{-6}$

d) N = 6 Pulses (i.e. 6 frequencies)

For this, from Di Franco and Rubin [4], page 397, we have

$$\overline{R}_p = \frac{2\overline{A^2}\mathcal{E}_p}{N_0} = 11.7 \text{ dB}$$

where $\overline{R}_p$ is the average of the peak received energy per pulse divided by the receiver front end noise spectral density. In particular, this is the center line SNR per pulse where the pulse time is one frequency dwell time (12.5 msec). In our case the Radar Cross Section is 1 sq. meter ($\overline{\sigma} = 1$), so that $\overline{A^2} = 1$. The definition of $\overline{R}_p$ involves an average since we are assuming a fluctuating target.

In order to determine the magnitude of the gain by using frequency diversity, we now consider performance without frequency diversity. To do so requires knowledge of the coherence time of the system. Since this cannot be specified precisely we consider two extreme cases so as to obtain bounds on the frequency diversity gain.

Case A. Assume the coherence time is minimum, namely, equal to one frequency dwell time when using frequency diversity (12.5 msec). This implies using a noncoherent receiver with a pulse length of 12.5 msec, and with a reception of N = 6 pulses. Therefore we have:

II) Without Frequency Diversity

Case A. Minimum Coherence Time (namely 12.5 msec)

a) Swerling I, Noncoherent Waveform (all pulses have the same random amplitude)

b) $P_d = 0.9$

c) $n' = 10^6$

d) N = 6 Pulses

The SNR required is found in Di Franco and Rubin [4], page 383, from which we have

$$\overline{R}_p = 18.2 \text{ dB}$$

The Frequency Diversity Gain under the assumptions in Case A is therefore given by

$$18.2 \text{ dB} - 11.7 \text{ dB} \quad \text{or}$$

$$\underline{\text{Diversity Gain}} = 6.5 \text{ dB}$$

Case B. We now assume the coherence time is maximum, namely equal to the spatial dwell time of t_d = 80 msec. This implies using a receiver which receives one long pulse of length 80 msec. In this case we have:

II) Without Frequency Diversity

Case B. Maximum Coherence Time (namely t_d= 80 msec)

a) Swerling I

b) $P_d = 0.9$

c) $n' = 10^6$

d) N = 1 Pulse

The SNR required is in Di Franco and Rubin [4], page 380, and is

$$\overline{R}'_p = 24.2 \text{ dB}$$

This SNR has been denoted with a prime since this is a SNR involving 6 times the observation period as in the other cases. To provide an equal comparison we consider

$$\overline{R}'_p = N\overline{R}_p$$

so that

$$\overline{R}_p = 24.2 \text{ dB} - 7.8 \text{ dB} = 16.4 \text{ dB}$$

since N = 6 implies 7.8 dB.

The Frequency Diversity Gain under the assumptions of Case B is therefore given by 16.4 dB - 11.7 dB or

$$\underline{\text{Diversity Gain}} = 4.7 \text{ dB}$$

Therefore the actual gain due to frequency diversity in this example can be expected to be between 4.7 dB and 6.5 dB. It is noted that the diversity gain is higher when the coherence time is assumed to be smaller. This is a result of the fact that a coherent pulse train is already very effective, thereby reducing the amount that can be gained by employing techniques (such as frequency diversity) which change the model of the fluctuating target from Swerling I to Swerling II.

We shall assume the minimum gain due to frequency diversity, namely 4.7 dB, when considering system performance for the cases which follow.

Required Transmitter Power

Using the results of all of the previous sections and the Appendices, we determine the required transmitter power for various receivers. We consider first the ideal receiver. The radar equation for the optimal receiver is

$$\overline{R}_p = \frac{\overline{2A^2 \mathcal{E}}_p}{N_0} = \frac{[2P_p d_t^2 \tau_t][G^2 \bar{\sigma} \lambda^2]}{[(4\pi)^3 R^4][FkT_0 d_r][L]}$$

The parameter definitions and values are as follows:

G = antenna gain = 35.4 dB

$\bar{\sigma}$ = average radar cross section = $1m^2$ = 0 dB

λ = (for 15 GHz) = 0.02m = -16.99 dB

$$[G^2 \bar{\sigma} \lambda^2] = \underline{36.82 \text{ dB}}$$

F = noise figure = 8 dB

k = Boltzman constant = 1.38×10^{-23} joules/^{o}K = -228.6 dB

T_0 = absolute temperature = 290^{o}K (63^{o}F) = 24.6 dB

d_r = receiver duty factor = 0.6 = -2.22 dB

$$N_0' = N_0 d_r = [FkT_0 d_r] = \underline{-198.2 \text{ dB}}$$

$(4\pi)^3 = 1984.4 = 32.98$ dB

R = 11 N.Mi. = 20,383 m.

$R^4 = 172.4$ dB

$$(4\pi)^3 R^4 = \underline{205.4 \text{ dB}}$$

Losses in Search Mode

RF Losses (assumed)	= 3.0 dB
Lateral Scan Loss	= 1.86 dB
Scan Alignment Loss	= 0.94 dB
Average Eclipsing Loss (d_t=0.4)	= 3.31 dB
Total Losses = L =	9.1 dB

$d_t^2 = (0.4)^2 = -7.9$ dB

τ_t = 12.5 msec = -19.03 dB

$[2d_t^2 \tau_t] = \underline{-24 \text{ dB}}$

In the ideal system, the bandwidth of the optimal receiver is much narrower than the IF filter, which in this case is the Doppler filter @ 1 KHz. This is the reason why the bandwidth of the Doppler filters does not affect the performance of the ideal system in the search mode of operation. For

the ideal system (in dB)

$$P_{peak} = \overline{R}_p + [(4\pi)^3 R^4] + N_0' + L - [G^2 \bar{\sigma} \lambda^2] - [2 d_t^2 \tau_t]$$

We consider now the following cases.

Case I. Ideal System With Frequency Diversity at R = 11 N. Mi.

With frequency diversity, and a fluctuating target, we have a Swerling II target. For the following assumptions

i) $P_d = 0.9$

ii) n' = false alarm number = 10^6

iii) N = 6 pulses (see discussion on frequency diversity).

we have from DiFranco and Rubin [4, p. 397], that

$$\overline{R}_p = 11.7 \text{ dB}$$

Therefore the peak power that is required is

$$P_{peak} = 15.18 \text{ dB}$$
$$= \underline{33 \text{ watts}} = \underline{\text{Peak Power}}$$

Then

$$P_{avg} = d_t P_{peak} = \underline{13.2 \text{ watts}} = \underline{\text{Average Power}}$$
$$= 11.2 \text{ dB}$$

Case II. Ideal System with Frequency Diversity at R = 12 N. Mi.

Repeating the same computation as in Case I at 12 N. Mi. instead of 11 N. Mi.

$$P_{peak} = 15.18 + 1.51 = 16.7 \text{ dB}$$
$$= \underline{46.8 \text{ watts}}$$

$$P_{avg} = \underline{18.7 \text{ watts}} \quad (d_t = 0.4)$$

Case III. Receiver with Post Detection Integration at R = 12 N. Mi.

For this implementable system, performance is obtained by referring to Cases I and II, and adding the additional loss due to post detection integration. Then

$$P_{peak} = 15.18 \quad \text{from Case I}$$
$$+ \ 1.51 \quad \text{from Case II}$$
$$+ \ 4.8 \quad \text{Post detection integration loss (see Appendix D)}$$
$$P_{peak} = 21.5 \text{ dB}$$
$$= \underline{141.3 \text{ watts}}$$

Therefore

$$\underline{P_{avg} = 57 \text{ watts}}$$

Case IV. Receiver with Post Detection Integration at R = 11 N. Mi.

This is the same computation as Case III, except at R = 11 N. Mi. The result is

$$P_{peak} = 15.18 + 4.8 = 20 \text{ dB}$$
$$= \underline{100 \text{ watts}}$$

So that

$$P_{avg} = \underline{40 \text{ watts}}$$

Discussion

1) The required transmitter power of a specific pulsed doppler radar has been determined. No extensive attempt has been made to optimize

the choice of the many system parameters. This will be the topic of a later report.

2) The system which employs post detection integration has been assumed to be the implementable system. The ideal system can be implemented with little loss by considering a digital implementation, and sampling no later than at the IF level before the bank of Doppler filters.

3) If there existed a bank of range gates, there would be a range gate loss on the average to take into account range gate straddling.

4) Another loss is velocity filter response loss. If the received signal is not totally within one Doppler filter, then additional loss is incurred on the average. The amount of this loss is reduced substantially by designing the bank of Doppler filters with 100% overlap.

5) In some receivers, a hard-limiter is placed ahead of the Doppler filter bank, with the result that a constant false alarm rate can be maintained over a large dynamic range. There is a small loss for doing this, called CFAR Loss (Constant False Alarm Rate Loss).

ADDENDUM A

When choosing multiple PRF's, there are two criteria which could be used:

i) To provide continuous estimation of unambiguous range.

ii) To maximize the average received power, or minimize the eclipsing loss.

In ii) the eclipsing loss to be minimized could be the average eclipsing loss, or the minimization of the maximum eclipsing loss. This criterion will be considered in Addendums B and C.

In this addendum we discuss the choice of PRFs using criterion i). This is a direct application of the Chinese Remainder Theorem. We develop the algorithms and then apply it to examples.

It does not follow necessarily that choosing multiple PRF's to provide unambiguous range information will minimize the eclipsing loss. This will become clear in the discussion in Addendum B.

When choosing PRF's to provide unambiguous range, a maximum unambiguous range is first choosen. The corresponding time between pulses if a low PRF were used is designated by T_r as shown in Figure A-1. In the simple example in Figure A-1, the returns of PRF #1 and PRF #2 are shown with the same time reference, namely over the same maximum range time T_r. When the PRF's are properly chosen, only returns from the true target range overlap. This matching is performed over each range time T_r.

Equivalently, there must be no overlap among all of the false range positions, which is the case in the example in Figure A.1.

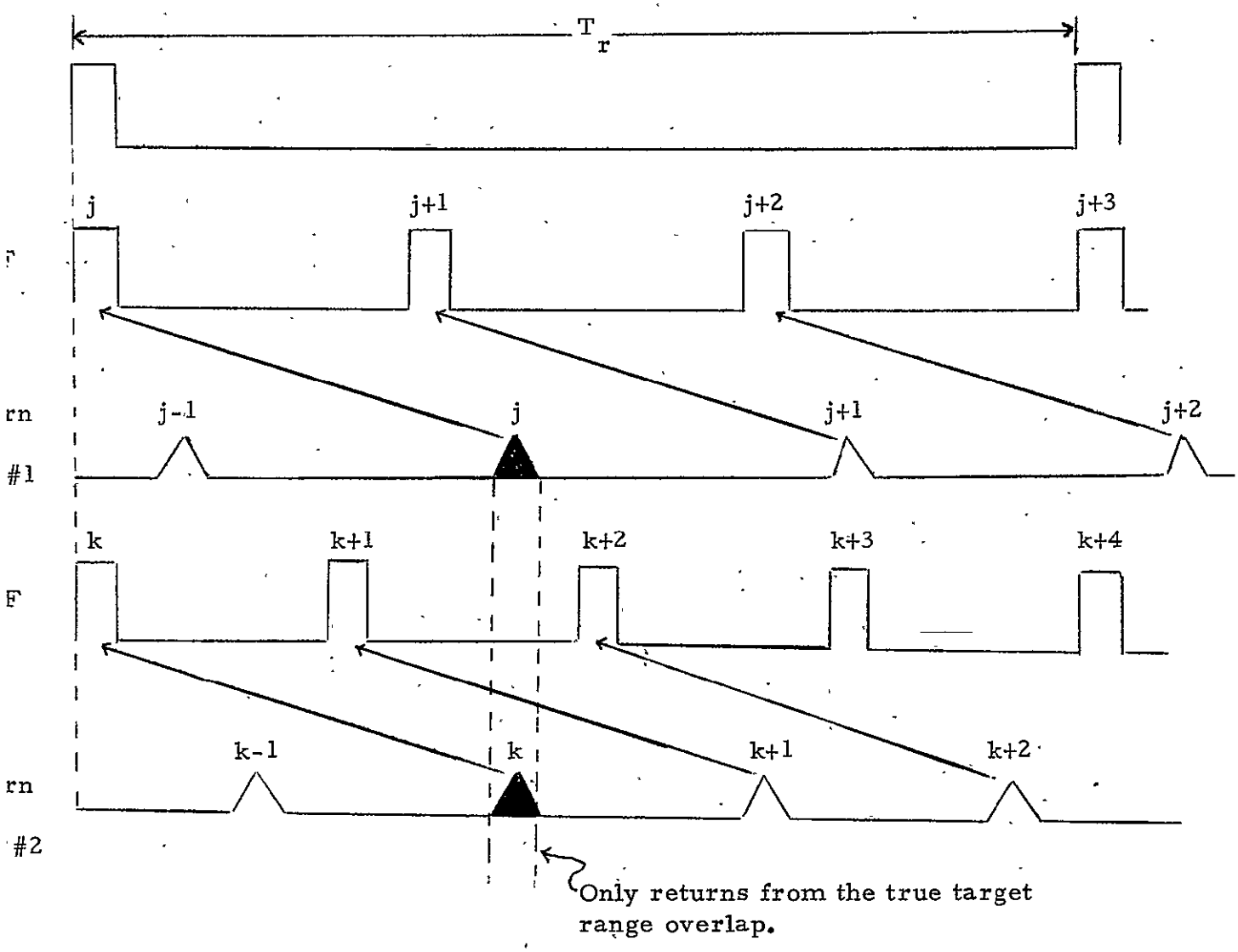

Figure A-1. Choosing Multiple PRF's that Provide Unambiguous Range.

Claim: (Application of the Chinese Remainder Theorem). There will be no false range overlaps among multiple PRF's, if the reciprocal of the PRF's are selected as multiples of a Basic Range Time, τ, where the set of multipliers are selected from relatively prime numbers.

Proof: Designate the Basic Range Time as τ. Choose a set of relatively prime numbers $n_1, n_2, \ldots, n_K$ where K = no. of PRF's. Then the PRF times are

$$T_k = n_k \tau \qquad k = 1, \ldots, K \tag{A-1}$$

and the multiple PRF's are given by

$$f_k = 1/T_k \qquad k = 1, \ldots, K . \tag{A-2}$$

If there is to exist no overlap across the false range times, then there must exist no integers i, j, that

$$iT_k = jT_\ell \qquad k \neq \ell \tag{A-3}$$

$$k, \ell = 1, \ldots, K$$

$$i \leq \max_k n_k$$

$$j \leq \max_k n_k$$

This is the same as saying that the $\{n_k\}$ have no common factors which is the definition of sets of relatively prime numbers. Q.E.D.

If a set of relatively prime numbers is chosen, then the basic range time is given by

$$\tau = \frac{T_r}{\prod_{k=1}^{K} n_k} \tag{A-4}$$

This provides the relationship between the maximum unambiguous range and the basic range element τ. A simple way of choosing relatively prime numbers is to choose a set of consecutive integers. For example, with 5 PRF's, one could choose N, N+1, N+2, N+3, N+4. Then

$$\tau = \frac{T_r}{N(N+1)(N+2)(N+3)(N+4)} \tag{A-5}$$

$$T_1 = N\tau$$
$$T_2 = (N+1)\tau$$
$$T_3 = (N+2)\tau \qquad \text{(A-6)}$$
$$T_4 = (N+3)\tau$$
$$T_5 = (N+4)\tau$$

and finally

$$f_k = 1/T_k$$

We now list 3 examples which will be used in the discussion in Appendix B.

Example 1.

Maximum Unambiguous Range = 100 N. Mi.

$T_r = 1.24$ msec.

$N = 1$

$N + 1 = 2$

$N + 2 = 3$

$N + 3 = 4$

$N + 4 = 5$

$\tau = 1.033 \times 10^{-5}$ sec.

$T_1 = 1.033 \times 10^{-5}$ sec. $\qquad f_1 = 96774$ PPS

$T_2 = 2.066 \times 10^{-5}$ sec $\qquad f_2 = 48387$

$T_3 = 3.1 \times 10^{-5}$ sec $\qquad f_3 = 32258$

$T_4 = 4.133 \times 10^{-5}$ sec $\qquad f_4 = 24194$

$T_5 = 5.166 \times 10^{-5}$ sec $\qquad f_5 = 19355$

Example 2. $T_r = .01$

Maximum Unambiguous Range = 809 N. Mi.

$$R_{max} = T_r \, c/2$$

$$\tau = 3.97 \times 10^{-6}$$

$N = 3,\ N + 1 = 4,\ N + 2 = 5,\ N + 3 = 6,\ N + 4 = 7$

$T_1 = 1.19 \times 10^{-5}$ sec.	$f_1 = 84,000$ PPS
$T_2 = 1.59 \times 10^{-5}$	$f_2 = 63,000$
$T_3 = 1.98 \times 10^{-5}$	$f_3 = 50,400$
$T_4 = 2.38 \times 10^{-5}$	$f_4 = 42,000$
$T_5 = 2.77 \times 10^{-5}$	$f_5 = 36,000$

Example 3. $T_r = .02$

Maximum Unambiguous Range = 1619 N. Mi.

$$\tau = 1.32 \times 10^{-6}$$

$N = 5,\ N + 1 = 6,\ N + 2 = 7,\ N + 3 = 8,\ N + 4 = 9$

$T_1 = 6.61 \times 10^{-6}$ sec.	$f_1 = 151,200$ PPS
$T_2 = 7.94 \times 10^{-6}$	$f_2 = 126,000$
$T_3 = 9.26 \times 10^{-6}$	$f_3 = 108,000$
$T_4 = 1.06 \times 10^{-5}$	$f_4 = 94,500$
$T_5 = 1.19 \times 10^{-5}$	$f_5 = 84,000$

ADDENDUM B

PERFORMANCE OF MULTIPLE PRF'S

The performance of specific sets of multiple PRF's is described. Thirteen sets of 5 PRF's have been studied; their values are listed in Table B-1. The first 10 sets were chosen from a variety of heuristic criteria. The last three sets were chosen via the criterion of providing unambiguous range out to some maximum range. Also the last three sets are the examples considered in Addendum A as applications of the Chinese Remainder Theorem.

The performance of a set of multiple PRF's from the point of view of eclipsing loss can be judged in three ways:

i) The average eclipsing loss.

ii) The maximum eclipsing loss over a specified range.

iii) The minimum value of signal-to-noise ratio over a specified range.

We consider performance from the first two points of view. First, the average eclipsing loss is independent of the choice of PRF's, where by average we mean over range. In all cases considered, the eclipsing loss, averaged over the interval of 1 to 20 N. Mi., agrees exactly with the theoretical average. The theoretical average eclipsing loss is shown in Table B-2 for a variety of a transmitter duty factors. The specific plots of eclipsing loss versus range for the cases considered is given in Addendum C. In summary, average eclipsing loss is dependent only on the transmitter duty factor and as a result does <u>not</u> provide a satisfactory criterion for choosing sets of multiple PRFs.

TABLE B-1

List of PRF's Considered

		Sets of 5 PRFs				
		1	2	3	4	5
Case	1-4	17,000	19,000	23,000	31,000	37,000
	5-8	85,000	87,000	88,000	89,000	91,000
	9-12	31,000	32,000	33,000	35,000	37,000
	13-16	77,500	80,000	82,000	87,500	92,500
	17-20	17,000	37,000	53,000	83,000	97,000
	21-24	79,000	83,000	89,000	97,000	101,000
	25-28	31,000	47,000	61,000	73,000	89,000
	29-32	82,200	85,000	87,000	90,350	93,000
	33-36	81,000	85,000	89,000	93,000	97,000
	37-40	81,000	85,000	89,000	92,000	97,000
Ex. 1, App. A	41-44	96,774	48,387	32,258	24,194	19,355
Ex. 2, App. A	45-48	84,000	63,000	50,400	42,000	36,000
Ex. 3, App. A	49-52	151,200	126,000	108,000	94,500	84,000

TABLE B-2

Average Eclipsing Loss*

XTMR Duty Factor d_t	Average Eclipsing Loss $E\{[\tau_s/\tau_t]^2\}$	Average Eclipsing Loss dB
0.3	0.6	2.22 dB
0.35	0.533	2.73
0.4	0.467	3.31
0.45	0.4	3.98
0.5	0.333	4.77
0.625	0.18	7.45

*From development on pp. 21-24

The second criterion is the maximum eclipsing loss over a specified range. In our study, the interval considered is 1 to 20 Nautical Miles. Plots of the eclipsing loss versus range are given in Addendum C for all cases considered. Several observations are worthy of note.

i) The structure of the eclipsing loss as a function of range is dependent only on the choice of the PRF's, and not on the duty cycle. On the other hand, recall that the average over range is dependent only on the duty cycle.

ii) There is no easy way to recognize patterns of the eclipsing loss versus range plots in Addendum C.

iii) Approximate values of the maximum eclipsing loss over the range 1 to 20 N.Mi. are tabulated in Table B-3. It is noted that the examples of Addendum A, namely Cases 41-52, do not have a maximum eclipsing loss which is smaller than the best of those which were chosen heuristically. For example, for $d_t = 0.30$, Case 41 has a maximum eclipsing loss of 7. dB, while the best set of multiple PRF's via this criterion is the first set. For $d_t = 0.30$, Case 1 has a maximum eclipsing loss of 5.8 dB. Both of these values are substantially higher, however, than the average, namely 2.22 dB for $d_t = 0.30$. This points out, as well as direct observation of the plots in Addendum C, the extensive variation about the mean value of the deterministic eclipsing loss of a set of multiple PRF's.

iv) No simple technique is known to the author for chosing sets of multiple PRF's which will minimize the maximum eclipsing loss over a specified interval of range.

TABLE B-3

Maximum Eclipsing Loss Over 1-20 N. Mi. (in dB)

Case	d_t = duty factor .30	.35	.40	.45	Case	d_t .30	.35	.40	.45
1	5.8				29	11			
2		7.0			30		12.1		
3			8.0		31			13	
4				9.2	32				14
5	16.5				33	7.5			
6		18			34		9		
7			19		35			10	
8				20	36				11
9	13.5				37	7.5			
10		15			38		9		
11			16		39			10.2	
12				17	40				11
13	7.5				41	7.0			
14		8.5			42		7.5		
15			10		43			8.5	
16				11	44				10
17	7.0				45	10			
18		8.5			46		11		
19			9.5		47			12.5	
20				10.5	48				13
21	7.5				49	7.5			
22		9.0			50		9		
23			10		51			10	
24				11	52				11
25	9.7								
26		11							
27			12.2						
28				13					

The third criterion for choosing multiple PRFs is the minimum value of signal-to-noise ratio over a given interval of range. This is the most satisfying criterion but also involves the most computation. It is satisfying in as much as the eclipsing loss is weighted by the range to the target. If a large eclipsing loss occurs at a close range, the signal-to-noise ratio may still be well above the minimum threshold to maintain satisfactory performance.

For fixed peak power, from page 25

$$\frac{\tilde{P}_c}{\tilde{N}_0} = \frac{P_p}{N_0} \, d_t^2 \, \frac{E(d_s/d_t)^2}{1 - d_t}$$

If we substitute deterministic eclipsing loss, which we denote EL(R), and insert the dependence on range, then

$$\frac{\tilde{P}_c}{\tilde{N}_0}(R) = \frac{P_p}{N_0} \, \frac{d_t^2}{1-d_t} \, EL(R) \left(\frac{R}{R_0}\right)^{-4}$$

where R_0 is a normalizing range, which in this example would be chosen to be 20 N. Mi.

For a fixed average power, from page 26, we have that

$$\frac{\tilde{P}_c}{\tilde{N}_0} = \frac{P_{avg}}{N_0} \, \frac{d_t}{1-d_t} \, EL(R) \left(\frac{R}{R_0}\right)^{-4}$$

The dependence on range and eclipsing loss is the same for both expressions.

Evaluation of these expressions are expected to be completed soon.

In Addendum C, a normalized signal loss is plotted for each case, where normalized signal loss is given by

$$EL(R) \, \frac{d_t^2}{1-d}$$

CASE 1

PRFS= 17000. 19000. 23000. 31000. 37000.DUTY FACTOR= .30

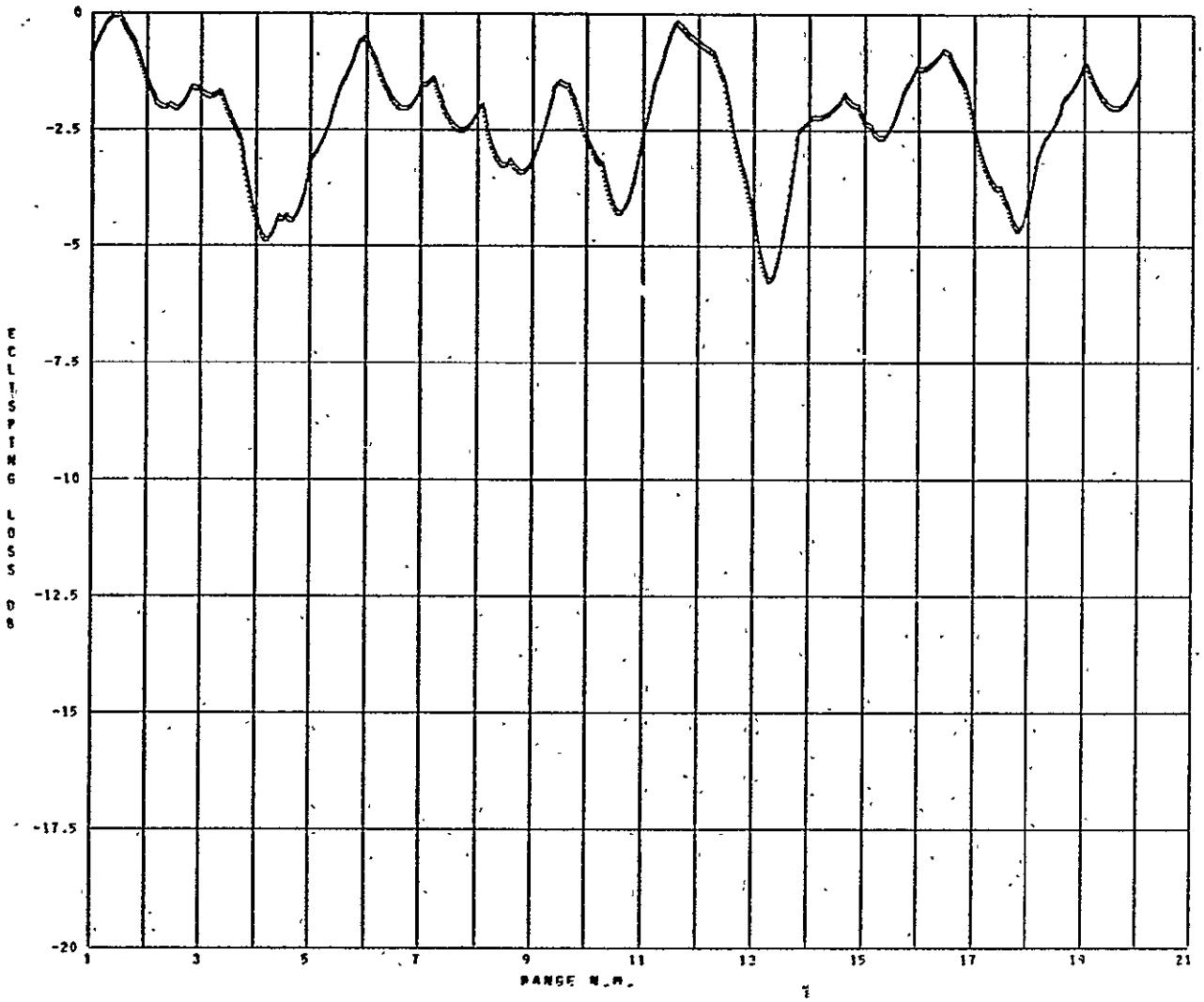

11-21X10# 06/06/74 UNIVAC 1108 SC-4020

PAGE 73.

CASE 1

PRFS= 17000. 19000. 23000. 31000. 37000.DUTY FACTOR= .30

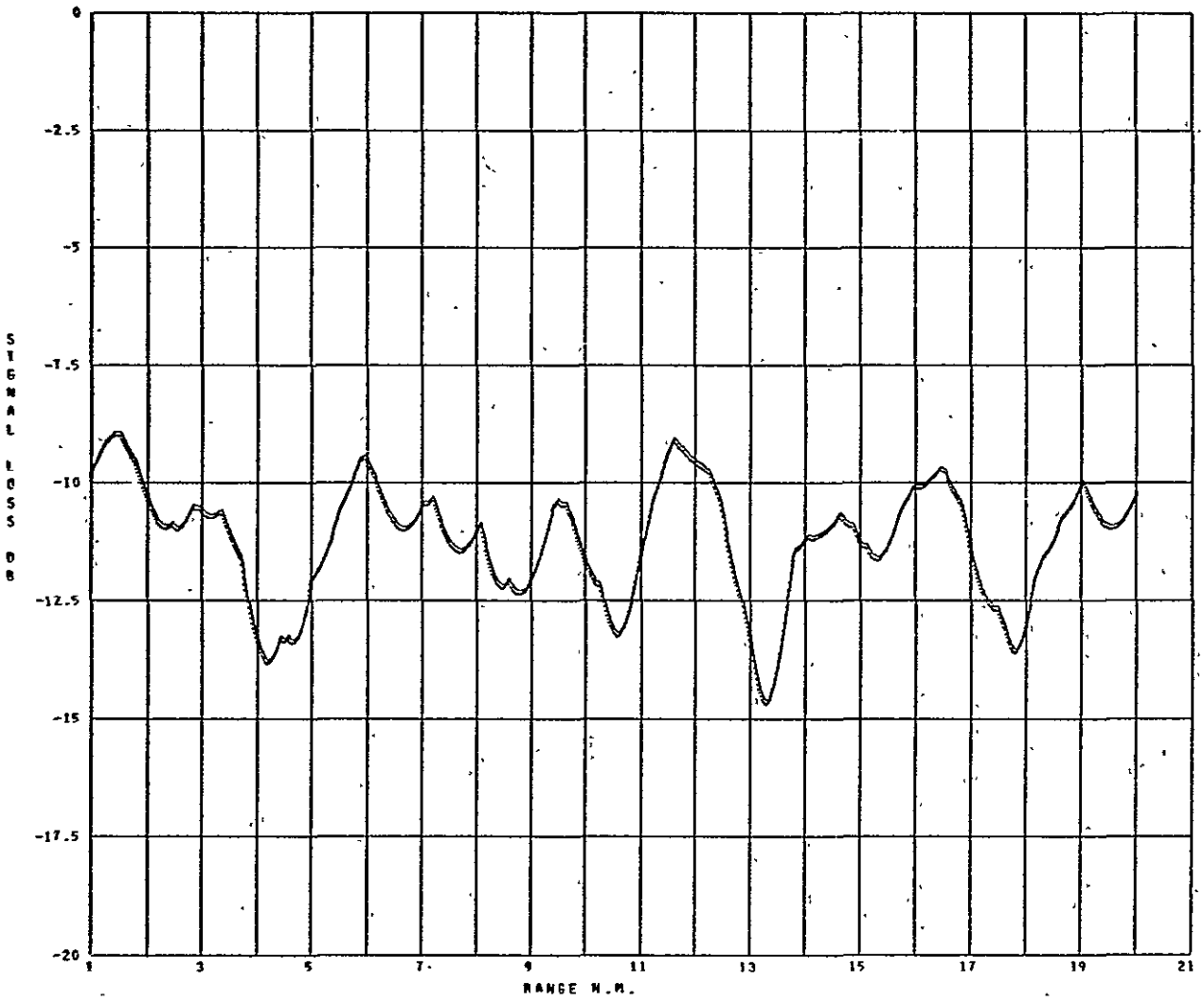

11-21R11# 06/06/74 UNIVAC 1108 SC-4020

CASE 1

PRFS= 17000. 19000. 23000. 31000. 37000.DUTY FACTOR= .30

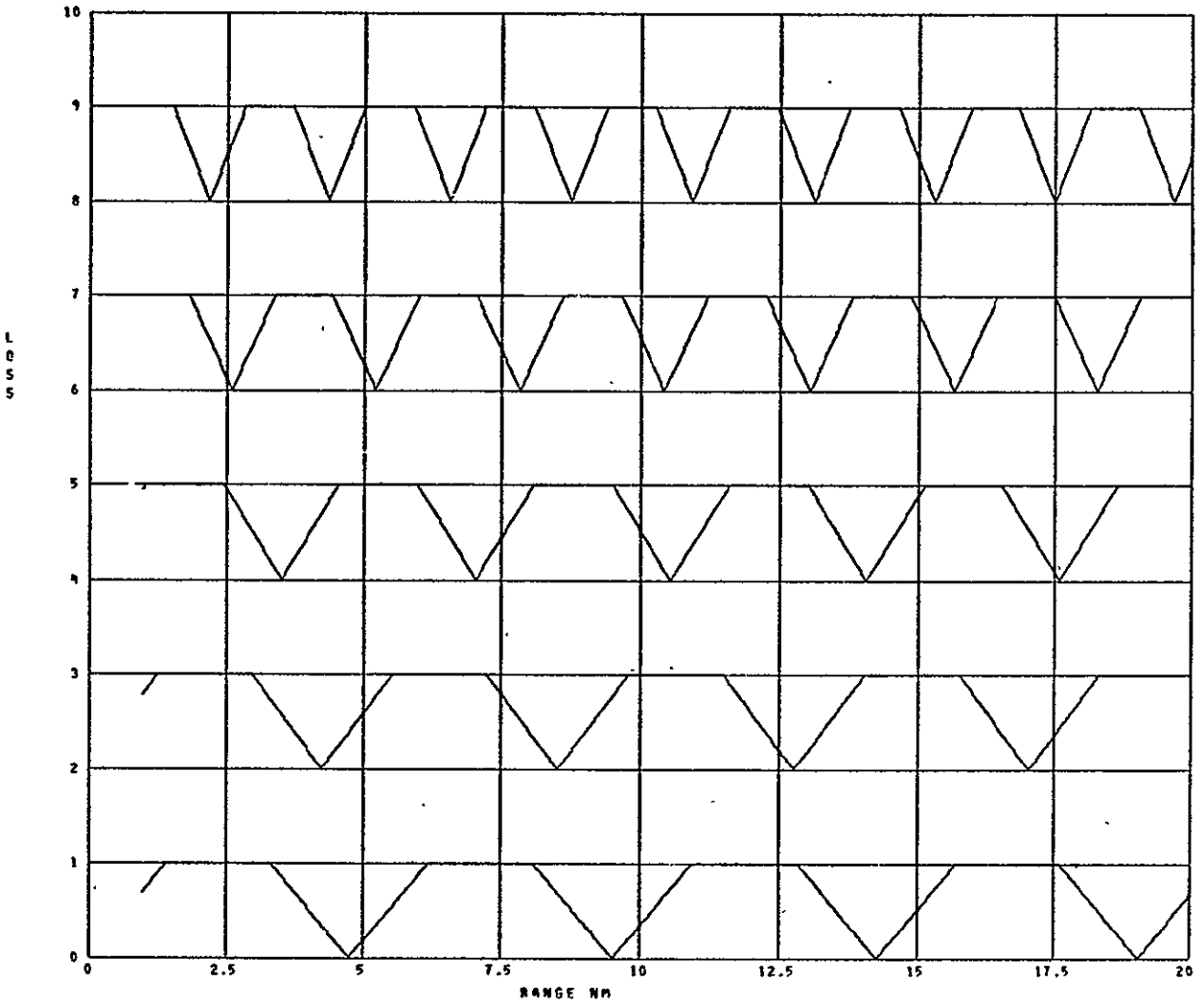

11-21R15# 06/06/74 UNIVAC 1108 SC-4020

ADDENDUM D

ANALYSIS OF POST DETECTION INTEGRATION LOSS

There appears to be no simple rigorous method for determining the exact post detection integration loss for pulsed doppler radar systems. In this example there is the additional consideration of a fluctuating target.

We have simplified the analysis somewhat by assuming that the improvement due to frequency diversity for the suboptimal implementable system is approximately the same as for the ideal optimal system. We therefore look at the suboptimal system over one spatial dwell time, namely t_d = 80 msec.

We shall assume that the low pass filter after the detector (see Figure D-1) can be replaced by a sampler and summer. This model of one channel of the receiver in Figure 1 is shown in Figure D-1, where the same notation has been employed. This is a satisfactory model of the analo receiver in Figure 1. If a digital implementation of the receiver is used, then this model would be even more representative.

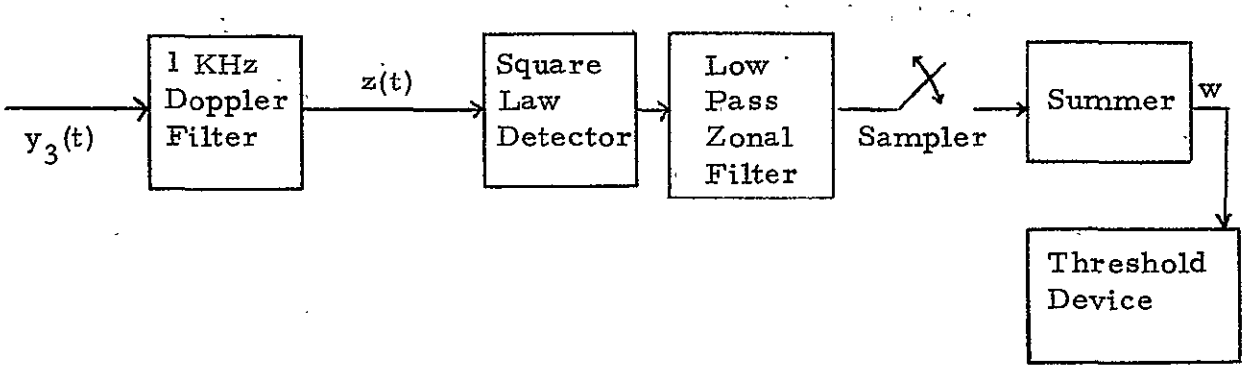

Figure D-1. Model of Implementable System.

The sampling rate for the sampler in Figure D-1 is at 1 KSPS. If the 1 KHz Doppler filter is an ideal BPF, then the sampled values will be conditionally independent random variables. When a nonfluctuating signal is present, the waveform at the output to the appropriate Doppler filter is

$$z_f(t) = \sqrt{2P_{cd}}\sin(\omega_0 t+\theta_0) + n_f(t) \qquad \text{(D-1)}$$

where

$$n_f(t) = \sqrt{2}\, n_s(t)\sin(\omega_0 t+\theta_0) + \sqrt{2}\, n_c(t)\cos(\omega_0 t+\theta_0) \qquad \text{(D-2)}$$

In (D-1), (D-2), we have that

i) P_{cd} is the received center line power of the coherent radar waveform at the output of the 1 KHz Doppler filter,

ii) $n_c(t)$ and $n_s(t)$ are independent identically distributed Gaussian stochastic processes, whose spectrum is dictated by the shape of the preceding Doppler filter.

iii) ω_0 is the center frequency of the correct Doppler filter. We assume the received signal is the center of the correct Doppler filter.

This simplification will be accounted for subsequently.

The autocorrelation function and spectral density of $n_f(t)$ are given by

$$R_n(\tau) = 2R_L(\tau)\cos\omega_0\tau \qquad \text{(D-3)}$$

$$= 2(N_0' B_d/2)\sin(\pi B_d\tau)/(\pi B_d\tau)$$

and

$$S_n(f) = S_L(f-f_0) + S_L(f+f_0) \qquad \text{(D-4)}$$

respectively where $R_L(\tau)$ and $S_L(f)$ are the autocorrelation and spectral density of $n_c(t)$ and $n_s(t)$. If the Doppler filter in Figure D-1 is ideal, then $S_L(f)$ is as shown in Figure D-3.

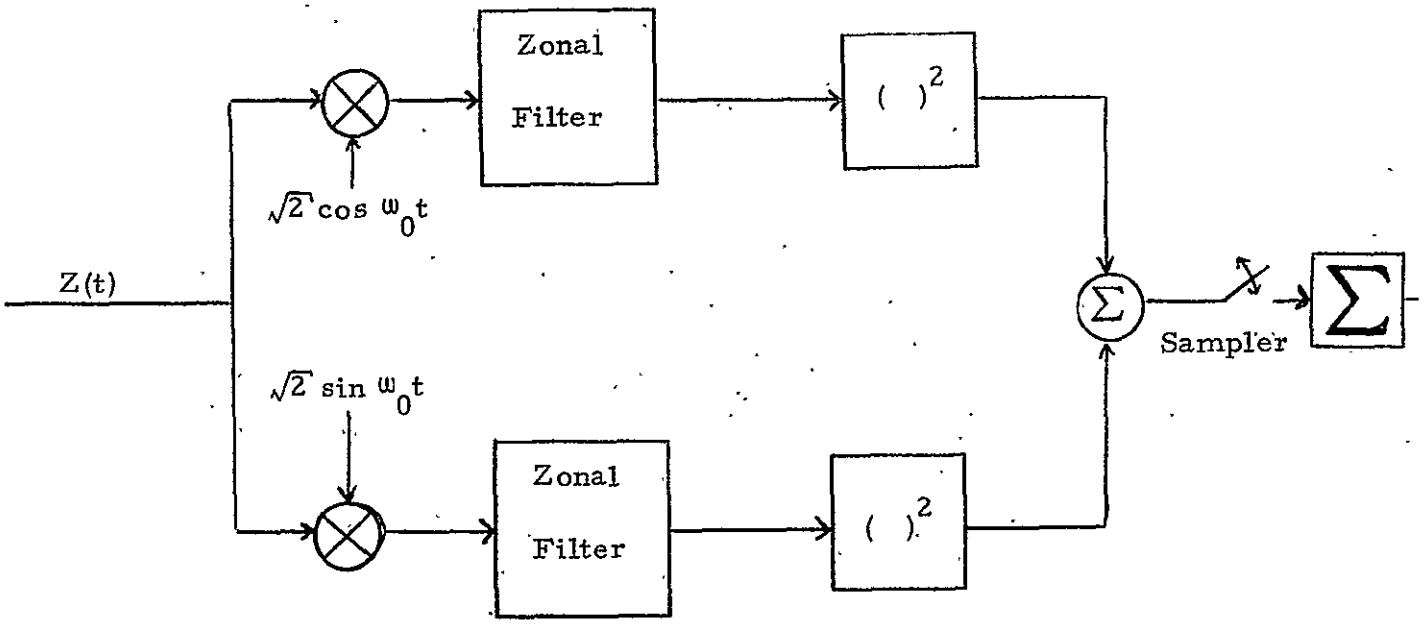

Figure D-2. Model of Square Law Detector and Zonal Low Pass Filter in Figure D-1.

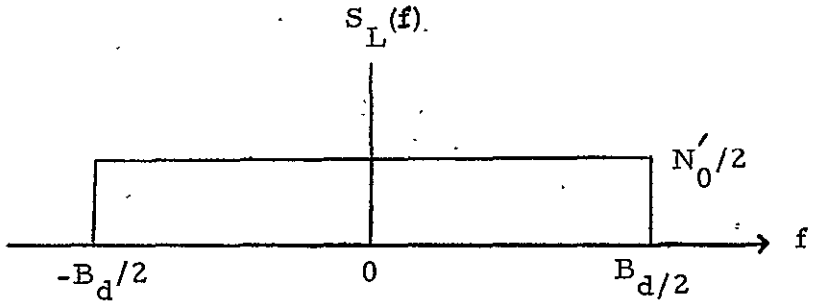

Figure D-3. Spectral Density of $n_c(t)$ and $n_s(t)$.

Over on spatial dwell time we have that

$$w = \sum_{j=1}^{J} (\sqrt{P_{cd}} + n_{sj})^2 + (n_{cj})^2 \qquad \text{(D-5)}$$

where $n_{sj} = n_s(t_j)$ and $n_{cj} = n_c(t_j)$. The time sampling interval is 1 msec, and the $\{n_{sj}\}$ and $\{n_{cj}\}$ are independent Gaussian random variables, with zero mean and variance given by

$$\sigma_n^2 = N_0' B_d / 2 \qquad \text{(D-6)}$$

In (D-6)

N_0' = spectral density of the receiver front end noise taking into account the receiver duty factor.

B_d = Doppler filter bandwidth = 1 KHz.

The number of samples that are summed to give w, namely J, could be 30 if the received energy from the entire spatial dwell time is considered. To account for the somewhat optimistic assumptions that have been made in the analytical model for the implementable detector, we have set J = 60 samples (10 samples for each of the six frequency dwell times).

Since the sum of identically distributed statistically independent random variables in (D-5) is sufficiently large, we invoke the central limit theorem [6] and conclude that w is approximately a Gaussian random variable. The first moment is given by

$$\begin{aligned} E[w] &= J\sigma_n^2 + JE[(\sqrt{P_{cd}} + n_{si})^2] \\ &= 2J\sigma_n^2 + JP_{cd} \\ &= J[N_0' B_d + P_{cd}] \end{aligned} \qquad \text{(D-7)}$$

Therefore

$$E[w \,|\text{Noise only}] = JN_0'B_d = 2J\sigma_n^2 \tag{D-8}$$

and

$$E[w \,|\text{Signal + Noise}] = J(N_0'B_d + P_{cd}) = J(P_c + 2\sigma_n^2) \tag{D-9}$$

Employing similar methods the second moment of $\bar{w}$ is given by

$$E[\bar{w}^2] = J^2P_{cd}^2 + 4J(J+1)(\sigma_n^2)(P_{cd}+\sigma_n^2) \tag{D-10}$$

The variance is then given by

$$\sigma_w^2 = 4J\sigma_n^4\left(1 + \frac{P_{cd}}{\sigma_n^2}\right) \tag{D-11}$$

Therefore

$$\sigma_w^2(\text{noise only}) = 4J\sigma_n^4 \tag{D-12}$$

and

$$\sigma_w^2(\text{signal+noise}) = 4J\sigma_n^4\left(1 + \frac{P_{cd}}{\sigma_n^2}\right) \tag{D-13}$$

Following the procedure described for example in [5], we determine detection performance in terms of the appropriate system parameters. Making reference to the probability density funxtions pictorially represented in Figure D-4, we note that the False Alarm Probability is

$$\begin{aligned} FAP &= \int_{w_0}^{\infty} p(w\,|n)dw = \int_{w_0}^{\infty} G(w, E(w\,|n), \sigma_{w\,|n}^2)dw \\ &= \text{erfc}\left[\frac{w_0 - E(w\,|n)}{\sigma_{w\,|n}}\right] \end{aligned} \tag{D-14}$$

where $G(x, m, \sigma^2)$ is a Gaussian pdf of x with mean m and variance σ^2, and erfc( ) is the complementary error function

$$\text{erfc}(\gamma) = \int_{\gamma}^{\infty} \frac{\exp(-\frac{1}{2}\tau^2)d\tau}{\sqrt{2\pi}} \tag{D-15}$$

The threshold, w_0, is set so that a prespecified FAP is maintained. Solving for w_0 in (D-14)

$$w_0 = E(w|n) + \sigma_{w|n}\, \text{erfc}^{-1}(\text{FAP}) \tag{D-16}$$

With this threshold setting, the detection probability is given by

$$\begin{aligned} P_d &= \int_{w_0}^{\infty} p(w|s+n)dw = \int_{w_0}^{\infty} G(w, E(w|s+n), \sigma^2_{w|s+n})dw \\ &= \text{erfc}\left[\frac{w_0 - E(w|s+n)}{\sigma_{w|s+n}}\right] \\ &= 1 - \text{erfc}\left[\frac{E(w|s+n) - w_0}{\sigma_{w|s+n}}\right] \end{aligned} \tag{D-17}$$

What we are ultimately interested in is transmitted signal power which is imbedded in $E(w|s+n)$. Solving for $E(w|s+n)$ in (D-17)

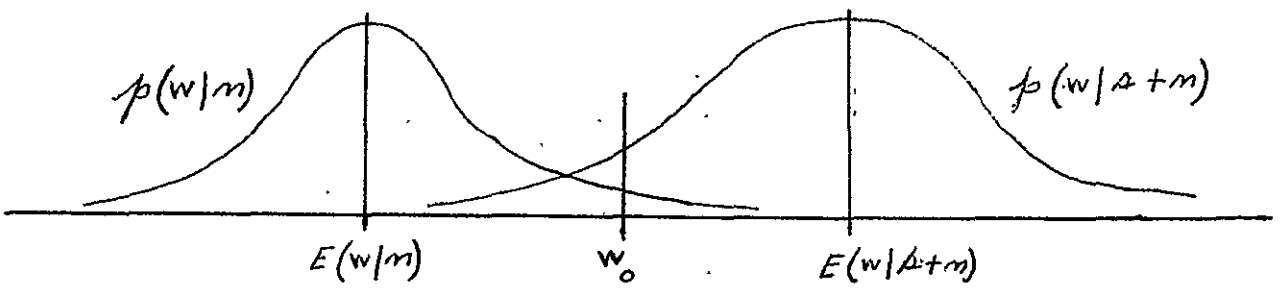

$$E[w|s+n] = w_0 + \sigma_{w|s+n}\, \mathrm{erfc}^{-1}(1-P_d) \tag{D-18}$$

Substituting (D-16) into (D-18)

$$\boxed{\begin{aligned} E(w|s+n) &= E(w|n) + \sigma_{w|n}\, \mathrm{erfc}^{-1}(FAP) \\ &\quad + \sigma_{w|s+n}\, \mathrm{erfc}(1-P_d) \end{aligned}} \tag{D-19}$$

This is the main result from which we can obtain a measure of post detection integration loss. In (D-19), FAP and P_d are specified, and, $E(w|s+n)$, $E(w|n)$, $\sigma^2_{w|n}$, and $\sigma^2_{w|s+n}$ are given by (D-9), (D-8), (D-12) and (D-13) respectively. Signal power appears in $E(w|s+n)$ and $\sigma^2_{w|s+n}$, from which we shall obtain an implicit expression for transmitted signal power. Consider first a nonfluctuating target. In our case $P_d = 0.1$ and $FAP = \alpha = 2.5 \times 10^{-6}$ so that, using [7]

$$b \triangleq \mathrm{erfc}^{-1}(1-P_d) = \mathrm{erfc}^{-1}(0.1) \approx 1.28 \tag{D-20}$$

and

$$a \triangleq \mathrm{erfc}^{-1}(\alpha) = \mathrm{erfc}(2.5 \times 10^{-6}) \approx 4.57 \tag{D-21}$$

After making the above indicated substitution into (D-19), we have that

$$\sqrt{J}\, \frac{P_{cd}}{\sigma_n^2} = 2\left\{a + b\left[1 + \left(\frac{P_{cd}}{\sigma_n^2}\right)\right]^{\frac{1}{2}}\right\} \tag{D-22}$$

or equivalently

$$(J/4)\lambda^2 - (\sqrt{J}a+b^2)\lambda + (a^2+b^2) = 0 \tag{D-23}$$

where $\lambda = P_{cd}/\sigma_n^2$. With J = 60, a = 4.57, b = 1.28, the solutions are $\lambda_1 = 1.72$ and $\lambda_2 = 0.74$. The second solution is an extraneous one, so that

$$\lambda \triangleq \frac{P_{cd}}{\sigma_n^2} \approx 1.72 \quad (2.36 \text{ dB}) \tag{D-24}$$

is the required signal-to-noise ratio at the input to the detector from the output of the 1 KHz Doppler filter.

We next need to relate this requirement back to the power required at the transmitter. The average noise power is given by (D-6) where, from section IV,

$$N_0' = N_0 d_r = FkT_0 d_r = -198.2 \text{ dB}$$

$$B_d = 1 \text{ KHz} \quad (30 \text{ dB})$$

Therefore

$$N_0' B_d = -168.2 \text{ dB} \tag{D-25}$$

The center line power into the detector is given in terms of the following radar equation

$$P_{cd} = \frac{[P_{peak} d_t^2][G^2 \bar{\sigma} \lambda^2]}{[(4\pi)^3 R^4][L]} \tag{D-26}$$

Combining (D-6) and (D-26)

$$\frac{P_{cd}}{\sigma_n^2} = \frac{[2P_{peak} d_t^2][G^2 \bar{\sigma} \lambda^2]}{[(4\pi)^3 R^4][L][N_0' B_d]} \tag{D-27}$$

From the above analysis

$$\frac{P_{cd}}{\sigma_n^2} = 2.36 \text{ dB}$$

From the discussion on system performance in section IV

$$G^2 \bar{\sigma} \lambda^2 = 36.82 \text{ dB}$$

$$(4\pi)^3 R^4 = 205.4 \text{ dB} \quad (@ R = 11 \text{ N. Mi.})$$

$$L = 9.1 \text{ dB} \tag{D-28}$$

Carrying out the computation

$$2 P_{peak} d_t^2 = 11.84 \text{ dB} \tag{D-29}$$

or, with a transmitter duty factor of $d_t = 0.4$, we have

$$\boxed{P_{peak} = 16.8 \text{ dB} \quad (48 \text{ watts, peak})}$$

or

$$\boxed{P_{avg} = 12.8 \text{ dB} \quad (19.2 \text{ watts avg.})} \tag{D-30}$$

The entire discussion to this point has been for a nonfluctuating target. We now account for the target fluctuations via the following.

The effect of employing frequency diversity has already been taken into account. The smallest gain from using frequency diversity is being assumed throughout, namely 4.7 dB. Therefore, one long pulse, or a Swerling I target model is assumed. We need

i) Swerling I target model,

ii) $P_d = 0.90$,

iii) FAP $= 10^{-6}$,

iv) N = 1 pulse,

for which, the required signal-to-noise ratio is given in DiFranco and Rubin [4, page 312],

$$\overline{R}_p = 24. \text{ dB} \qquad \text{(D-31)}$$

On the other hand, for a nonfluctuating target the required signal-to-noise ratio is

$$R_p = 16.1 \text{ dB} \qquad \text{(D-32)}$$

Therefore the increase in required SNR by assuming a Swerling I fluctuation target instead of a nonfluctuating target is 7.9 dB. This result is quite insensitive to the number of pulses that are assumed (we assumed N = 1), but very dependent on the probability of detection that is chosen. This is shown for example in DiFranco and Rubin [4, pp. 442-443]. As P_d is increased, the difference in required SNR between a nonfluctuating target and a Swerling I fluctuating target increases.

To determine the peak power in our case we have the following:

i) $P_{peak} = 16.8$ dB, for a nonfluctuating target, N = 1 pulse, from (D-30)

ii) + 7.9 dB, for the assumption of a fluctuating target Swerling I, N = 1 pulse, from the above discussion.

iii) -4.7 dB due to diversity gain, see Section IV of this report.

Therefore

$$P_{peak} = 100 \text{ watts } (20 \text{ dB}) \qquad \text{(D-33)}$$

is the peak power required for the suboptimal system with a fluctuating target and account for frequency diversity at a range of 11 N.Mi. Compared to Case I in Section IV, where P_{peak} = 15.18 dB for the ideal systems where all other assumptions are identical, we conclude the post detection integration loss with respect to the ideal system is 4.8 dB.

REFERENCES

1. M. I. Skolnik, Radar Handbook, McGraw-Hill, 1970.

2. D. K. Barton and H. R. Ward, Handbook of Radar Measurement, Prentice-Hall, 1969.

3. S. O. Hovanessian, Radar Detection and Tracking Systems, Artech House, 1973.

4. J. V. Di Franco and W. L. Rubin, Radar Detection, Prentice-Hall, 1968.

5. C. L. Weber, Elements of Detection and Signal Design, McGraw-Hill, 1968.

6. W. Feller, An Introduction to Probability Theory and Its Applications, Vol. I, Wiley, 1968.

7. M. Abramowitz and I. Stegun, Handbook of Mathematical Functions, National Bureau of Standards, June 1964.

APPENDIX G

INTEGRATED KU-BAND ORBITER RADAR/COMMUNICATION SYSTEM DESCRIPTION

1.0 INTRODUCTION

The concept of combining the Shuttle Orbiter's rendezvous radar and the TDRS communication subunits into one integrated system is an appealing one from many viewpoints and thus this concept has been under consideration for quite some time. The feasibility of such integration is due to the fact that the radar and the communication functions do not occur simultaneously and, consequently, time sharing some of the equipment between the two functions appears possible. The requirements for the communication function are relatively well defined, for they are constrained by such factors as TDRS frequency assignments, link budgets, and data rates specifications. In comparison, optimizing the radar function involves a multitude of tradeoffs and assumptions, some of which are still under study. Nevertheless, sufficient information has been generated to date to permit block diagram designs for an integrated radar/communication system.

Ideally, the maximum degree of integration would be achieved with a radar design which permits all three major subunits, such as the antenna assembly, the receiver, and the transmitter, to be shared by both the radar and the communication functions. Information available to date indicates that the antenna assembly can be shared. The receiver functions, which include monopulse tracking, can also be shared between the radar and the communication modes, provided that the radar operating frequency is either within or close to the 13.8 GHz communication receive band.

Whether the transmitter unit can be shared will depend on the type of radar selected. The two extremes of the candidate radar designs are represented by (1) a noncoherent pulse system and (2) a coherent pulse doppler system. The pulse radar is characterized by high peak power, 20 to 40 kw, and low duty cycle, 0.001 being typical. The pulse doppler radar requires 20 to 40 watts peak power, but its duty cycle is in the 0.1 to 0.5 range.

Because the peak power requirements for the pulse doppler radar are close to the requirements for the communication transmitter (50 watts CW at 15 GHz), it is reasonable to assume that, if a gridded TWTA of sufficient bandwidth is available, it can be utilized by the pulse doppler radar. On the other hand, if pulse radar is selected, a separate and switchable magnetron transmitter must be used for the radar function.

In this report, we describe preliminary block diagram designs for two types of integrated radar/communication systems. One system employs a noncoherent pulse radar; the other utilizes a coherent pulse doppler radar. The Ku-band microwave losses for the integrated system (regardless of radar type) are summarized and compared to similar losses for separated communication and radar systems. Also, the RF filtering requirements for the integrated radar/communication system are defined.

2.0 KU-BAND RADAR/COMMUNICATION INTEGRATED SYSTEMS

2.1 Noncoherent Pulse Radar/Communication System

The functional block diagram for an integrated radar/communication system which utilizes noncoherent pulse radar is shown in Figure 1. To reduce the complexity of the diagram, only those subunits which are pertinent to noncoherent radar operation are shown in detail. Other subunits, such as the communication modulator and demodulator, as well as antenna angle search and track functions, are included only in their generalized form. The salient features of the integrated block diagram are discussed below.

2.1.1 Transmitter Switching

Noncoherent pulse radar transmitter requirements call for peak powers in the order of 20 to 40 kw with a typical duty cycle of about 0.001. Thus, although the average power requirement for the radar is of the same order of magnitude as that for the communication transmitter, which is

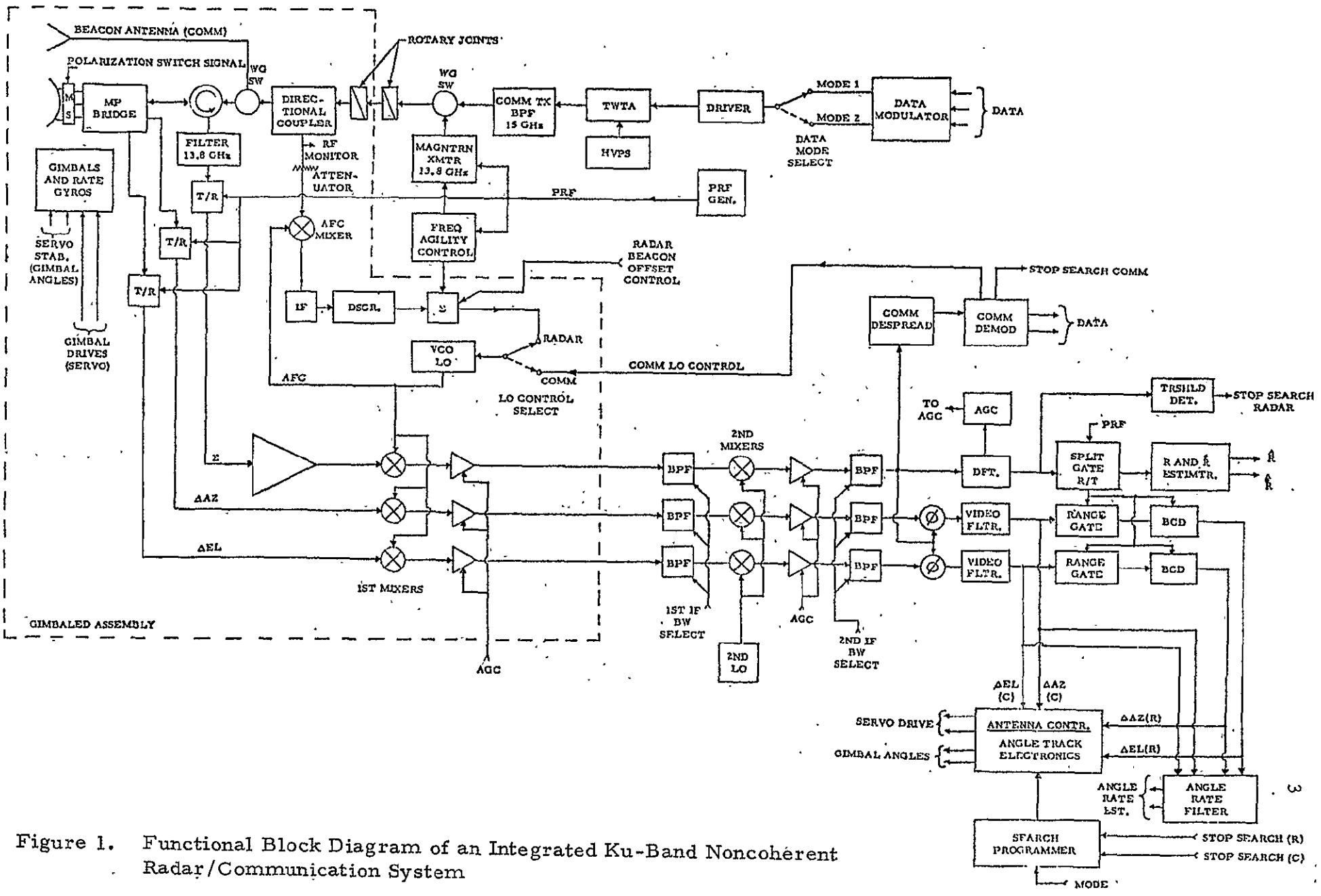

Figure 1. Functional Block Diagram of an Integrated Ku-Band Noncoherent Radar/Communication System

currently baselined at 50 watts CW, separate transmitter tubes must be used for the two functions. A frequency agile magnetron is a logical candidate for the radar transmitter and a TWTA for the communication transmitter. To minimize RF losses, both transmitters are located within the deployed assembly. Depending on the mode, their outputs are selected by a remotely controlled waveguide switch and applied via a rotary joint to the gimbaled antenna assembly. In radar search and track modes, as well as in the communication track mode, the main (20-inch nominal diameter) antenna is used. The wide beam "beacon" antenna is used only in the communication mode during TDRS acquisition procedures.

2.1.2 AFC Implementation

Automatic frequency control (AFC) is required in the radar mode for two reasons: (1) to reduce the effects of the magnetron transmitter's long-term frequency drifts, and (2) to vary the LO's frequency in step with the frequency hopped radar transmitter output during the passive target acquisition and tracking mode. To implement the AFC, a sample of transmitted radar signals is mixed with a sample of the LO output and the difference signal, whose frequency is approximately equal to the IF frequency, is applied to an IF amplifier followed by a discriminator. The output of the discriminator is then applied to the frequency control terminal of the first LO (actually a VCO) and the LO frequency is corrected accordingly to keep the IF constant.

Note that the AFC circuit is shown located within the gimbaled antenna assembly. This is consistent with the design philosophy of limiting the Ku-band interfaces between the deployed and the gimbaled assembly to the transmitter output rotary joints only. In the frequency diversity mode the frequency steps may be wider than the bandwidth of the AFC loop. Therefore, a first order frequency correction information is supplied to the LO by the magnetron's frequency agility device. The correction is,

typically, either a DC or a low frequency signal which has a known relationship to the instantaneous frequency of the magnetron. Because of the relatively low frequency nature of this correction signal it can be supplied to the gimbaled assembly via a cable wrap.

As the correction signal brings the LO signal within the bandwidth of the AFC loop, the latter takes over and provides the final adjustment to bring the IF within a workable range.

2.1.3 Receiver Front End

To provide for maximum receiver commonality, the operating frequency of the radar is made approximately equal to the 13.8 GHz nominal frequency of the communication receive signal. As shown, the monopulse bridge provides the Σ, the ΔAz and the ΔEl channel outputs. However, because the Σ receive channel is shared with the transmit channel, it is supplied to the receiver input via a circulator. This circulator provides some degree of isolation from the transmit signal in the communication mode. Also, as discussed in section 4.0, additional isolation must be provided by a 13.8 GHz filter to keep the 15 GHz signal from saturating the Σ channel in the communication mode where CW transmission and reception take place simultaneously at their respective frequencies.

In the radar mode all three channels must be protected by the T/R switches. These may consist of conventional gas ionization cavities followed by solid-state switches. Such sequential switching may prevent overloading of the receivers with spikes and residual leakages during the transmission of the high power radar pulse. Also, if reduced power is used for radar at short ranges, ionization may not take place and the T/R function may have to be performed by the solid-state switches alone.

The first mixers for both the radar and the communication function are located on the gimbaled assembly. Thus, after the first conversion to the first IF, which for a Ku-band system may be in the 300 to 1000 MHz range, the three monopulse channel signals are preamplified and supplied

to the deployed assembly via a set of cable wraps.

The question of whether to use the paramp in the radar Σ-channel is an open one, because the answer depends on the frequency allocation of the radar function. If the radar frequency is close to the communication receive frequency, improvement in radar Σ-channel noise figures can be realized by the use of the paramp. If the paramp is used for the radar function, one must insure that its bandwidth, as well as the bandwidth of the bandpass filter which precedes it, can accommodate the frequency spread required by the frequency agility during radar operation with a passive target.

Similar considerations pertain to sharing the first LO between the radar and communication functions. Because of the tunable nature of the radar LO, such sharing appears feasible. Specifically, one can implement a configuration which will force the output of the radar LO to be phase-locked to a stable reference during the communication mode.

2.1.4 Range, Range Rate and Angle Tracking

After conversion to the first IF the Σ and the two Δ channels can be shared by the radar and communication functions. The only difference may be in the bandwidth of the IF filters required for each of these modes. Specifically, for the radar mode the final bandwidth may be in the 1 to 10 MHz range, while for the communication mode the bandwidth prior to despreading may be in the 30 to 40 MHz range.

The second local oscillator converts the first IF to the second IF which may be in the 70 to 200 MHz range, the lower end being limited by the requirement to support the 30 to 40 MHz unspread bandwidth of the communication mode. The radar data recovery and angle tracking detection for both modes can be performed at the second IF. Note that despreading is not used in the communication mode prior to angle track information recovery. It has been shown in a recent report that despreading is not

required for TDRS signal angle tracking.

The output of the sum channel is applied to the communication despreader and to the radar processor. In the radar mode, the target acquisition is declared when the sum channel output exceeds a preset threshold. Antenna scan is then terminated and tracking initiated.

For range tracking a split-gate tracker is used. The output of this tracker is then applied to a processor which performs an optimal estimation of range and range rate.

The sum channel data is also used as a reference signal in the two separate phase detectors which generate, respectively, the ΔAz and ΔEl error signals. Because the system under consideration utilizes amplitude monopulse bridge, the "phase" detectors act essentially as coherent amplitude detectors (CAD). The output signals of these detectors are applied to video filters and in the radar mode these signals are first range-gated and then applied to the box car detectors. The function of these detectors is to enhance the DC component of the range-gated error samples. Because the angle error data can be either positive or negative the box car detectors are bi-polar.

The outputs of the box car detectors are applied to the angle tracking electronics subunit. This unit performs additional smoothing of the angle error data and supplies the angle correction commands to the antenna servos. Note that because the signal in the communication mode is continuous the outputs of the video filters are applied directly to the angle tracking electronics subunit.

2.2 Coherent Pulse Doppler Radar/Communication System

Figure 2 shows the block diagram for an integrated radar/communication system which utilizes a coherent pulse doppler radar. Similar to

---

*C. L. Weber, "Shuttle Monopulse System for Ku-Band Communication Signal from TDRS," Appendix I to this report.

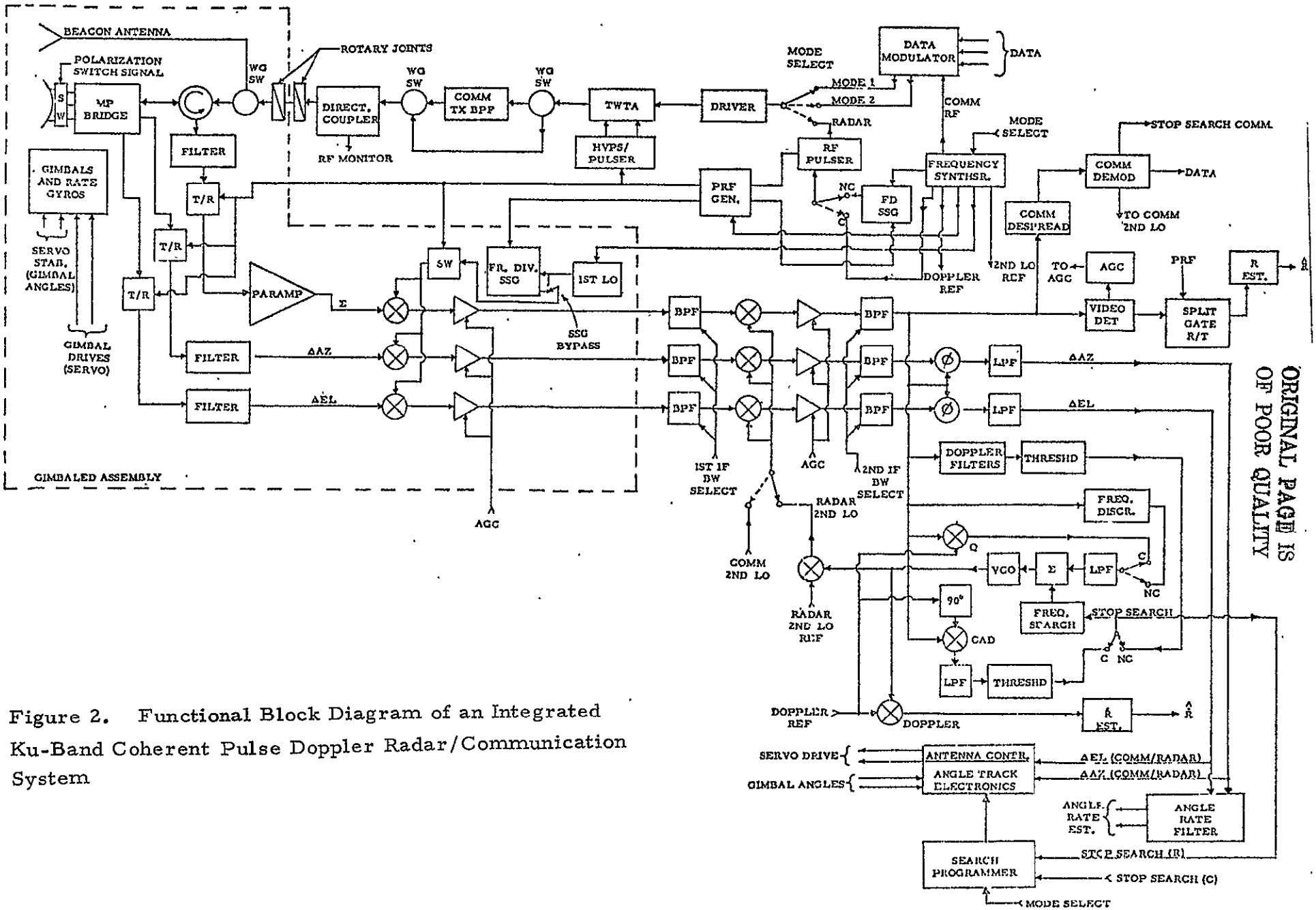

Figure 2. Functional Block Diagram of an Integrated Ku-Band Coherent Pulse Doppler Radar/Communication System

the block diagram in Figure 1, only the subunits which are pertinent to the radar function are shown in detail. The radar function is described below.

2.2.1 Radar Transmitter

The salient feature of the coherent pulse doppler radar is an inherent capability to provide simultaneous measurement of range and range rate, with the particular advantage over the noncoherent pulse radar being the accuracy of the range rate estimation. The duty cycle of such radar is relatively high, approximately 0.1 to 0.5, as compared to a typical duty cycle of 0.001 used for pulse radars. Also, the accuracy of the velocity measurement depends on the coherency and frequency stability of the transmitter and the local oscillator signals. Therefore, as shown in Figure 2, the transmitter drive and most of the local oscillator signals are derived from a stable crystal-controlled frequency synthesizer source.

The TWTA which is used for the communication signal transmission is used for the radar function. However, the RF drive signal, as well as the tube grid are pulsed at the rate determined by the PRF and the duty cycle. Since it is assumed that the radar is either equal or close to the communication receive frequency of 13.8 GHz, the 15 GHz communication transmitter filter is bypassed in the radar mode. The peak output of the transmitter is the range of 20 to 50 watts.

In the passive (skin tracking) mode the transmitter frequency diversity can be provided by the single sideband generator (SSG) which offsets the nominal transmitter frequency by a number of preselected steps to achieve the required frequency diversity span of 250 to 300 MHz. In the cooperative (transponder-aided) mode the transponder offsets the frequency of the return by the amount equal to the radar's first IF. Thus, in the cooperative mode, the transmitter and first LO signals are the same.

Similar to the pulse radar/communication system described in Section 2.1, the Ku-band transmitter is located within the deployed assembly to minimize RF line losses. Its output is applied via a rotary joint to the gimbaled antenna assembly.

2.2.2 Receiver Front End

As for the case of the noncoherent pulse radar, the goal of maximum component commonality requires that the operating frequency of the pulse doppler radar be either close to or equal to the communication receive frequency of 13.8 GHz. As shown in Figure 2, similar to the pulse radar, the monopulse bridge provides the Σ, the ΔAz and the ΔEl channel outputs. The Σ channel, which is shared with the transmit channel, is supplied to the receiver input via a circulator.

There are certain differences, however, which are peculiar to the pulse doppler radar. First, the T/R switching at all three receiver inputs is performed by solid state switches, rather than ionization type cavities. This is to insure that the T/R function can be performed at high PRF rates (tens of kpps) with minimum residual leakage and without recovery time limitations. Additional receiver protection is provided by turning off the LO drive to all three first mixers during the transmission of the radar pulse.

To protect the receivers from the 15 GHz transmit signal leakage during the communication function, filters are included in all three receiver channels. The requirement for these filters is explained in detail in Section 4.0. Here it is only proper to mention the fact that without the ionization cavity type switches in the receive channels the filter action provided by these cavities in their unfired state is not available. Hence, special filters are included in the two delta channels. Because the transmitter signal and the LO signals are derived from a coherent synthesizer, the AFC action is not required for the pulse doppler radar. In the passive mode, when the frequency diversity is required, the first LO signal is stepped in synchronism with the transmitter signal. A single sideband generator, similar to the one used to change the transmitter frequency, can be used for this purpose. In the cooperative mode, as was mentioned previously, the first LO frequency is the same as that of the transmitter.

After the conversion to the first IF and preamplification, the three monopulse channel signals are supplied to the deployed assembly via a set of cable wraps.

With respect to the sharing of the paramps and the first LO between the radar and the communication functions, the same considerations as were expressed at the end of Section 2.1.3 pertain. In other words, if the radar frequency is the same as the communication receive frequency, or is close to it, sharing of these components between the two functions appears feasible.

2.2.3 Signal Acquisition and Tracking

After conversion to the second IF and amplification, the output of the sum channel is applied to the communication and radar processors. The communication processor is the same as that used with the pulse radar, but the radar processor is different. The main difference is that special circuitry is added for acquiring and tracking the doppler-shifted center line of the target return spectrum.

In the passive target tracking mode, the target signal is detected by a bank of doppler filters. When the signal in one of the filters exceeds a preset threshold, angular search is terminated and the frequency tracking commences. Because in the passive mode the coherency of the return may be destroyed by target characteristics, a discriminator and a VCO are used to perform the tracking. The output of the VCO is then compared against a fixed reference and the frequency difference is used to estimate the range rate, i.e., the target velocity.

In the cooperative mode the transponder return is coherent and a phase-lock loop is used to acquire and track the frequency of the transponder's reply.

The range acquisition is performed by cycling the PRFs through several values to resolve the range ambiguity caused by the high values of the PRFs used by the pulse doppler radar. Once the range ambiguity

is resolved by applying the Chinese remainder theorem algorithm, split-gate target tracking in true range is initiated.

Because of the presence of a strong center line component, the angle tracking can be performed directly on this component without resorting to range gating. Similar to the pulse radar, the sum channel provides the reference signal to the "phase" detectors which coherently recover the amplitude and the polarity of the two delta channel error signals. The errors are then lowpass filtered and applied to the angle tracking electronics unit which keeps the radar antenna pointed at the target.

In the communication mode, as was mentioned earlier, the angle tracking is performed directly on the unspread downlink signal.

3.0 SYSTEM LOSSES

The numerous RF components utilized by the Ku-band integrated system introduce losses which must be accounted for when the estimates of system performance for radar and communication modes are carried out.

Generally, one may expect that an integrated radar/communication system may involve several minor RF components which may not be required by either a radar or a communication system alone. For example, transmitter and receiver filtering may not be required for a radar system alone, because the transmitter/receiver isolation is provided by the T/R switches. Also, the communication system requires circular polarization, while the best radar performance with passive targets may be obtained with linear polarization. Thus, antenna polarization switching may be required with an integrated system.

Table 1 presents a comparison of microwave losses for an integrated Ku-band radar/communication system and the separate radar and communication systems. This table has been supplied to Axiomatix by John Griffin of NASA/JSC and is included in this report as a useful guideline.

TABLE 1

COMPARISON OF MICROWAVE LOSSES,
KU-BAND SYSTEM (dB)

	Integrated System	Comm Only	Radar Only
TRANSMIT			
Filter	0.5	0.5	Not Used
Waveguide Switches	0.4	0.2	Not Used
Rotary Joints	0.5	0.4	0.4
Directional Coupler	0.15	0.1	0.1
Ferrite Circulator	0.5	0.5	0.5
Windows, Flanges, Seals, etc.	0.3	0.2	0.2
Monopulse Bridge/Feed	0.3	0.3	0.3
Waveguide	0.3	0.15	0.15
Bends	0.3	0.3	0.3
Polarization	0.1	0.1	Not Used
Switchable Polarization	0.25	Not Used	Not Used
TOTAL	3.6	2.75	1.95
RECEIVE			
Monopulse Bridge/Feed	0.3	0.3	0.3
Ferrite Circulator	0.5	0.5	0.5
T/R	0.5	Not Used	0.5
Waveguide	0.1	0.1	0.1
Bends	0.3	0.2	0.2
Filter	0.5	0.5	Not Used
Windows, Flanges, Seals, etc.	0.3	0.2	0.2
Polarization	0.1	0.1	Not Used
Switchable Polarization	0.25	Not Used	Not Used
TOTAL	2.85	1.9	1.8

4.0 RF FILTER REQUIREMENTS FOR AN INTEGRATED RADAR/COMMUNICATION SYSTEM

The RF filtering considerations for an integrated radar/communication system are determined primarily by the requirement for minimizing the transmitter-to-receiver interference during the operation in the communication mode. In this mode, the Shuttle transmitter supplies about +47 dBm (50 watts) CW power to the antenna, while the TDRS signal delivered by the antenna to the receiver is on the order of -100 dBm. The approximate frequencies of the transmit and receive signals are 15 GHz and 13.8 GHz, respectively. Therefore, the frequency separation of about 1.2 GHz constitutes a guard band across which the required signal isolation must be achieved.

Because the sum terminal of the monopulse bridge is common to the transmit and receive functions, it appears that providing adequate transmitter/receiver isolation in the Σ-channel of the receiver is of primary importance. As can be seen from Figures 1 through 3, apart from any RF filtering, the only electrical separation between the transmit and receive signals in this channel is through the circulator. The Δ-channels, however, are used for the receive function only and thus achieving transmitter/receiver isolation in these channels should be less problematic.

As shown in Figure 3, the sum channel of the receiver will, in addition to the desired low level communication signal, accept at least four spurious components which are all generated by the transmitter TWTA. These components are:

$P_N(13.8)$ - Noise generated by the TWTA and the receive frequency of 13.8 GHz. Suppression of this component requires either a bandpass or a high pass filter at the output of the TWTA transmitter.

$P_{CL}(15)$ - This component is the transmitter signal leakage between ports (1) and (3) of the circulator. Placing a 13.8 GHz bandpass or a lowpass filter between

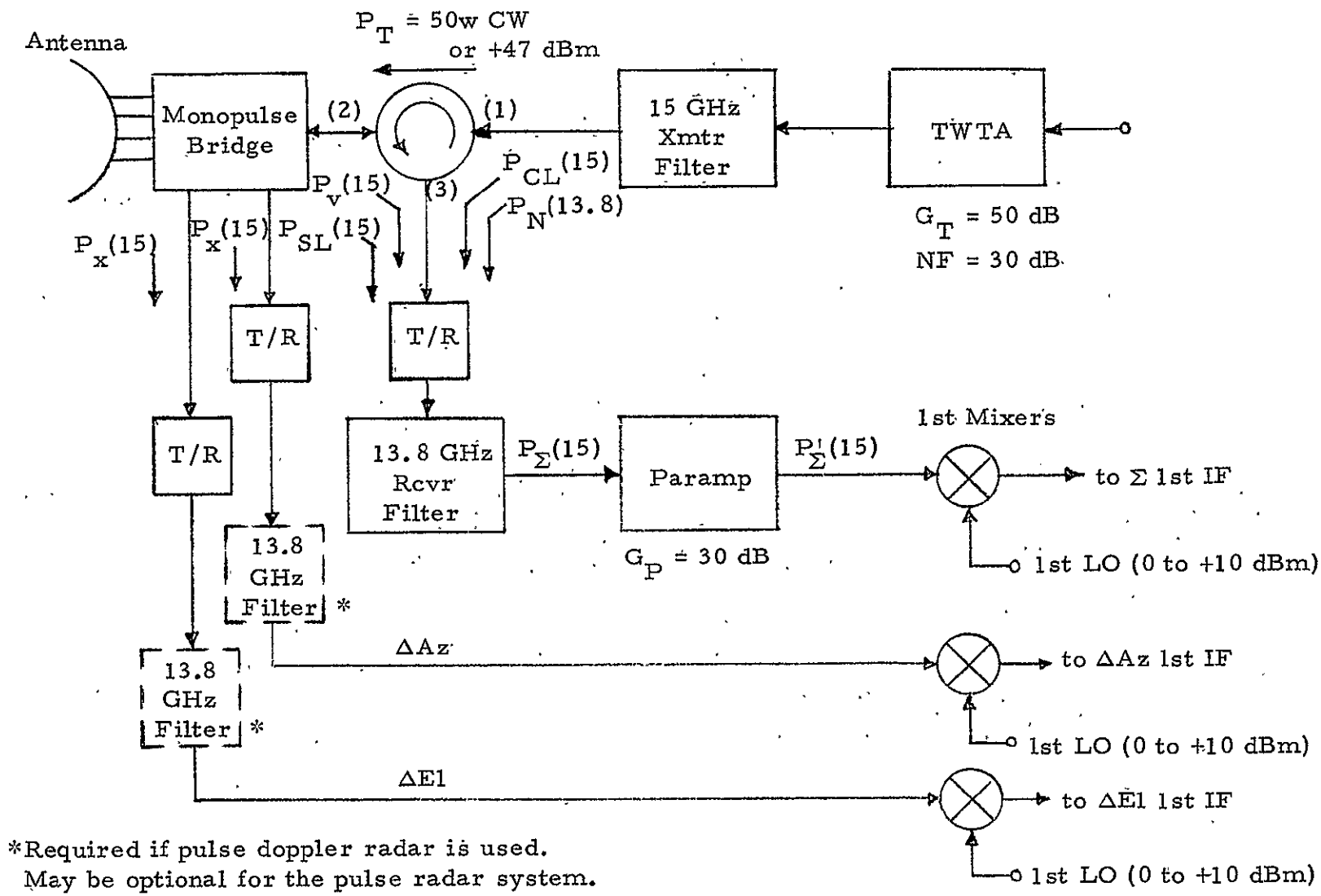

*Required if pulse doppler radar is used.
May be optional for the pulse radar system.

Figure 3. Transmitter and Receiver Filtering Required for Communication Mode of the Integrated Ku-Band Radar/Communication System

port (3) of the circulator and paramp input will attenuate this component.

$P_v(15)$ - The 15 GHz communication transmitter power reflected to the receiver input because of VSWR on the circulator-to-antenna line. Filter at receiver input will provide suppression of this component.

$P_{SL}(15)$ - 15 GHz power due to antenna sidelobe reflections at certain antenna angles. The level of this component is difficult to predict at this point without having actual measurements on either a full-size or scale model mockup. However a filter at the receiver input will provide suppression for this component.

Also, as shown in Figure 3 the 15 GHz signal leakage, $P_x(15)$, may also appear at the inputs to the Δ-channel receivers. The magnitudes of these components will be determined primarily by the monopulse bridge implementation.

The filtering of the undesirable receiver input components is discussed below.

4.1 TWTA Transmitter Output Filter

In the communication mode the Shuttle transmitter TWTA provides a return link signal at an approximate frequency of 15 GHz. However, because the TWT is generally a broadband device (bandwidth of 10% or more), a considerable amount of noise may be generated at the nominal receive frequency of 13.8 GHz. This is particularly true if the TWTA is also used for the radar function, and thus it must have the same gain at 13.8 GHz as it provides at 15 GHz. Consequently, to minimize the transmitter-generated noise at the receiver input, a filter must be included between the TWTA output terminal and the circulator. The filter may be either a bandpass or a high pass type, as long as it passes the 15 GHz with minimum loss and provides sufficient attenuation at 13.8 GHz.

The attenuation requirements for this filter can be estimated using the following assumptions:

$$\text{TWT gain:} \quad G_T = 50 \text{ dB at } 13.8 \text{ GHz}$$
$$\text{TWT noise figure:} \quad NF_T = 30 \text{ dB at } 13.8 \text{ GHz} .$$

Thus, if we start with a nominal noise floor of -114 dBm/MHz at TWT input, the noise floor at TWT output will be, approximately,*

$$N_0 = N_i + NF_T + G_T = -114 \text{ dBm/MHz} + 30 \text{ dB} + 50 \text{ dB}$$
$$= -34 \text{ dBm/MHz} . \quad (1)$$

The circulator may provide, typically, 20 dB isolation between ports 1 and 3. Thus, without a filter, the transmitter noise, $P_N(13.8)$, at the receiver input will be:

$$P_N(13.8) = N_0 - I = -34 \text{ dBm/MHz} - 20 \text{ dB}$$
$$= -54 \text{ dBm/MHz} , \quad (2)$$

where I is circulator isolation expressed as a positive value.

A conservative design may require that transmitter noise contribution be, say, at least 10 dB below the thermal noise at receiver input. Consequently, the required absolute attenuation at 13.8 GHz provided by the transmitter output filter should be:

$$P_N(13.8) - A \leq -114 \text{ dBm} - 10 \text{ dB} , \quad (3)$$
$$-54 \text{ dBm} - A \leq -124 \text{ dBm} ,$$

or $A \geq 70$ dB, where A is the required attenuation expressed as a positive number.

---

*For the purpose of simplicity, we disregard such second-order effects as saturation, intermod products, etc.

The 70 dB attenuation is not excessive from a standpoint of being provided by a multi-section filter, but this number does approach a limit set by "across-the-device" leakage. Therefore, when specifying the 15 GHz transmitter filter, not only the attenuation at 13.8 GHz must be defined but also the maximum allowable leakage.

In arriving at the results of (3), we have used a step-by-step procedure for the purpose of clarity. But, because the values of the parameters used in (1) through (3) may actually differ from those assumed, it is convenient to obtain one expression which combines them all.

Thus, if we define M(dB) as a margin by which we wish to suppress the transmitter noise below the nominal receiver noise floor of -114 dBm/MHz, we can combine equations (1), (2) and (3) into a generalized form which can be easily interpreted:

$$A(dB) \geq NF_T(dB) + G_T(dB) + M(dB) - I(dB) \quad . \tag{4}$$

This expression can be amended to include various correction factors and tradeoffs.

4.2 Receiver Filter Requirements

4.2.1 Sum Channel Filtering

4.2.1.1 Circulator Leakage

The communication transmitter output level will be about 50 watts CW or +47 dBm. The major portion of this signal will flow from terminal (1) to terminal (2) of the circulator and then via the monopulse bridge to the antenna feed. A small portion, determined by isolation between circulator ports (1) and (2), will reach the input of the receiver. If no filtering is used, this spurious signal, $P_{CL}(15)$, when amplified by the paramp, will saturate the first mixer of the Σ-channel receiver. Furthermore, it may also saturate the paramp itself.

Consider first the mixer saturation problem. A typical microwave mixer accepts an LO power on the order of 0 to +10 dBm. Thus, to prevent the spurious 15 GHz signals from interfering with LO action, one must keep these signals at least 10 dB or more below the LO level. Assume that -10 dBm is the maximum allowable spurious level at the mixer. If A is the filter attenuation required and I is the port (1) to port (3) isolation, we can write:

$$P_T(\text{dBm}) - I(\text{dB}) - A(\text{dB}) + G_P(\text{dB}) \leq -10 \text{ dBm} . \quad (5)$$

For I = 20 dB and G_P = 30 dB (paramp gain), we have

$$+47 \text{ dBm} - 20 \text{ dB} - A(\text{dB}) + 30 \text{ dB} \leq -10 \text{ dBm} , \quad (6)$$

or $\underline{A \geq 67 \text{ dB}}$, a requirement which approaches the "across-the-device" leakage limitation.

So far, we have assumed that only a filter external to the paramp performs all the filtering. This means that at the input to the paramp the spurious signal may be as high as -40 dBm. Depending on the paramp used, this may be too high a level to handle without saturating the paramp unit itself. Consequently, an additional transmit-reject filter may be incorporated into the paramp unit. This filter may provide additional 20 to 30 dB of the transmitter signal rejection.

4.2.1.2 VSWR Reflection

Mismatches in the transmission path between port (2) of the circulator and the antenna feed will cause some of the 15 GHz transmit signal to be reflected back to port (2) and then via port (3) to the receiver input. We designate this component as $P_v(15)$. Assuming VSWR of 1.5 (S = 1.5), the voltage reflection coefficient is

$$\left|\rho_v\right| = \frac{S-1}{S+1} = \frac{1.5-1}{1.5+1} = \frac{0.5}{2.5} = 0.2 \quad (7)$$

and the power reflection coefficient is

$$\rho_p = \rho_v^2 = (0.2)^2 = 0.04 \text{ or } -14 \text{ dB} . \quad (8)$$

Therefore, the level of the transmitted power reflected to the receiver will be

$$P_v(15) = +47 \text{ dBm} - 14 \text{ dB} = +33 \text{ dBm or } \underline{2 \text{ watts}}! \quad (9)$$

This is a considerable amount of power and to keep its level at -40 dBm at the paramp input would require 77 dB of attenuation from the receiver filter at the 15 GHz frequency.

Additional trassmit-reject filtering may thus have to be included within the paramp itself to prevent its own saturation and the overloading of the sum channel mixer. It is also evident that the VSWR in the sum channel is one of the driving factors in determining the transmit-reject filtering requirements in the sum channel of the receiver.

4.2.1.3 Sidelobe Reflection

At some of the pointing angles, the antenna sidelobes may be directed at various portions of the Orbiter's fuselage and, as a result, some transmitter power may be reflected back to the antenna. The magnitude of such a reflected component is difficult to predict, however, without carrying out the actual measurements with either a full-size mockup or a scaled-down model. Thus, for the present, we will <u>assume</u> that the sidelobe reflections will be, in the worst case, of the same order of magnitude as the aforementioned circulator leakage and line mismatch reflection signals. Consequently, the receiver filtering requirements, if met for these other signals, should be satisfactory to handle the sidelobe reflections.

4.2.2 Delta Channel Filtering

Filtering requirements for the two delta channels will be determined by the isolation achievable in the monopulse bridge between the transmitter

channel (sum channel) and the delta output ports. The isolation available ranges typically from 20 to 30 dB, depending on the tolerance, bandwidth, environmental conditions, etc. If we assume that at best 26 dB of isolation is available, the transmitter signal leakage to the two delta ports will be, not counting sidelobe reflections,

$$P_x(15) = +47 \text{ dBm} - 26 \text{ dB} = +21 \text{ dBm} , \tag{10}$$

or ≈ 0.12 watts. This is a sizeable signal and unless attenuated, it will saturate the first mixers of the two delta channel receivers.

Applying our previously used criterion that the input to the first mixers at the receive signal terminals should not exceed -10 dBm, the attenuation of the 15 GHz signal in the delta receiver channels can be determined:

$$+21 \text{ dBm} - A_\Delta(15) \leq -10 \text{ dBm} \tag{11}$$

or $$A_\Delta(15) \geq \underline{31 \text{ dB}} .$$

Although this requirement is not as imposing as those for the sum channel, which includes the paramp, nevertheless it indicates that some filtering must be provided in the delta channels.

One argument is that if the T/R switches used for the radar function are of the ionization/cavity type, such as may be used with a pulse radar, some filtering action may be obtained from frequency selectivity of the unfired cavities of these switches. The amount of signal rejection at 15 GHz will depend on the filter configuration, the number of sections per filter, and the filter bandwidth.

The minimum bandwidth is determined by the requirement to pass the frequency diversity radar signal. The nominal bandwidth required for the frequency diversity is 250 MHz. Thus, let us assume that 1 dB filter bandwidth is 300 MHz. Also let us assume that maximum number of sections (or cavities) per filter is <u>two</u>. This may be typical of a T/R switch.

Table 2 shows the attenuation available from several common filter configurations.

Table 2. Attenuation at 15.8 GHz vs. Filter Configuration and Number of Sections (Filter 1 dB BW = 300 MHz, center frequency ≅ 13.8 GHz)

Filter Type	Number of Sections	Attenuation at 15.8 GHz (dB)
Single Tuned	1	10
Maximally Flat Time Delay	2	23
Butterworth (0 dB ripple)	2	31
Chebishev (1 dB ripple)	2	36

From Table 2, it is evident that with two sections or cavities, the required minimum attenuation of 31 dB can be achieved with either a Butterworth or a 1 dB ripple Chebishev filter. Thus, in principle, if two-cavity T/R switches of the proper design are used in the delta receiver channels they may provide the necessary attenuation of the undesired 15.8 GHz signal in the communication mode. It must also be noted that an inclusion of such T/R switches in the sum channel provides additional filtering in that channel.

For the pulse doppler radar the gas T/R switches are not applicable and thus receiver filters of the type described in Table 2 must be included in the delta receiver channels to suppress the 15.8 GHz signal leakage in the communication mode. These filters are shown by dotted lines in Figure 3.

5.0 CONCLUSIONS

Functional block diagram designs for the integrated radar/communication system indicate that a considerable degree of component commonality can be achieved if the radar operates at the frequency equal to, or close to, the communication receive frequency.

In this case, at least the receivers and the angle tracking circuits can be shared. If a noncoherent pulse radar characterized by high peak power (20 to 30 kw) is used, separate transmitters are required, however. On the other hand, if a coherent pulse doppler system which requires only 20 to 40 watts of peak power is used, transmitter time sharing is a good possibility, provided that the TWTA transmitter can be gated (grid gating preferred) during the radar operation.

Integration of the radar and communication functions imposes special requirements for transmitter and receiver filtering, but the preliminary estimates indicate that these requirements can be met with good conventional filter design.

APPENDIX H

RF SPECTRA AND FILTERING CONSIDERATIONS FOR AN INTEGRATED KU-BAND SHUTTLE ORBITER RADAR/COMMUNICATION SYSTEM

1.0 INTRODUCTION

The RF filtering considerations for an integrated Ku-band Shuttle radar/communication system are determined primarily by the requirement for minimizing the transmitter-to-receiver interference during the operation in the communication (comm) mode. In the comm mode the Shuttle transmitter supplies about +47 dBm (50 watts) CW power to the antenna, while the TDRS signal delivered by the antenna to the receiver is in the order of -100 dBm. The approximate frequencies of the transmit and receive signals are 15 GHz and 13.8 GHz, respectively. Therefore, the frequency separation of about 1.2 GHz provides a guard band across which the required signal isolation must be achieved.

Basically, there are two types of transmitter signal components which are deleterious to receiver operation. These are:

(1) Transmitter output components which fall within the receiver bandwidth, and

(2) Transmitter signal components which, although outside the receive band, are of sufficient level to present a saturation threat to the sum and delta channels of the receiver.

Referring to the block diagram of Figure 1, the in-band and out-of-band components can be identified as follows:

Receiver In-Band Components

$P_T(13.8)$ - That portion of transmitter signal spectrum which extends to and beyond the receive band, i.e., spectrum sidelobes, or splatter.

$P_N(13.8)$ - Noise generated by the TWTA within the receive band.

Components Outside Receive Band

$P_{CL}(15)$ - Transmitter signal leakage between ports (1) and (3) of the circulator.

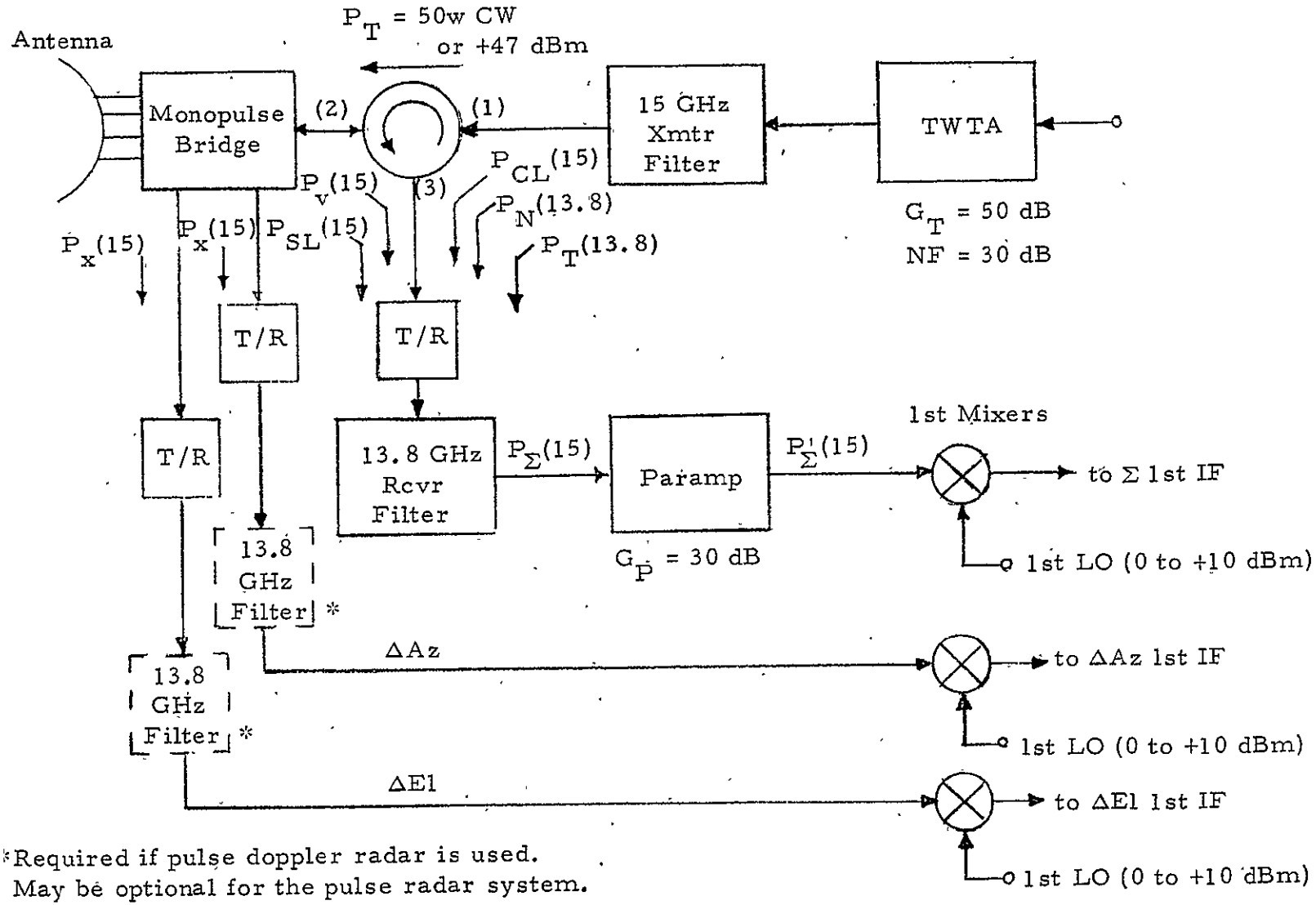

*Required if pulse doppler radar is used.
May be optional for the pulse radar system.

Figure 1. Transmitter and Receiver Filtering Required for Communication Mode of the Integrated Ku-Band Radar/Communication System

$P_V(15)$ - The 15 GHz comm transmitter power reflected to the receiver input because of VSWR on the circulator-to-antenna line.

$P_{SL}(15)$ - The 15 GHz transmitter signal reflected back to antenna via sidelobes at certain antenna angles.

$P_X(15)$ - The 15 GHz components appearing at delta channel output of the monopulse bridge.

The in-band components can be suppressed only by passing the TWTA output through either a bandpass or a highpass filter. As shown in Figure 1, this filter must be located between the output of the TWTA and port (3) of the circulator. The out-of-band components can be suppressed by providing either a bandpass or a lowpass filter at the inputs to the sum and delta receive channels.

The estimates of magnitudes for most of the components listed above and the corresponding filtering requirements have been discussed in an earlier report.* The effect of transmitter spectrum sidelobes, $P_T(15)$, falling in the receive band have not been covered, however. It is thus the main purpose of this report to reconsider the comm transmitter filtering requirements in terms of the spectral characteristics of the transmitted comm signal. The requirements for the receiver filtering are also reviewed.

2.0 COMMUNICATION SPECTRA AND FILTERING REQUIREMENTS

Part (a) of Figure 2 presents a qualitative description of the transmit and receive spectra for the communication mode. The receive signal is located in the 13.75 GHz to 13.8 GHz band. Its bandwidth is determined by the forward link PN code, whose clock rate is in the 11 to 14 Mbps range. Thus, the "bandwidth" of this signal is in the 30 to 40 MHz range,

*S. Udalov, "Integrated Ku-Band Orbiter Radar/Communication System Description," Appendix G to this report.

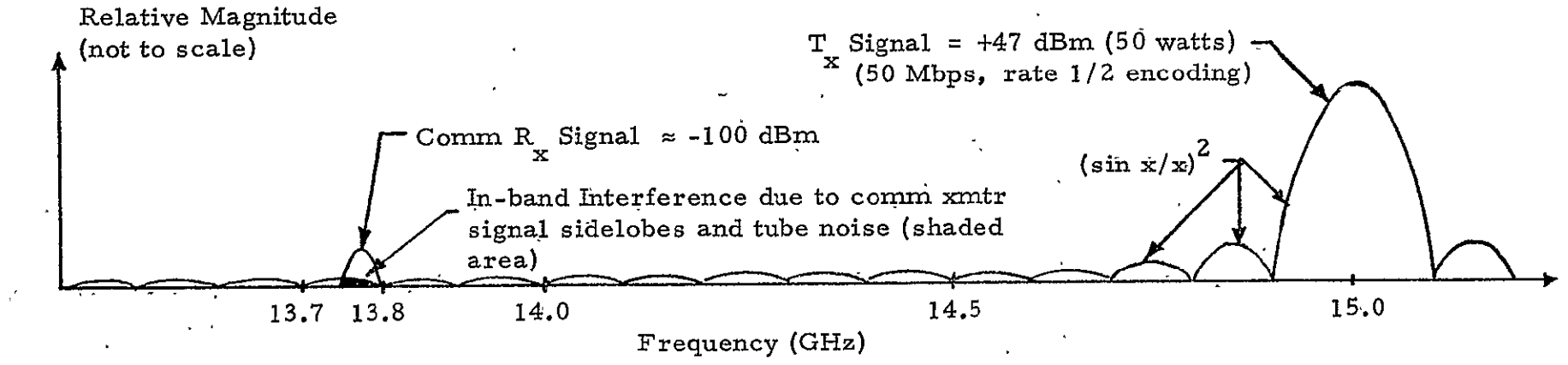

(a) Comm Mode T_x and R_x Spectra Prior to Filtering

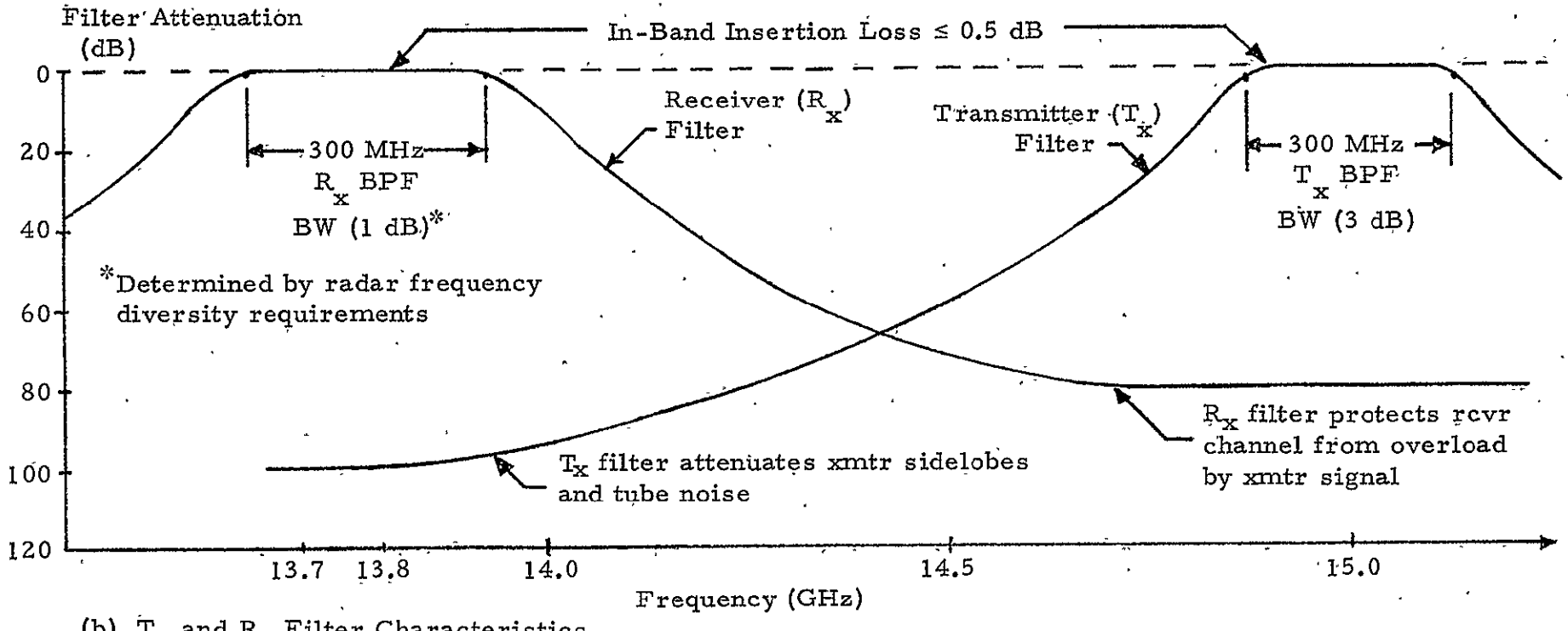

(b) T_x and R_x Filter Characteristics

Figure 2. Comm Mode T_x and R_x Spectra (a) and Filter Characteristics (b)

depending on the filtering employed at the transmitting end. The power level of this signal at the output of the Shuttle antenna is in the order of -100 dBm. This signal also appears at port (3) of the circulator which is the input to the sum channel of the receiver.

The unfiltered spectrum of the comm transmitter signal is also shown. This signal is centered at approximately 15 GHz and its maximum power level is +47 dBm or 50 watts. It is important to consider the shape of this spectrum. For a 50 Mbps rate transmission, which is rate 1/2 encoded, the effective symbol rate is 100 Mbps. Consequently, the power spectrum has $(\sin x/x)^2$ envelope with the first nulls at 100 MHz on either side of the nominal 15 GHz carrier frequency. Because the envelope of this spectrum falls off only at a rate of 20 dB/decade it becomes clear that unless adequate filtering of transmitter output is provided the sidelobes may cause considerable in-band interference to the receive signal. As shown below, this interference is considerably higher than that caused by the tube noise alone.

For a +47 dB signal and the effective symbol rate of 100 Mbps, the maximum spectral density of the main lobe is

$$D_m(15) = +47 \text{ dBm} - 20 \text{ dB}(100 \text{ MHz}) = +27 \text{ dBm/MHz} . \quad (1)$$

According to the $(\sin x/x)^2$ law, this density in the region of the receive band will be reduced by about 31 dB. Thus, the maximum possible interference density in the receive band is:

$$D_m(13.8) = +27 \text{ dBm/MHz} - 31 \text{ dB} = -4 \text{ dBm/MHz} . \quad (2)$$

In comparison, if we estimate the tube noise density in this region,* we obtain

---

*S. Udalov, ibid.

$$N_0(13.8) = N_i + NF_T + G_T = -114 \text{ dBm/MHz} + 30 \text{ dB} + 50 \text{ dB}$$

$$= -34 \text{ dBm/MHz} , \quad (3)$$

based on the assumptions that

$$G_T = \text{TWT gain} = 50 \text{ dB at } 13.8 \text{ GHz}$$

$$NF_T = \text{TWT noise figure} = 30 \text{ dB at } 13.8 \text{ GHz} .$$

Thus, it is evident that, unless adequately filtered, the transmitter sidelobe splatter at the maximum transmission rate of 50 Mbps is potentially a much greater source of receiver interference than the TWT noise.

One may argue, however, that the density calculated in (2) is only a maximum possible density and that there are transmitter spectrum nulls in the region of the receive band which may alleviate the problem. But, since the position of the nulls, as well as of the peaks, is determined by the data rate which is variable, one should consider the worst case value indicated by (2).

One can also consider prefiltering the transmitter signal prior to amplification. This is a valid approach, provided that the tube is not operating in the saturation mode. However, for maximum efficiency, the tube is usually run in or near saturation and this brings back the spectrum sidelobes despite prefiltering.*

If we assume that the circulator provides 20 dB isolation, we can estimate the filter attenuation required to keep the transmitter sidelobe splatter at, say, -124 dBm, which is 10 dB below the basic noise floor of the receiver:

$$-4 \text{ dBm/MHz} - A - 20 \text{ dB} \leq 124 \text{ dBm/Hz} \quad (4)$$

or $A \geq 100$ dB.

---

*Prefiltering to reduce spectrum sidelobes at the output of a saturated or a limiting amplifier is effective only if a staggered quadriphase modulation (SQPM) is used. So far, this type of modulation has not been considered for Shuttle return link.

This requirement is quite stringent and it demands special considerations to minimize signal leakages across the microwave components used. Choke flanges with electrical gaskets may have to be used at critical waveguide interconnections.

From the standpoint of filter design, however, the attenuation requirement may be met with 5-pole or higher order filters. The general shape of the transmitter filter characteristics is shown in part (b) of Figure 2 (page 4). This characteristic does not include circulator isolation. As shown, a 3 dB bandwidth (two-way) of 300 MHz is assumed. An approximate selectivity contour for the receiver sum channel filter is also shown in part (b) of the figure. The requirements for this filter are discussed later.

Figure 3 shows in detail the effect of transmitter filter and circulator isolation on the suppression of transmitter spectrum splatter and tube noise. The envelope of the unfiltered transmitter spectrum, as well as the tube noise level, are shown in the upper portion of the figure. The effect of a 5-pole, 0.01 dB ripple Chebichev filter on the transmitter signal sidelobes and noise is also shown. The 3 dB bandwidth (two-way) of this filter is 300 MHz. The filter characteristics are typical of the type used for such applications but are rather conservative because higher order pole filters with more ripple could be used to yield steeper attenuation characteristics.

The reason for using the idealized filter response not limited by leakage is that the attenuation is for the lower side of the transmitter bandpass. From the implementation standpoint, such idealized attenuation response on the low frequency side is generally easier to obtain in practice than it is for the high frequency side of a bandpass filter.

As shown in the lower left portion of Figure 3, the filter attenuation, plus 20 dB of circulator isolation, push the transmitter signal sidelobes below the -124 dBm/MHz level. The tube noise is attenuated below this level by the filter alone and the circulator isolation provides additional suppression.

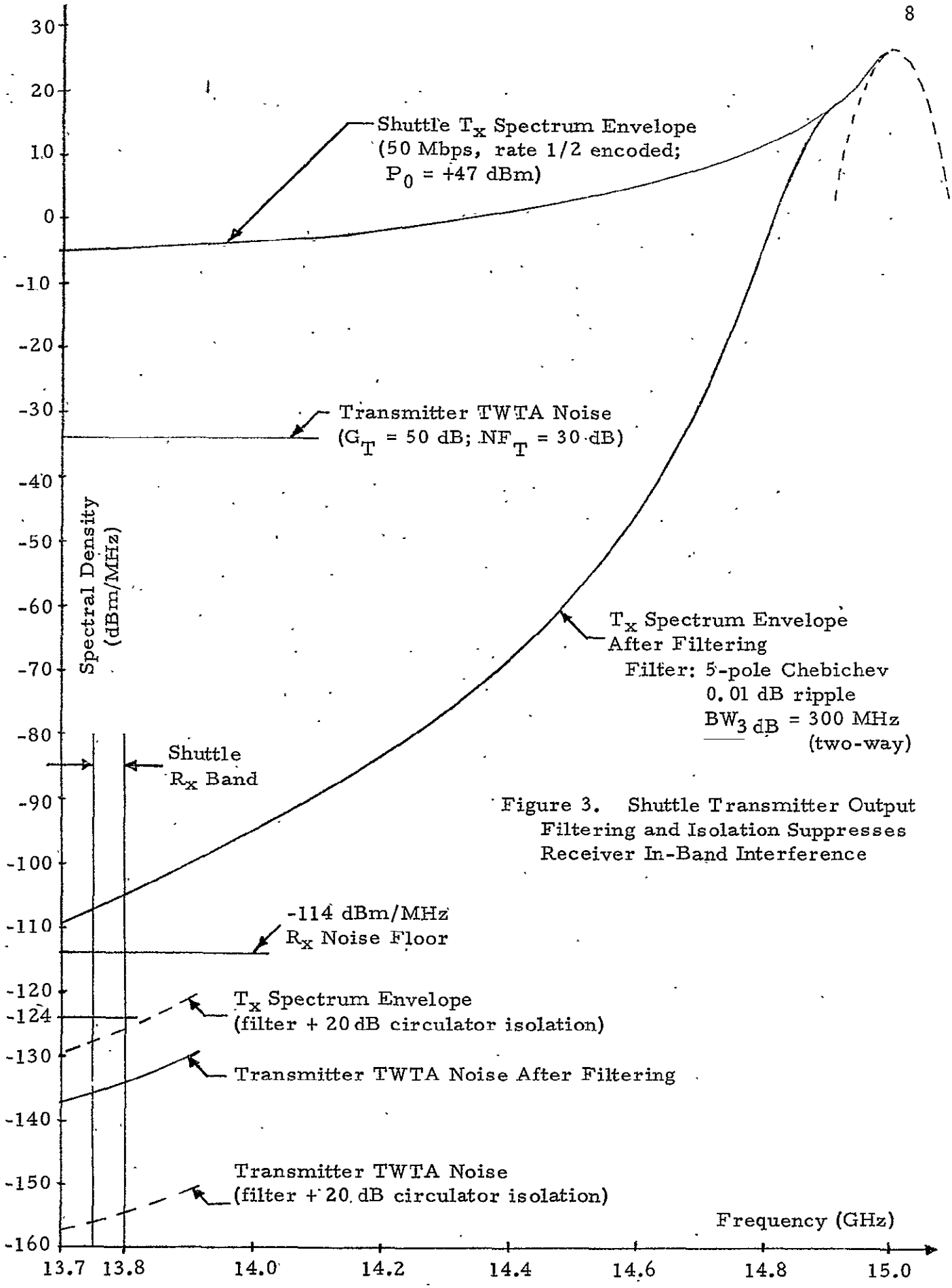

Figure 3. Shuttle Transmitter Output Filtering and Isolation Suppresses Receiver In-Band Interference

3.0 INTEGRATED RADAR/COMM RECEIVER FILTERING REQUIREMENTS

Because the radar function with either a pulse or pulse doppler radar accomplishes the transmitter-receiver isolation by time gating the receiver filtering is required primarily in the comm mode. The function of such filtering is to keep the 15 GHz signal leakage from saturating the inputs of the sum and delta receive channels. The sum channel is particularly vulnerable to overload because of the presence of the parametric amplifier.

If we assume that the 15 GHz leakage must be held below -40 dBm at the sum channel input and below -10 dBm at the delta channel inputs, we can construct the table which identifies the 15 GHz leakage components and the minimum requirements for their attenuation. Table 1 shows these requirements. It is evident from this table that the most severe requirement is placed by the VSWR of 1.5:1 in the antenna port channel. With such VSWR, about 4% of transmitted power (2 watts!) is reflected to port (2) of the circulator and subsequently to port (3), the receiver input.

The bandwidth of the receiver filters is determined by the requirement to pass the frequency diversity radar signal. The bandwidth of this signal is about 250 MHz. Thus, a filter 1 dB bandwidth (two-way) of 300 MHz is assumed. For a 5-pole, 0.01 dB ripple Chebichev filter the corresponding 3 dB bandwidth (two-way) would be about 325 MHz and attenuation of 73 dB would be reached at about 14.5 GHz. The frequency response of this filter is shown in part (b) of Figure 2 (page 4).

Table 1 shows that delta channel attenuation requirements are not as demanding as those for a sum channel. Thus, fewer sections can be used to provide the required filtering. For example, the cavities of the unfired T/R switches used with a pulse radar/comm system could serve as filters for the delta channels and provide extra filtering for the sum channel. In a pulse doppler radar/comm system, the ionization type

Table 1. Receiver Filter Attenuation Requirements vs. 15 GHz Leakage Components

15 GHz Leakage Component	Initial Magnitude M, dBm	Suppression Prior to Filtering I, dB	M - I dBm	Required Level dBm	Receiver Filter Attenuation Requirement dB	Comments
$P_{CL}(15)$	+47	20	+27	-40	67	Port (1) to Port (2) circulator leakage
$P_{v}(15)$	+33	0	+33	-40	73	VSWR = 1.5:1 Antenna port
$P_{x}(15)$	+47	26	+21	-10	31	Monopulse bridge isolation to delta channels ≈ 26 dB

NOTE: $P_{SL}(15)$ cannot be estimated at this time, but it is assumed that it will not exceed the worst case of $P_{\_}(15)$ shown above.

T/R switches are not used and special filters must be provided for the delta channels. In either case a 2-pole filter configuration should be adequate for the delta channels.

A qualitative comparison of spectra in the comm and radar modes is provided in Figures 4 and 5, respectively. As mentioned earlier, it is the radar frequency diversity which is the driving factor in determining the bandwidth of the receiver channel filters. This, of course, is based on the assumption that, for maximum receiver component commonality, the radar operates in the vicinity of the comm receive band. For this case one must also specify that the phase ripple of the receiver filters in the delta and sum channels be minimized across the frequency diversity bandwidth in order not to degrade monopulse tracking performance in the radar mode.

4.0 CONCLUSIONS

The transmitter and receiver filtering requirements for an integrated Ku-band Shuttle Orbiter radar/communication system are determined by the comm mode operation. Transmitter output filtering is particularly important to keep the transmit signal sidelobes at an acceptably low level with the 13.8 GHz receive band. Receiver input filtering is required in the sum and delta channels to prevent the leakages of the main (15 GHz) lobe of the transmitter signal from saturating the receiver channels. For an integrated system which places the radar operation in the vicinity of the comm receive band, the bandwidth of the receiver filters must be at least 250 MHz wide to accommodate the radar frequency diversity signal.

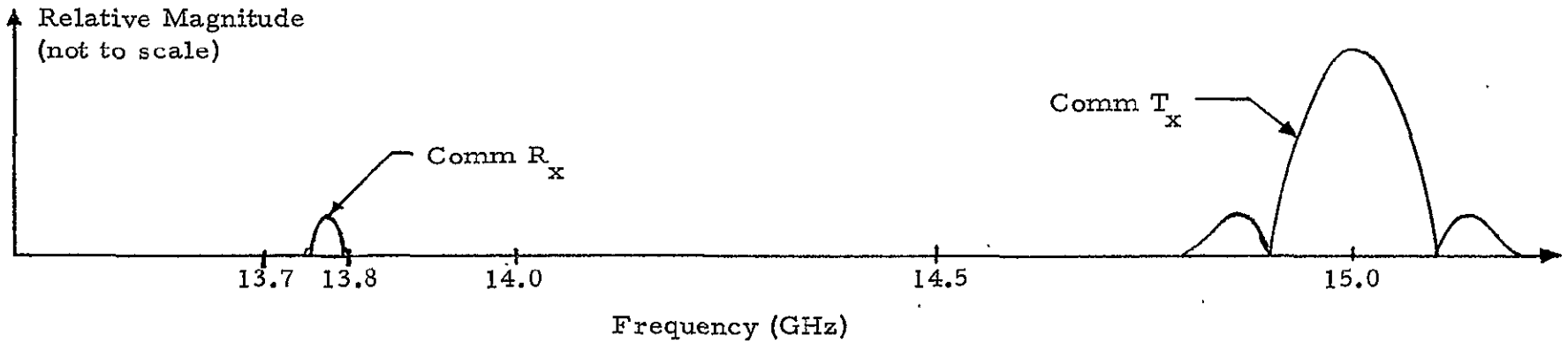

Figure 4. Comm R_x and T_x Spectra After Filtering

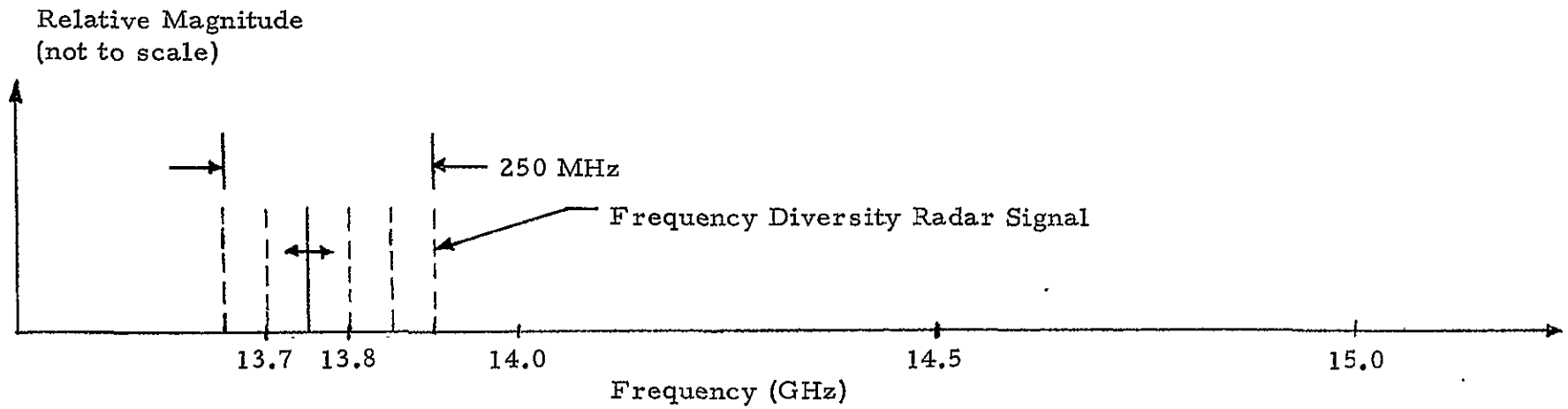

Figure 5. Radar Spectrum in Passive (Skin Tracking) Mode

APPENDIX I

SHUTTLE MONOPULSE SYSTEM FOR KU-BAND COMMUNICATION SIGNAL FROM TDRS

SHUTTLE MONOPULSE SYSTEM FOR KU-BAND COMMUNICATION SIGNAL FROM TDRS

Charles L. Weber

1. INTRODUCTION

This report verifies that angle tracking of the TDRS PN spread, communication signal received by the Shuttle can be carried out directly on the unspread wideband waveform. Hence, PN despreading is not necessary in the angle tracking loop, thereby significantly simplifying the acquisition sequence of the TDRS waveform by the Shuttle Ku-band communication receiver.

We consider in particular a coherent amplitude comparison monopulse angle tracking system for the Ku-band communication signal from TDRS. Only a single channel of monopulse angle tracking is considered. The results are sufficiently optimistic, however, so as to allow more than ample safety margin for any crosstalk which may be encountered in a two-channel monopulse system. Specific characteristics of the particular system considered are:

(a) the monopulse angle tracking is performed directly from the PN spread received signal, with no spectrum compression and no data wipe-off;

(b) a noncoherent AGC is used; and

(c) a coherent amplitude phase detector (CAD) is employed to generate the angle error information. For this system, the RMS angle tracking error due to receiver front-end noise is shown to be

$$\sigma_{\Delta_\epsilon} \approx 10^{-3} \text{ degrees}$$

when the ratio of the average receiver power in the sum channel at boresight to one-sided noise spectral density is

$$\frac{P_{REC}}{N_0} = 73.8 \text{ dB-Hz} \quad .$$

This result was determined when using conservative values for the IF bandwidth, the antenna error angle gain characteristic, and the servo control system loop bandwidth.

This RMS error is very small compared to any realistic specification that is expected. This performance result is also approximately three orders of magnitude below the specification for the angle tracking of the Ku-band Shuttle radar in both the skin-track and cooperative modes of operation.

2. MONOPULSE SYSTEM DESCRIPTION

A block diagram of the monopulse angle tracking system is shown in Figure 1. The sum channel is described by $\Sigma(t)$ and the difference channel by $\Delta(t)$.

With respect to the monopulse feed, sum and error patterns of a four-horn antenna system are usually determined experimentally, in order to account for the effects of coupling between horns, and of introduction of high-order transmission modes at the mouth of the horn assembly. Studies of actual parabolic antenna patterns [1-3] have shown that the sum pattern can be represented very closely by

$$E_r = \cos^2 (1.18 \ \Delta_\epsilon / \theta_B) \tag{1}$$

where Δ_ϵ is the angle off the boresight axis, and θ_B is the 3 dB beamwidth. The measured error pattern for the same type parabolic antenna is

$$E_\Delta = 0.707 \sin (2.36 \ \Delta_\epsilon / \theta_B) \quad . \tag{2}$$

Differences between these approximations and actual patterns appear only at the edges of the main beam, way beyond the 3 dB beamwidth.

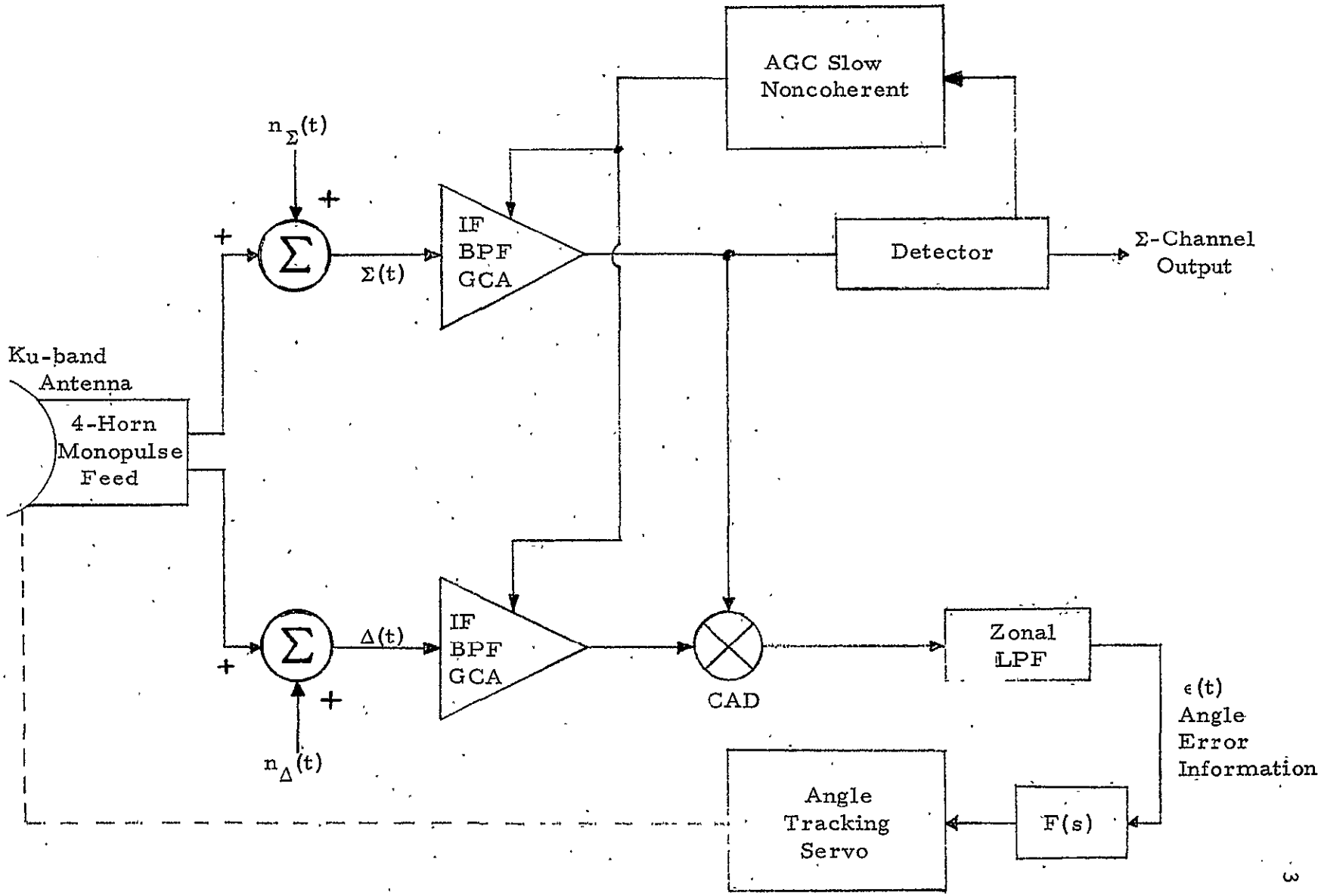

Figure 1. System Block Diagram of Monopulse Angle Tracking for Shuttle Communication Forward Link. (Only one error channel is shown.)

In this region, the actual pattern is modified by side lobes and neither equation can be considered reliable. In the angle tracking we are considering, as well as in most cases, only the variation within the 3 dB beamwidth is of interest, in which case the approximations are very satisfactory. The actual error pattern is approximately linear to one-third of the beamwidth off the boresight. The normalized error pattern E_Δ/E_r which results from the AGC action in the receiver system is linear over more than 0.6 of the beamwidth. The slope increases as the received signal approaches the half power point of the sum channel beam. The error slope is designated as k_m and is approximately 1.57 in the example shown. The error voltage is

$$\text{Error voltage} = \frac{E_\Delta}{E_r} = k_m \left(\Delta_\epsilon / \theta_B\right) \tag{3}$$

or, equivalently, the angle error is

$$\Delta_\epsilon \Big|_{\text{deg}} = \theta_B \Big|_{\text{deg}} \frac{1}{k_m} \frac{E_\Delta}{E_r} \quad . \tag{4}$$

The actual value of the antenna error slope, k_m, varies over different monopulse feed designs. A conservative interval is

$$1.2 \leq k_m \leq 2 \quad . \tag{5}$$

Referring again to Figure 1, the sum channel signal is given by

$$\Sigma(t) = E_r \left\{ A_c \, d_c(t) \cos\left(\omega_0 t + \theta_r\right) + A_s \, d_s(t) \sin\left(\omega_0 t + \theta_r\right) \right\} + n_\Sigma(t) \quad , \tag{6}$$

where E_r represents the effect of the sum of the four ports of the monopulse horn,

ω_0 is the RF carrier in radians/second,

θ_r is the sum channel reference phase;

$d_c(t) = PRN(t)\, m_c(t)$;

PRN(t) is the pseudo noise spectrum spreading-code signal;

$m_c(t)$ is one channel of ±1 digital symbols which are asynchronous with PRN(t) and $m_s(t)$;

$m_s(t)$ is the other channel of ±1 digital symbols which are at a different rate than $m_c(t)$;

A_s and A_c are in-phase and quadrature-phase signal amplitudes, which are unequal. The power in the TDRS channels is unbalanced at 80% and 20%, respectively.

The average received signal power is

$$P_{rec} = \frac{A_c^2}{2} + \frac{A_s^2}{2} \quad . \tag{7}$$

The noise $n_\Sigma(t)$ is assumed to have already been passed through an IF with noise bandwidth B_{IF}. The narrowband noise is represented by

$$n_\Sigma(t) = \sqrt{2}\, n_1(t) \cos \omega_0 t + \sqrt{2}\, n_2(t) \sin \omega_0 t \quad , \tag{8}$$

where n_1 and n_2 are independent Gaussian processes, and

$$R_{n_\Sigma}(\tau) = 2\, R_n(\tau) \cos \omega_0 \tau \tag{9}$$

$$R_n(\tau) = R_{n_1}(\tau) = R_{n_2}(\tau) \tag{10}$$

$$S_{n_\Sigma}(f) = S_n(f - f_0) + S_n(f + f_0) \quad . \tag{11}$$

These spectral densities are shown in Figure 2. The coefficient E_r in (6) represents the sum channel of the four-port monopulse horn, as indicated in (1).

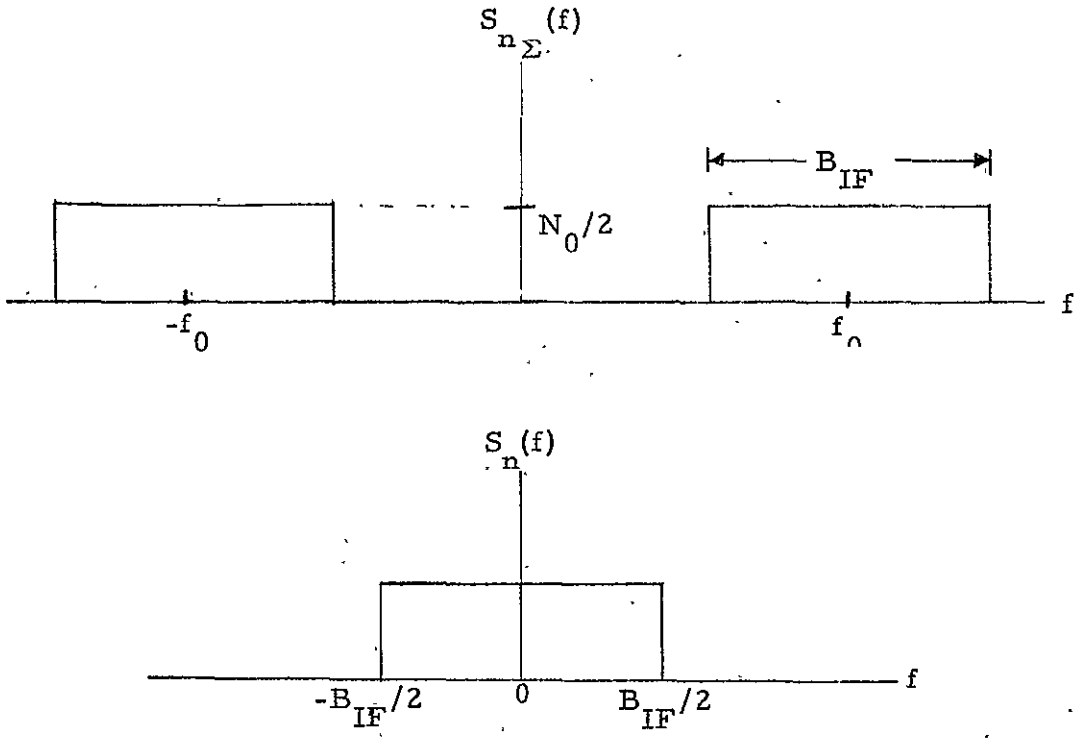

Figure 2. Noise Spectral Densities

The error channel signal is similarly described, in particular,

$$\Delta(t) = E_\Delta\{A_c\, d_c(t) \cos(\omega_0 t + \theta_\Delta) + A_s\, d_s(t) \sin(\omega_0 t + \theta_\Delta)\} + n_\Delta(t) \quad , \tag{12}$$

where E_Δ is the difference channel error signal from the horn, and θ_Δ is the RF reference phase of the difference channel which ideally is equal to θ_r in the sum or reference channel.

The narrowband additive noise in the error channel is modeled as

$$n_\Delta(t) = \sqrt{2}\, n_3(t) \cos \omega_0 t + \sqrt{2}\, n_4(t) \sin \omega_0 t \quad , \tag{13}$$

which has the same statistics but is assumed to be independent of $n_\Sigma(t)$.

Referring to Figure 1, both $\Sigma(t)$ and $\Delta(t)$ are passed through identical IF bandpass filters with noise bandwidth B_{IF}, which is sufficiently large for us to assume that there is no signal distortion. These BPFs have gain controlled amplifiers, and we designate their gain as

$$\text{IF Gain} = \frac{1}{A_{GCA}} \quad . \tag{14}$$

We consider the effects of the AGC on these IF amplifiers in Appendix A. Under the assumption of an ideal AGC from a noncoherent energy detector, we show that

$$(A_{GCA})^2 = E_r^2 P_{rec} + 2 R_N(0) \quad . \tag{15}$$

The output of the coherent amplitude detector (CAD), also a phase detector, after being passed through a zonal low pass filter, is designated as $\epsilon(t)$ which is the angle error signal in the single channel system we are considering. This dynamic angle error is

$$\begin{aligned}
\epsilon(t) &= \left.\frac{\Delta(t)\,\Sigma(t)}{(A_{GCA})^2}\right|_{\text{Low Pass}} \\
&= \left(\frac{1}{A_{GCA}}\right)^2 \left\{\left[E_\Delta\left\{A_c d_c(t)\cos(\omega_0 t + \theta_\Delta) + A_s d_s(t)\sin(\omega_0 t + \theta_\Delta)\right\}\right.\right. \\
&\qquad \left. + \sqrt{2}\, n_3(t)\cos\omega_0 t + \sqrt{2}\, n_4(t)\sin\omega_0 t\right] \\
&\qquad \cdot \left[E_r\left\{A_c d_c(t)\cos(\omega_0 t + \theta_r) + A_s d_s(t)\sin(\omega_0 t + \theta_r)\right\}\right. \\
&\qquad \left.\left. + \sqrt{2}\, n_1(t)\cos\omega_0 t + \sqrt{2}\, n_2(t)\sin\omega_0 t\right]\right\}_{\text{Low Pass}} \\
&= \left(\frac{1}{A_{GCA}}\right)^2 \left\{E_\Delta E_r\left[\frac{A_c^2}{2}\cos\theta_E + \frac{A_s^2}{2}\cos\theta_E\right] + n'_{eq}(t)\right\} \quad ,
\end{aligned} \tag{16}$$

where the difference in IF phase delays between the sum and difference channels is

$$\theta_E = \theta_\Delta - \theta_r \tag{17}$$

and the equivalent additive noise is given by

$$\begin{aligned} n'_{eq}(t) &= n_1(t)\, n_3(t) + n_2(t)\, n_4(t) \\ &+ \frac{E_\Delta}{\sqrt{2}}\Big[A_c d_c(t) \cos\theta_\Delta\, n_1(t) - A_c d_c(t) \sin\theta_\Delta\, n_2(t) \\ &+ A_s d_s(t) \sin\theta_\Delta\, n_1(t) + A_s d_s(t) \cos\theta_\Delta\, n_2(t)\Big] \\ &+ \frac{E_r}{\sqrt{2}}\Big[A_c d_c(t) \cos\theta_r\, n_3(t) - A_c d_c(t) \sin\theta_r\, n_4(t) \\ &+ A_s d_s(t) \sin\theta_r\, n_3(t) + A_s d_s(t) \cos\theta_r\, n_4(t)\Big] \quad . \end{aligned} \tag{18}$$

From (16), the angle error signal can be expressed as

$$\begin{aligned} \epsilon(t) &= \frac{E_\Delta E_r P_{rec} \cos\theta_E}{(A_{GCA})^2} + \frac{n'_{eq}(t)}{(A_{GCA})^2} \\ &= \frac{E_\Delta E_r P_{rec} \cos\theta_E}{E_r^2 P_{rec} + 2 R_N(0)} + \frac{n'_{eq}(t)}{(A_{GCA})^2} \\ &= \frac{E_\Delta}{E_r}\left[\frac{\cos\theta_E}{1 + \dfrac{2 R_N(0)}{E_r^2 P_{rec}}}\right] + \frac{n'_{eq}(t)}{(A_{GCA})^2} \\ &= k_m \frac{\Delta_\epsilon}{\theta_B}\left[\frac{\cos\theta_E}{1 + \dfrac{2 R_N(0)}{E_r^2 P_{rec}}}\right] + \frac{n'_{eq}(t)}{(A_{GCA})^2} \end{aligned}$$

$$\epsilon(t) = K_{eq}\,\Delta_\epsilon + \frac{n'_{eq}(t)}{(A_{GCA})^2} \quad . \tag{19}$$

where

$$K_{eq} \triangleq \frac{k_m}{\theta_B}\,\frac{\cos\theta_E}{\left[1 + \dfrac{2\,R_N(0)}{E_r^2\,P_{rec}}\right]} \quad . \tag{20}$$

3. PERFORMANCE - RMS ERROR

If the angle error signal is scaled by K_{eq}^{-1}, then a linearized antenna angle control system is as shown in Figure 3, where

$$\epsilon_n(t) = \frac{\epsilon(t)}{K_{eq}} = \Delta_\epsilon + n_{eq}(t) \tag{21}$$

and

$$n_{eq}(t) = K_{eq}^{-1}\,n'_{eq}(t)\Big/(A_{GCA})^2 \quad . \tag{22}$$

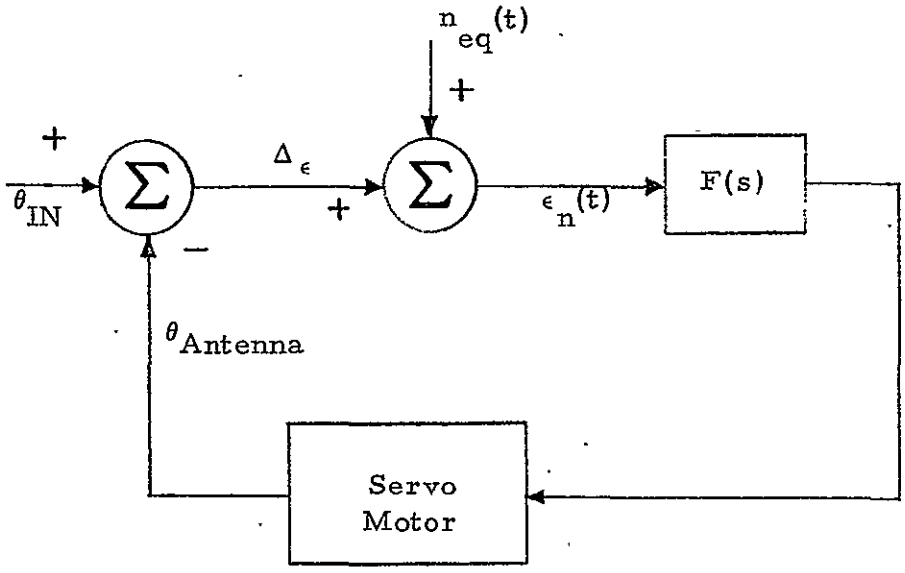

Figure 3. Linearized Diagram for Antenna Angle Control

From linear tracking loop theory [7-8], the variance of the angle error due to thermal noise is given by

$$\sigma^2_{\Delta_\epsilon} = \int_{-\infty}^{\infty} \left|H_s(f)\right|^2 S_{n_{eq}}(f)\, df \tag{23}$$

where $H_s(f)$ is the closed loop transfer function of the antenna angle control and $S_{n_{eq}}(f)$ is the two-sided spectral density of equivalent loop noise.

When the bandwidth of the noise is very large with respect to the noise bandwidth of the antenna angle control, the variance of the angle error is

$$\sigma^2_{\Delta_\epsilon} = N_{eq}\, B_s \tag{24}$$

where N_{eq} is the one-sided spectral density of the equivalent loop noise and B_s is the one-sided noise bandwidth of the angle control loop

$$B_s = \int_0^{\infty} \left|H_s(f)\right|^2 df \ . \tag{25}$$

Equivalently stated, the requirement is $B_s \ll B_{IF}$.

The one-sided spectral density of $n_{eq}(t)$ is given in terms of that of $n'_{eq}(t)$ by

$$N_{eq} = \frac{N'_{eq}}{K^2_{eq}\,(A_{GCA})^4} \ . \tag{26}$$

In Appendix B, we show that the one-sided spectral density of $n'_{eq}(t)$ is given by

$$N'_{eq} = N_0\, P_{rec}\left[\frac{N_0\, B_{IF}}{P_{rec}} + \left(\frac{E_\Delta}{E_r}\right)^2 + 1\right] . \tag{27}$$

Upon substitution of (27) into (26), and (15), (20) and (26) into (24), we have that

$$\sigma_{\Delta_\epsilon} = \frac{\theta_B}{k_m \cos \theta_E} \sqrt{\frac{N_0}{P_{rec}} \left[\frac{N_0 B_{IF}}{P_{rec}} + \left(\frac{E_\Delta}{E_r} \right)^2 + 1 \right] B_s} \tag{28}$$

where we have consolidated E_r into P_{rec} by setting $E_r = 1$.

4. COMPUTATION

Assuming that

$$\theta_B = 2.8 \text{ degrees}$$

$$B_{IF} = 40 \text{ MHz}$$

$$\frac{P_{rec}}{N_0} = 73.8 \text{ dB-Hz}$$

$$\left| \frac{E_\Delta}{E_r} \right| \leq 1$$

and $$B_s = 10 \text{ Hz}$$

we have

$$\sigma_{\Delta_\epsilon} \approx 2.2 \times 10^{-3} \text{ degrees} \tag{29}$$

or $$3\sigma_{\Delta_\epsilon} \approx 6.6 \times 10^{-3} \text{ degrees} .$$

This compares very favorably with the 3σ values for the radar angle tracking specifications in both the skin-tracking and beacon modes of operation, namely:

$3\sigma = 0.573$ degrees due to random noise .

We conclude from (29), therefore, that it is unnecessary to use the PN despreading of the communication signal from TDRS for angle tracking performance.

POST-NOTE

In Figure 1, the paramp in the sum channel is not shown. With the paramp present, the gain in the sum channel is substantially increased with respect to that in the difference channel. This does not present any problem. The GCA in each channel may be different as a result. What is important, however, is that the RF phase delay of each channel be the same so as to minimize θ_E. This may require a small delay in the difference channel to compensate for the phase delay through the paramp.

REFERENCES

1. D. K. Barton. Radar System Analysis. Prentice-Hall, 1964.

2. P. W. Hannan. "Optimum Feeds for All Three Modes of a Monopulse Antenna." IRE Trans. Ant. Prop., Vol. AP-9, No. 5, September 1961, pp. 444-461.

3. S. F. George and A. S. Zannamaker. "Multiple Target Resolution of Monopulse vs. Scanning Radars." Proc. NEC, No. 15, 1959, pp. 814-823.

4. M. Skolnik. Radar Handbook. McGraw-Hill, 1970.

5. D. K. Barton and H. R. Ward. Handbook of Radar Measurement. Prentice-Hall, 1969.

6. W. C. Lindsey and M. K. Simon. Telecommunication Systems Engineering. Prentice-Hall, 1973.

7. A. J. Viterbi. Principles of Coherent Communication. McGraw-Hill, 1966.

8. W. C. Lindsey. Synchronization Systems in Communication and Control. Prentice-Hall, 1972.

APPENDIX A

AUTOMATIC GAIN CONTROL CONSIDERATIONS

A typical noncoherent AGC is shown in Figure A-1. The input is $\Sigma(t)$ as shown in Figure 1 and described in (6). The noncoherent detector is modeled as a square law device followed by a low pass filter. The gain controlled amplifier has gain $A_{GCA}^{-1}(t)$, so that

$$v_{AGC}(t) = \frac{1}{A_{GCA}(t)} \Sigma(t) \quad . \tag{A-1}$$

In a slowly varying AGC, the control voltage is essentially given by the DC value of $e_{AGC}(t)$, which is

$$e_{AGC}(t) = \left(\frac{1}{A_{GCA}(t)}\right)^2 \left[\Sigma(t)\right]^2 \quad . \tag{A-2}$$

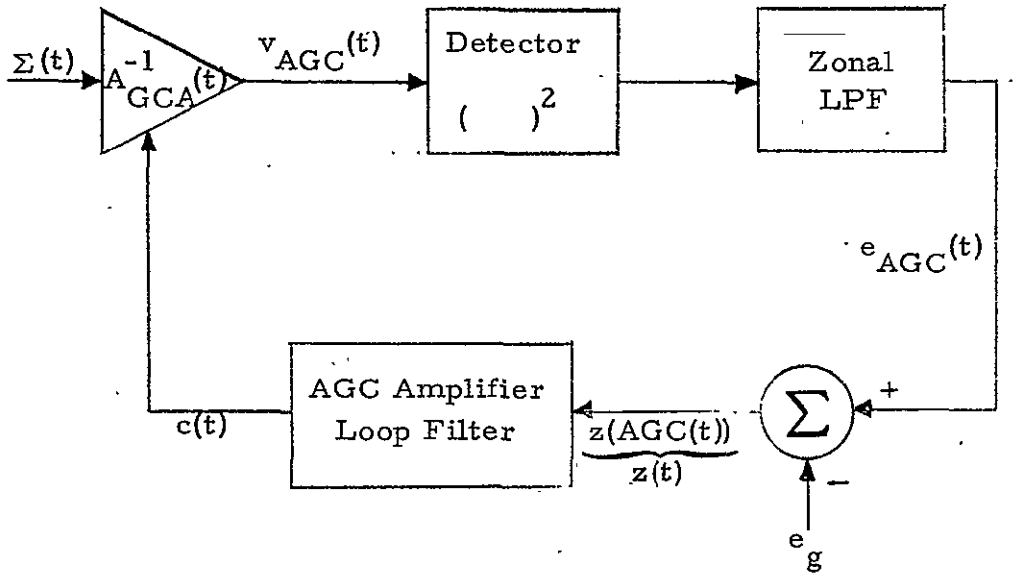

Figure A-1. Noncoherent Automatic Gain Control (AGC)

From (6), the baseband part of $\left[\Sigma(t)\right]^2$ is given by

$$\left[\Sigma(t)\right]^2_{\substack{\text{base}\\\text{band}}} = \frac{E_r^2}{2}\left[A_c^2 + A_s^2\right] + \frac{1}{2}\left[n_1^2(t) + n_2^2(t)\right] \quad . \tag{A-3}$$

The average value of $\left[\Sigma(t)\right]^2$ is

$$E\left\{\left[\Sigma(t)\right]^2\right\} = E_r^2 P_{rec} + 2 R_N(0) \quad . \tag{A-4}$$

In the ideal noncoherent AGC which has unlimited range of operation, an excellent approximation for A_{GCA} is

$$A_{GCA}^2 = E_r^2 P_{rec} + 2 R_N(0) \quad . \tag{A-5}$$

This is the relationship used in the analysis to evaluate angle tracking capability of the Ku-band communication signal from TDRS. More sophisticated analysis of AGC could have indeed been carried out. In view of the design margin in the result, however, any small deterioration in performance due to non-ideal AGC will still result in an RMS angle error well below any anticipated specification.

APPENDIX B

EQUIVALENT NOISE SPECTRAL DENSITY

In this appendix, the one-sided noise spectral density of the equivalent loop noise $n'_{eq}(t)$ as given by (18) is determined. The auto-correlation function of $n'_{eq}(t)$ is

$$R_{n'_{eq}}(\tau) = 2 R_N^2(\tau) + \frac{1}{2}\left[(E_\Delta^2 + E_r^2)\left(A_s^2 R_{d_s}(\tau) + A_c^2 R_{d_c}(\tau)\right) R_N(\tau)\right] . \tag{B-1}$$

Under the assumption of an ideal bandpass filter with noise band width B_{IF}, the Fourier transform and hence spectral density of $2 R_N^2(\tau)$ is

$$S_1(f) = 2 \int_{-\infty}^{\infty} e^{-j\omega\tau} R_N^2(\tau)\, d\tau = 2 \int_{-\infty}^{\infty} S_N(f') S_N^*(f - f')\, df \tag{B-2}$$

which, when evaluated at $f = 0$, is

$$S_1(0) = 2 \int_{-\infty}^{\infty} S_N^2(f')\, df' = 2 (N_0/2)^2 B_{IF} . \tag{B-3}$$

The contribution to the spectral density of $n'_{eq}(t)$ from the second term in (B-1) is

$$S_2(f) = (E_\Delta^2 + E_r^2) \bullet \mathcal{F}\left\{\left[\frac{A_s^2}{2} R_{PRN}(\tau) R_{m_s}(\tau) + \frac{A_c^2}{2} R_{PRN}(\tau) R_{m_c}(\tau)\right] R_N(\tau)\right\} . \tag{B-4}$$

Although some of the data sequences are slow with respect to the chip time of the PN sequence, all of these sequences have wide bandwidth with respect to the bandwidth of the antenna angle control loop B_s. We therefore make the approximation that

$$R_{m_s}(\tau) = R_{m_c}(\tau) = 1 \qquad \text{for } |\tau| < T_c \tag{B-5}$$

where T_c is the PN sequence chip time. Then

$$S_2(f) = (E_\Delta^2 + E_r^2)\, P_{rec} \bullet \mathcal{F}\left\{R_{PRN}(\tau)\, R_N(\tau)\right\} . \tag{B-6}$$

Evaluating this at f = 0,

$$S_2(0) = (E_\Delta^2 + E_r^2)\, P_{rec} \frac{N_0}{2} \int_{-B_{IF}/2}^{B_{IF}/2} S_{PRN}(f)\, df . \tag{B-7}$$

The spectral density of a PRN sequence of ±1's with chip time T_c is approximately

$$S_{PRN}(f) \approx T_c \left(\frac{\sin(\omega T_c/2)}{\omega T_c/2}\right)^2 . \tag{B-8}$$

In addition, we will approximate the integral

$$\int_{-B_{IF}/2}^{B_{IF}/2} S_{PRN}(f)\, df \approx \int_{-\infty}^{\infty} T_c \left(\frac{\sin(\omega T_c/2)}{\omega T_c/2}\right)^2 df$$

$$\approx 1 \tag{B-9}$$

since we assume that $B_{IF} \geq 3 T_c/2$. (B-10)

Upon substitution

$$S_2(0) = (E_\Delta^2 + E_r^2)\, P_{rec} \frac{N_0}{2} \tag{B-11}$$

and

$$N'_{eq} = 2 S_{n'_{eq}}(0) = 2\left[S_1(0) + S_2(0)\right]$$

$$= N_0 P_{rec}\left[\frac{N_0 B_{IF}}{P_{rec}} + \left(\frac{E_\Delta}{E_r}\right)^2 + 1\right] \qquad \text{(B-12)}$$

where we absorb E_r into P_{rec} by assuming $E_r = 1$ without any loss of generality. This result is used in (27).

APPENDIX J

SHUTTLE MONOPULSE SYSTEM FOR KU-BAND COMMUNICATION SIGNAL FROM TDRS

PART II

SHUTTLE MONOPULSE SYSTEM FOR KU-BAND COMMUNICATION SIGNAL FROM TDRS

PART II

Charles L. Weber

1.0 INTRODUCTION

This report extends the results of [1], and familiarity with that report is assumed. The conclusion remains unchanged, namely, that angle tracking of the TDRS PN spread communication signal received by the Shuttle can be carried out directly on the unspread wideband waveform.

2.0 MONOPULSE SYSTEM DESCRIPTION

A system block diagram of the monopulse angle tracking system is shown in Figure 1. The sum channel signal is designated by $\Sigma(t)$ and the difference channel signal by $\Delta(t)$. In this part of the system evaluation, separate IF strips are assumed. Also shown are paramps in the sum channel and difference channel, and the PN sequence despreader operating on each channel. We shall determine angle tracking performance for the configuration shown, as well as with one or both paramps removed, and with the PN despreader removed. We shall see that satisfactory angle tracking performance is possible for all configurations.

Reference [1] determined system performance for the system shown in Figure 1 with paramps in all channels and without the PN despreader. We consider in this part of the analysis only one of the difference channels. We shall consider both error channels when we consider alternate implementations.

The parabolic antenna patterns are those described in [1]. The beamwidth θ_B and the error angle off boresight Δ_ϵ represent mechanical motion of the antenna in degrees as opposed to RF phase angle. For completeness, we shall repeat some of the representations in this report so as to make it reasonably self-contained.

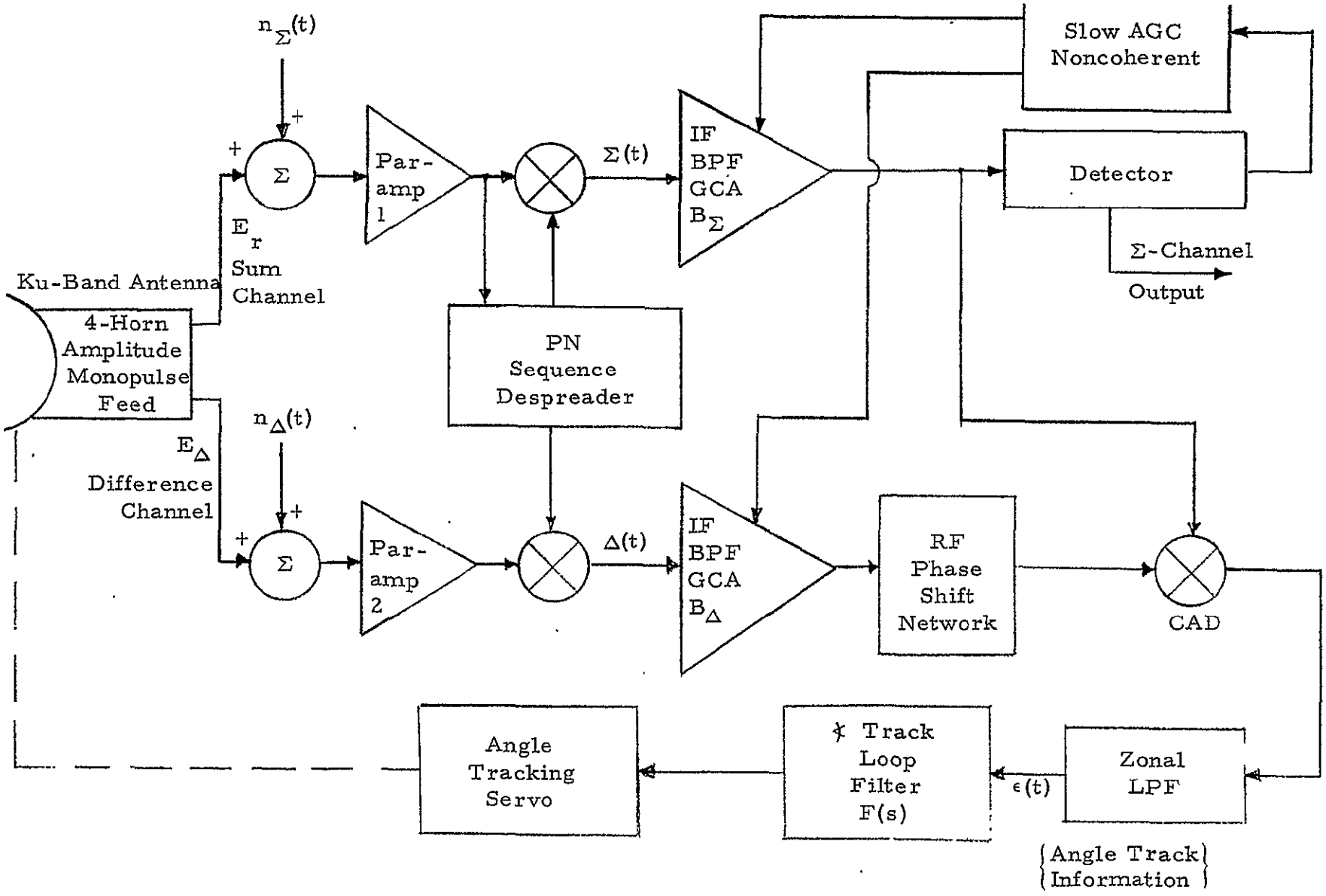

Figure 1. System Block Diagram of Monopulse Angle Tracking for Shuttle Communication Forward Link (Only one error channel is shown)

The sum amplitude pattern can be closely approximated by

$$E_r = \cos^2 (1.18\ \Delta_\epsilon/\theta_B) \ . \tag{1}$$

The error pattern is given by

$$E_\Delta = 0.707 \sin (2.36\ \Delta_\epsilon/\theta_B) \ . \tag{2}$$

In the linear region, which is our only interest, the error voltage is

$$\text{Error voltage} = \frac{E_\Delta}{E_r} = k_m\ \Delta_\epsilon/\theta_B \tag{3}$$

or

$$\Delta_\epsilon = (\theta_B/k_m)(E_\Delta/E_r) \ . \tag{4}$$

The actual value of the antenna error slope, k_m, varies over different four-horn monopulse feed designs within the interval

$$1.2 \le k_m \le 1.9 \tag{5}$$

with typical values being $1.55 \le k_m \le 1.6$.

Referring again to Figure 1, the sum channel signal at the input to the sum channel IF strip is given by

$$\Sigma(t) = E_r \Big\{ A_c\, d_c(t) \cos (\omega_0 t + \theta_r) + A_s\, d_s(t) \sin (\omega_0 t + \theta_r) \Big\} + n_\Sigma(t) \ , \tag{6}$$

where E_r represents the effect of the sum of the four ports of the monopulse horn,

ω_0 is the RF carrier in radians/second,

θ_r is the sum channel reference phase;

$d_c(t) = \text{PRN}(t)\ m_c(t)$;

PRN(t) is the pseudo noise spectrum spreading-code signal;

$m_c(t)$ is one channel of ±1 digital symbols which are asynchronous with PRN(t) and $m_s(t)$;

$m_s(t)$ is the other channel of ±1 digital symbols which are at a different rate than $m_c(t)$;

A_s and A_c are in-phase and quadrature-phase signal amplitudes, which are unequal. The power in the TDRS channels is unbalanced at 80% and 20%, respectively.

The average received signal power is

$$P_{rec} = \frac{A_c^2}{2} + \frac{A_s^2}{2} \quad . \tag{7}$$

The noise $n_\Sigma(t)$ is assumed to have already been passed through an IF with noise bandwidth B_{IF}. The narrowband noise is represented by

$$n_\Sigma(t) = \sqrt{2}\ n_1(t) \cos \omega_0 t + \sqrt{2}\ n_2(t) \sin \omega_0 t \quad , \tag{8}$$

where n_1 and n_2 are independent Gaussian processes, and the autocorrelations and spectral densities are given by

$$R_{n_\Sigma}(\tau) = 2\, R_{L\Sigma}(\tau) \cos (\omega_0 \tau) \tag{9}$$

$$R_{L\Sigma}(\tau) = R_{n_1}(\tau) = R_{n_2}(\tau) \tag{10}$$

$$S_{n_\Sigma}(\tau) = S_{L\Sigma}(f - f_0) + S_{L\Sigma}(f + f_0) \quad . \tag{11}$$

These spectral densities are shown in Figure 2.

The error channel signal is similarly described. In particular, at the input to the error channel bandpass filters:

$$\Delta(t) = E_\Delta \Big\{ A_c\, d_c(t) \cos (\omega_0 t + \theta_\Delta) + A_s\, d_s(t) \sin (\omega_0 t + \theta_\Delta) \Big\} + n_\Delta(t) \quad , \tag{12}$$

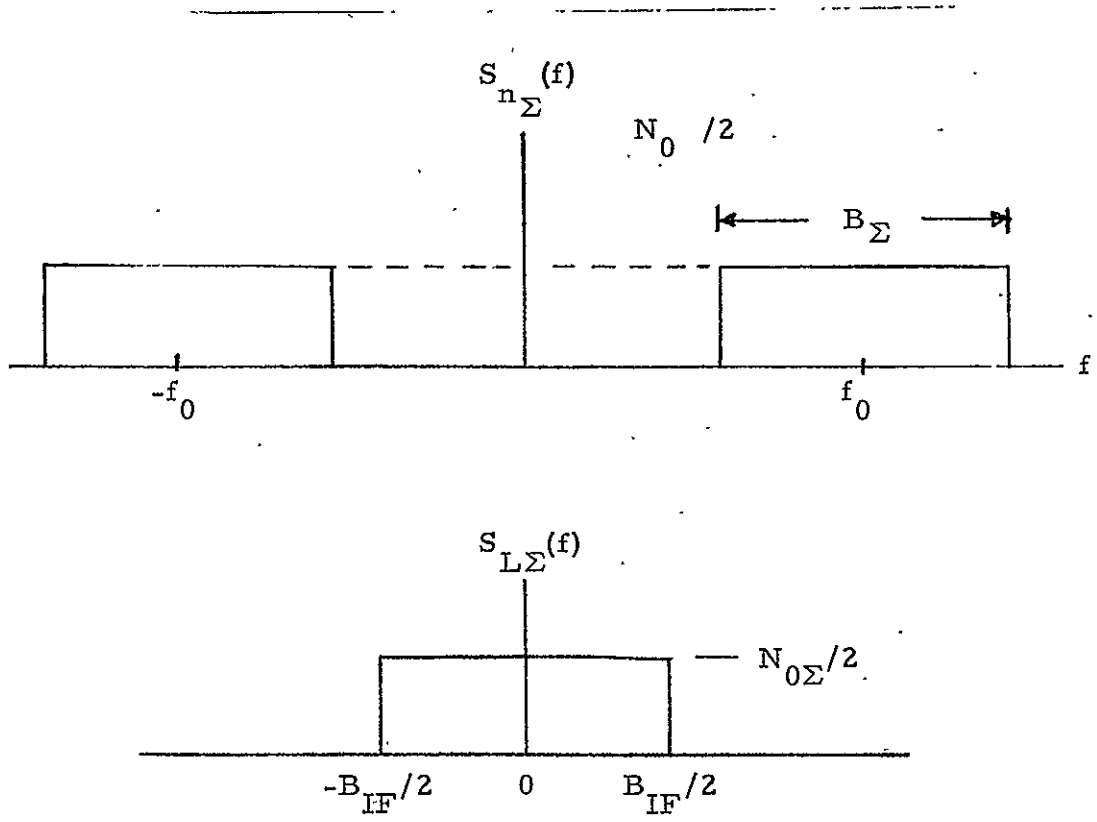

Figure 2. Noise Spectral Densities

where E_Δ is the difference channel error signal from the horn, and is the RF reference phase of the difference channel which ideally is equal to θ_r in the sum or reference channel.

The narrowband additive noise in the error channel is modeled as

$$n_\Delta(t) = \sqrt{2}\ n_3(t) \cos \omega_0 t + \sqrt{2}\ n_4(t) \sin \omega_0 t\ , \tag{13}$$

which is independent of $n_\Sigma(t)$. In (13), n_3 and n_4 are independent, and the autocorrelations and spectral densities are given by

$$R_{n_\Delta}(\tau) = 2\, R_{L\Delta}(\tau) \cos(\omega_0 \tau) \tag{14}$$

$$R_{L\Delta}(\tau) = R_{n_3}(\tau) = R_{n_4}(\tau) \tag{15}$$

$$S_{n_\Delta}(f) = S_{L\Delta}(f - f_0) + S_{L\Delta}(f + f_0) \quad . \tag{16}$$

The spectral shape is the same as the sum channel in Figure 2, with the exception that the one-sided spectral density is N_{0_Δ} watts/Hz instead of N_{0_Σ} watts/Hz. This additional parameterization allows us to account for different noise levels in the sum and difference channels due to the presence or absence of the paramps.

Referring to Figure 1, both $\Sigma(t)$ and $\Delta(t)$ are passed through identically shaped IF bandpass filters with noise bandwidth B_Σ and B_Δ, which is sufficiently large for us to assume that there is no signal distortion. These BPFs have gain controlled amplifiers, and we designate their gain as

$$\text{IF Gain} = \frac{1}{A_{GCA}} \quad . \tag{17}$$

We consider the effects of the AGC on these IF amplifiers in Appendix A of [1]. Under the assumption of an ideal AGC from a noncoherent energy detector, we show that

$$(A_{GCA})^2 = E_r^2 P_{rec} + 2 R_{n_\Sigma}(0) \quad . \tag{18}$$

The output of the coherent amplitude detector (CAD), also a phase detector, after being passed through a zonal low pass filter, is designated as $\epsilon(t)$ which is the angle error signal in the single channel system we are considering. This dynamic angle error is

$$\epsilon(t) = \left.\frac{\Delta(t)\,\Sigma(t)}{(A_{GCA})^2}\right|_{\substack{\text{Low}\\\text{Pass}}}$$

$$= \left(\frac{1}{A_{GCA}}\right)^2 \left\{\left[E_\Delta\left\{A_c d_c(t)\cos(\omega_0 t + \theta_\Delta) + A_s d_s(t)\sin(\omega_0 t + \theta_\Delta)\right\}\right.\right.$$

$$\left. + \sqrt{2}\, n_3(t)\cos\omega_0 t + \sqrt{2}\, n_4(t)\sin\omega_0 t\right]$$

$$\cdot \left[E_r\left\{A_c d_c(t)\cos(\omega_0 t + \theta_r) + A_s d_s(t)\sin(\omega_0 t + \theta_r)\right\}\right.$$

$$\left.\left. + \sqrt{2}\, n_1(t)\cos\omega_0 t + \sqrt{2}\, n_2(t)\sin\omega_0 t\right]\right\}_{\substack{\text{Low}\\\text{Pass}}}$$

$$= \left(\frac{1}{A_{GCA}}\right)^2 \left\{E_\Delta E_r\left[\frac{A_c^2}{2}\cos\theta_E + \frac{A_s^2}{2}\cos\theta_E\right] + n'_{eq}(t)\right\} \quad , \tag{19}$$

where the difference in IF phase delays between the sum and difference channels is

$$\theta_E = \theta_\Delta - \theta_r \tag{20}$$

and the equivalent additive noise is given by

$$\left.\begin{aligned} n'_{eq}(t) = {} & n_1(t)\, n_3(t) + n_2(t)\, n_4(t) \\ & + \frac{E_\Delta}{\sqrt{2}}\left[A_c d_c(t)\left(\cos\theta_\Delta\right) n_1(t) - A_c d_c(t)\left(\sin\theta_\Delta\right) n_2(t)\right. \\ & \left. + A_s d_s(t)\left(\sin\theta_\Delta\right) n_1(t) + A_s d_s(t)\left(\cos\theta_\Delta\right) n_2(t)\right] \\ & + \frac{E_r}{\sqrt{2}}\left[A_c d_c(t)\left(\cos\theta_r\right) n_3(t) - A_c d_c(t)\left(\sin\theta_r\right) n_4(t)\right. \\ & \left. + A_s d_s(t)\left(\sin\theta_r\right) n_3(t) + A_s d_s(t)\left(\cos\theta_r\right) n_4(t)\right] \quad . \end{aligned}\right\} \begin{array}{l} \text{N x N terms} \\ \\ \\ \\ \text{S x N terms} \end{array} \tag{21}$$

The terms in $n'_{eq}(t)$ are designated as noise x noise (N x N) terms and signal x noise (S x N) terms as indicated in (21).

There may be some question as to whether the output of the CAD can truly be represented as the mathematical product of the two input waveforms when both inputs are broadband. In this case, with the despreader absent, the bandwidth is $B_\Sigma = B_\Delta = 40$ MHz, and with the despreader present in both channels, the bandwidth is approximately $B_\Sigma = B_\Delta = 9$ MHz (3 Mbps data rate of bi-ϕ-L signals). In all cases, there is no spectral component in either signal. To our knowledge, if the signal level of one of the inputs is kept substantially higher than the other, say by a factor of 10, then the CAD will act as an ideal multiplier independent of the bandwidth of either input waveform.

From (19), the angle error signal may be expressed as

$$\epsilon(t) = \frac{E_\Delta E_r P_{rec} \cos\theta_E}{(A_{GCA})^2} + \frac{n'_{eq}(t)}{(A_{GCA})^2}$$

$$= \frac{E_\Delta E_r P_{rec} \cos\theta_E}{E_r^2 P_{rec} + 2R_{n\Sigma}(0)} + \frac{n'_{eq}(t)}{(A_{GCA})^2}$$

$$= \frac{E_\Delta}{E_r}\left[\frac{\cos\theta_E}{1 + \dfrac{2R_{n\Sigma}(0)}{E_r^2 P_{rec}}}\right] + \frac{n'_{eq}(t)}{(A_{GCA})^2}$$

$$= k_m \frac{\Delta_\epsilon}{\theta_B}\left[\frac{\cos\theta_E}{1 + \dfrac{2R_{n\Sigma}(0)}{E_r^2 P_{rec}}}\right] + \frac{n'_{eq}(t)}{(A_{GCA})^2}$$

$$= K_{eq}\Delta_\epsilon + \frac{n'_{eq}(t)}{(A_{GCA})^2} \quad , \tag{22}$$

where

$$K_{eq} \triangleq \frac{k_m}{\theta_B}\left[\frac{\cos\theta_E}{1+\frac{2\,R_{n\Sigma}(0)}{E_r^2\,P_{rec}}}\right] . \tag{23}$$

3.0 PERFORMANCE - RMS ERROR

If the angle error signal is scaled by K_{eq}^{-1}, then a linearized antenna angle control system is as shown in Figure 3, where

$$\epsilon_n(t) = \frac{\epsilon(t)}{K_{eq}} = \Delta_\epsilon + n_{eq}(t) \tag{24}$$

and

$$n_{eq}(t) = K_{eq}^{-1}\, n'_{eq}(t)\Big/(A_{GCA})^2 . \tag{25}$$

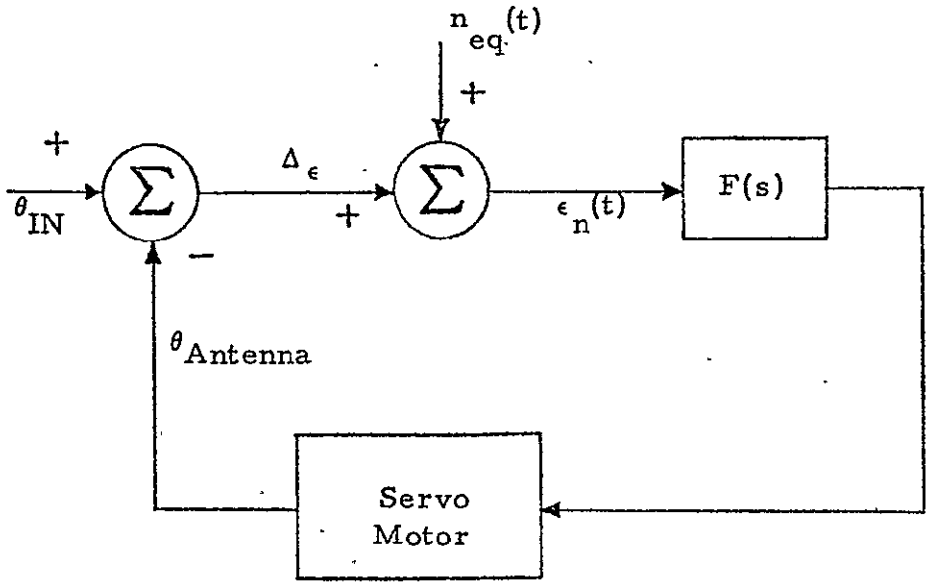

Figure 3. Linearized Diagram for Antenna Angle Control

From linear tracking loop theory [2-3], the variance of the angle error due to thermal noise is given by

$$\sigma^2_{\Delta_\epsilon} = \int_{-\infty}^{\infty} \left|H_s(f)\right|^2 S_{n_{eq}}(f)\, df \tag{26}$$

where $H_s(f)$ is the closed loop transfer function of the antenna angle control and $S_{n_{eq}}(f)$ is the two-sided spectral density of equivalent loop noise.

When the bandwidth of the noise is very large with respect to the noise bandwidth of the antenna angle control, the variance of the angle error is

$$\sigma^2_{\Delta_\epsilon} = N_{eq} B_s \tag{27}$$

where N_{eq} is the one-sided spectral density of the equivalent loop noise and B_s is the one-sided noise bandwidth of the angle control loop:

$$B_s = \int_0^{\infty} \left|H_s(f)\right|^2 df \ . \tag{28}$$

Equivalently stated, the requirement is $B_s \ll B_\Sigma$, and $B_s \ll B_\Delta$.

The one-sided spectral density of $n_{eq}(t)$ is given in terms of that of $n'_{eq}(t)$ by

$$N_{eq} = \frac{N'_{eq}}{K^2_{eq} (A_{GCA})^4} \ . \tag{29}$$

In Appendix A, we show that the one-sided spectral density of $n'_{eq}(t)$ is given by

$$N'_{eq} = P_{rec} N_{0\Sigma}\left[\frac{N_{0\Sigma} B_\Sigma}{2 P_{rec}} + \left(\frac{N_{0\Delta}}{N_{0\Sigma}}\right)\left(\frac{N_{0\Delta} B_\Delta}{2 P_{rec}}\right) + E_r^2\left(\left(\frac{E_\Delta}{E_r}\right)^2 + \frac{N_{0\Delta}}{N_{0\Sigma}}\right)\right] \tag{30}$$

This result agrees with (27) of [1] when $N_{0\Delta} = N_{0\Sigma}$ and $B_\Sigma = B_\Delta$. Upon substituting (30) into (29), and (18), (23), and (29) into (27), the RMS angle error due to thermal noise is given by

$$\sigma_{\Delta_\epsilon} = \frac{\theta_B}{k_m \cos\theta_E}\left\{\left(\frac{N_{0\Sigma} B_s}{P_{rec}}\right)\left[\frac{N_{0\Sigma} B_\Sigma}{2 P_{rec}}\left\{1 + \left(\frac{N_{0\Delta}}{N_{0\Sigma}}\right)^2\left(\frac{B_\Delta}{B_\Sigma}\right)\right\} + \left(\frac{E_\Delta}{E_r}\right)^2 + \frac{N_{0\Delta}}{N_{0\Sigma}}\right]\right\}^{1/2} \tag{31}$$

where we have consolidated E_r into P_{rec} by setting $E_r = 1$.

4.0 COMPUTATIONS

The RMS phase error due to thermal noise as given in (31) has been evaluated under a variety of conditions.

The constants used in the computation are:

1. Tracking Loop Bandwidth

$$B_s = 10 \text{ Hz}$$

This is considered a relatively conservative value since the angular motion of the Shuttle with respect to the TDRS is expected to be very small.

2. 3 dB Antenna Beamwidth

$$\theta_B = 2.8 \text{ degrees}$$

Using the rule-of-thumb

$$\theta_B \approx 70\ \lambda/D \tag{32}$$

for paraboloid (circular aperture) antenna dishes, where λ = RF wavelength and D = antenna diameter, if we set

$$\lambda = 0.02 \text{ m} \quad (f_0 = 15 \text{ GHz}) \tag{33}$$

and $$D = 20 \text{ inches}, \tag{34}$$

then $$\theta_B = 2.76 \text{ degrees} \tag{35}$$

3. We shall assume that the paramp improves the noise figure by 6 dB with respect to RF balanced diode mixers at Ku-band. This agrees well with [4, Ch. 5]. Typical noise figures for paramps at Ku-band are 2-3 dB and 6-8 dB for balanced diode mixers at Ku-band.

4. Based on the discussion above, the IF filter bandwidth is chosen to be

40 MHz for the PN spread waveform

9 MHz for the despread waveform .

5. The antenna error slope is set at

$$k_m = 1.57 \tag{36}$$

which is in the center of the interval of typical values for circular apertures.

6. The initial computations are performed assuming the RF phase delay of the error channel with respect to the sum channel is $\theta_E = 0$. The effect of θ_E on RMS angle error is considered later.

7. The ratio of E_Δ/E_r is bounded by its maximum value of $\left|E_\Delta/E_r\right| = 1$.

With these constants, the RMS angle error is shown in Figure 4 versus the sum channel $P_{rec}/N_{0\Sigma}$ either at the input to the paramp or at the input to the balanced diode mixer, if the paramp is not in the tracking loop.

Considering the performance curves individually, we note the following:

Curve 1 is the case where all channels have the same noise figure and there is no despreading of the PN sequence. Therefore,

$$N_{0\Delta} = N_{0\Sigma} \quad \text{and} \quad B_\Delta = B_\Sigma = 40 \text{ MHz} \ .$$

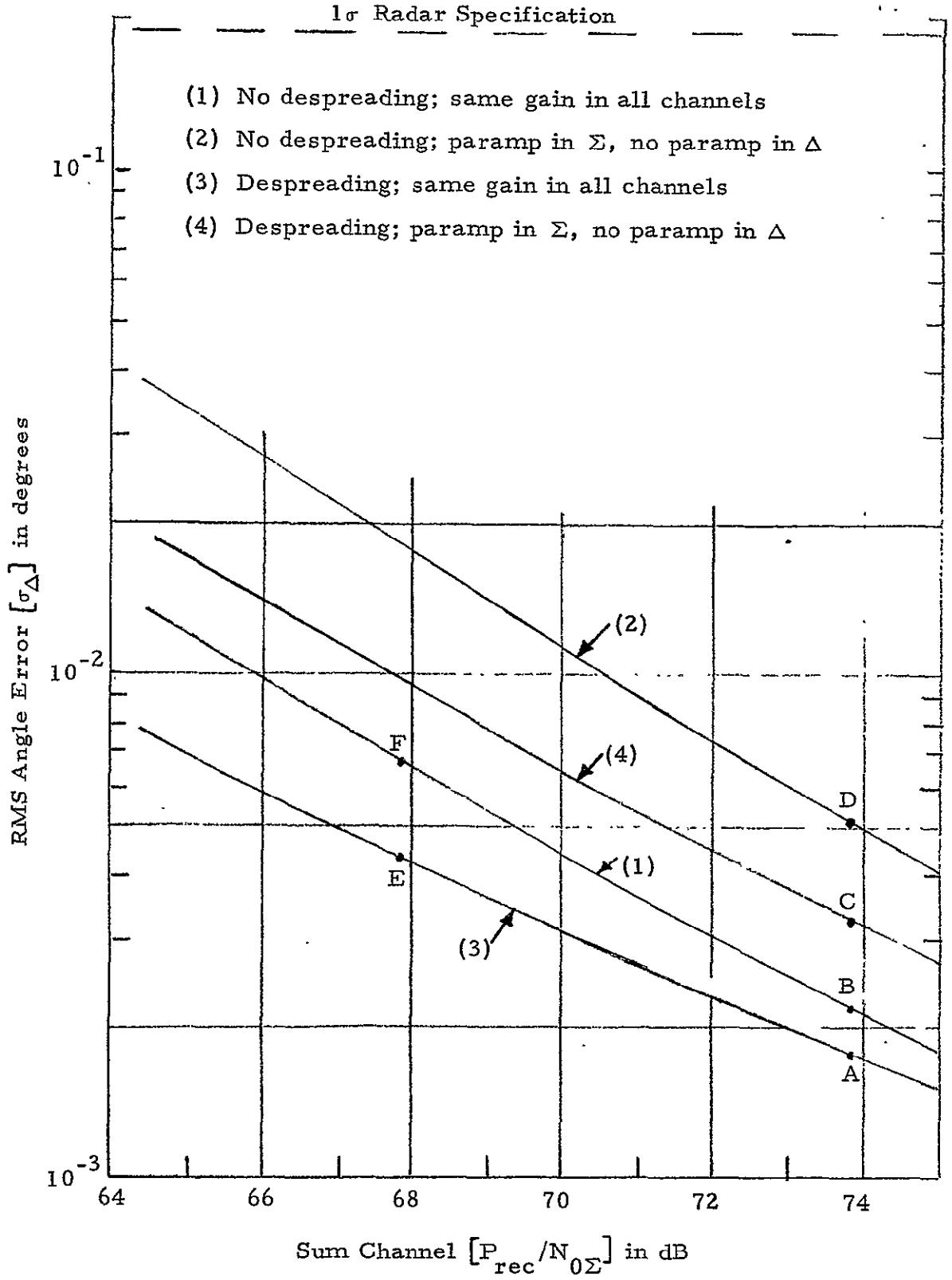

Figure 4. RMS Angle Error vs. P_{rec}/N_0

Point B on Curve 1 is at $P_{rec}/N_{0\Sigma}$ = 73.8 dB, which is the presently quoted value* when the paramp is present. Therefore, the performance when there is a paramp in all channels and there is no despreading is given by point B. This agrees with the results in [1].

Alternatively, if there is no paramp in any of the three channels, the performance is given by Point F when there is no despreading. This corresponds to $P_{rec}/N_{0\Sigma}$ = 67.8 dB, or 6 dB lower than Point B.

Any alterations in the present power budget could easily be taken into account by choosing the appropriate values of $P_{rec}/N_{0\Sigma}$.

Curve 2 also assumes no PN sequence despreading, but also assumes there is a paramp in the sum channel only. Therefore,

$$B_{\Delta} = B_{\Sigma} = 40 \text{ MHz} \tag{37}$$

and

$$\frac{N_{0\Delta}}{N_{0\Sigma}} = 4 \quad (6 \text{ dB}) . \tag{38}$$

Point D on Curve 2 corresponds to the present design point of $P_{rec}/N_{0\Sigma}$ = 73.8 dB.

Curve 3 assumes the PN sequence despreader is present in the receiver tracking loop and is functioning ideally. In addition, all channels are assumed to have the same noise figure. Therefore,

$$B_{\Delta} = B_{\Sigma} = 9 \text{ MHz} \tag{39}$$

and

$$N_{0\Sigma} = N_{0\Delta} . \tag{40}$$

In this case, Point A at $P_{rec}/N_{0\Sigma}$ = 73.8 dB assumes a paramp is present in all channels, and Point E assumes the paramp is absent in all channels.

Finally, Curve 4 assumes ideal PN despreading with a paramp present in the sum channel only, and Point C corresponds to the present design point of $P_{rec}/N_{0\Sigma}$ = 73.8 dB.

---

*From power budgets issued by B. H. Batson, NASA/JSC.

It can be seen that all design points that have been considered have an RMS angle error substantially less than 10^{-2} degrees.

One might ask why the RMS angle error due to thermal noise is so small. The reason is that the P_{rec}/N_0 (signal power to noise spectral density) is very large because of the requirements due to the wideband digital signal. The result is an abundance of signal-to-noise ratio for angle tracking purposes.

Effect of RF Phase Error

In order to obtain a measure of additional RMS angle error due to RF phase differences between sum and error IF channels, we compute

$$\sigma_0 \triangleq \left[\cos \theta_E\right]^{-1} \tag{41}$$

which is plotted in Figure 5. Because of the cos θ_E function, the effect on RMS angle error is very small for $|\theta_E|$ less than 20 degrees.

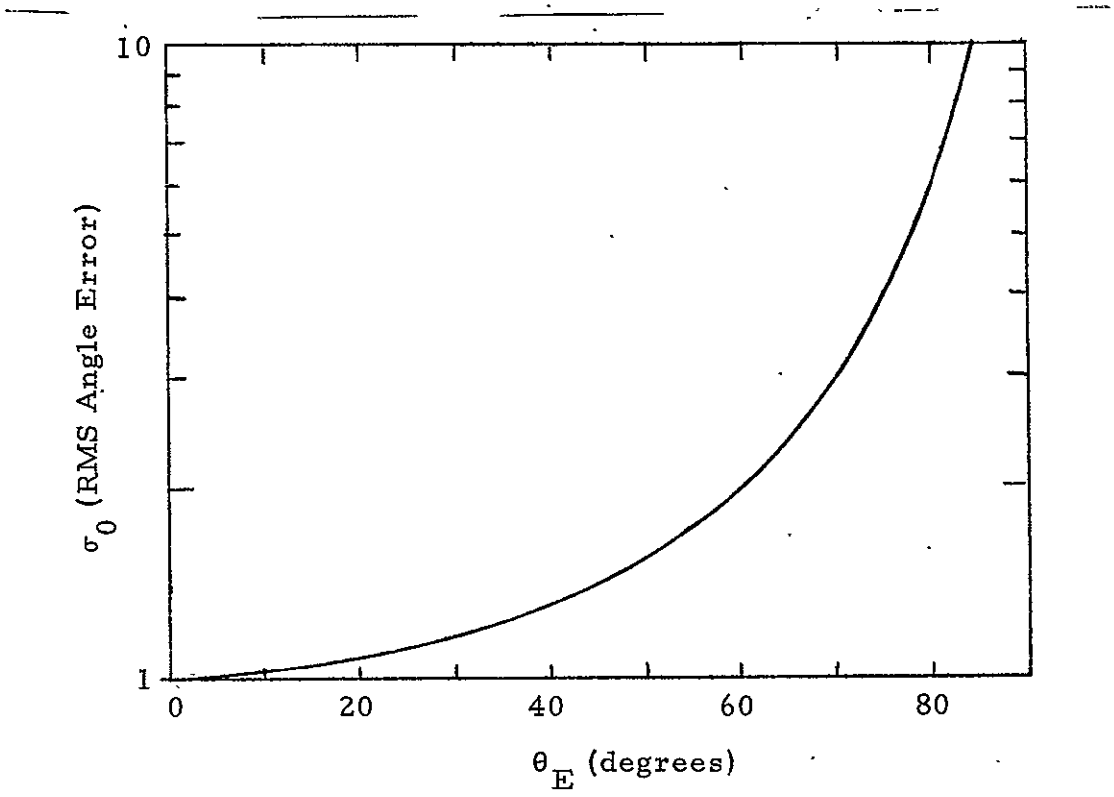

Figure 5. Angle Error Versus RF Phase Difference Between Sum and Error IF Channels

5.0 IMPLEMENTATION CONSIDERATIONS

The above system performance evaluation was carried out under the assumption that there are three separate IF channels for the angle tracking loops.

One possible alternative implementation which has also been proposed for the Japanese Broadcast Satellite is shown in Figure 6. The two error channels are multiplied by PN sequences which are either different sequences or shifted versions of the same sequence. The outputs of these mixers are then added and combined with part of the power from the sum channel, which in turn is processed by a single IF strip which will have a somewhat wider bandwidth. At the end of the IF amplification strip, the signals are demultiplexed in the same manner in which they were multiplexed. The coherent amplitude detection is then carried out in each channel.

More quantitatively, the input to the single channel IF is

$$x(t) = \Sigma(t) + PRN_E(t)\,\Delta_E(t) + PRN_A(t)\,\Delta_A(t) \quad , \tag{42}$$

where the sum channel signal is described by (6) and each error channel is described by (12).

Considering the azimuth channel only:

$$\begin{aligned} y_A(t) &= x(t)\,PRN_A(t) \\ &= \Delta_A(t) + \Sigma(t)\,PRN_A(t) + \Delta_E(t)\,PRN_E(t)\,PRN_A(t) \\ &= \Delta_A(t) + \Sigma(t)\,PRN_A(t) + \Delta_E(t)\,PRN'_E(t) \end{aligned} \tag{43}$$

where

$$PRN'_E(t) = PRN_E(t)\,PRN_A(t) \tag{44}$$

is a shifted version of $PRN_E(t)$.

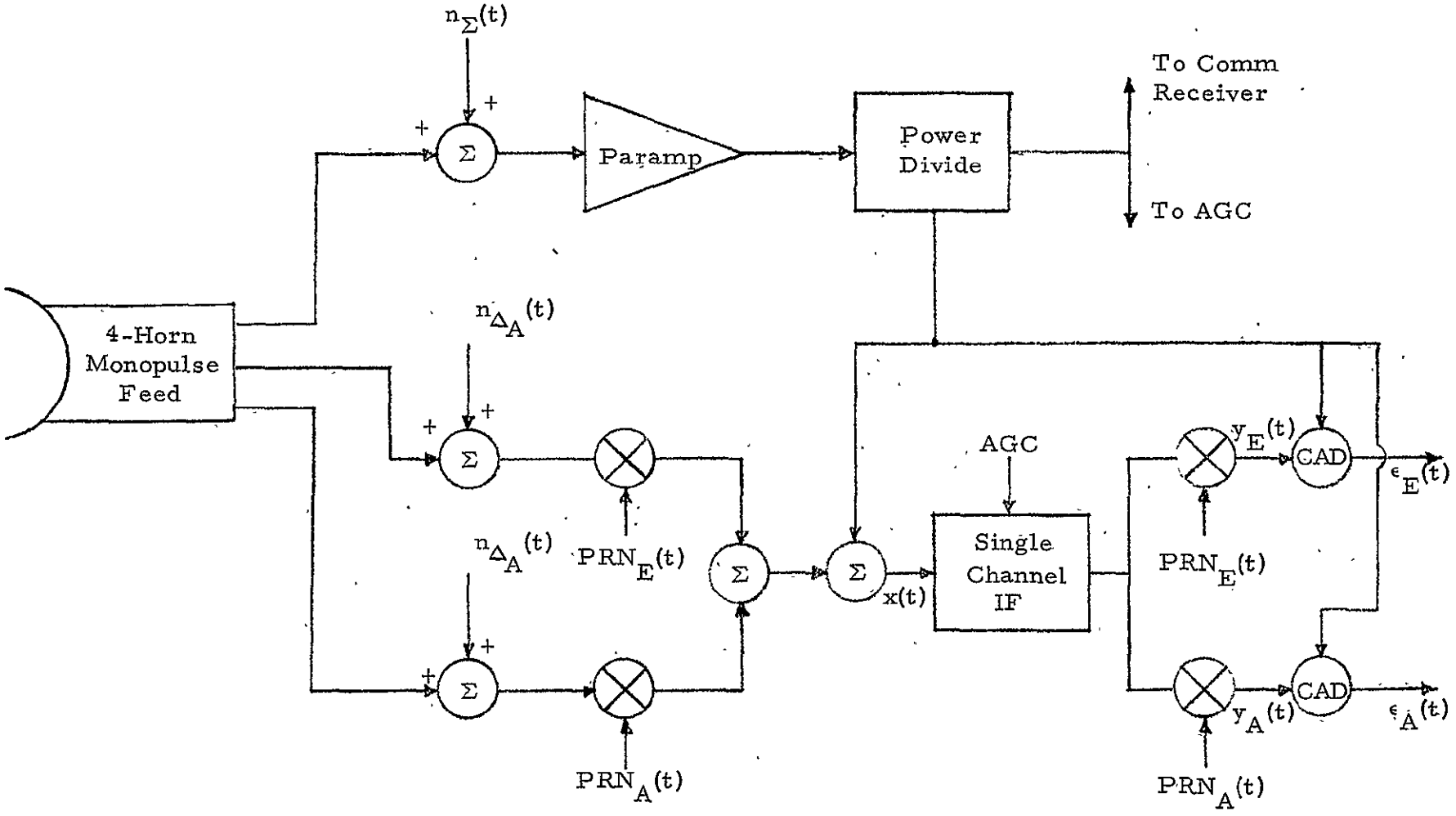

Figure 6. One Possible Single Channel IF Implementation of Communication Angle Track From TDRS

The output of the CAD for the azimuth channel is then given by

$$\epsilon_A(t) = \Delta_A(t)\,\Sigma(t) + [\Sigma(t)]^2\,PRN_A(t) + \Delta_E(t)\,\Sigma(t)\,PRN'_E(t) \quad . \qquad (45)$$

The first term in (45) is the desired output, as given by (19). The remaining two terms are additional noise (self-noise and cross-modulation) terms which resulted from the multiplexing and demultiplexing operations, so as to implement a single IF strip.

Neglecting the effect of the AGC, the low frequency portion of $\epsilon_A(t)$ in (45) is given by

$$\begin{aligned}
\epsilon_A(t) = {} & E_{\Delta_A} E_r P_{rec} && \Big\} 1 \\
& + n_1(t)\,n_3(t) + n_2(t)\,n_4(t) && \\
& + \frac{E_{\Delta_A}}{\sqrt{2}}\left[A_c d_c(t)\,n_1(t) + A_s d_s(t)\,n_2(t)\right] && \Big\} 2 \\
& + \frac{E_r}{\sqrt{2}}\left[A_c d_c(t)\,n_3(t) + A_s d_s(t)\,n_4(t)\right] && \\
& + PRN_A(t)\left\{E_r^2 P_{rec} + n_1^2(t) + n_2^2(t)\right. && \Big\} 3 \\
& \qquad \left. + \sqrt{2}\,E_r\left[A_c d_c(t)\,n_1(t) + A_s d_s(t)\,n_2(t)\right]\right\} && \\
& + PRN'_E(t)\left\{E_{\Delta_E} E_r P_{rec} + n_1(t)\,n_5(t) + n_2(t)\,n_6(t)\right. && \\
& \qquad + \frac{E_{\Delta_E}}{\sqrt{2}}\left[A_c d_c(t)\,n_1(t) + A_s d_s(t)\,n_2(t)\right] && \Big\} 4 \\
& \qquad \left. + \frac{E_r}{\sqrt{2}}\left[A_c d_c(t)\,n_5(t) + A_s d_s(t)\,n_6(t)\right]\right\} && \qquad (46)
\end{aligned}$$

where $n_5(t)$ and $n_6(t)$ have the same statistics as $n_3(t)$ and $n_4(t)$. All noises are statistically independent. In (46):

(1) is the desired error signal;

(2) is the $n'_{eq}(t)$ noise described by (21);

(3) is noise, self-noise, and cross-modulation, all spread by $PRN_A(t)$. This is the $[\Sigma(t)]^2\ PRN_A(t)$ term in (45);

(4) is noise, self-noise, and cross-modulation, all spread by $PRN'_E(t)$.

As the PN housekeeping sequences have decreased chip time, the spectral densities of the self-noise terms decreases. This, however, forces the IF bandwidth to be increased, thereby increasing the power in the noise terms in (46). There is an optimal choice of IF bandwidth and PN sequence chip time which will maximize the signal-to-noise ratio in the angle tracking loop. This optimization has not been performed. It is anticipated, however, that an IF bandwidth and PN sequence chip time can be chosen so that the resulting degradation in RMS angle tracking error is not significant and that the resulting RMS error is still well below any anticipated specifications.

1. C. L. Weber, "Shuttle Monopulse System for Ku-Band Communication Signal from TDRS," Appendix I to this report.

2. A. J. Viterbi, Principles of Coherent Communication, McGraw-Hill, 1966.

3. W. C. Lindsey, Synchronization Systems in Communication and Control, Prentice-Hall, 1972.

4. M. Skolnik, Radar Handbook, McGraw-Hill, 1970.

APPENDIX A

In this appendix, the one-sided noise spectral density of the equivalent loop noise, $n'_{eq}(t)$, as given by (21) is determined. The autocorrelation function of $n'_{eq}(t)$ is

$$R_{n'_{eq}}(\tau) = R^2_{n\Sigma}(\tau) + R^2_{n\Delta}(\tau) + \left[\frac{E^2_\Delta}{2} R_{n\Sigma}(\tau) + \frac{E^2_r}{2} R_{n\Delta}(\tau)\right]\left[A^2_c R_{d_c}(\tau) + A^2_s R_{d_s}(\tau)\right] \tag{A-1}$$

The Fourier transform of the first two terms in (A-1) is designated as $S_1(f)$. This spectral density evaluated at $f = 0$ is

$$S_1(0) = \left(\frac{N_{0\Sigma}}{2}\right)^2 B_\Sigma + \left(\frac{N_{0\Delta}}{2}\right)^2 B_\Delta \ . \tag{A-2}$$

The contribution to the spectral density of $n'_{eq}(t)$ from the last term in (A-1) is designated as $S_2(f)$. It is the Fourier transform of

$$\left[\frac{E^2_\Delta}{2} R_{n\Sigma}(\tau) + \frac{E^2_r}{2} R_{n\Delta}(\tau)\right]\left[A^2_c R_{d_c}(\tau) + A^2_s R_{d_s}(\tau)\right]$$

$$= \left[E^2_\Delta R_{n\Sigma}(\tau) + E^2_r R_{n\Delta}(\tau)\right]\left[\frac{A^2_c}{2} R_{PRN}(\tau) R_{m_c}(\tau) + \frac{A^2_s}{2} R_{PRN}(\tau) R_{m_s}(\tau)\right] . \tag{A-3}$$

We compute $S_2(0)$ for two cases: (I) PN sequence present (not removed), and (II) the PN sequence absent (i.e., despread ideally).

Case I. PN sequence present in all channels, and not despread.

In Figure A-1, the autocorrelation functions of the data sequences and the PN sequence are shown. Since $T_c \ll T_s$, we make the approximation that

$$R_{m_s}(\tau) = R_{m_c}(\tau) \approx 1 \qquad \text{for } |\tau| \leq T_c \tag{A-4}$$

where T_c is the PN sequence chip time. Then,

$$S_2(f) = P_{rec}\, \mathcal{F}\left\{\left[E_\Delta^2\, R_{n\Sigma}(\tau) + E_r^2\, R_{n\Delta}(\tau)\ \ R_{PRN}(\tau)\right]\right\} \tag{A-5}$$

and

$$S_2(0) = P_{rec}\left\{E_\Delta^2 \int_{-B_\Sigma/2}^{B_\Sigma/2} \frac{N_{0\Sigma}}{2}\, S_{PRN}(f)\, df + E_r^2 \int_{-B_\Delta/2}^{B_\Delta/2} \frac{N_{0\Delta}}{2}\, S_{PRN}(f)\, df\right\} . \tag{A-6}$$

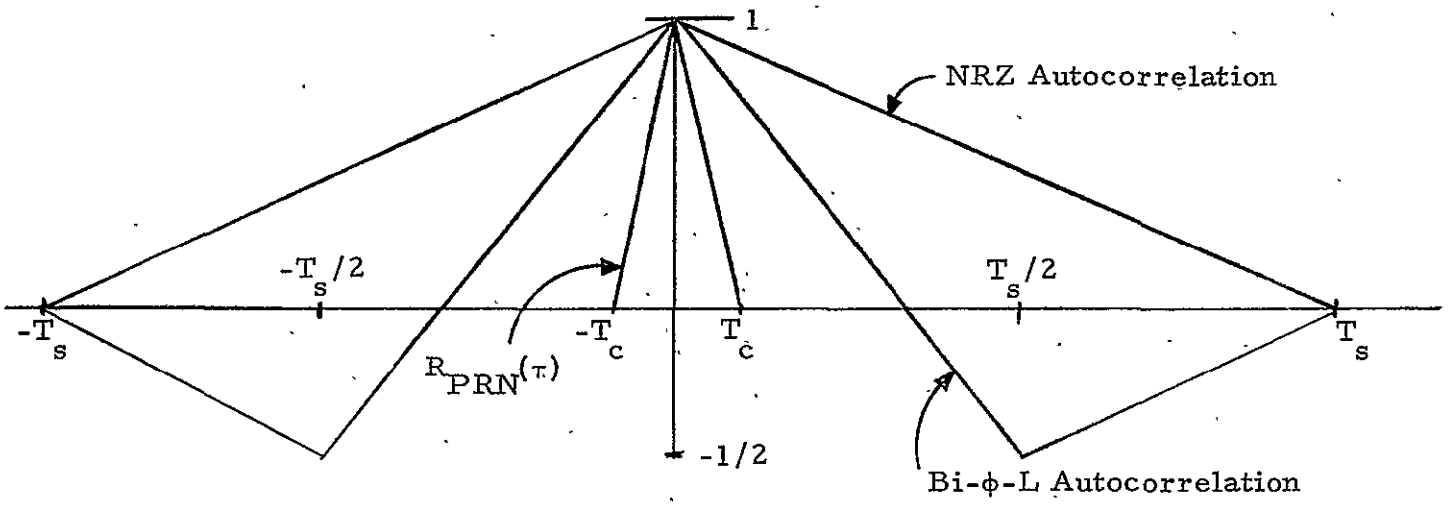

Figure A-1. Autocorrelation Functions

From Figure A-2, it is seen that the values of PRN chip time and IF bandwidth are such that the IF filters pass the PN sequence without distortion and without loss of signal power. The integrals in (A-6) can then be carried out with the result that, for Case I:

$$S_2(0) = \frac{P_{rec}}{2}\left[E_\Delta^2 N_{0\Sigma} + E_r^2 N_{0\Delta}\right] . \qquad (A-7)$$

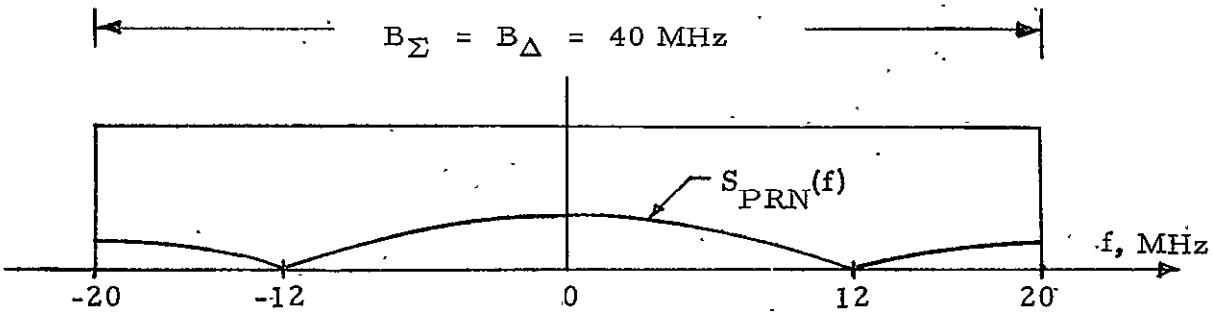

Figure A-2. PN Sequence Spectrum and IF Filter

Case II. PN sequence despread ideally in all channels

When the PN sequence has been despread, then

$$S_2(f) = \left[E_\Delta^2 R_{n\Sigma}(\tau) + E_r^2 R_{n\Delta}(\tau)\right]\left[\frac{A_c^2}{2} R_{m_c}(\tau) + \frac{A_s^2}{2} R_{m_s}(\tau)\right] . \qquad (A-8)$$

The maximum data rate is 3 Mbps of Bi-ϕ-L waveforms. This spectrum is shown in Figure A-3, where it is seen that a 9 MHz IF filter will pass essentially all of the signal energy. We assume that a 9 MHz

IF in the sum and difference channels does pass all of the signal energy without distortion.

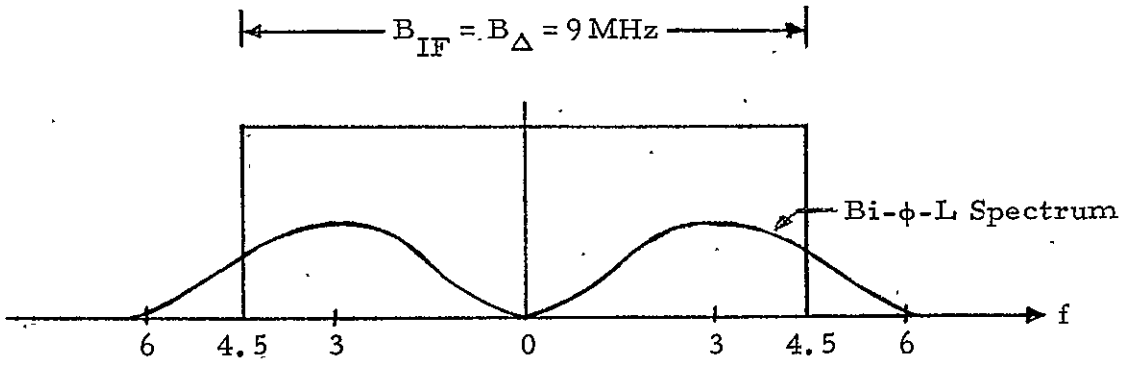

Figure A-3. Bi-ϕ-L Data Spectrum and IF Filter

The transform in (A-8) can then be evaluated at f = 0, with the result that

$$S_2(0) = \frac{P_{rec}}{2}\left[E_{\Delta}^2 N_{0\Sigma} + E_r^2 N_{0\Delta}\right] \qquad \text{(A-9)}$$

which is the same as in Case I. The value of bandwidths are different, however.

Upon addition of (A-9) or (A-7) and (A-2), we have

(A-10)

We can absorb E_r into P_{rec} by assuming $E_r = 1$ without any loss of generality. This result is (30), which is used to compute the RMS angle error due to thermal noise.

APPENDIX K

FREQUENCY CONSIDERATIONS

If the radar function is to be considered independently of the communications function, one may pose a question of whether there is an "optimum" frequency at which the radar should operate. The answer to this question may not be an easy one, because the term "optimum" itself involves many parameters which vary in a number of ways with frequency, or equivalently with wavelength. Thus, one can only consider general trends without trying to establish exact quantitative answers. As the first step we can look at the radar equation. Assuming that the antenna aperture is relatively independent of the operating wavelength we can express the ratio of received power to the transmitted power in terms of wavelength-dependent terms:

$$\frac{P_r}{P_t}(\lambda) = G_t(\lambda) \times \left(\frac{1}{4\pi R^2}\right)^2 \times \sigma(\lambda) \times A \times F(\lambda) \qquad \text{(K}$$

$$= \frac{4\pi A}{\lambda^2} \times \left(\frac{1}{4\pi R^2}\right)^2 \times \sigma(\lambda) \times A \times F(\lambda) \qquad \text{(K}$$

$$= \frac{1}{4\pi R^4} \times \frac{A^2}{\lambda^2} \times \sigma(\lambda) \times F(\lambda) \qquad \text{(K}$$

where

P_r = received power
P_t = transmitted power
R = range
σ = radar cross section
A = antenna aperture
F = secondary factors affecting the radar equation.

The question now is how do the $\sigma(\lambda)$ and $F(\lambda)$ vary. The dependence of the radar cross section on λ is a function of the target shape and it can vary from $k\lambda^{-2}$, as for flat plate reflectors, to $k\lambda^2$ for reflectors such as a cone whose apex is pointed at the radar. Because the exact shape of the

expected passive targets is not known, a compromise assumption would be that the σ may be independent of the λ, such as is the case for a sphere.

The term $F(\lambda)$ may contain $1/L(\lambda)$, a loss factor of RF components, such as waveguides, which typically varies inversely with λ.* Thus, one would enter that portion of the $F(\lambda)$ term as $k\lambda$, where k is a constant associated with a particular waveguide. If the λ-dependence exploration was stopped at this point, one would conclude that as the wavelength decrease (i.e., the frequency increases) the performance improves. There may be a slight offset of this trend due to increasing noise temperature with frequency, but this term deteriorates performance relatively slowly, at least in the range from 5 to 15 GHz.**

But, from the component standpoint, weight may be important. If one considers a typical ensemble of available magnetrons, such as would be used for a pulse radar system the general profile is as shown in Figure 1. This profile is based on Litton frequency-tuned magnetrons. The data on a typical fixed tuned magnetron is also included to fill in the gap. From this profile it is evident that for a relatively equal peak power, the weight decreases to about one half in the region of 15 to 25 GHz. Thus, the baseline frequency of 15 GHz or in the close range within it, appears reasonable from the standpoint of weight.

Also considering weight dependence of waveguide on frequency, as shown in Figure 2, we see that weight goes down with increasing frequency. The same is also true of a typical component such as a monopulse converter which may be used for combining all three monopulse channels into one composite signal. The volume of the converter is particularly indicative since it employs a number of components such as switchable circulators and waveguide junctions. We see that this volume remains practically constant

---

*ITT, Reference Handbook for Radio Engineers, 5th edition, Howard W. Sams and Co., Inc., 1968, p. 23-13.

**M. Skolnik, Radar Handbook, McGraw-Hill, 1970, Figure 4, p. 5-1

above 8 GHz. Thus, again we may conclude that from the standpoint of volume and weight, operation in the 13 to 15 GHz range, compatible with the Shuttle communication mode, is desirable, even if the radar function is considered by itself.

Figure 1. Typical Peak Powers and Weights of Frequency Tuned Magnetrons

NOTE: Numbers refer to Litton Industries magnetron type.

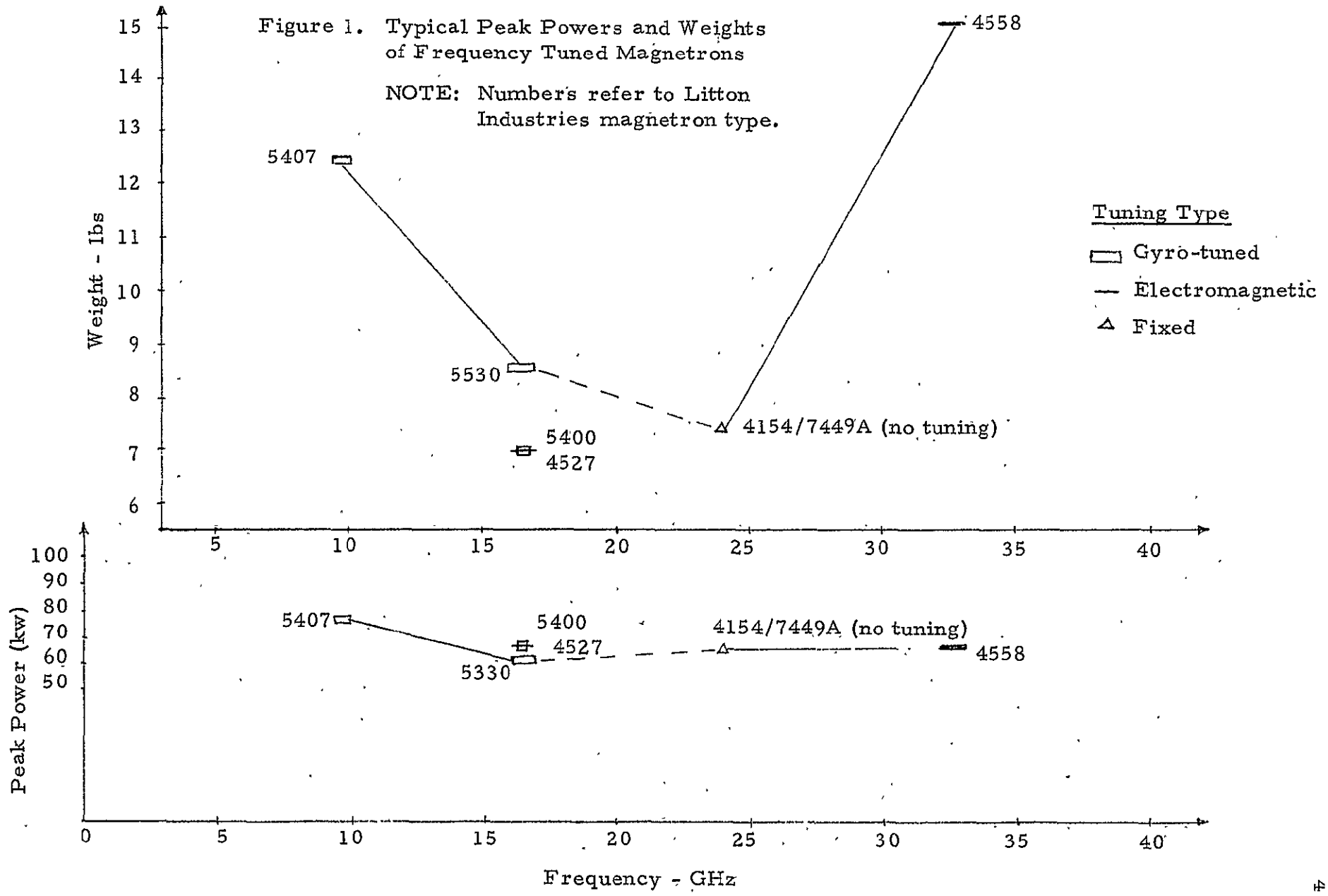

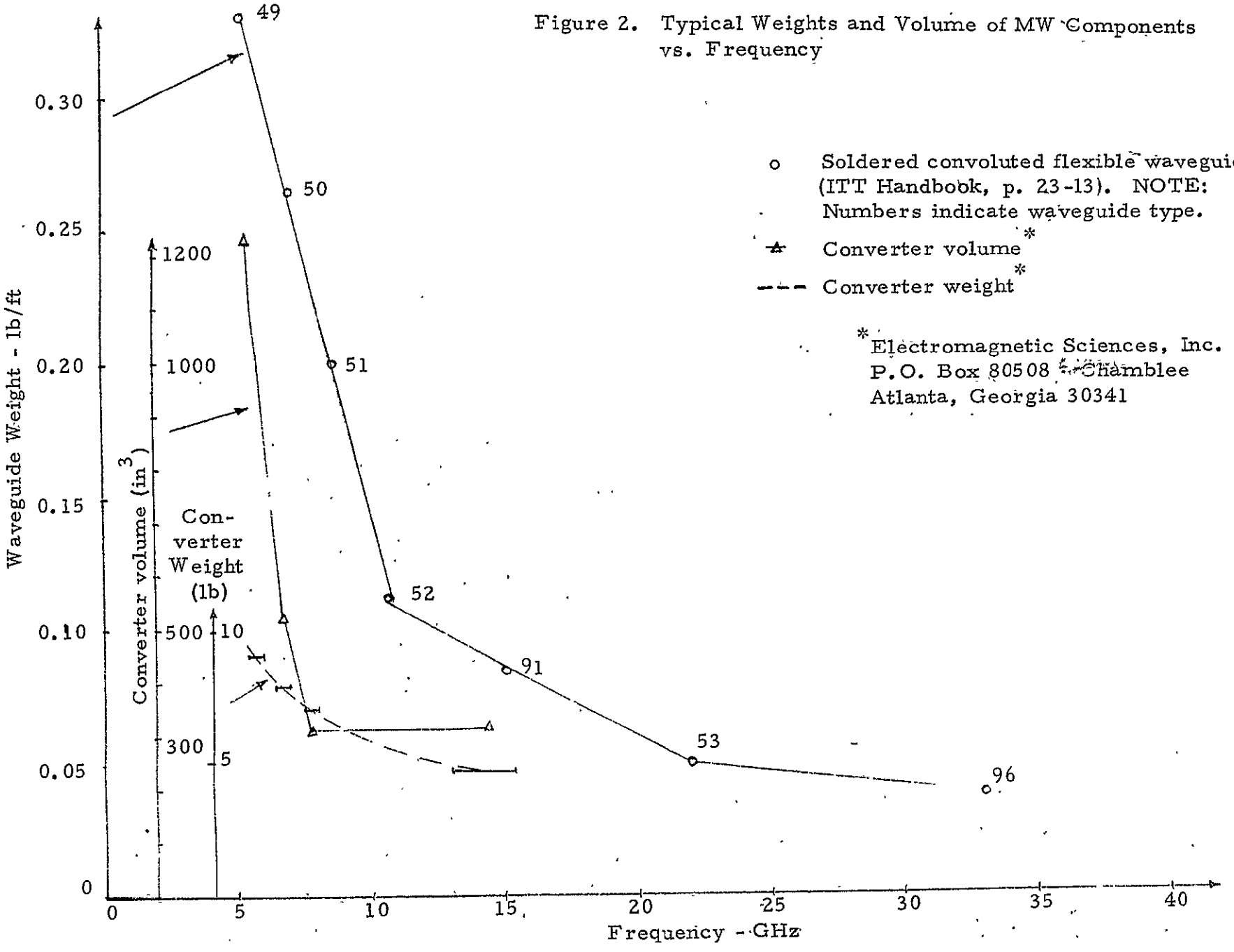
Figure 2. Typical Weights and Volume of MW Components vs. Frequency
o Soldered convoluted flexible waveguide (ITT Handbook, p. 23-13). NOTE: Numbers indicate waveguide type.
Converter volume*
Converter weight*
*Electromagnetic Sciences, Inc.
P.O. Box 80508 - Chamblee
Atlanta, Georgia 30341
Waveguide Weight - lb/ft
0.30
0.25
0.20
0.15
0.10
0.05
0
49
50
51
52
91
53
96
1200
1000
500
300
10
5
Converter volume (in^3)
Con-
verter
Weight
(lb)
0
5
10
15
20
25
30
35
40
Frequency - GHz